UNIVERSITE PICARDIE JULES VERNE
FACULTE DE MEDECINE ET PHARMACIE
ET
UNIVERSIDADE DE LISBOA – FACULDADE DE MEDICINA

Année 2010/2011

Nº attribué par la bibliothèque

Thèse en co-tutelle pour l'obtention du

Diplôme de Docteur de l'Université Picardie Jules Verne

Specialité: ***Biologie et Santé***

et de

Docteur de l'Université de Lisbonne

Specialité: ***Dermatologie***

Par

João Nuno Maia Rodrigues da SILVA

Directeurs de thèse:

MORLIÈRE, Patrice

MAZIÈRE, Jean-Claude

FILIPE, Paulo

Le Novembre 2010

Titre: **Étude des effets photosensibilisés de nouvelles molécules de synthèse : applications potentielles en photochimiothérapie antitumoral cutanée.**

[*Study of photosensitizing events triggered by new synthetic photosensitizers. Potential use in photodynamic therapy of skin cancers.*]

JURY:

Monsieur le Professeur	R. VICTORINO	Président
Monsieur le Professeur	J.C. BÉANI	Rapporteur
Monsieur le Professeur	A. FIGUEIREDO	Rapporteur
Monsieur le Professeur	R. SANTUS	Examinateur
Monsieur le Professeur	M. MARQUES GOMES	Examinateur
Monsieur le Professeur	P. FILIPE	Directeur de thèse
Monsieur le Professeur	J.C. MAZIÈRE	Directeur de thèse
Monsieur le Docteur	P. MORLIÈRE	Directeur de thèse

To my family and friends

As opiniões expressas nesta publicação são da exclusiva responsabilidade do seu autor.

ACKOWLEDGEMENTS

This thesis is the result of the research that I have pursued for several years, none of which would have been accomplished without the help and guidance from several persons to whom I am gratefully indebted.

First and foremost, I am very grateful to Professor Paulo Filipe and Dr. Patrice Morlière for becoming, along with Professor Jean-Claude Mazière, the co-directors of this thesis. I very much appreciate the time and effort that they have devoted to guide me in a wide variety of research problems. They have always been available to train me in research methodology and in the process of scientific writing. Their careful proofreading has also been valuable in the writing of this document.

I would like to acknowledge Professor Paulo Filipe, with whom I have had the honor to work since 1994, first as my teacher in the Faculty of Medicine of Lisbon, then as my tutor during my internship in Dermatology and later as a co-director of this thesis. For almost 16 years, Professor Paulo Filipe continuously inspired me to pursue higher scientific studies and gave me precious guidance ranging from research problems, difficulties in the practice of Dermatology, to career directions. His teachings, advice and enlightening example during our long working days at the laboratory and at the Dermatology clinic, have deeply enriched me as a researcher and as a dermatologist.

It is difficult to overstate my gratitude to Dr. Patrice Morlière, for introducing me to the world of porphyrins and for the decisive contribution to the achievement of the objectives of this thesis. His constant scientific advice, along with that of Professor Paulo Filipe, has been the driving force throughout this study. His inspiration and his great efforts to explain things clearly and simply have been a great help in the performance of the photophysical and photochemical studies. I greatly appreciate his devotion to science, his scientific knowledge in photobiology and his outstanding scientific methodology.

After referring to my co-directors, I wish to express my deepest gratitude to Professor René Santus for his advice, his spontaneity leading to great scientific ideas and for his help in writing reports. I appreciate his encouragement and enthusiastic constructive discussions about my work and about the different perspectives for improvement of photodynamic therapy. It has been a real honor to have such a world-class expert as a mentor during this thesis. His patient and careful proofreading has also been of inestimable value in the development of this document.

I want to express my gratitude to Professor Marques Gomes and Professor Jean-Claude Mazière for allowing me to use their research facilities. They have always supported this work creating all the conditions to pursue it. Their contributions during the thesis have been very much appreciated as they helped to reinforce the connection between the basic research and its clinical application. I also want to thank Dr. Larry Patterson from Notre Dame University, Indiana, USA, for the exceptional opportunity given me to carry out part of this work at the Radiation Laboratory.

I wish to express my sincere thanks to Professor José Cavaleiro and his co-workers at the University of Aveiro, Portugal, for synthesizing the new porphirinic derivatives studied in this thesis. I look forward to continue our good collaboration in the future.

I am also most grateful to Professor Afonso Fernandes and Professor Guerra Rodrigo for supporting me through the first years of my research activity. They were decisive to my formation as they have helped me to see medicine and science in their full depth, and have taught me how to appreciate good scientific work.

I greatly appreciate the interest of Admiral Macieira Fragoso and Admiral Teles Martins in this work and for allowing me to dedicate precious time to the elaboration of this thesis. Their valuable advice highlighting the search of excellence in every aspect of professional and personal life has been of the upmost importance.

During these years, I have been privileged to work with several scientists from the Université Picardie Jules Verne who greatly helped me with this work. I had the opportunity to work closely with Professor Antoine Galmiche who has been extremely helpful with matters related to cell transfection and other molecular biology aspects of the experiments. Dr. Agnès Boullier is warmly thanked for her contribution, as well as for her cheerful friendship and valuable advice in various issues. Dr. Jean-Claude Capiod is gratefully acknowledged for his help in the flow cytometry studies.

I have never ceased to admire the excellent work, friendly guidance and great atmosphere created by the technicians Mrs. Marie-Alix Conte, Mrs. Cathy Gomila, Mr. Christophe Louandre and Mrs. Corinne Godin. They are gratefully acknowledged for their skilled assistance and for their excellent organizing skills. I also want to thank Mrs. Maria do Céu Menezes and Mrs. Josiane Haigle for their careful and thorough work, as well as, for their kind help and company.

The company of my friends and colleagues during the execution of this thesis has been invaluable. The many joyful moments I have had with them will remain in my mind as fond and inspiring memories.

I am deeply thankful to my wife Joana for her emotional support, whose love and boundless patience has made the completion of this work possible. I thank Joana and her parents for the support and for all the encouragement during my studies abroad. Finally, I gratefully acknowledge the encouragement and influence of my parents. Their precious support has been constant and unconditional. Whatever I have learned from them since my childhood, has been crucial in shaping my character and mindset. My deepest gratitude goes to all who always encouraged me to make my plans become a reality.

TITRE: **ÉTUDE DES EFFETS PHOTOSENSIBILISES DE NOUVELLES MOLECULES DE SYNTHESE; APPLICATIONS POTENTIELLES EN PHOTOCHIMIOTHERAPIE ANTITUMORAL CUTANEE**

INSERM ERI12, Laboratoire de Biochimie, CHU Amiens-Hôpital Nord, place Victor Pauchet, 80054 Amiens Cedex 1, France
Clínica Universitária de Dermatologia, Hospital de Santa Maria, Avenida Prof. Egas Moniz, 1649-028 Lisboa, Portugal

RESUME

La thérapie photodynamique (PDT) cutanée est utilisée pour traiter les kératoses actiniques, la maladie de Bowen et les carcinomes basocellulaires. Malgré des résultats prometteurs, elle manque d'efficacité pour les lésions profondes et l'amélioration des photosensibilisateurs est d'actualité.

Nous avons étudié les propriétés photophysiques et photosensibilisatrices de porphyrines tricationiques substituées. Elles sont fluorescentes et leur état excité triplet a une grande durée de vie et un rendement quantique élevé à l'exception du conjugué poly-*S*-lysine. L'oxygène singulet est formé quantitativement depuis ce triplet.

L'étude chez des kératinocytes cutanés humains hyperprolifèrants de l'incorporation et de la photocytotoxicité montrent que 3 d'entre eux soutiennent favorablement la comparaison avec la protoporphyrine IX induite par l'acide δ-aminolévulinique (traitement actuel en PDT cutanée). Ils se localisent dans des vésicules d'endo- et pinocytose mais pas dans le noyau ni les mitochondries. La structure de leur chaîne substituée conditionne l'incorporation, la localisation et donc la phototoxicité.

Les mécanismes de mort cellulaire étudiés avec le dérivé le plus efficace montrent l'absence de fixation de l'annexine V, d'activation des caspases, de condensation de la chromatine et donc d'apoptose. L'apparition de vésicules LC3-positives dans ces cellules transfectées par GFP-LC3 et la dégradation de p62 démontrent l'implication de l'autophagie dans la photocytotoxicité avec une régulation négative par JNK.

En conclusion, ce sont des photosensibilisateurs intéressants nécessitant des études complémentaires dans des modèles cellulaires et animaux.

Mots-clés: thérapie photodynamique; porphyrines tricationiques; fluorescence; état excité triplet; oxygène singulet; incorporation cellulaire; localisation intracellulaire; photocytotoxicité; autophagie; nécrose; MAPK.

RESUME DETAILLE

INTRODUCTION

La thérapie photodynamique (PDT) utilise la combinaison d'un médicament photosensibilisant et de la lumière visible pour causer des dommages sélectifs au tissu tumoral cible. La nature locale plutôt que systémique des effets de la thérapie photodynamique doit être soulignée. Elle contribue à la fois aux limites et aux possibilités de la PDT dans un traitement efficace contre le cancer. Une limitation de la PDT est qu'elle ne peut être envisagée pour des tumeurs avancées et disséminées, car l'irradiation du corps entier avec des doses appropriées n'est pas possible. Néanmoins, la PDT peut être une thérapie sélective et curative appropriée, avec des avantages potentiels par rapport à d'autres propositions thérapeutiques pour des tumeurs précoces et/ou localisées ou encore certains troubles infectieux. Pour des cancers avancés, la PDT peut améliorer la qualité de vie et prolonger la survie.

En dermatologie, l'administration intraveineuse de Photofrin®, premier médicament "PDT" approuvé par la FDA en 1993, a montré son efficacité dans le traitement de diverses lésions cutanées, mais l'administration systémique de ce médicament n'est pas justifiée pour le traitement à grande échelle de pathologies localisées. En outre, la complexité et la variabilité du mélange de plus de 60 composés ayant des propriétés et activités différentes constituant le Photofrin®, sa lente élimination de l'organisme ajoutées à la photosensibilité cutanée résiduelle, due à la faible sélectivité pour les tissus tumoraux ont limité son utilisation en Dermatologie. La PDT utilisant l'acide aminolévulinique (ALA) ou son ester méthylique (MAL) comme pro-drogues a partiellement résolu ces problèmes en raison de sa commodité et de sa simplicité d'utilisation. L'ALA ou le MAL permettent la synthèse endogène localisée de la protoporphyrine IX (PPIX) comme photosensibilisant et ne sont donc pas associés à d'importants effets toxiques systémiques, à savoir la photosensibilité cutanée résiduelle. Bien qu'étant approuvés pour le traitement des cancers non-mélaniques de la peau, comme la maladie de Bowen (BD) et le carcinome basocellulaire superficiel (SBCC), et pour les lésions cutanées pré-néoplasiques, telles que la kératose actinique (AK), ALA et MAL présentent quelques limitations cliniques. Ils présentent en effet une pénétration cutanée limitée, et comme le Photofrin ®, la protoporphyrine IX induite possède des coefficients d'extinction molaire modestes dans le domaine visible rouge où est réalisée l'irradiation car correspondant à la fenêtre thérapeutique optimale. En outre, l'ALA et le MAL sont difficilement solubles en milieu aqueux.

En raison des inconvénients présentés par les photosensibilisateurs actuellement utilisés, de nombreux nouveaux composés, les photosensibilisateurs dits de deuxième génération, ont été synthétisés. La recherche dans ce domaine vise à l'élaboration de

médicaments photosensibilisants qui sont chimiquement purs, qui absorbent plus fortement à longueurs d'onde élevées et qui présentent des propriétés biologiques améliorées. Avec des capacités d'absorption de la lumière meilleures que la PPIX, ces photosensibilisateurs de deuxième génération permettraient de diminuer les doses de médicaments et d'irradiation.

Notre groupe a porté son intérêt sur des dérivés de porphyrines tri-cationiques, hydrosolubles (PR), dont les structures sont données ci-dessous. Ils sont obtenus par substitution du groupe hydroxyl du carboxyphenyl en position *meta* sur le cycle tétrapyrrolique par un groupe méthoxy (P-Me), un groupe *N,N´*-dicyclohexylureidooxy (P-DDC), un groupe di-*O*-isopropylidene-α-D-galactopyranosyl (P-OGal), un groupe α/β-D-galactopyranosyl (P-Gal) ou par chaîne poly-S-lysine (P-$(Lys)_n$) des chaînes latérales (Figure 1.1). Ces dérivés porphyriniques ont été synthétisés par le groupe du Professeur Cavaleiro à l'Université d'Aveiro (Portugal).

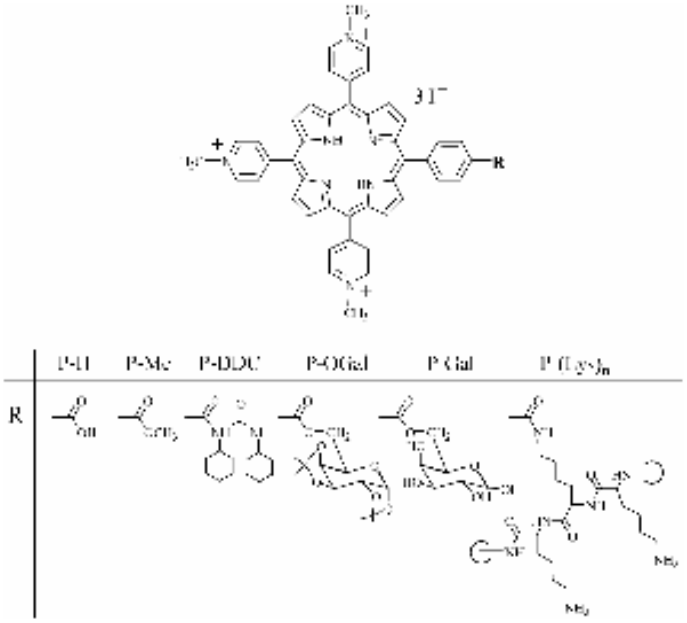

Figure 1.1 *Noms et structures chimiques des dérives étudiés dérivants de la 5-(4-carboxyphenyl)-10,15,20-tris(N-methylpyridinium-4-yl)porphyrine*

P-H *: 5-(4-Carboxyphenyl)-10,15,20-tris(N-methylpyridinium-4-yl)porphyrin tri-iodide.*

P-Me *: 5-(4-Methoxycarbonylphenyl)-10,15,20-tris(N-methylpyridinium-4-yl)porphyrin tri-iodide.*

P-DDC *: 5-[4-(N,N'-Dicyclohexylureidooxycarbonyl)phenyl]-10,15,20-tris(Nmethylpyridinium-4-yl)por-phyrin tri-iodide.*

P-OGal *: 5-[4-(1,2:3,4-Di-O-isopropylidene-R-D-galactopyranosyl-6-oxycarbonyl)phenyl]-10,15,20-tris (N-methylpyridinium-4-yl)porphyrin tri-iodide.*

P-Gal *: 5-[4-(R/_-D-Galactopyranosyl-6-oxycarbonyl)phenyl]-10,15,20-tris(Nmethylpyridinium-4-yl)por-phyrin tri-iodide.*

P-$(Lys)_n$ *: Porphyrin-poly-S-lysine conjugate.*

Les dérivés tri-cationiques porphyriniques sont des dérivés prometteurs. Ils peuvent interagir avec les cellules de la peau chargées négativement après la rupture de la barrière du stratum corneum. Il est intéressant de noter que les cellules cancéreuses peuvent porter une charge négative en raison de la surexpression de molécules anioniques telles les mucines O-glycosylées. Leurs propriétés hydrophiles semblent être une alternative intéressante au Photofrin® liposoluble et à l'ALA ou au MAL, pro-médicaments utilisés aujourd'hui dans la pratique clinique. La conjugaison à des acides aminés, des peptides et des sucres à des photosensibilisateurs peut favoriser un ciblage spécifique dans la mesure où ces groupes jouent un rôle clé dans la reconnaissance et le métabolisme de micro-organismes et de cellules pathologiques. Enfin, les conjugués porphyriniques tri-cationiques sont des molécules amphiphiles en raison des charges positives sur les trois groupes pyridinium et de la substitution par un groupe sans charge et plus hydrophobe sur le quatrième groupe carboxyphenyl. En règle générale les photosensibilisateurs amphiphiles sont censés être photodynamiquement plus actifs car pouvant se localiser aux interfaces hydrophobes-hydrophiles dans les membranes et à la surface des protéines. Le caractère amphiphile est également important car il permet de limiter l'agrégation et, par conséquent, de limiter la perte des propriétés photosensibilisantes de la molécule.

OBJECTIFS

L'objectif de cet travail est donc de détailler les caractéristiques photobiologiques de ces nouvelles substances.

Tout d'abord, les propriétés photophysiques et photochimiques des cinq conjugués porphyriniques tri-cationiques seront comparées à celle de la molécule mère. L'influence des substituants sur les propriétés des états excités singulet et triplet sera étudiée dans différents milieux (tampon aqueux, éthanol, et micelles neutres ou chargées négativement) compte tenu de la sensibilité de ces paramètres au microenvironnement;

La deuxième partie concerne l'évaluation des cinétiques d'absorption cellulaire, la localisation subcellulaire, ainsi que l'étude des mécanismes de la photocytotoxicité des nouveaux dériviés porphyriniques chez une lignée de kératinocytes humains cutanés hyperprolifèrants (NCTC-2544). Une telle étude permet de comparer les différents effets biologiques des molécules appartenant à la même classe de composés chimiques, mais dotées de propriétés physiques différentes. La justification d'une telle étude est que les différents substituants de la porphyrine tri-cationique sont susceptibles d'affecter leur pénétration cellulaire et le mode de distribution intracellulaire. En conséquence, une relation structure-activité photocytotoxique pourrait être établie. En outre, cette approche est préalable à une étude plus approfondie du mécanisme d'action et de la forme dominante de

la mort cellulaire. L'élucidation des voies de signalisation conduisant à ces réponses est importante, car elle fournit des indices pour mieux comprendre comment la PDT fonctionne aux niveaux cellulaire et moléculaire. Par ailleurs, il y a peu d'études concernant la participation des MAPK dans le stress induit par la PDT, notamment concernant des porphyrines cationiques. Nous examinerons donc le rôle de l'expression des MAPK au cours de la mort cellulaire induite par la PDT dans la lignée de kératinocytes NCTC 2544.

PRINCIPAUX RESULTATS ET DISCUSSION

APPROCHE PHYSICO-CHIMIQUE ET PHOTOPHYSIQUE

Spectres d'absorption et coefficients d'extinction molaires

Selon les conditions de solvant (tampon, PBS, éthanol, TX100, SDD), les spectres d'absorption de tous les dérivés présentent les caractéristiques des spectres d'absorption des porphyrines avec une bande de Soret (forte bande d'absorbance proche- UV) à ~ 420 nm et 4 maxima de moindre absorbance vers ~ 520, 550 et 630 - 650 nm. Ces différents solvants ont été utilisés pour simuler les différents milieux biologiques. Aucune différence majeure n'est observée pour ces différents environnements. Peu de différences sont observées dans leurs propriétés d'absorption suggérant que tous sont potentiellement intéressants en termes de capacité d'absorber la lumière. Par rapport à la PPIX actuellement utilisée en dermatologie oncologique, les propriétés d'absorption de ces photosensibilisateurs dans la fenêtre thérapeutique au-delà de 650 nm, où la pénétration de lumière est plus élevée, sont plus favorables.

Spectres et rendements quantiques de fluorescence

Dans un même solvant, tous les dérivés présentent des propriétés de fluorescence semblables avec des rendements quantiques de fluorescence très voisins à l'exception de P-$(Lys)_n$ dont le rendement quantique de fluorescence est sensiblement inférieur. Les rendements quantiques de fluorescence de ces dérivés dépendent peu des conditions de solvant à l'exception des solutions micellaires de SDS où ils sont nettement plus élevés. Malgré une excellente solubilité en milieu aqueux, on observe la formation de dimères ou d'oligomères de petite taille non covalents favorisant les processus de conversion non radiative, qui se traduisent par le raccourcissement de la durée de vie de fluorescence et un rendement quantique de fluorescence diminué.

L'existence d'une fluorescence est particulièrement intéressante dans le contexte de ce travail parce que la sensibilité des mesures de fluorescence permettra : 1 / des mesures

quantitatives de la concentration des dérivés dans les systèmes cellulaires, et 2 / l'étude de leur localisation intracellulaire. En outre, dans l'éventualité d'une utilisation clinique future de de ces dérivés, la fluorescence peut être utile pour le diagnostic et la délimitation du tissu tumoral. L'utilisation de ces dérivés à des fins diagnostiques sera néanmoins rendue plus délicate en raison de rendements quantiques modestes.

Les rendements quantiques de fluorescence de ces dérivés et la durée de vie de fluorescence indiquent que des voies non-radiatives sont impliquées dans la désactivation du premier état singulet excité $^1S_1^*$ de P-R vers l'état fondamental S_0. Ces paramètres laissent également présager que la conversion "intersystème" conduisant à la formation de l'état triplet $^3S_1^*$ de P-R est susceptible de se produire.

Photolyse "laser femtoseconde"

Les expériences de photolyse par éclair laser résolue à la femtoseconds ont été effectuées au laboratoire de Radiation Laboratory de l'Université of Notre Dame (USA, Indiana). Cette technique permet d'étudier les événements photophysiques qui ont lieu avant la formation de l'état triplet, à savoir le comportement des états singulets excités ($^1S_1^*$, $^1S_2^*$, ...$^1S_n^*$). Bien qu'importants dans la compréhension des processus physico-chimiques conduisant à la population du premier état excité $^1S_1^*$ de P-R, ils ne concernent pas ceux qui caractérisent l'état triplet, l'état excité essentiel en ce qui concerne les capacités photosensibilisantes photodynamiques.

Propriétés de l'état triplet

Les propriétés physico-chimiques de l'état triplet sont étudiées par photolyse par éclair laser avec une résolution temporelle inférieure à la microseconde. La résolution temporelle des spectres d'absorption transitoires permet de mesurer sa durée de vie. Elle se situe dans un intervalle de temps allant de la dizaine à la cinquantaine de microsecondes et elle est plus longue dans le PBS que dans les autres solvants. L'état triplet de P-$(Lys)_n$ présente la plus longue durée de vie. Ceci est probablement du à la présence des chaînes latérales poly-lysine volumineuses qui peuvent entraver les processus collisionnels rapide qui favorisent le retour de l'état triplet $^3T_1^*$ vers l'état fondamental S_0. Les durées de vie relativement longues de ces états triplets laissent présumer une activité photosensibilisante photodynamique de P-R dans les milieux aqueux.

Un autre paramètre important concernant l'état triplet est son rendement quantique de formation (Φ_T). Le rendement quantique de formation de l'état triplet de P-R peut être calculé à partir des spectres d'absorption de cet état triplet, à condition de connaitre son coefficient d'extinction molaire (ε_T) et la quantité de photons présents dans l'impulsion laser. Les

coefficients d'extinction molaires sont obtenus par des méthodes classiques impliquant un transfert d'énergie de l'état triplet de P-R vers l'état fondamental du β-carotène. Parallèlement, une actinométrie du faisceau laser est réalisée en utilisant une molécule (*méso*-tétraphenylporphyne) dont le rendement quantique et le coefficient d'extinction molaire de l'état triplet sont connus. Ainsi des rendements quantiques d'état triplet élevés, de l'ordre de 0,5-0,6, sont mesurés pour P-R dans les différents solvants, à l'exception de P-$(Lys)_n$ qui présente des rendements plus modestes. Ceci suggère que les dérivés prophyriniques tri-cationiques peuvent être des photosensibilisateurs efficaces dans la plupart des environnements.

Formation d'oxygène singulet

Les données ci-dessus suggèrent que l'oxygène singulet peut être produit avec un rendement quantique élevé. La formation de l'oxygène singulet a été quantifiée par la mesure de la dégradation de l'histidine dont l'oxydation se produit uniquement via un processus photodynamique de type II. Les rendements quantiques de dégradation de l'histidine sont de l'ordre de 0,08 à l'exception de celui du dérivé P-$(Lys)_n$ plus faible (0,02) en accord avec les données concernant les états triplets. Ces rendements quantiques sont nuls en absence d'oxygène. Ils sont augmentés en présence de D_2O et fortement réduits en présence de N_3^-, ce qui confirme la formation de l'oxygène singulet. Un étalonnage avec la *méso*-tétraphenylporphyne tétrasulfonée permet de calculer des valeurs théoriques pour les rendements quantiques d'état triplet légèrement supérieures à celles obtenues par photolyse par éclair laser, mais qui confirment donc le potentiel photosensibilisant de ces dérivés porphyriniques tri-cationiques.

APPROCHE BIOLOGIQUE ET CELLULAIRE

Capture cellulaire

La capture de P-H, P-Me, P-DDC, P-Gal et P-OGal par les kératinocytes NCTC 2544 est extrêmement rapide et atteint un plateau dans l'heure qui suit le début de l'incubation. Dans le cas de P-$(Lys)_n$, environ 3 heures sont nécessaires pour atteindre ce plateau. La capture est pour tous les dérivés une fonction linéaire de la concentration d'incubation. Les cinq conjugués sont plus efficacement captés par les cellules que P-H (facteur environ x6 pour P-$(Lys)_n$, environ x5 pour P-Me, P-DDC, et P-OGal, et seulement x2 pour P-Gal). Les incubations ont également été menées dans le HBSS, c'est-à-dire sans sérum, pour déterminer si les protéines sériques peuvent jouer un rôle particulier dans le processus de capture. Nous montrons que seule la capture du dérivé P-$(Lys)_n$ est influencée par la

présence des protéines, qui interagissent vraisemblablement avec la chaine poly-lysine.

Photocytotoxicité

La photocytotoxicité des dérivés P-R a été estimée par le test de capture intracellulaire du rouge neutre. L'ordre d'efficacité relative PDT - P-OGal > P-DDC = P-Me > P-$(Lys)_n$ >> P-Gal > P-H a été établi. P-H, P-Me, P-DDC, P-Gal et P-OGal ont tous les mêmes capacités intrinsèques de production d'oxygène singulet. Il peut être établi par ailleurs que ces dérivés ont intrinsèquement les mêmes capacités d'absorption de la lumière. Ainsi si la moindre photocytotoxicité de P-H et P-Gal correspond à une moindre capture cellulaire, les différences de photocytotoxicité entre P-Me, P-DDC, P-OGal ont probablement pour origine des différences de localisation cellulaire et pour conséquences des cibles primaires différentes. En ce qui concerne P-$(Lys)_n$ sa plus faible capacité intrinsèque à produire l'oxygène singulet que P-H et P-Gal, est en partie compensée par une plus forte capacité à absorber la lumière. Par ailleurs, Il est important de noter que les dérivés les plus efficaces, P-OGal, P-DDC et P-Me, supportent favorablement la comparaison avec la PPIX endogène induite par le traitement des cellules avec l'ALA. Étant donné que les quantités de lumière absorbée par P-R et PPIX dans les cellules sont proches, P-OGal, P-DDC et P-Me sont des photosensibilisateurs aussi puissants que PPIX.

Stress photo-oxydant

La peroxydation lipidique a été choisie comme un indice global de l'intensité du stress photo-oxydant. Elle a été évaluée par la mesure de la formation des substances réactives à l'acide thiobarbiturique (TBARS). La production de TBARS augmente de façon linéaire avec le temps d'irradiation, P-OGal, P-DDC, P-Me étant les plus efficaces pour induire la peroxydation lipidique. En fait, comme pour la photocytotoxicité, la peroxydation lipidique de P-OGal, P-DDC, P-Me et P-$(Lys)_n$ est supérieure à celle de P-H et P-Gal.

Microscopie de fluorescence

Les images de fluorescence des cellules traitées avec les derivés porphyriniques tri-cationiques ont été obtenues avec un système de microscopie de fluorescence très sensible de manière à éviter des expositions lumineuses importantes et donc l'interférence avec des phénomènes de photoblanchiment et de relocalisation après photoblanchiment. Ces expériences de fluorescence intracellulaire confirment que le P-H et P-Gal sont moins absorbés par les kératinocytes NCTC 2544 que P-Me, P-DDC et P-OGal. En outre, la fluorescence de P-Me, P-DDC, P-OGal et P-$(Lys)_n$ est plus particulièrement localisée dans les endroits pouvant correspondre à des vésicules d'endocytose ou de pinocytose. A

contrario, la fluorescence des cellules traitées avec le P-H et P-Gal est plutôt diffuse suggérant une localisation cytoplasmique et dans la membrane plasmique. Il convient de noter que les mitochondries et le noyau ne sont pas des sites de localisation de P-R. Ces observations démontrent que les substituants méthoxy (P-Me), di-O-isopropylidene-α-D-galactopyranosyl (P-OGal) et *N,N´*-dicyclo-hexylureidooxycarbonyl (P-DDC) sont plus critiques que la charge électrique de la porphyrine dans le contrôle de leur capture et de leur localisation et, par conséquent, dans l'expression de leur efficacité photosensibilisante.

Mécanismes de la mort cellulaire

Après avoir décrit le rôle de la chaîne substituée sur le potentiel photocytotoxique des dérivés porphyriniques tri-cationiques, nous avons étudié les mécanismes de mort cellulaire induite par P-R et leur importance relative. Comme P-Me, P-OGal et P-DDC présentent une localisation intracellulaire similaire, P-OGal, le photosensibilisateur le plus efficace a été choisi pour cette étude.

Rôle de l'apoptose

Il a été établi par le groupe d'Oleinick que la PDT est un inducteur puissant de l'apoptose. La translocation de la phosphatidylsérine de la couche interne vers la couche externe de la membrane plasmique est un marqueur précoce de l'apoptose. L'apoptose a donc été analysée par cytométrie de flux par l'observation simultanée de l'exposition de l'annexine V et de l'incorporation de l'iodure de propidium. Aucun changement significatif du pourcentage de cellules positives à l'annexine V est observé jusqu'à 9 h après l'irradiation. Des résultats similaires ont été obtenus avec différentes concentrations et durées d'incubation de P-OGal et avec différentes doses de lumière. Un autre marqueur bien établi de l'apoptose est la fragmentation de l'ADN nucléaire en unités oligonucléosomiques. Aucune augmentation significative de la fragmentation d'ADN (dosage immuno-enzymatique) n'est observée jusqu'à 24 h après l'irradiation. En outre, aucune activité de la caspase-3, de la caspase-8 et de la caspase-9 et aucun clivage de la pro-caspase-3, de la pro-caspase-8 et de la pro-caspase-9 sont observés jusqu'à 12 h après l'irradiation. Parallèlement, aucune fuite du cytochrome c mitochondrial est observée dans les cellules photosensibilisées par P-OGal. Toutes ces données confirment l'absence d'induction de l'apoptose photosensiblisée par P-OGal dans NCTC 2544 cellules. Deux contrôles positifs (5-methoxypsoralène + UVA et camptotécine) montrent l'induction de l'apoptose dès 24 h et 9 h respectivement après le traitement. Par conséquent, nos observations sont en contraste frappant avec la plupart des articles qui attribuent à l'apoptose la mort cellulaire après thérapie photodynamique. L'absence d'apoptose est conforme à la localisation non mitochondriale du photosensibilisateur.

Rôle de l'autophagie

Bien que l'autophagie ait été initialement décrite comme une réponse de survie de la cellule, elle a également été considérée comme une voie conduisant à la mort dans de nombreuses études. Comme pour l'apoptose, nous avons utilisé plusieurs critères pour étudier le développement de l'autophagie. Premièrement, l'activité autophagique a été étudiée en utilisant un marqueur fluorescent (GFP-LC3) (protéine de fusion entre la "protéine fluorescente verte" (GFP) et la chaine légère 3 de la protéine associée aux microtubules (LC3). Le processus de protéolyse et le recrutement de membranes d'autophagosomes de LC3, marqueur de l'autophagie, a été suivie par microscopie de fluorescence. Après irradiation, on observe le développement de multiples vacuoles cytosoliques avec un marquage ponctuel de GFP-LC3. Cette augmentation caractéristique du nombre de cellules présentant cet aspect vacuolaire de la GFP-LC3 dépend du temps écoulé après l'irradiation. Un autre marqueur de l'autophagie est la dégradation de p62/SQSTM1. L'analyse par Western blot montre que p62/SQSTM1 diminue (~ 60%) après irradiation des cellules traités par P-OGal. Un contrôle négatif a été réalisé avec des cellules traitées par ALA puis irradiées. Aucun des marqueurs mentionnés ci-dessus est modifié dans des conditions conduisant à une photocytotoxicité comparable à celle induite pour P-OGal. L'induction d'une autophagie dans la mort cellulaire induite par P-OGal est d'ailleurs confirmée par un traitement des cellules avec la 3-methyladenine (3-MA), inhibiteur bien caractérisé de l'autophagie. En effet, la pré-incubation des cellules avec la 3-MA supprime, comme attendu, le marquage ponctuel de GFP-LC3 et la dégradation de p62.

L'évaluation de la contribution de l'autophagie dans la mort cellulaire a été réalisée par cytométrie en utilisant l'exposition de l'annexine V et l'incorporation de l'iodure de propidium par les cellules mortes. La mort cellulaire photoinduite est inhibée d'environ 40% après une incubation avec le 3-MA mais aucune induction d'apoptose est observée après inhibition de l'autophagie par 3-MA. Cette série d'expériences suggère que: 1) l'autophagie joue un rôle dans la mort cellulaire dans notre système, 2) l'autophagie se produit indépendamment de l'apoptose, mais en liaison avec la nécrose.

Il y a quelques articles récents sur l'induction de la mort cellulaire autophagique par thérapie photodynamique. La plupart de ces travaux ont été réalisés avec des cellules déficientes pour l'apoptose. En outre, dans plusieurs études, l'autophagie n'a été observée qu'après l'inhibition de l'activité des caspases. Il est extrêmement important de noter que nous avons utilisé un modèle de cellules compétentes pour l'apoptose dans lequel la porphyrine cationique tri-conjuguée induit une mort cellulaire principalement par autophagie en l'absence de tout inhibiteur de l'apoptose. L'incorporation de P-R dans les lysosomes ou pré-lysosomes dans les environs du réticulum endoplasmique et l'appareil de Golgi et la

localisation non-mitochondriale sont en accord avec ces événements non-apoptotiques mais leur relation avec autophagie doit être élucidée. On peut supposer que l'autophagie induite par la photosensibilisation par P-OGal est un moyen pour la cellule pour supprimer les organites endommagés par la photo-oxydation ou pour dégrader les gros agrégats de protéines réticulées qui ne peuvent pas être éliminés par le système ubiquitine-protéasome. Selon le degré de dommages cellulaires, la persistance de l'autophagie peut conduire à un effondrement du métabolisme et, finalement, à la mort cellulaire autophagique. En outre, l'autophagie peut être initiée par plusieurs molécules de signalisation dont l'expression est modulée au cours de la thérapie photodynamique en réponse au stress oxydatif. Cette modulation peut passer ce processus d'une voie de survie à une voie de mortalité.

Participation des MAP kinases dans la mort cellulaire

Les résultats obtenus suggèrent que l'autophagie est impliquée dans la mort cellulaire photoinduite par P-R. En conséquence, on peut poser la question suivante: Les photosensibilisateurs peuvent-ils activer/inactiver une voie moléculaire spécifique qui module le processus d'autophagie ? Nous avons donc testé les voies de signalisation impliquées dans le stress oxydant, en particulier celles faisant intervenir JNK et p38 (généralement associées à l'apoptose et à l'autophagie) et ERK1/2 et AKT (généralement associées à la survie et la prolifération cellulaire).

Des immunoblots ont été réalisés pour visualiser la phosphorylation de JNK, p38, ERK1/2 et AKT. On observe une rapide, mais transitoire, activation de p38 et de JNK dans les cellules photosensibilisées par P-OGal. En revanche, on note une nette diminution dans le contenu de p-ERK et p-AKT. Le rôle des MAPK est également conforté par l'action des inhibiteurs de JNK (SP600125) et de p38 (SB203580). Après confirmation de leur spécificité en exposant des cellules à un stress osmotique, le marquage membranaire par l'annexine V et l'incorporation d'iodure de propidium ont été évalués par cytométrie. Le SB203580 mais pas le SP600125, augmente la mort par photosensibilisation des cellules. En outre, aucun effet significatif sur le pourcentage de cellules positives à l'annexine V est observé après photosensibilisation par P-OGal des cellules traitées par les inhibiteurs de p38 et de JNK .

Pour mieux comprendre comment SP600125 augmente la mort par photosensibilisation des cellules, on a mesuré le nombre des spots de fluorescence de la GFP-LC3 et effectué des immunoblots de p62. Le marquage ponctuel par GFP-LC3 est augmenté dans les cellules traitées avec P-OGal et le SP600125 alors que le SP600125 n'a aucun effet sur le niveau de base de GFP-LC3. Comme attendu, le SP600125 au contraire du SB203580 augmente la dégradation de p62 après la photosensibilisation. L'ensemble de

ces résultats confirment que JNK exerce un effet régulateur négatif sur l'autophagie induite par la photosensibilisation par P-OGal.

Le rôle de JNK dans la mort cellulaire a longtemps été controversé car il présente un effet "pro-survie" ou il déclenche la mort cellulaire en fonction de l'état physiologique ou pathologique étudié. Cet effet paradoxal est en partie dû à différents modes d'activation de JNK. Apparemment, une phase transitoire au début de l'activation de JNK détermine la survie des cellules, tandis que l'activation prolongée de JNK peut induire des signaux de mort cellulaire. Nos résultats sont en accord avec la première alternative puisque nous avons observé une activation rapide et transitoire de JNK associée à un effet de régulation négative sur la mortalité des cellules et sur l'autophagie.

Il existe également des données contradictoires concernant le rôle de p38 dans l'apoptose et l'autophagie. Certaines sont en accord avec un rôle de p38 comme inhibiteur de l'autophagie alors que d'autres montrent un effet inducteur de l'autophagie. Bien que nous ayons observé une activation de p38 après photosensibilisation par P-OGal, nos données suggèrent que p38 n'est pas directement impliqué dans l'induction de la mort cellulaire dans notre système. L'activation de ERK est un événement en aval dans la voie mitogène. L'activation de la voie Ras/Raf-1/ERK1/2 est en mesure de promouvoir des réponses cellulaires opposées, "pro-survie" ou antiprolifération, telles que l'apoptose et l'autophagie. Les données disponibles indiquent que la PDT peut moduler l'activité de ERK. Nous avons trouvé une diminution de p-ERK après photosensibilisation par les conjugués P-R, jusqu'à des niveaux pratiquement indétectables après l'irradiation, malgré l'expression de niveaux de base élevés. Le rôle de ERK1/2 dans les mécanismes de mort cellulaire induite par la PDT dans notre modèle doit cependant être précisée par des études ultérieures.

L'activation de la PI3-K/AKT est une autre voie de signalisation importante connue pour inhiber l'apoptose et pour promouvoir la survie cellulaire. Les données concernant l'effet de la PDT sur la phosphorylation de AKT sont quelque peu contradictoires allant de la dé-phosphorylation et l'activation subséquente de la mort cellulaire impliquant la voie des caspases à la stimulation de la phosphorylation de AKT. Nos résultats montrent une diminution dépendante du temps de p-AKT après le traitement par la PDT avec les P-R. Il convient de noter que plusieurs études ont montré que les voies de signalisation ERK et PI3-K/AKT peuvent être aberrantes dans divers cancers humains. Comme les conjugués porphyriniques tri-cationiques inhibent ERK1/2 et PI3-K/AKT, nous pourrions proposer leur rôle potentiellement bénéfique dans le traitement du cancer.

CONCLUSIONS ET PERSPECTIVES

L'objectif de ce travail était de détailler les propriétés photobiologiques de six dérivés porphyriniques tri-cationiques dans le contexte d'une utilisation potentielle en dermatologie.

Dans la première partie du travail, nous avons mené une étude approfondie de leurs propriétés photophysiques et photochimiques mettant l'accent sur l'influence de la structure de la chaîne conjuguée sur les propriétés des états excités singulets et triplets. Cette approche nous a permis de montrer que tous possèdent des propriétés d'absorption compatibles avec une utilisation thérapeutique. En ce qui concerne leur premier état triplet excité, sa durée de vie assez longue (jusqu'à ~ 60 ms) et le rendement quantique élevé de sa formation (~ 0,5) - sauf pour le P-(Lys)n pour lequel ces valeurs sont de l'ordre de 3 à 4 fois inférieures - conduit à une production efficace d'oxygène singulet. L'analyse de ces résultats suggère que tous les composés sont potentiellement intéressants mais à un degré moindre pour le conjugué poly-lysine. A ce stade des travaux, il était clair que, à l'exception du conjugué poly-lysine, la différence éventuelle dans l'activité photocytotoxique de ces dérivés ne pouvait pas être expliquée par une plus grande efficacité photodynamique intrinsèque. D'autres facteurs peuvent être impliqués tels que la différence dans leur taux de pénétration cellulaire et leur localisation intracellulaire

La deuxième partie de notre travail a été consacrée à l'étude de l'efficacité et les mécanismes photocytotoxiques des dérivés porphyriniques tri-cationiques chez des kératinocytes cutanés humains en culture. En terme de photocytotoxicité globale nous avons pu établir l'ordre d'efficacité suivant P-OGal > P-CDD = P-Me > P-(Lys) n >> P-Gal > PH. En particulier, P-OGal, P-DDC, P-Me supportent aisément la comparaison avec PPIX, produit de façon endogène par un traitement par ALA et constituant," l'étalon-or" de la PDT topique en dermatologie. Une attention particulière a été accordée à l'évaluation des voies de mort cellulaire et les mécanismes moléculaires impliqués dans la phototocytoxicité, en utilisant P-OGal, le dérivé le plus efficace. Nous avons constaté que l'autophagie joue, avec la nécrose, un rôle majeur dans la mort cellulaire induite par la photosensibilisation photodynamique par P-OGal. Cette observation est en désaccord avec la majorité des articles qui attribuent la mort cellulaire induite par PDT à l'apoptose. En fait, l'apoptose n'a pas été observée, même après l'inhibition de l'autophagie, probablement en raison de la localisation non-mitochondriale de P-OGal. Pour faire la lumière sur les mécanismes moléculaires impliqués, nous avons étudié le rôle des MAPK dans la photocytotoxicité induite par P-OGal. Nous avons montré que JNK exerce une régulation négative de l'autophagie. Nous avons également observé une activation de p38 et une inhibition de AKT et de ERK. L'induction d'un mode spécifique de mort cellualire et l'inhibition de AKT et ERK pourraient constituer un avantage thérapeutique.

La conclusion que l'on peut tirer après l'achèvement de ce travail est que les porphyrines tri-cationiques substituées que nous avons étudiées, particulièrement P-OGal, sont des photosensibilisateurs intéressants dans le contexte d'une utilisation thérapeutique en dermatologie. Ceci n'est pas sans poser quelques nouvelles questions et ouvrir la voie à quelques perspectives de développement.

1 - Il serait intéressant de préciser et détailler le rôle de l'autophagie dans la mort cellulaire photoinduite par les dérivés porphyriniques tri-cationiques les plus efficaces. Il est d'intérêt majeur de clarifier le rôle de la modulation des MAPK dans la photocytotoxicité et dans l'autophagie associée. À cet égard, l'utilisation de la technologie "siRNA" serait très pertinente pour comprendre le rôle joué par la voie JUNK dans le mécanisme de cette mort cellulaire.

2 - Il serait également judicieux d'étendre cette étude à des lignées de cellules squameuses et de carcinomes basocellulaires.

3 - Ces dérivés porphyriniques tri-cationiques devraient également être testés *in vivo* dans des modèles murins de tumeurs cutanées permettant alors, après l'évaluation de leur toxicité aiguë, l'étude de leur pharmacocinétique, de leur sélectivité et de leur efficacité.

4 - Enfin, si les nouvelles études sur des modèles animaux sont encourageantes, des "photopatch tests" chez l'homme pourraient être exécutés en préambule à une future utilisation clinique.

Mots-clés: thérapie photodynamique; porphyrines tricationiques; fluorescence; état excité triplet; oxygène singulet; incorporation cellulaire; localisation intracellulaire; photocytotoxicité; autophagie; nécrose; MAPK.

TÍTULO: **ESTUDO DO EFEITO FOTOCITOTÓXICO DE NOVAS MOLÉCULAS DE SÍNTESE. POTENCIAIS APLICAÇÕES EM FOTOQUIMIOTERAPIA ANTITUMORAL EM DERMATOLOGIA**

INSERM ERI12, Laboratoire de Biochimie, CHU Amiens-Hôpital Nord, place Victor Pauchet, 80054 Amiens Cedex 1, France
Clínica Universitária de Dermatologia, Hospital de Santa Maria, Avenida Prof. Egas Moniz, 1649-028 Lisboa, Portugal

RESUMO

A terapêutica fotodinâmica (TFD) tópica é um dos métodos utilizados no tratamento de ceratoses actínicas, doença de Bowen e de carcinomas basocelulares superficiais. Apesar dos resultados promissores, tem reduzida eficácia no tratamento de lesões com maior espessura, pelo que o desenvolvimento de novos fotossensibilizadores mais eficazes é de actual relevância.

Estudámos as propriedades fotofísicas e fotosensibilizantes de cinco novas porfirinas tricatiónicas substituídas. Os derivados porfirínicos são moderadamente fluorescentes e têm um estado excitado tripleto de longa duração de vida associado a um elevado rendimento quântico, à excepção do conjugado com poli-*S*-lisina. Foi demonstrada a formação de oxigénio singuleto a partir do estado excitado tripleto.

O estudo da sua incorporação celular e fototoxicidade, efectuados numa linhagem de ceratinócitos humanos hiperproliferativos, mostrou que três das porfirinas tricatiónicas substituídas são superiores à protoporfirina IX induzida pelo ácido aminolevulínico (tratamento actual em TFD cutânea). Estes compostos localizam-se preferencialmente em vesículas de endocitose ou pinocitose, mas não nas mitocondrias nem nos núcleos. A estrutura química da cadeia conjugada condiciona a sua incorporação, a localização e, consequentemente, a sua fototoxicidade.

O estudo dos mecanismos de morte celular, com o derivado porfirínico mais eficaz, mostrou a ausência de fixação de anexina V, de activação das caspases 3, 8 e 9, da condensação da cromatina, sugerindo que a via apoptótica não é estimulada. A formação de vesículas LC3 positivas nas células transfectadas com GFP-LC3 e a degradação da p62 demonstraram a presença da autofagia. Esta é regulada negativamente pelo JNK.

Em conclusão, trata-se de fotossensibilizadores eficazes *in vitro* sendo, contudo, necessário estudos complementares em modelos celulares e animais.

RESUMO DETALHADO

INTRODUÇÃO

A terapêutica fotodinâmica (TFD), ou fotoquimioterapia antitumoral, é uma terapêutica antitumoral recente. A base da TFD assenta na utilização de um fotossensibilizador do tipo porfirínico. Este interage com a radiação visível passando, por diversos processos fotofísicos, ao estádio excitado tripleto. Na presença de oxigénio molecular, a transferência de energia do estádio tripleto para o oxigénio molecular conduz à formação de oxigénio singuleto, espécie reactiva de oxigénio (efeito fotodinâmico do tipo II). O oxigénio singuleto é considerado uma das principais fototoxinas responsáveis pelo efeito terapêutico. Devido à sua grande reactividade, o oxigénio singuleto lesa as principais biomoléculas celulares na sua proximidade tais como os lípidos, proteínas e ADN, levando à morte das células transformadas.

Em Dermatologia, a TFD tópica usando como pró-fámaco o ácido δ-aminolevulínico (ALA), ou o seu derivado metilado, é a mais utilizada por ser a que demonstrou maior eficácia. A TFD tópica consiste na aplicação no local a tratar de ALA (pró-fármaco) que, após captação selectiva pelas células alvo, leva à síntese endógena de protoporfirina IX, o fotossensibilizador. A TFD tópica está aprovada no tratamento de ceratoses actínicas, doença de Bowen e carcinoma basocelular superficial. Apesar dos seus resultados encorajadores, a TFD cutânea necessita de desenvolvimento para maximizar a sua eficácia e poder ser eficiente no tratamento de tumores cutâneos profundos. Uma das estratégias de investigação possíveis passa pelo desenvolvimento e estudo de novos fotossensibilizadores mais eficazes.

OBJECTIVO

Escolhemos deste modo cinco novos fotossensibilizadores do tipo porfirínico, tricatiónicos e hidrossolúveis, substituídos com as seguintes cadeias laterais: *5-(4-Metoxicarbonilfenil)* (**P-Me**), *5-[4-(N,N'-Diciclohexilureidooxicarbonil)fenil]* (**P-DDC**), *5-[4-(1,2:3,4-Di-O-isopropilidene-R-D-galactopiranosil-6-oxicarbonil)fenil]* (**P-OGal**), *5-[4-(R-D-Galactopiranosil-6-oxicarbonil)fenil]* (**P-Gal**) e poli-*S*-lisina (**P-(Lys)$_n$**).

Estas moléculas foram escolhidas porque: 1) podem ligar-se às células tumorais da pele com expressão aumentada de moléculas aniónicas, como as mucinas; 2) as suas propriedades hidrofílicas constituem alternativa aos fotossensibilizantes lipofílicos actuais; 3) a conjugação de diferentes grupos (aminoácidos, péptidos e açúcares) poderão conferir

vantagens melhorando a selectividade e captação pelas células tumorais; 4) são moléculas anfifílicas pelo que poderão exercer a sua acção fotossensibilizante na interface hidrofílica-hidrofóbica das membranas na proximidade de proteínas, fenómeno associado a maior eficácia fotossensibilizante.

O objectivo geral desta tese foi o estudo de cinco novos derivados porfirínicos tricatiónicos, em particular:

1. A caracterização das suas propriedades fotofísicas e fotossensibilizantes intrínsecas, preâmbulo indispensável a um projecto deste tipo;
2. O efeito comparativo das suas propriedades fotosensibilizantes num modelo de ceratinócitos humanos hiperproliferativos, seguido do estudo dos mecanismos moleculares implicados na morte celular.

RESULTADOS

Inicialmente, estudámos as propriedades de absorção e de fluorescência por espectroscopia convencional dos novos derivados porfirínicos tricatiónicos. O estudo dos estádios excitados singuleto dos fotossensibilizadores foi efectuado por "espectroscopia de feixe laser no regime de femtosegundos" e pela determinação do tempo de vida da fluorescência. Verificámos que as propriedades de absorção destas moléculas são compatíveis com a sua utilização terapêutica, e que as suas propriedades de fluorescência permitem a sua detecção e quantificação em células vivas. Por "espectroscopia de feixe laser no regime de nanosegundo" estudámos o estádio excitado tripleto destas substâncias que se caracteriza por uma duração de vida relativamente longa (> 50 ms) e um rendimento quântico elevado (~0,5) permitindo antever uma forte probabilidade de formação de oxigénio singuleto a nível celular. A formação de oxigénio singuleto, evidenciada de forma indirecta pela oxidação da histidina como substrato específico, é idêntica em todos os derivados porfirínicos à excepção do substituído com a cadeia poli-*S*-lisina que tem menor eficácia.

Após a caracterização das propriedades fotofísicas e fotoquímicas, estudámos as propriedades fotobiológicas dos novos derivados porfirínicos através de abordagem *ex-vivo* usando linha celular de ceratinócitos humanos hiperproliferativos (NCTC 2544). Este modelo celular foi escolhido atendendo a que a TFD tópica é usada em lesões pré-neoplásicas e neoplásicas cutâneas epiteliais, respectivamente, ceratoses actínicas e doença de Bowen. Estudámos a incorporação, a indução de "*stress*" oxidativo, a fotocitotoxicidade e a localização intracelular dos derivados porfirínicos. Demonstrámos que todos os derivados porfirínicos são fotocitotóxicos, neste modelo celular, com a seguinte ordem de eficácia relativa: P-OGal > P-DDC = P-Me > P-$(Lys)_n$ >> P-Gal > P-H. Um resultado interessante foi a

constatação de que três dos derivados porfirínicos são ligeiramente mais fotocitotóxicos que a protoporfirina IX induzida pelo tratamento das células com ácido δ-aminolevulínico, pró-fármaco utilizado actualmente na prática clínica. Observámos a correlação entre a eficácia fotocitotóxica dos derivados porfirínicos e a sua capacidade de induzir a peroxidação lipídica. Verificámos que a eficácia fotocitotóxica depende da elevada incorporação celular e da localização intracelular dos derivados porfirínicos. Os derivados porfirínicos mais eficazes localizam-se em vesículas de endocitose e pinocitose, não tendo sido evidenciado a sua presença mitocondrial ou nuclear.

A fim de esclarecer os mecanismos moleculares de morte celular, prosseguimos o estudo com o derivado porfirínico mais fotocitotóxico (P-OGal). Começámos por estudar que vias de morte celular são induzidas pela TFD com P-OGal em ceratinócitos NCTC 2544. A apoptose é habitualmente descrita como a via de morte celular predominante induzida pela maioria dos fotossensibilizadores usados em TFD. No entanto, ao contrário do habitualmente considerado, não observámos o aparecimento de marcadores de apoptose após TFD com P-OGal, nomeadamente, fixação de anexina V (citometria de fluxo), activação das caspases 3, 8, 9 (actividade enzimática e *immuno blotting*), de condensação da cromatina (técnica ELISA) e libertação de citocromo *c* mitocondrial (imunofluorescência). Podemos, deste modo, admitir que a apoptose não constitui via preferencial de morte celular induzida pelo P-OGal.

Esta observação levou-nos a estudar vias alternativas de morte celular, nomeadamente a autofagia e a necrose. Após TFD com P-OGal verificámos, por microfluorescência, a formação de vesículas LC3-positivas em células NCTC 2544 transfectadas com GFP-LC3, sugerindo a presença de autofagia na morte celular. Esta hipótese foi confirmada pela observação da degradação de p62, por técnica de *immuno blotting*. Após inibição da autofagia com 3-metiladenina observámos uma redução de aproximadamente 40% na fotocitotoxicidade total induzida pelo P-OGal. Podemos, deste modo, concluir que na morte celular induzida pelo P-OGal participam simultaneamente a autofagia e necrose. O facto de a apoptose não constituir via preferencial de morte celular poderá ser consequência da reduzida presença mitocondrial do derivado porfirínico, uma vez que uma localização lisossomial ou pré-lisossomial na proximidade do retículo endoplasmático parece favorecer os fenómenos anti-apoptóticos e pro-autofágicos.

Atendendo a que as MAPKs participam na regulação das vias de morte celular induzidas pelo *"stress"* oxidativo, decidimos estudar por *immuno blotting* a expressão de p38, JNK, ERK1/2 e AKT. Verificámos, após TFD com P-OGal, a activação transitória do p38 e JNK, associada à inibição do ERK1/2 e AKT. Demonstrámos, ainda, que o JNK exerce regulação negativa na fotocitotoxicidade. Consideramos potencialmente relevante salientar que vários

tumores têm uma expressão aberrante de ERK1/2 e AKT, pelo que a sua inibição pelos novos derivados porfirínicos poderá resultar em vantagem terapêutica futura.

CONCLUSÃO

Neste trabalho demonstrámos que as porfirinas tricatiónicas estudadas possuem propriedades fotofísicas e fotosensibilizantes intrínsecas compatíveis com a sua utilização como agentes fotoquimioterapêuticos eficazes. A abordagem celular demonstrou que a sua incorporação e localização intracelulares dependem fortemente da natureza da cadeia lateral de substituição e condicionam a eficácia fotocitotóxica. Paralelamente à necrose, a autofagia parece estar fortemente implicada. Contribuímos para a clarificação do papel das MAPKs na morte celular induzida pela TFD. Atendendo aos resultados, as nossas perspectivas futuras passam pela realização de técnicas, como o *small interfering RNA*, que permitirão detalhar o papel das MAPKs no processo de autofagia. A nossa abordagem deverá, igualmente, evoluir para o estudo destes novos derivados porfirínicos em linhas celulares de carcinoma basocelular e em modelos animais.

Palavras-chave: Terapêutica fotodinâmica; porfirina tricatiónica; fluorescência; estado tripleto; oxigénio singuleto; captação celular; localização intracelular; fotocitotoxicidade; autofagia; necrose; MAPK.

TITLE: **STUDY OF PHOTOSENSITIZING EVENTS TRIGGERED BY NEW SYNTHETIC PHOTOSENSITIZERS. POTENTIAL USE IN PHOTODYNAMIC THERAPY OF SKIN CANCERS**

INSERM ERI12, Laboratoire de Biochimie, CHU Amiens-Hôpital Nord, place Victor Pauchet, 80054 Amiens Cedex 1, France

Clínica Universitária de Dermatologia, Hospital de Santa Maria, Avenida Prof. Egas Moniz, 1649-028 Lisboa, Portugal

ABSTRACT

Topical photodynamic therapy (PDT) has been approved for treating actinic keratosis, Bowen's disease and basal cell carcinoma. Despite promising results, PDT still lacks efficacy in treating deeper lesions, and the search for new photosensitizers is of current interest.

In this work, photophysical and photosensitizing properties of new water-soluble tri-cationic porphyrin derivatives (P-R) were investigated. Except for the poly-*S*-lysine conjugate, rather fair fluorescence and long-lived excited triplet state with a high quantum yield (~0.5) have been characterized. Quantitative formation of singlet oxygen from the excited triplet has been observed.

Uptake in and photocytotoxicity toward cultured proliferating human skin keratinocytes have shown that three of them compare favourably with protoporphyrin IX induced by δ-aminolevulinic acid treatment, protocol currently used in Dermatology. They localize in endocytotic or pinocytotic vesicles but not in mitochondria or nuclei. The nature of the conjugated side chain is critical in controlling the uptake and localization of P-R and the photocytotoxic efficacy.

Molecular mechanisms of cell death have been studied using the most efficient derivative (Di-*O*-isopropylidene-α-*D*-galactopyranosyl substituted). Lack of annexin V binding, caspase activation and chromatin condensation has shown the absence of apoptosis. Photocytotoxicity correlates with the appearance of LC3 marked vesicles in GFP-LC3 transfected cells and p62 degradation, suggesting that autophagy along with necrosis, plays a major role. JNK exerts a negative regulatory effect on autophagy.

In conclusion, P-R are interesting photosensitizers which merit further studies in cellular and animal models.

Key words: Photodynamic therapy; tricationic porphyrin; fluorescence; triplet state; singlet oxygen; cellular uptake; cellular localization; photocytotoxicity; autophagy; necrosis; MAPK

ABBREVIATIONS

ABTS	2,2'-azino-di-[3-ethylbenzthiazoline sulfonate
AIF	Apoptosis inducing factor
AlPcSn	Sulfonated chloroaluminium phthalocyanine
AK	Actinic keratosis
AKT	Protein kinase 1
ALA	δ-aminolevulinic acid (Levulan®)
ALAD	ALA dehydratase
AMC	Aminomethylcoumarin
AP-1	Activator protein-1
APAF	Apoptotic peptidase activating factor 1
apo	Apoprotein
ASK1	Apoptosis signal regulating kinase 1
Atg	Gene required for autophagossome formation
ATMPn	Porphycene
ATP	Adenosine triphosphate
BAPTA	Intracellular Ca^{2+} chelator
BD	Bowen's disease
BF-200 ALA	Nanoemulsion-based ALA formulation
BOPP	Boronated protoporphyrin
BPD-MA	Benzoporphyrin derivative monoacid A (Verteporfin, Visudyne®))
cAMP	Cyclic adenosine monophosphate
CDFC	*meso*-tetrakis(pentafluorophenyl)chlorin bearing a *N*-benzylisoxazolidine ring conjugated to four β-cyclodextrins
CNV	Choroidal neovascularization
CPO	Porphycene
CTCL	Cutaneous T-cell lymphoma
Cys	Cysteine
cyt *c*	Cytochrome *c*
DMSO	Dimethylsulfoxide
DNA	Deoxyribonucleic acid
Drp1	Dynamic related protein 1
DPBS	Dulbecco's phosphate-buffered saline
EDTA	Ethylenediaminetetraacetic acid
EGFR	Epidermal growth factor receptor
EMEM	Minimum essential medium with Earle's salts
EMPD	Extramammary Paget's disease
ER	Endoplasmic reticulum
ERK	Eextracellular signal regulated kinases
FC	*meso*-tetrakis(pentafluorophenyl)chlorin bearing a *N*-benzylisoxazolidine ring

FCS	Fetal calf serum
FITC	Fluorescein isothiocyanate
GABA	Gamma aminobutyric acid
GFP	Green fluorescent protein
Grx	Glutaredoxin
Hb	Hemoglobin
HBSS	Hanks' balanced saline solution containing 20 mM Hepes
HEPES	4-(2-hydroethyl)-1-piperazineethanesulfonic acid
His	Histidine
HMGB1	High mobility group box 1
HO-1	Heme oxygenase
HpD	Hematoporphyrin derivatives
HPPH	2-[1-hexyloxyethyl]-2-devinyl pyropheophorbide-a (Photochlor®)
ICAM-1	Intracellular cell adhesion molecule-1
IκB	Class of inhibitor proteins of NF-kB
IL	Interleukin
IPL	Intense pulsed light
ISC	Intersystem crossing
KTP	Potassium–titanium–phosphate
JNK/SAPKs	c-Jun NH_2 terminal kinases/stress activated protein kinases
LC3	Microtubule-associated protein 1 light chain
LCI	Lysyl chlorin e6 imide
LCP	Zinc octyloxyethilporphyrin
LDL	Low-density lipoproteins
LEDs	Light emitting diodes
LOOH	Lipid hydroperoxides
Lu-Tex	Lutetium(III) texaphyrin
3-MA	3-methyladenine
MAL	Methyl aminolaevulinate (Metvix®)
MAPKs	Mitogen activated protein kinases
MCP	Monocationic porphyrin
MDA	Mmalondialdehyde
MLu	Motexafin lutetium
MKP-1	Mitogen-activated protein kinase phosphatase 1
m-THPC	*meta*-tetra hydroxyphenyl chlorin (Temoporfin, Foscan®)
mTOR	Mammalian target of rapamycin
NAD	Nicotinamide adenine dinucleotide
nBCC	Nodular basal cell carcinoma
NCTC 2544	Nation collection of type culture, clone 2544
NF-κB	Nuclear transcription factor κB
NO	Nitric oxide
NPe6	Mono-L-aspartyl-chlorin e6

NR	Neutral Red
PARP	Poly(ADP-ribose) polymerase
PBG	Porphobilinogen
PBGD	Porphobilinogen deaminase
PBR	Peripheral-benzodiazepine receptor
Pc-4	Silicon phthalocyanine-4
PCD	Programmed cell death
P-DDC	Cationic *meso*-tetra-porphyrins dicyclohexylureidooxy group substituted
PDT	Photodynamic therapy
P-Gal	*meso*-tetra-porphyrins α/β-D-galactopyranosyl group substituted
PI3	Inositol-1,4,5-trisphosphate
P-$(Lys)_n$	*meso*-tetra-porphyrins poly-*S*-lysine chain substituted
P-Me	*meso*-tetra-porphyrins methyl substituted
P-OGal	*meso*-tetra-porphyrins di-*O*isopropylidene-α-D-galactopyranosyl substituted
PPIX	Protoporphyrin IX
RIP1	Receptor-interacting protein 1
RNA	Ribonucleic acid
ROS	Reactive oxygen species
sBCC	Superficial basal cell carcinoma
SDS	Sodium dodecyl sulfate
SDS-PAGE	SDS polyacrylamide gel electrophoresis
SnET2	Tin ethyl etiopurpurin (Purlytin®)
SnOPA	Tin octaethylpurpurin amidine
SCC	Squamous cell carcinoma
TBARS	Thiobarbituric Acid Reactive Substances
TCA	Tricholoacetic acid
TNF	Tumor necrosis factor
TPP	*meso*-tetraphenylporphyrin
TPPS	*meso*-Tetrasulfonatophenylporphyrin
TRADD	TNF receptor-associatedprotein with death domain
TRAF	TNF-associated factor
TRAIL	TNF-related apoptosis-inducing ligand
Trp	Tryptophan
Trx	Thioredoxin
Tyr	Tyrosine
TX100	Neutral Triton X100
UV	Ultraviolet radiation
VCAM-1	Vascular cell adhesion molecule- 1
VIN	Vulval intraepithelial neoplasia
XRCC1	DNA repair protein

CONTENTS

CHAPTER 1

GENERAL INTRODUCTION

1.1 OBJECTIVES OF THE WORK IN THE VIEW OF THE ROLE AND LIMITATIONS OF PHOTODYNAMIC THERAPY

Photodynamic therapy (PDT) uses the combination of a photosensitising drug and light to cause selective damage in the target tissue. The local rather than systemic nature of the photodynamic therapy effect should be highlighted because it contributes to both the limitations and the opportunities for PDT as a successful treatment of cancer. A limitation of PDT is that it cannot cure advanced disseminated tumors because irradiation of the whole body with appropriate doses is not possible. Nevertheless, PDT can be a valuable selective and curative therapy with many potential advantages over available alternatives in early or localized diseases, either neoplasms or certain infectious disorders. For some advanced cancers, PDT can improve quality of life and may lengthen survival.

In dermatology, intravenous administration of Photofrin® - the first PDT drug approved by the FDA in 1993 - was shown to be effective in treatment of several cutaneous lesions but systemic administration of this drug was shown to be unjustified for large-scale treatment of localized pathologies. Furthermore, the complex and variable mixture of more than 60 compounds with different properties and activity which constitutes Photofrin® added to the long-lasting cutaneous photosensitivity due to its low selectivity for tumour tissues; and its slow elimination rate from the body have limited its use in dermatological practice. Photodynamic therapy using topical applications of either δ-aminolevulinic acid (ALA) or its methyl ester (MAL) pro-drugs has partially resolved these problems as it is simple and convenient. It permits topical pro-drug delivery and thus is not associated with substantial systemic toxic effects, namely, long-lasting cutaneous photosensitivity. Although approved for the treatment of non-melanoma skin cancer, such as Bowen's disease (BD) and superficial basal cell carcinoma (sBCC), as well as for pre-neoplasic skin lesions, such as actinic keratosis (AK), ALA and MAL still present several clinical limitations. They have limited skin penetration and, as Photofrin®, have low absorbance coefficients in the red region corresponding to the optical therapeutic window irradiation (see Section 1.7). Moreover, ALA and MAL are rather insoluble in water.

Owing to the disadvantages presented by the photosensitizers presently used, many new compounds - the so-called second generation photosensitizers - have been synthesized. As detailed in Section 2.1, research in this area is aimed at the development of photosensitizing drugs that are chemically pure, that absorb more strongly at longer wavelengths and that have improved biological properties. The second-generation photosensitizers present

stronger absorption coefficients at longer wavelengths than for protoporphyrin IX (PPIX) and thus, a PDT treatment with any of these compounds would require lower doses of drug and light for efficacy. Phthalocyanines were first thought to represent a better option than porphyrins for improving topical PDT because of their superior absorbance in the 700 nm region (molar absorptivity: ~2×10^5 $M^{-1}cm^{-1}$). However, they are not currently used in the PDT of epidermal skin lesions as they tend to form aggregates with reduce skin uptake and photosensitizing properties. Furthermore, the phthalocyanine ring resists biodegradation which may determine long-lasting cutaneous photosensitivity. In fact, none of the previously referred systemically administered photosensitizers have been specially developed for topical application to treat skin lesions. Finally, achievement of effective PDT through the injection of photosensitizers directly into the lesion has been unsuccessful.

To summarize, the main current efforts in relation to skin PDT are related to: 1) the development of new photosensitizers with better (photo)biological activity, 2) the improvement of the selectivity of the treatment thus minimizing its side-effects, 3) an easy formulation especially in view of large scale use on an out-patient basis in dermatological practice.

A strategy that can be used to overcome these challenges is to design new photosensitizers with different structures, electric charges and hydrophobicity. These factors will determine how photosensitizers interact with themselves and with their surroundings, how they are accumulated by cells, to which sites, which molecular pathways they modulate and the type of programmed cell death they induce. Structure-activity relationship studies must thus be performed to identify and quantify the contribution of the physicochemical characteristics that may affect the biological activity of the compounds.

Our group has focused his interest on tri-cationic porphyrin derivatives. Effective photosensitizers have been synthesized whose water solubility and biological activity have been improved by conjugating cationic *meso*-tetra-substituted porphyrins to a methyl (P-Me), a dicyclohexylureidooxy group (P-DDC), a di-*O*isopropylidene-α-D-galactopyranosyl group (P-OGal), a α/β-D-galactopyranosyl group (P-Gal) or a poly-*S*-lysine chain (P-$(Lys)_n$) side chains (Figure 1.1).

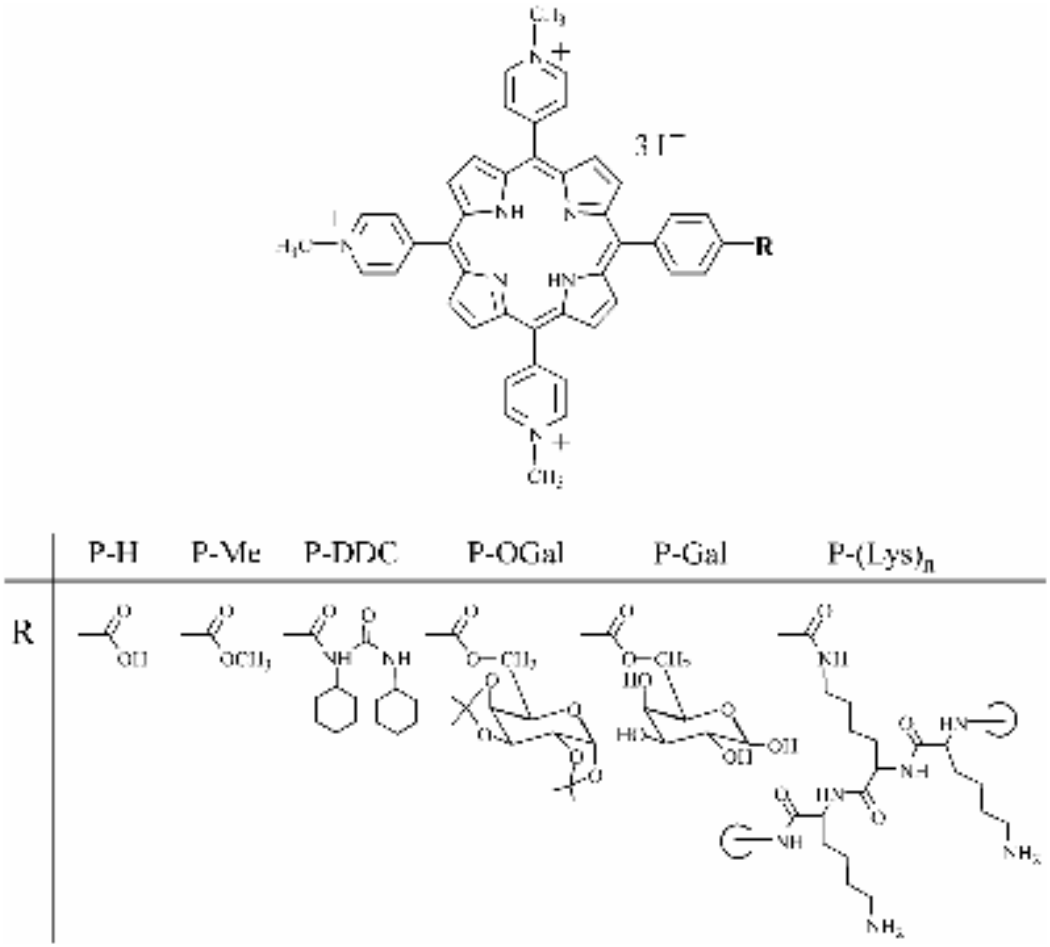

Figure 1.1 *Names and chemical structures of 5-(4-carboxyphenyl)-10,15,20-tris(N-methylpyridinium-4-yl)porphyrin derivatives under study.* ***P-H****: 5-(4-Carboxyphenyl)-10,15,20-tris(N-methylpyridinium-4-yl)porphyrin Tri-iodide.* ***P-Me****: 5-(4-Methoxycarbonylphenyl)-10,15,20-tris(N-methylpyridinium-4-yl)porphyrin Tri-iodide.* ***P-DDC****: 5-[4-(N,N'-Dicyclohexylureidooxycarbonyl)phenyl]-10,15,20-tris(Nmethylpyridinium-4-yl)porphyrin Tri-iodide.* ***P-OGal****: 5-[4-(1,2:3,4-Di-O-isopropylidene-R-D-galactopyranosyl-6-oxycarbonyl)phenyl]-10,15,20-tris(N-methylpyridinium-4-yl)porphyrin Tri-iodide.* ***P-Gal****: 5-[4-(R/_-D-Galactopyranosyl-6-oxycarbonyl)phenyl]-10,15,20-tris(Nmethylpyridinium-4-yl)porphyrin Tri-iodide.* ***P-(Lys)$_n$****: Porphyrin-poly-S-lysine conjugate.*

Tri-cationic porphyrin derivatives are promising molecules. (1) They may bind to negatively charged skin cells after the disruption of the *stratum corneum* barrier. It is of note that cancer cells may carry a net negative charge due to over-expression of anionic molecules such as O-glycosylated mucins. (2) Their hydrophilic properties appear to be a valuable alternative to the liposoluble Photofrin® and ALA/MAL pro-drugs used nowadays in the clinical practice. (3) The conjugation of amino-acids, peptides and sugars to photosensitizers further favors specific targeting as such groups play key roles in the recognition and metabolism of microorganisms and pathological cells. Finally, (4) the tricationic porphyrin conjugates are

amphiphilic photosensitizers due to their positive charges and their side chain conjugated to the hydrophobic porphyrin ring. Amphiphilic photosensitizers are thought to be more photodynamically active as they can localize to the hydrophobic-hydrophylic interfaces in membranes and at the surface of proteins. Amphiphilicity is also important because it can limit aggregation and, consequently, improve the photosensitizing properties of the molecule.

As a consequence, the main goal of this thesis is to elucidate the photobiological/biochemical characteristics of new photoactive substances - namely: tri-cationic porphyrin conjugates – which make them suitable for therapeutic applications in dermatology.

To this end, specific topics will be developed as follows:

Chapter 2- State of the art and bibliographic synthesis

Chapter 3- Experimental methods

Chapter 4- As a pre-requisite for the analysis of their photobiological activity, the fourth chapter presents the physico-chemical properties of the tri-cationic conjugates and a thorough study of their photophysics with emphasis on the influence of the conjugation on their excited state properties

Chapter 5- The fifth chapter deals with the photocytotoxicity effectiveness of tri-cationic porphyrin derivatives in cultured proliferating human skin keratinocytes. Photosensitizers photodynamic activity are determined as a function of their physicochemical characteristics, cellular uptake kinetics and photosensitizer intracellular localization. Finally, attention is paid to the assessment of cell death pathways and molecular mechanisms involved in the photocytotoxicity induced by tri-cationic porphyrin derivatives, the induction of a specific death mode might be susceptible to result in a therapeutic advantage

Chapter 6- General Conclusions and Perspectives

CHAPTER 2

STATE OF THE ART AND BIBLIOGRAPHIC SYNTHESIS

2.1 PHOTODYNAMIC THERAPY: AN OUTLINE

After a short historical overview, I will detail in this first part of the introduction the following topics:

- Historical overview
- Basic principles of photodynamic therapy
- Photosensitizers
- Photodegradation and photomodification
- Subcellular localization and relocalization
- Basis for tumor selectivity
- Principles of light interaction with tissue and light sources used for PDT

2.1.1 HISTORICAL OVERVIEW

Light has been used in the treatment of various diseases from antiquity. Ancient Egyptian, Indian and Chinese cultures (3000 BC-1500 BC) used the beneficial effect of the sun to treat a variety of diseases including vitiligo, psoriasis and even psychosis [1]. The ancient Greeks used whole-body sun exposure or heliotherapy in the treatment of different diseases. Around 500 BC, the famous Greek physician, Herodotus, the father of heliotherapy, introduced the importance of sun exposure for the restoration of health [1]. However, only rather recently has the therapeutic effect of sunlight been used to a significant degree in medicine, when ancient habits like lying nude in the sun became a popular pastime (Figure 2.1).

Figure 2.1 *Children take sun at a sanatorium in the Swiss Alps, the region in which heliotherapy originated [2].*

The Danish physician Niels Finsen further developed phototherapy and was awarded a Nobel Prize in 1903 for his work on the bactericidal effects of phototherapy after having successfully treated smallpox using red light (in 1893) and lupus vulgaris, a cutaneous

tuberculosis, with ultraviolet light generated by an arc lamp (in 1895) [3]. Phototherapy uses light in the treatment of disease while photochemotherapy involves the administration of a chemical agent followed by the exposure to light of tissues in which the agent is localized [4]. The concept of cell death being induced by the interaction of light and chemicals has been recognized for 100 years. The therapeutic use of photochemotherapy, as we know it, begins in 1900 when Raab reported that the combination of acridine orange and light can destroy living organisms. Raab, a medical student working for von Tappeiner in Munich, described the lethal effect of combining acridine red and light on Infusoria, a species of paramecium responsible for a type of malaria [5]. In a series of successive experiments he established that this lethal effect on the paramecium occurred to a greater extent with acridine plus light than with acridine alone, light alone or acridine exposed to light and then added to the paramecium. Raab, therefore, concluded that it was not the light but rather "some product of the fluorescence" that induced *in vitro* toxicity. He postulated that this effect was caused by the transfer of energy from light to the chemical, similar to that seen in plants after the absorption of light by chlorophyl. In 1903, using eosin and sunlight in the treatment of a number of human skin conditions, Jesionek and Tappeiner demonstrated the basic principle of phototherapy [6]. In order to distinguish these phenomena from the sensitization of photographic plates by dyes, the term *Photodynamische Wirkung* (photodynamic effect) was coined for the oxygen-requiring photosensitized reactions in biological systems. Von Tappeiner also predicted the potential future application of "fluorescent substances" in medicine [6-8].

At the same time as Raab's discovery, Prime, a French neurologist, reported photosensitive reactions in sun-exposed areas, in a patient who had been given parenteral eosin for the treatment of epilepsy [9]. In 1908, Haussmann introduced a new concept in photochemotherapy by using hematoporphyrin prepared from bovine blood and the related tetrapyrrole derivative, chlorophyll, in photodynamic therapy of cultured cell and mice [10]. The first report of endogenous porphyrin photosensitisation was given in 1913 by Meyer-Betz [11]. After injecting himself 200mg of hematoporphyrin, Meyer-Betz noted severe pain and swelling of that part of the body exposed to light, showing a massive phototoxic reaction. His pictures are shown in figure 2.2 before and after treatment.

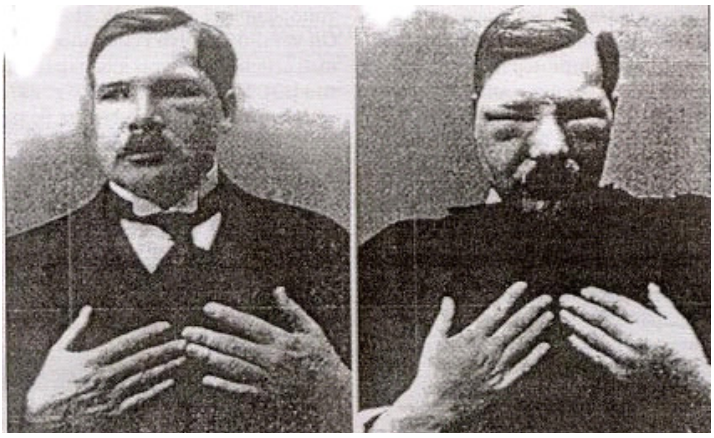

Figure 2.2 *First report of exogenous porphyrin photosensitisation. In 1913, after injecting himself 200mg of HpD, Meyer-Betz noted severe pain and swelling of the part of his body exposed to light, showing a massive phototoxic reaction. This illustration shows the pictures of him before and after treatment [11].*

The first report of fluorescent porphyrin localization in a malignant tumour appeared in 1924 when a Frenchman from Lyon, Policard, observed the characteristic red fluorescence of hematoporphyrin in an experimental rat sarcoma illuminated with ultraviolet light from a Wood's lamp [12]. Since then, porphyrins and hematoporphyrin derivatives (HpD) have been studied and used for diagnosis.

In the 40's, the term photodynamic therapy was introduced by Blum, according to the original definition by Von Tappeiner, as a photosensitized reaction in the presence of oxygen [13]. Latter in the 50's Ronchese activated endogenous fluorescent molecules in tumor tissue to delineate its boundaries [14]. At the same time, Figge *et al.* [15] and Rasmussen-Taxdal *et al.* [16] administered natural porphyrins to patients and tumor-bearing animals in an attempt to more accurately detect tumor tissue by fluorescence. Winkelman used synthetic porphyrins (tetraphenylporphyrins) to detect tumor tissue [17-19]. However, the photodynamic therapy field was silent until the collaboration of Richard Lipson and Samuel Schwartz in the 1960's. Schwartz had isolated a tumor localizing impurity from hematoporphyrin preparations that was later named hematoporphyrin derivative. Lipson was investigating how to detect tumor tissue by observing the intratumoral fluorescence of hematoporphyrin. Unable to obtain reproducible results with hematoporphyrin, Lipson used Schwartz's HpD as a tumor detection agent and found that it could be used as a photosensitizer to destroy tumor tissue [20].

In the 1970's, Dougherty rediscovered that fluorescein diacetate could photodynamically destroy TA-3 cells *in vitro* [21]. Dougherty then began treating tumor-bearing animals with fluorescein and found that it could work as a photosensitizer [22]. Following this observation, Weishaupt *et al.* identified the cytotoxic product of the photochemical reaction to be singlet

oxygen [23]. However, fluorescein has a low singlet oxygen quantum yield and a long wavelength absorption in the green portion of the electromagnetic spectrum that does not penetrate deeply into skin. Porphyrins were then examined as photosensitizers because they are efficient singlet oxygen producers and have absorbance maxima in the red portion of the electromagnetic spectrum. Schwartz's HpD was then re-discovered since it has been proved to have a high singlet oxygen quantum yield, an absorbance maximum in the red, and is selectively retained in tumor tissue [21]. After several years a purified version named Photofrin, was produced. In the following years Photofrin was approved for use in the United States against early- and late-stage lung cancers and esophageal cancers and dysplasias with other indications pending [21].

As I will show later, photodynamic therapy has been increasingly adopted over the last few decades and many new photosensitizers and light delivery systems have been developed (this will be fully detailed in Section 2.1.3 and Section 2.1.8, respectively). By now, PDT with various photosensitizers has been clinically applied and approved for the treatment of several malignant and non-malignant diseases (Table 2.1).

Generic name	Chemical name	Approval	(Potential) Indications
Benzvix	Benzyl δ-aminolevulinic acid	No [a]	Gastrointestinal tumors
BOPP	Boronated protoporphyrin	No [a]	Brain tumors
Hexvix	Hexyl δ-aminolevulinic acid	Yes [b]	Bladder cancer
Levulan	δ-Aminolevulinic acid	Yes [c]	Actinic keratosis, Bowen's disease, Basal cell carcinoma
		No [a]	Head and neck tumors, gynecological tumors
Lu-Tex	Lutetium texaphyrin	No [a]	Cervical cancers, prostate cancer, brain tumors
Metvix	Methyl δ-aminolevulinic acid	Yes [d]	Actinic keratosis, Bowen's disease, Basal cell carcinoma
Pc-4	Phthalocyanine-4	No [a]	Cutaneous/subcutaneous lesions of diverse solid tumor origins
Photochlor	2-(1-Hexyloxyethyl)-2-devinyl pyropheo-phorbide-alpha	No [a]	Basal cell carcinoma
Photofrin	Porfimer sodium Hematoporphyrin derivative, polyhematoporphyrin	Yes [e]	Barrett's high-grade dysplasia
		Yes [f]	Cervical dysplasia and cervical cancers
		Yes [g]	Endobroncheal cancer
		Yes [h]	Esophageal cancer
		Yes [f]	Gastric cancer
		Yes [i]	Papillary bladder cancer
		No [a]	Cholangiocarcinoma, brain tumors
Photosense	Aluminum phthalocyanine	Yes [j]	Head and neck cancer
Foscan	Temoporfin Meso-tetrahydroxy-phenyl chlorine	Yes [k]	Palliative therapy of head and neck cancer
		No [a]	Prostate cancer, pancreas cancer, cholangiocarcinoma
SnET2	Tin ethyl etiopurpurin	No [a]	Breast cancer, Kaposi sarcoma, prostate cancer
Visudyne	Verteporfin Benzoporphyrin derivative monoacid ring A	Yes [e]	Age-related macular degeneration
		No [a]	Basal cell carcinoma

Table 2.1 *Overview of photosensitizing agents currently used in clinical application ([a] Not yet approved; [b] European Union (EU); [c] EU, USA; [d] EU, Australia; [e] Canada, EU, UK, USA; [f] Japan; [g] Canada, Denmark, Finland, France, Germany, Ireland, Japan, The Netherlands, UK, USA; [h] Canada, Denmark, Finland, France, Ireland, Japan, The Netherlands, UK, USA; [i] Canada; [j] Russia; [k] EU, Iceland, Norway)*

While PDT has focused on cancer since 1975, it has become clear within the past decade that PDT may also be of interest for the treatment of gram-positive and gram-negative microbial infections (since it overcomes the problem of (multi-) drug resistance of bacteria) and could be useful in the management of viral, fungal and parasitic diseases.

2.1.2 BASIC PRINCIPLES OF PHOTODYNAMIC THERAPY

Phototherapy can be defined as the use of light alone for therapeutic purposes (eg. ultraviolet B irradiation for the treatment of vitiligo) while photochemotherapy involves the therapeutic use of light in combination with a chromophoric chemical, a chromophore called a photosensitizer. The photosensitizer triggers the photochemotherapeutic reaction (eg. ultraviolet A irradiation in combination with 8-methoxypsoralen for the treatment of psoriasis and cutaneous T cell lymphoma). As defined by Blum (see Section “Historical overview”) photodynamic therapy is a modality of photochemotherapy in which the photosensitized reaction requires the presence of oxygen, as will be fully detailed below.

Photodynamic therapy is, nowadays, a medical technology that has been developed for the removal of harmful or unwanted cells, mainly to treat cancer [24]. It consists of the systemic or topical application of a drug (a dye or a dye precursor), called a photosensitizer (P), that localizes more or less selectively in the target tissue at nontoxic concentrations. The principle is based on the capacity of these substances to be excited by light and to restitute energy in a chemical form by transferring excess energy to molecular oxygen. The latter is transformed into an activated species called “singlet oxygen” ($^1O_2$) as will be detailed below [25-26].

A photosensitizer molecule (P) in its ground state ($^1P_0$) is characterized by paired electrons with a total spin of S=0 and a spin multiplicity of 1 thus called the singlet state. Illuminating the chromophore with light brings it to an excited singlet state in which one electron of the occupied orbital of highest energy of the ground state is brought to a previously unoccupied orbital of higher energy. Depending on the energy of the excitation wavelength, the photosensitizer undergoes a transition to an excited singlet state $^1P_1^*$, $^1P_2^*$,.... or $^1P_n^*$ (in the order of increased energetic states). The shorter the wavelength, the higher the energy and consequently the higher is the excited singlet state. Then the molecules in the upper singlet states ($^1P_n^*$, n≥2) are rapidly deactivated (within less than a picoseconds) into the $^1P_1^*$ state. In their first excited singlet state ($^1P_1^*$) most molecules return to the ground state by losing their excess energy to the environment as heat (so-called internal conversion followed by vibrational relaxation). Another deactivation path from $^1P_1^*$ consists in the emission of a fluorescence (radiative process). As a result, the shape of the fluorescence emission spectrum is not dependent on the excitation wavelength. Furthermore, the emitted quanta have lower energies and higher wavelengths than those used for excitation of the molecule

[27-28]. It is important to note that most molecules undergo a return process via the internal conversion followed by vibrational relaxation. As a consequence, their singlet states $^1P_1^*$ have a very short life and the molecules exhibit neither fluorescence nor photosensitizing properties. The fluorescence pathway is thus favored by the relative inefficiency of internal conversion and vibrational relaxation which is associated with a longer lifetime of $^1P_1^*$ in the nanosecond range. Beside internal conversion/vibrational relaxation or fluorescence emission, the excited singlet state ($^1P_n^*$) can also cross to an isoenergetic level of the triplet state, most generally the first excited triplet state ($^3P_1^*$), where two electrons are unpaired and have the same spin. This non-radiative process is called intersystem crossing (ISC). Most PDT photosensitizers have high quantum efficiency for this transition. Then, the return to the ground state from the first excited triplet state $^3P_1^*$ can occur via phosphorescence (radiative process) or via intersystem conversion to $^1P_1^*$ followed by vibrational relaxation. Because these processes are thermodynamically unfavorable, they are therefore relatively slow. As a result, triplet states are generally characterized by a relatively long lifetime (up to seconds). From $^1P_1^*$ or $^3P_1^*$, whose lifetime is long enough, photochemical reactions with the environment may occur confering photosensitizing properties to the molecules. Because of the longer lifetime of the triplet excited state (compared to that of singlet excited states) most photosensitizing processes occur via the triplet state. This sequence of reactions can be summarized by the simplified "Jablonski diagram" (Figure 2.3).

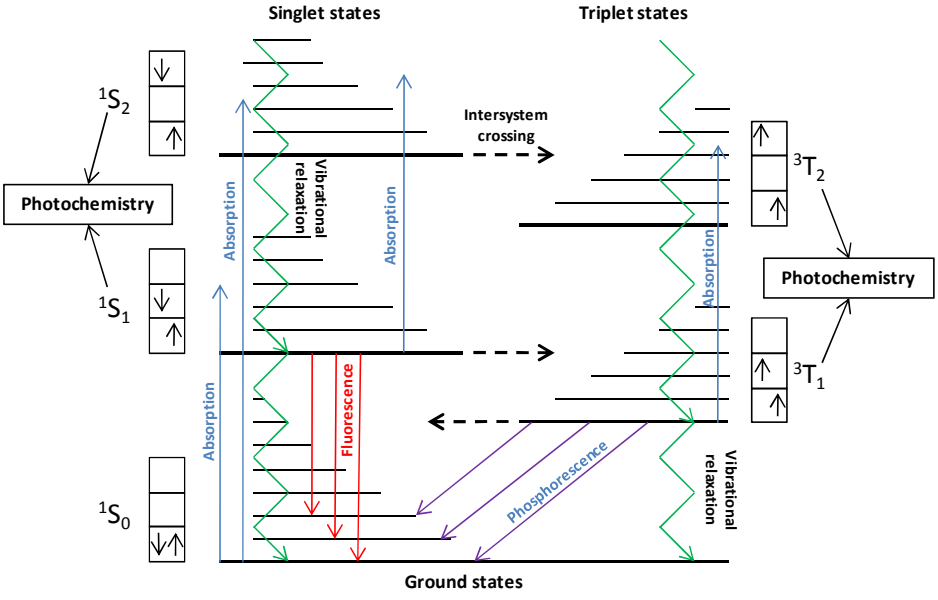

Figure 2.3 *Simplified Jablonski diagram showing porphyrin (singlet and triplet states) [adapted from Kohen et al., 2002 [29]]*

An overview of photophysical processes in photosensitizer molecules is also given in Table 2.2.

Process	Reaction	Timescale [s]	Rate (s^{-1})
Excitation	$h\upsilon + {}^1S_0 \rightarrow {}^1S_1, {}^1S_2, ..., {}^1S_n$	$\sim 10^{-15}$	
Internal conversion	${}^1S_n, ..., {}^1S_2 \rightarrow {}^1S_1$ + heat	$\sim 10^{-13} - 10^{-12}$	
Internal conversion	${}^1S_1 \rightarrow {}^1S_0$ + heat	$\sim 10^{-7}$	$k_{IC}[{}^1S_1]$
Intersystem crossing	${}^1S_1 \rightarrow {}^3T_1$ + heat	$\sim 10^{-7}$ - 10^{-6}	$k_{ISC}[{}^1S_1]$
Chemical reaction	${}^1S_1 + X \rightarrow S_0$ + reaction product or ${}^1S_1 \rightarrow S'$ (photoproduct)		$k_{R(S)}[{}^1S_1]$
Fluorescence	${}^1S_1 \rightarrow {}^1S_0 + h\upsilon_{Fluor}$	$\sim 10^{-11} - 10^{-6}$	$k_{FI}[{}^1S_1]$
Internal conversion	${}^3T_1 \rightarrow {}^1S_0$ + heat	$\sim 10^{-11} - 10^{-6}$	$K_{ICT}[{}^3T_1]$
Phosphorescence	${}^3T_1 \rightarrow {}^1S_0 + h\upsilon_{Phosp}$	$>10^{-6}$	$K_P[{}^3T1]$
Chemiluminescence X*: unstable chemical	$X^* \rightarrow {}^1S_1 \rightarrow {}^1S_0 + h\upsilon_{Chem}$	$>10^{-6}$	$k_C[A^*]$
Chemical reaction	${}^3T_1 + X \rightarrow {}^1S_0$ + reaction product or ${}^3T_1 \rightarrow S''$ (photoproduct)		$k_{R(T)}[{}^3T_1]$

Table 2.2 *General characteristics of primary photophysical/photochemical processes in aromatic molecules. (k_x rate constant, ${}^1S_n$ singlet state molecule, ${}^3T_n$ triplet state molecule, [${}^1S_n$ or ${}^3T_n$] concentration of excited molecules, X reaction substrate).*

Damage to the environment produced by ${}^3P_1{}^*$ which will not be detailed here [30]. As an example we may mention the photoaddition of psoralens to DNA. Other pathways constitute the so-called photosensitized reactions. In such processes the photosensitizer will modify the

environment without direct reaction. Most photosensitized reactions involve molecular oxygen. They are called photodynamic reactions.

The literature distinguishes two photodynamic processes depending on the intervention of molecular oxygen (more correctly called dioxygen). In its ground state, molecular oxygen (e.g. oxygen we breathe) possesses 2 unpaired electrons in isoenergetic orbitals. Thus these 2 electrons have the same spin. Consequently, the ground state of oxygen is a triplet state and its low-lying excited state is a singlet state. This makes possible an energy transfer between the first excited triplet state of the photosensitizer and the triplet ground state of oxygen. The ground state of the photosensitizer is restored while oxygen becomes excited as a singlet state, as illustrated by the following scheme:

$$^1P_0 + h\nu \rightarrow {}^1P_1^*$$
$$^1P_1^* \rightarrow {}^{ISC}\rightarrow {}^3P_1^*$$
$$^3P_1^* + {}^3O_2 \rightarrow {}^1P_0 + {}^1O_2^*$$

Scheme 2.1 Singlet oxygen generation via photosensitization (P = Porphyrin; ISC = Intersystem Crossing). Note that $^3O_2$ as well as $^1O_2$ are conventional notations since $^3O_2$ is a ground state molecule while $^1O_2^*$ is a molecule in the first excited singlet state.

The energy required for the triplet to singlet transition of oxygen is 22 kcal/mol corresponding to a photon energy of 1274 nm (infrared light). Thus, relatively low energy is needed to produce singlet oxygen.

Singlet oxygen, which is the lowest excited electronic state of oxygen, is cytotoxic. It readily reacts with electron-rich biomolecules such as unsaturated lipids, amino acids and DNA. In homogenous solutions, the $^1O_2$ lifetime varies from the µs (aqueous media) to several hundreds of µs (in some organic solvents). In cells, there is much controversy regarding the lifetime and diffusion distance of the transient oxygen species. Recent studies have shown that the intracellular lifetime of singlet oxygen is ~3 µs in a viable, metabolically active, H_2O-containing cell [31]. This lifetime is significantly longer than that previously reported [32]. The intracellular diffusion distance of singlet oxygen has been estimated to be 2–4x10^{-6} cm^2s^{-1} [33]. This short singlet oxygen lifetime and resulting limited diffusion distance makes PDT a highly selective form of cancer treatment due to the localized effect it produces. Therefore, the site of its generation is also the site of initial damage. Photosensitizing reactions of this type are known as Type-II photodynamic reactions and are characterized by their dependence on oxygen concentration [34]. This type II process is thus defined as an

interaction between the excited triplet state of the photosensitizer and oxygen. It is the primary process of the photosensitized sequence of events. Another process related to type II reaction, although generally not frequent, is a charge transfer for $^3P_1^*$ to $^3O_2$ instead of energy transfer:

$$^3P_1^* + {}^3O_2 \rightarrow P_0^{+\bullet} + O_2^{-\bullet}$$

In contrast to type II reactions, where molecular oxygen interacts directly with the photosensitizers, there exists a so-called type I process in which molecular oxygen intervenes after the reaction of the $^3P_1^*$ with the substrate (Sub). Most frequently, the initial step in this type I reaction is an electron (or hydrogen atom) transfer between $^3P_1^*$ and the ground state of the substrate:

$$^3P_1^* + Sub_0 \rightarrow P^{-\bullet} + Sub^{+\bullet}$$

Then, molecular oxygen can react with the semioxidized substrate, leading to oxidative damage. Note that during this process, the formation of superoxide anion leads to the photosensitizer regeneration:

$$P^{-\bullet} + O_2 \rightarrow P_0 + O_2^{-\bullet}$$

The superoxide radical-anion can in turn damage the biological environment.

Photosensitizers are characterized by photophysical parameters which help to understand their photobiological activities. The relevant singlet and triplet state parameters are the excited singlet and triplet transient absorbance spectra, the fluorescence quantum yield (Φ_F), the triplet-state quantum yield (Φ_T), the triplet-state energy (ΔE_T), the singlet state (τ_S) and triplet-state (τ_T) lifetimes. The Φ_F is the probability for a photosensitizer to emit fluorescence when returning to the $^1S_0$ ground state after absorption of a quantum of light. The Φ_T is the probability for a photosensitizer to convert to the $^3T_1$ state, after absorption of a quantum of light. From them, important parameters of their chemical reactivity can be deduced: the rate constant for the interaction of $^3T_1$ with oxygen ($k_{R(T)}$), the singlet oxygen quantum yield (Φ_Δ) and the S_Δ parameter. The latter measures the effectiveness of the $^3T_1 + {}^3O_2 \rightarrow {}^1O_2 + {}^1S_0$ process to generate $^1O_2$. The singlet oxygen quantum yield (Φ_Δ) is defined as the probability that a photosensitizer generates $^1O_2$ after absorption of a quantum of light. The S_Δ parameter is defined by the equation [35]:

$$\Phi_{\Delta} = S_{\Delta}\, \Phi_{T}$$

Nearly all photosensitizers employed in PDT yield high Φ_{Δ} (~0.3 to 0.8) [36].

The singlet oxygen quantum yield depends on the rate of the chemical reaction of the P triplet state and is reduced by processes such as phosphorescence, internal conversion from the triplet to the singlet ground state, or chemical reactions of the photosensitizer excited in the singlet state manifold. Finally, the energy of singlet oxygen (ΔE_{Δ}) is the energy difference between $^1O_2$ and $^3O_2$ (ΔE_{Δ} = 94 kJ mol^{-1} = 7882 cm^{-1} = 0.97 eV).

Aggregation of photosensitizers may change their photophysical properties. It shortens τ_F and τ_T and decreases Φ_{Δ} by dissipating the energy through internal conversion. Therefore highly aggregated photosensitizers are generally considered to be less effective photosensitizers than monomeric forms *in vivo* [37]. It appears that amphiphilicity contributes to aggregation modulation which in turn determines how compounds accumulate into various targets within a tumor cell. Amphiphilic molecules, that are partially hydrophobic and hydrophilic, are thought to bind most efficiently to membranes and/or proteins at the interface between the hydrophilic surface and hydrophobic interior of proteins and membranes. Several researchers have suggested that amphiphilic photosensitizers are more photodynamically active [38].

2.1.3 PHOTOSENSITIZERS

After reading this brief photophysical and photochemical review, it turns out that an ideal photosensitizer must absorb as much as light as possible, and possess a high ability to trigger photosensitized reactions, mainly by efficient intersystem conversion to its excited triplet state. An ideal photosensitizer should also be minimally toxic, taken up more quickly by abnormal (target) tissue than by normal tissue, cleared rapidly from normal tissue and activated at wavelengths that penetrate the target tissue.

This group of chemicals includes ‘first-generation’ derivatives of natural porphyrins, which became available about 30 years ago, and a broad group of new ‘second-generation’ and ‘third-generation’ synthetic compounds, which are currently under laboratory and clinical investigation.

2.1.3.1 *FIRST GENERATION PHOTOSENSITIZERS*

Porphyrins, as illustrated in Figure 2.4, are tetrapyrrole macrocycles. As a result of the extended conjugation, porphyrins are strongly colored compounds. The visible absorption spectrum shows an intense Soret band around 400 nm and weaker bands in the visible-near IR region. The longest wavelength maximum absorbance corresponds to the $^1S_0 \rightarrow {}^1S_1$ transition.

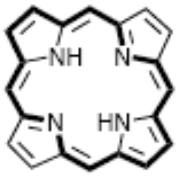

Figure 2.4 *The tetrapyrrolic porphyrin ring: note the 22 π electron system.*

Porphyrins and other closely related tetrapyrrolic pigments occur widely in nature with major roles in various biological processes. For example, heme, the iron (II) protoporphyrin-IX complex, is the prosthetic group in hemoglobins and myoglobins responsible for oxygen transport in red blood cells and oxygen storage in tissue. Heme is also essential for the structure and function of cytochromes.

In 1884, Nencki isolated the first pure porphyrin by preparing hematoporphyrin hydrochloride directly from isolated heme [39]. In 1912, Kuster first proposed the structure of porphyrins as four pyrrole units linked by four methine bridges [40]. This structure was later confirmed in 1926 when Fisher synthesized etioporphyrin-1 [41] thereby demonstrating that the aromatic structure initially proposed by Kuster was correct (Figure 2.5).

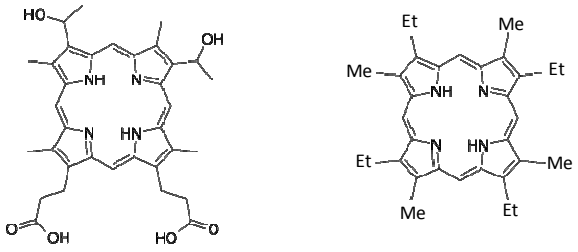

Hematoporphyrin **Etioporphyrin-1**

Figure 2.5 *Early porphyrins synthesized by Nencki and Fisher*

Haematoporphyrin (Hp) was first isolated from haemoglobin using concentrated sulfuric acid [42]. It has been shown later that treatment with sulfuric and acetic acids led to

hematoporphyrin derivative (HpD) [43] a very complex mixture of several components with about 50% identifiable as oligomeric haematoporphyrins and protoporphyrins having a low *in vivo* photosensitizing activity [44-45]. It turned out that HpD had better tumour localizing properties than crude Hp [20]. Chromatographic analysis of tumour extracts showed that it was mainly the "impurities" that were retained in the tumours. Many groups attempted to identify these impurities [46-48], and it was concluded that they were composed of dimers, oligomers and aggregates of porphyrins. Kessel *et al.* showed that diethers and diesters were central [49]. Kessel proposed that aggregates were monomerized in tumour cells and became trapped, rendering the cells photosensitive.

HpD was further chromatographically purified by Dougherty's group to Photofrin, which is still the most widely used clinical PDT photosensitizer [25, 48]. The HpD chemical purification allows for the preparation of porfimer sodium (Photofrin®). The latter is a lyophilized and concentrated form of monomeric (haematoporphyrin, protoporphyrin and monohydroxyethylvinyl- deuteroporphyrin) and oligomeric (dimer to hexamer derivatives of haematorphyrin units linked through ether or esters bonds) porphyrins. It also contains a reduced fraction of components that are not photoactive.

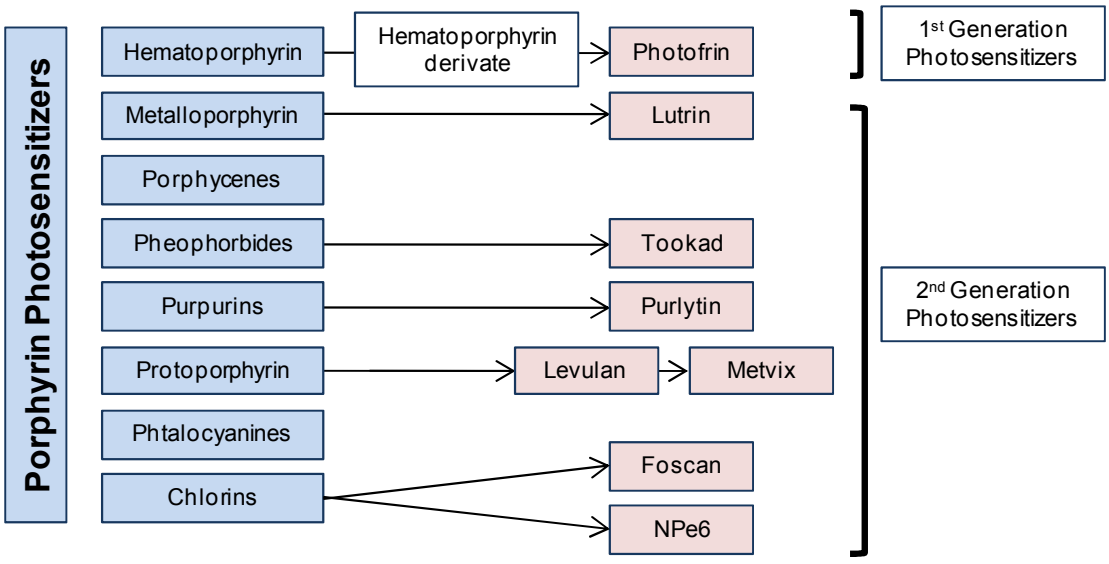

Figure 2.6 *Classification of porphyrin-based photosensitizers molecules.*

Photofrin® was approved for treatment of early stage lung cancer in 1998 and for Barrett's esophagus in 2003. The clinical applicability of Photofrin® has been limited by several factors. First, its longer wavelength light absorption peak occurs at too short wavelength (630 nm) to allow deep light penetration in tissue (about 5–10 mm in therapeutic PDT). Second, Photofrin® is a complex mixture of oligomers. Finally, administration of Photofrin® results in

cutaneous photosensitivity lasting up to 6 weeks. These limitations have inspired the development of a second generation of photosensitizers with longer-wavelength light absorption peaks (see Section 2.1.3) and more rapid clearance from skin.

2.1.3.2 *SECOND GENERATION PHOTOSENSITIZERS*

The second generation photosensitizers (phthalocyanines, naphthalocyanins, benzoporphyrins, chlorins, purpurins, texaphyrins, porphycenes, pheophorbides, bacteriochlorins, *etc.*) were introduced to overcome the problems encountered with HpD [50-55]. Various chemical modifications of the tetrapyrrolic ring of the porphyrins characterize the different groups of the 'second-generation' photosensitizers (figures 2.6 and 2.7).

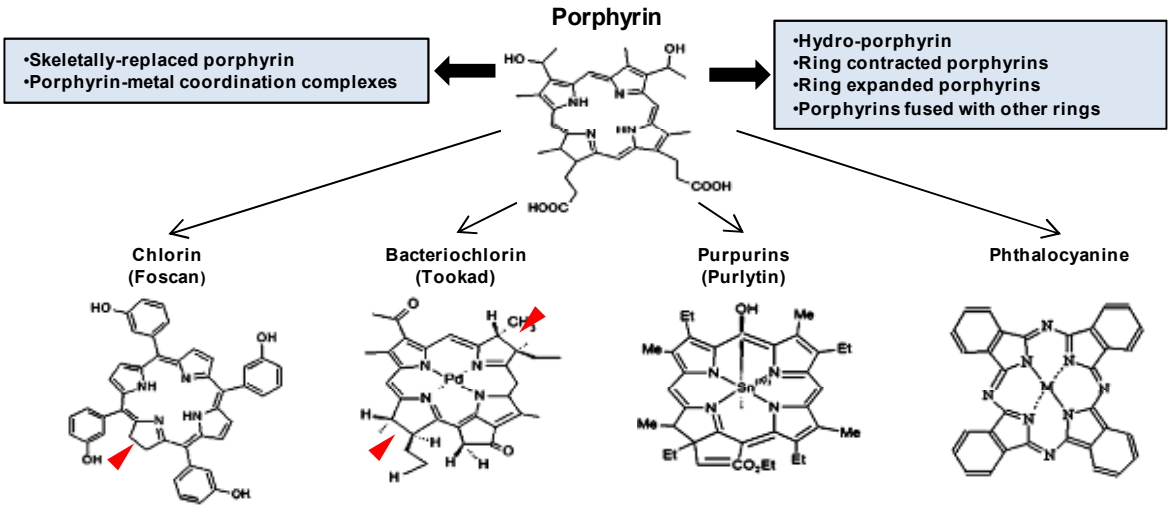

Figure 2.7 *Chemical structure of porphyrin-derived sensitizers (►- reduced).*

Unlike HpD and Photofrin®, they may be obtained as chemically pure substances. They are effective generators of singlet oxygen and have high absorbance in the far red (660–700 nm) or near infrared (700–850 nm) regions. At these wavelengths, the penetration depth into mammalian tissues is up to 20 mm, as developed in Section 2.1.8.2 "Light interaction with tissue and light sources" [42, 56]. The serum half-lives of the second-generation sensitizers are short and tissue accumulation is selective and quick (within 1–6 h after injection). In addition, the risk of burns by accidental sun exposure is low because clearance from normal tissues is rapid. Toxicity to skin and internal organs in the absence of light (so-called 'dark' toxicity) is absent or minimal.

Most sensitizers currently under investigation belong to two chemical groups: the phthalocyanines and the chlorins. The joining of four benzenes or naphthalene rings to the β-pyrrolic positions of porphyrins and the substitution of the methine-bridge carbons with nitrogen produce phthalocyanines and naphthalocyanines, respectively. Polar substituents are often linked to avoid solubility problems caused by their strong hydrophobicity [42]. The presence of aluminium, zinc(II), silicon(IV) and other ions gives hexacoordination and guarantees a satisfactory yield of singlet oxygen generation (Table 2.3) [57].

Chlorins differ from porphyrins by the hydrogenation of a double bond of one pyrrole ring (figure 2.7). They exhibit a high extinction coefficient and an absorption peak in the far red waveband [57] and a rapid, high and selective accumulation in the target tissue.

The second generation photosensitizers benzoporphyrin derivative monoacid A (BPD-MA (Verteporfin; Visudyne®, QLT Inc. and Novartis Opthalmics) and *meta*-tetra hydroxyphenyl chlorin (m-THPC; Foscan®, Biolitec AG) are approved for clinical use (Table 2.1) [58-60]. Benzoporphyrin derivative monoacid ring A is a semisynthetic porphyrin derived from protoporphyrin which is approved for the treatment of age-related macular degeneration [61]. It has poor water solubility but it can be formulated successfully, either in liposomes or emulsions [62]. In preclinical trials, it was observed that Verteporfin® preferentially targeted neovasculature. This selectivity has been exploited for the treatment of choroidal neovascularization (CNV), an abnormal growth of vessels in the retina associated with age-related macular degeneration, the leading cause of blindness in the developed world. Verteporfin® was approved in the U.S. under the tradename Visudyne® for CNV treatment in 2000.

Mesotetrahydroxyphenyl chlorin (m-THPC) (Temoporfin, Foscan®; Biolitech Pharma, Edinburgh, Scotland, UK) is another second generation photosensitizer, a pure synthetic chlorin compound, hydrophobic, which is activated by 652 nm light [63]. The major advantages of mTHPC are a short duration of skin photosensitivity (15 days), a high quantum yield for singlet oxygen, and depth of tumor necrosis of up to 10 mm in preclinical models [64]. mTHPC has been used for treatment of pleural mesothelioma [65], head-and-neck cancers [66-67], esophagus [68-69], prostate [70-71], pancreas [72], arthritic joints [73], and skin cancers [74]. It has been approved in Europe in 2001 for the PDT of head-and-neck cancers and other tumors.

Mono-L-aspartyl-chlorin e6 (NPe6, Porphyrin Products Inc., Logan, UT, USA) and chlorin e6 (Dialek Ltd, Minsk, Belarus) are hydrophilic compounds with some amphiphilicity and similar

photobiological properties [42, 75-76]. The hydrophobic Tin ethyl etiopurpurin (SnET2) (Purlytin®, Miravant Medical Technologies, CA, USA) has been proposed for dermatological indications [58-60, 77].

Several other second generation photosensitizers are currently under clinical evaluation. These include BOPP (boronated porphyrin; Pacific Pharmaceuticals Inc.), hypericin (Pharmaceuticals Inc.), HPPH (2-[1-hexyloxyethyl]-2-devinyl pyropheophorbide-a, Photochlor; Roswell Park Cancer Institute), AlPcSn (sulfonated aluminium phthalocyanine, Photosense; State Research Center), ATMPn (porphycene; Glaxo-Wellcome Inc.), lutetium(III) texaphyrin (Lu-Tex, Antrin; Pharmacyclics Inc.), motexafin lutetium (MLu), *etc*. [78-80].

Near-infrared absorbing photosensitizers may be useful for the treatment of highly pigmented tumours, such as melanoma metastases, which do not respond to treatment with photosensitizers that absorb in the visible range. Bacteriochlorins display a significant absorption around 780 nm with a high extinction coefficient (150000 $M^{-1}cm^{-1}$) and might be particularly useful for the PDT of pigmented tumours [57]. Light with wavelengths longer than 850 nm cannot be used because it does not yield enough energy to trigger a photochemical reaction.

2.1.3.3 *THIRD GENERATION PHOTOSENSITIZERS*

Second generation photosensitizers bound to carriers for improving the effectiveness of PDT, are often called “third generation photosensitizers” [50, 81]. Briefly, different approaches have been developed to improve photosensitizers targeting into tumour cells such as photoimmunotargeting (eg. monoclonal antibodies directed against specific antigens on cancer cells) and peptide mediated targeting (eg. peptides that mimick the natural ligands of receptors that are specifically overexpressed on cancer cells) [50, 81-82]. Theoretically, these approaches have several advantages: high affinity of the binding moiety to the receptor or antigen on the targeted cell surface; direct and more specific localization with increased efficiency and selectivity; and lower dose of photosensitizer.

Other strategies recently developed to improve the delivery of photosensitizers to target tissue involve lipoprotein-mediated delivery and photosensitizer encapsulation in colloidal carriers (*eg*. liposomes, oil-dispersions, biodegradable polymeric particles and hydrophilic polymers) to facilitate drug delivery [82-84].

In this context, we have synthesized a *meso*-tetrakis(pentafluorophenyl)chlorin bearing a *N*-benzylisoxazolidine ring (FC) conjugated to four β-cyclodextrins (CDFC) to further assess the potential interest of this new class of chlorins as PDT photosensitizers. We have shown a good photocytotoxic effectiveness of CDFC towards cultured human keratinocytes. The study of their excited singlet and triplet state properties by means of time resolved femto and nanosecond spectroscopies demonstrates that the presence of four β-cyclodextrin macrocycles on CDFC leads to a long-lived triplet state which is formed in a good yield in aqueous media. Microenvironmental-dependent interactions of the cyclodextrin moieties with the fluorinated chlorin ring in the singlet and triplet excited states have been observed (aqueous media, buffer, ethanol and neutral Triton X100). These results are not included in the present thesis as they are outside its major objectives. However, they have been recently published and the article is presented as Annex I.

2.1.3.4 δ-AMINOLEVULINIC ACID AND ITS DERIVATIVES

a) Heme biosynthesis pathway

The study of porphyria diseases showed that metal-free porphyrins can be endogenously produced [85-89]. Each of the porphyrias has a specific enzyme defect in the pathway of heme biosynthesis. There are 8 enzymes involved in the synthesis of heme, and, with the exception of the first one, defects of these enzymes lead to tissue accumulation and excessive excretion of porphyrins and/or their precursors, such as δ-aminolevulinic acid and porphobilinogen. In the cytoplasm, ALA is metabolized by porphobilinogen synthase, also called ALA dehydratase (ALAD), which induces the condensation of two molecules of ALA to yield porphobilinogen (PBG). The concerted action of porphobilinogen deaminase (PBGD) and uroporphyrinogen III (co)-synthase combines four molecules of PBG and cyclizes the tetrapyrrole chain catalyzing ring closure to form uroporphyrinogen III [90]. Uroporphyrinogen decarboxylase then removes four acetic acid carboxyl groups, converting them to methyl groups, to form coproporphyrinogen III. The latter is oxidized by the mitochondrial coproporphyrinogen oxidase, which decarboxylates and oxidizes the propionic side chains to vinyl groups leading to protoporphyrinogen IX. The subsequent oxidation of the tetrapyrrole ring, which adds more double bonds, is catalysed by protoporphyrinogen oxidase in the mitochondrion. It is the final step in the synthesis of PpIX [91]. Then, iron incorporation into the tetrapyrrole structure is catalysed by ferrochelatase in the inner mitochondrial membrane resulting in heme synthesis.

b) *ALA effects on porphyrin formation and mechanism of action*

Heme biosynthesis is normally so tightly regulated that the concentrations of intermediate products are below the threshold of photosensitization. In 1951 Berlin *et al.* demonstrated that excess administration of exogenous ALA bypasses the cellular feedback control mechanism leading to abnormally large quantities of PpIX in humans [92-93]. Later on, Batlle *et al.* found that addition of ALA to the culture medium of soybean callus, a vegetable tumour, led to accumulation of porphyrins associated with fluorescence during UV exposure, inhibition of growth, and, finally destruction of tissue [94]. Clinical research on erythropoietic protoporphyria revealed that PpIX was an efficient photosensitizer. Protoporphyrin IX was shown to cause skin photodamage *via* mitochondrial destruction [92, 94]. In 1987, two groups proposed to use ALA as a porphyrin precursor in PDT [95-96]. It was demonstrated that exogenous ALA-induced PpIX together with light led to inactivation of Friend erythroleukemic cells [95]. In 1990 Kennedy *et al.* reported the first clinical trials using ALA-PDT for the treatment of malignant and precancerous skin abnormalities [97]. PpIX has a high absorption peak corresponding to the Soret band at about 405 nm and other absorption maxima, the Q-bands, at approximately 510, 545, 580 and 630 nm. As detailed below, although the Q-bands are 10–20-fold smaller than the peak in the Soret band, most clinical studies have used 625–633 nm red light, which allows for a deeper penetration into the skin [42]. However, green and blue wavelengths were found to be just as effective as red light for the treatment of actinic keratosis (AK), while being less painful [98-99].

c) *ALA pharmacokinetics*

Introduction of ALA as a PpIX precursor was a milestone in the development of PDT for several reasons. It is naturally produced in the body, and shows low cytotoxicity. It is the only PDT agent that is a biochemical precursor of the photosensitizer. Endogenously produced PpIX is rapidly cleared from the body (24–48 h) because natural clearance mechanisms exist. Although ALA is usually administered topically, it can also be administered intravenously or orally. Topical delivery of ALA avoids systemic photosensitivity, because the drug can be selectively applied on the areas to be treated. Moreover it is selectively uptaken by target cells. A short time interval (1–8 h, depending on the mode of administration) is needed between the administration of ALA and the maximal accumulation of PpIX in target tissues [100-102].

d) *Methyl aminolevulinate advantages over ALA*

In 1999, ALA was approved for the treatment of actinic keratoses. However, the hydrophilic nature of ALA was thought to limit its penetration through biological membranes. In mammalian cells, it is taken up mainly by active transport mechanisms, that is the Na^+/Cl^- dependent β-amino acid transporters, including those of glycine, and gamma aminobutyric acid (GABA) [103]. These systems require energy, depend on pH and temperature, are saturable and slow, and are only slightly faster in tumour cells [104-105].

Chemical derivatization of ALA, were proposed to improve ALA delivery and porphyrin production. A large number of derivatives have been synthesized in the search for compounds that penetrate the plasma membrane of targeted cells and diffuse through epidermal layers more easily than ALA itself does. Most of the results indicate that many of the esters are more efficient in inducing porphyrin accumulation in cells *in vitro* than ALA itself. The methyl ester, MAL is more lipophilic than ALA and, in WiDr adenocarcinoma cells, is taken up by active mechanisms mainly through transporters of non-polar amino acids such as L-alanine, L-methionine, L-tryptophan and glycine. Most importantly, MAL is also taken up by passive transmembrane diffusion [106]. This mechanism does not require energy and it is unsaturable. It is very efficient in normal cells and even more in neoplastic cells. The plurality and efficiency of these various mechanisms determine the enhanced penetration of MAL in comparison to ALA and the difference is even more significant in malignant cells [101].

As the esterified form is more lipophilic than ALA, it was anticipated that MAL could penetrate more deeply into lesions. Peng *et al.* [107] reported that MAL penetrated to a 2 mm depth in BCC, contrasting with a more limited penetration with ALA [108]. Other investigators also found highly variable ALA uptake into nodular and infiltrating BCC [109]. However, Ahmadi *et al.* showed, in human skin biopsies, that ALA applied for 4 h penetrates to at least 2 mm depth from the lesion surface [110]. Using similar protocols, ALA is reported to produce higher PpIX levels than MAL, but with less selectivity for the diseased tissue [111-112].

Soon after cell penetration, MAL is rapidly demethylated to ALA and therefore the subsequent metabolic steps are the same as those described for ALA [104]. When excess PpIX is synthesized, it can diffuse from the mitochondrion to the endoplasmic reticulum and also to the plasma membrane, which are the other known sites of cellular damage through PDT [113]. These agents are relatively selectively concentrated in the target tissue, possibly related to alterations in surface permeability and tumour porphyrin metabolism. The rate of ALA-induced porphyrin synthesis and accumulation is higher in malignant and premalignant cells than in their normal counterparts with a 10:1 ratio of PpIX accumulation in tumours of the keratinocyte lineage in comparison to surrounding healthy skin [111].

e) *ALA and MAL: therapeutic efficacy and diagnosis*

As I will present on Section "Clinical applications of PDT" on Section 2.3, ALA (Levulan®, DUSA Pharmaceuticals) and ALA methyl ester (MAL: Metvix®, PhotoCure ASA) are widely used for the treatment of skin premalignancies and malignancies. Meanwhile, ALA hexyl ester (Hexvix®, PhotoCure ASA) is being developed for the diagnosis of bladder cancer (Table 1).
Briefly, PDT with topically applied ALA or MAL is an effective treatment for lesions less than 2mm depth [100]. Recent studies have attempted to compare the efficacy of MAL-PDT and ALA-PDT in diseased tissue, with application of each prodrug for 3h [112]. Patients with nodular BCC were randomly assigned to either ALA-PDT or MAL-PDT (ALA⁄MAL for 3 h, 600–730 nm, 75 J/cm^2, 100 mW/cm^2) and in each group half the tumours were debulked prior to PDT. On histological analysis after 8 weeks, no difference was found in lesional response. A further randomized double-blind study compared ALA and MAL for the treatment of extensive scalp AK [114]. MAL was applied for 3 h, but ALA for 5 h (580–740 nm, 50 J/cm^2, 50 mW/cm^2). No significant difference in mean lesion count reduction was observed 1 month after treatment, although pain was more intense on the ALA side.

Besides its usefulness in therapy, ALA and MAL can also be applied for diagnostic purposes [115-118]. After topical or systemic ALA application, PpIX is induced in epithelial tumours, with a high tumour to surrounding tissue ratio, and the tumours can be visualized under exposure to blue light. Fluorescence images can be utilized either to guide biopsy sampling or as an aid during surgery [119].

f) Novel ALA derivatives and strategies to increase production of PpIX by the target tissue

New ALA derivatives are continuously being designed [120-121]. Therapy and diagnosis with ALA are being used in dermatology [100, 122-124], gynaecology [125-130], urology [131-134], gastroenterology [135-138], neurosurgery [119], *etc.* Low doses of ALA-PDT are already useful for photorejuvenation [139-141] and photochemoprevention of skin tumours [142-145]. Several other methods, such as use of different formulations (creams, lotions, gels, *etc.* alone, with penetration enhancers and/or iron chelators), physical methods (curettage, ultrasound, iontophoresis, electroporation and electrophoresis) were also

proposed to improve ALA delivery and porphyrin production. A stable nanoemulsion-based ALA formulation, BF-200 ALA, is currently under clinical development for PDT of AK, showing patient and lesion complete clearance rates after illumination of 96.4% and 98.8%, respectively [146]. The accumulation of PpIX and other porphyrin intermediates is dependent on the activity of ferrochelatase and the availability of iron. The source of ferrous iron is probably the intramitochondrial pool. The simultaneous delivery of ALA together with the iron chelators, such as ethylenediaminetetraacetic acid (EDTA) and desferrioxamine, increases the rate of accumulation of porphyrins [147].

2.1.3.5 *CHARACTERISTICS OF A GOOD PHOTOSENSITIZER*

As I highlighted earlier, a photosensitizer should ideally possess several properties (Table 2.3) that may be associated with therapeutic efficacy and tolerability.

Purity	• Single pure substance of known composition that is stable at room temperature.
Selectivity	• Accumulation within tumor tissue is favorable. • Subcellular localization within organelles which induce apoptosis rather than necrosis
Toxicity	• Minimal toxicity in the absence of light and only cytotoxic in the presence of light of defined wavelengths. • Photosensitizer should not yield toxic metabolites. • Eliminated quickly enough to avoid generalized skin photosensitization.
ADME	• Optimal absorption, distribution, metabolism and excretion (ADME) properties.
Quantum yield	• High single oxygen quantum yield for photochemical event.
Activation	• Absorb light wavelengths between ~700 and 850 nm for maximum light penetration in the optical window for PDT. • Stable enough to avoid photobleaching
Mutagenicity	• Neither mutagenic nor carcinogenic effects
Cost and availability	• Inexpensive and commercially available.

Table 2.3 *Characteristics of an ideal photosensitizer*

First, the ideal photosensitizer is preferably a pure compound with a constant composition and no toxicity in the absence of light. It should also be selectively enriched in the target tissue and eliminated from the body quickly enough to avoid generalized skin photosensitization.

As previously mentioned, efficient triplet energy transfer is required for $^1O_2$, formation. As a consequence, the photosensitizer should also have a high triplet state yield, with a triplet

state energy larger than the energy of singlet oxygen (> 94 $kJmol^{-1}$). Optimally, it should not self-aggregate, as the aggregation decreases triplet state yield and singlet-oxygen yield [148].

The photosensitizer should absorb light of longer wavelengths so that the therapeutic effect of PDT can be as deep as possible [57]. However, the absorption wavelengths should not be too long as the triplet state energy can be too low for producing $^1O_2$ [148]. Also, the photostability of a compound often decreases when its absorption wavelength increases [148]. Preferably, the photosensitizer should not strongly absorb light of the region 400–600 nm, to reduce the risk of generalized photosensitivity caused by sunlight [148].

In addition to those I mentioned above, there are other characteristics that could prove useful in PDT. Strong absorption of the light used in PDT decreases the amount of photosensitizer required for a certain therapeutic effect. However, this should be cautiously taken into account as a too strong absorption of photosensitizers may limit the penetration of light into the tissue and thus reduce the treatment depth (this phenomenon is known as selfshielding) [61]. The photosensitizer should also be stable enough to avoid degradation processes, e.g. photobleaching. However, the photobleaching tendency can be an advantage as well, because it can shorten the duration of generalized photosensitivity after PDT [149], and also because it can increase the treatment selectivity.

The use of photosensitizers that need a short period of incubation before irradiation (within a few hours after administration) makes it possible to complete the treatment within a single visit to the hospital [150]. The fluorescence emitted by the photosensitizer is also useful in tumor detection, in the estimation of tumor size and limits, and in the determination of the photosensitizer concentration. However, as the triplet state quantum yield of strongly fluorescing compounds cannot be high, the compounds developed as photosensitizers for PDT are probably different from those intended to act as fluorophores for tumor detection [51].

Finally, synthesis of the photosensitizer should be relatively easy while the starting materials should be readily available and cheap. Its large-scale production should also be feasible to make it cost-effective and widely applicable [151].

2.1.4 PHOTODEGRADATION AND PHOTOMODIFICATION OF PHOTOSENSITIZERS

Upon illumination, all photosensitizers are chemically modified [32, 149, 152-155]. Photobleaching is the destruction of the photosensitizer by light-mediated processes. It was observed that light degrades photosensitizers in solution according to the following equation where β is specific for each compound, and J is the total light fluence [156]:

$$C=C_0e^{-\beta j}$$

Photosensitizer degradation by light through singlet oxygen mediated processes can occur due to: (1) photosensitizer fragmentation, resulting in loss of absorbance and fluorescence, and/or (2) photosensitizer modification, forming fluorescent photoproducts, which are often photosensitizers themselves and usually more water-soluble than the parent compounds [149, 157-161]. These processes have a high probability, since the photosensitizers are close to the reactive molecules, in the biological environment.

The main photoproducts of porphyrin photofragmentation do not absorb in the visible spectral region and are non-fluorescent. Photobleaching is therefore followed by the decrease in the fluorescence over time assuming that fluorescence intensity and concentration are proportional [156]. It was proposed that one pathway of porphyrin photodegradation may be epoxidation at the double-bond between the ring and the methine bridge of Hp, HpD, PpIX and mesoporphyrin [162]. Formation of bilirubin and biliverdin that are quite photolabile pigments may be the result. As a consequence, photodegraded photosensitizers may lose their photodynamic activity [149, 153, 155]. On the other hand, other photolytic pathways may also take part. It has been shown that photomodification of porphyrins such as PPIX typically creates chlorines, accompanied by a red shift of fluorescence. For PPIX, it has been published that some of the photoproducts are more effective photosensitizers than the mother molecule [155, 161, 163].

As stated above, most photosensitizers are photodegraded and phototransformed according to first order processes, *i.e.* the degradation rates are independent on the initial dye concentration. However, as opposed to homogenous solutions, in biological samples, photodegradation does not follow simple exponential kinetics due to heterogeneous binding to biological structures and oxygen depletion during light exposure [157, 164-167]. There are large differences in the photostability of the different photosensitizers. Water-soluble dyes tend to be more stable than the lipophilic ones, at least when present in cells and tissues [156, 162]. The reason for this might be related to the intracellular localization of the photosensitizer. Binding of a photosensitizer to a protein are also important as it generally decreases photosensitizer photostability. Aggregates of a photosensitizer are more photostable than monomers [168]. Although photobleaching decay constants for several

porphyrins have been measured in solution, there is no agreement as to whether photobleaching has any effect on PDT activity [156, 169]. Photobleaching of a photosensitizer may nevertheless limit its efficacy in PDT and has to be taken into account when choosing optimal light fluences and photosensitizer concentrations. On the other hand, photobleaching can prevent photodamage to normal tissue adjacent to the tumour area [157, 165]. Photobleaching requires singlet oxygen just as tumour destruction does. Thus, photodegradation rates may be used for clinical dosimetry [156, 166-167, 170-171].

2.1.5 CELLULAR UPTAKE OF PHOTOSENSITIZERS

Photosensitizer uptake kinetic is a major determinant of the photocytotoxic efficacy as it determines the final photosensitizer intracellular concentration. It depends on the structural features of the photosensitizers such as: the net ionic charge which can range from -4 anionic to +4 cationic charges; the degree of hydrophobicity expressed as the logarithm of the octanol/water partition coefficient; the degree of asymmetry and the existence of conjugated chains [54].

The different uptake pathways of photosensitizers in tumor tissues are summarized in Figure 2.8.

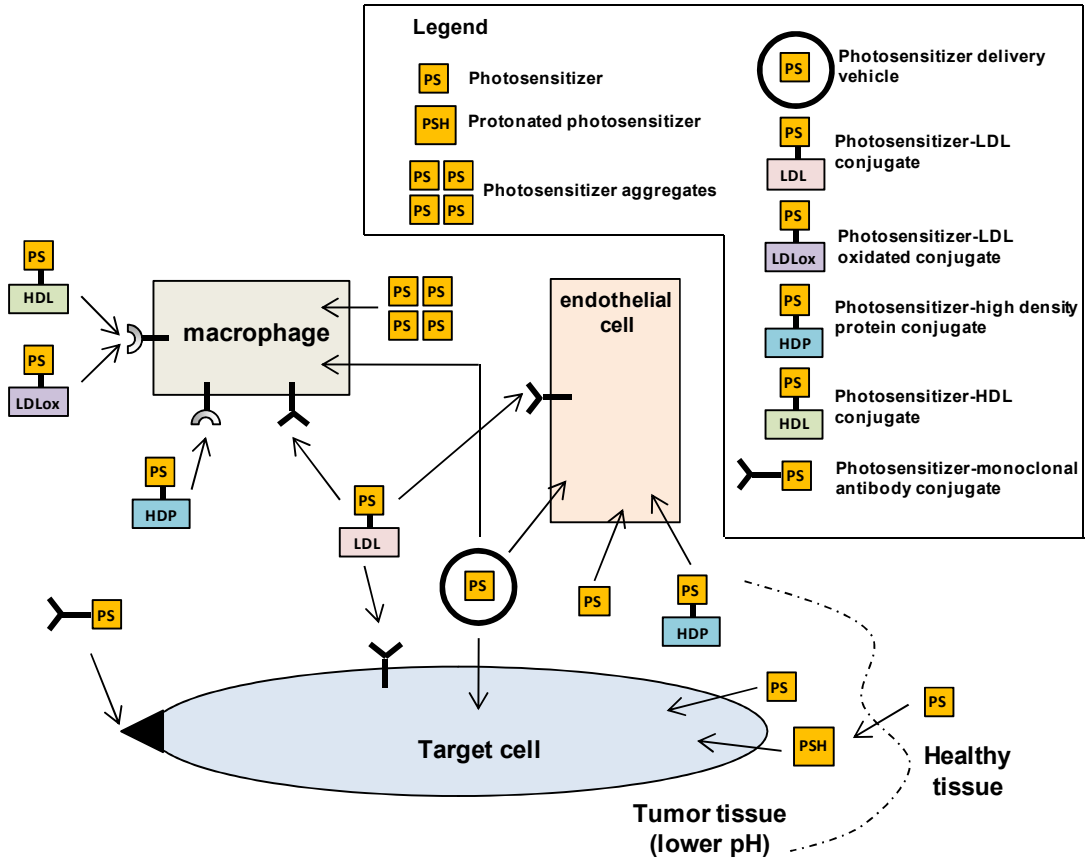

Figure 2.8 *Overview of photosensitizer uptake pathways in tumour tissue [adapted from Osterloh et al., 2002 [172]]*

Porphyrins can diffuse as monomers or small aggregates through the plasma membranes of tumor cells or they may bind to membrane proteins. Photosensitizers which are hydrophobic and electronically neutral (or have two or less negative charges) may diffuse across the plasma membrane, and then relocate to other intracellular membranes. These photosensitizers also tend to have the greatest uptake by cells *in vitro*, especially when present at relatively low concentration in the cell culture medium. Photosensitizers which are less hydrophobic and have less than two negative charges tend to be too polar to diffuse across the plasma membrane, and are therefore taken up by endocytosis [54]. Low-density lipoproteins (LDL)-bound photosensitizers target LDL apoB/E receptors at the surface of all cell membranes whereas other porphyrin-protein assemblies such as modified LDL-porphyrin complexes are recognized by macrophage scavenger receptors. Photosensitizers bound to monoclonal antibodies target specific antigens at the surface of neoplastic cell membranes and porphyrin-peptide conjugates with nuclear localization sequences are taken up by endocytosis, and can target the cell nucleus. Highly aggregated porphyrins are taken up by phagocytosis. In the case of vehicle-bound porphyrins in topical

formulations, they are incorporated *via* plasma membrane fusion or receptor or non-receptor-mediated endocytosis. High density lipoprotein (HDL)-porphyrin complexes target the tumor stroma and preferentially accumulate in macrophages.

2.1.6 SUBCELLULAR LOCALIZATION AND RELOCALIZATION

Along with cellular uptake, an important factor determining the outcome of PDT is how the photosensitizer interacts with cells within the target tissue or tumor. The structural features of the photosensitizer also determine its affinity for sub-cellular organelles and thus the primary targets of PDT-mediated damage. The knowledge of the photosensitizer localization allows to predict the consequences of specific photodamage to cellular organelles and the subsequent steps leading to photokilling. Data obtained from localization studies may also be useful as they may suggest an indication of PDT efficacy [173].

PDT sensitizers with known clinical or pre-clinical efficacy can target mitochondria/endoplasmic reticulum (ER), ER alone, ER/lysosomes or lysosomes alone. It is not yet clear whether any particular target is especially effective (Figure 2.9) [174].

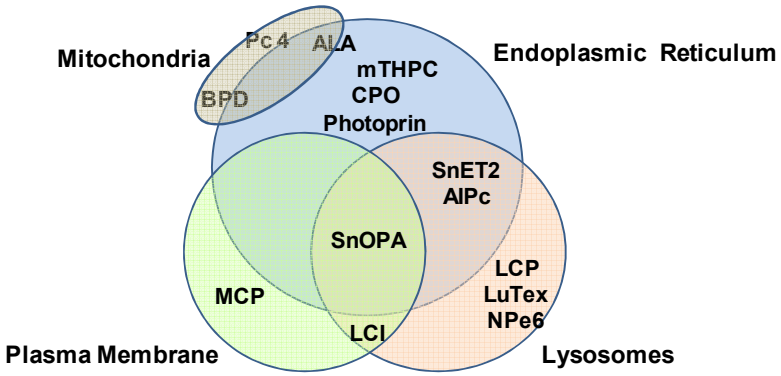

Figure 2.9 *Sites of localization of different photosensitizers using murine leukemia L1210 cells in culture (ALA, δ-aminolevulinic acid; PC4,* sulfonated aluminium phthalocyanine*; BPD benzoporphyrin derivates; m-THPC, mesotetrahydroxyphenyl chlorin; CPO, porphycene; SnET2, tin ethyl etiopurpurin; AlPc, sulfonated aluminium phthalocyanine; LCP, zinc octyloxyethilporphyrin; LuTex, lutetium texaphyrin; MCP monocationic porphyrin, NPe6, mono-L-aspartyl-chlorin e6; SnOPA, tin octaethylpurpurin amidine; LCI lysyl chlorin e6 imide). [adapted from Kessel et al., 2004 [175]]*

Depending on the nature of the photosensitizer, mitochondria, lysosomes and cytoplasmic membranes, but not the nucleus, are primary targets of PDT-mediated damage [176]. The main targets of PDT are summarized below.

2.1.6.1 *MITOCHONDRIA*

Mitochondria have long been considered as a main target of photodynamic damage since ATP, required to power cellular functions, is produced by this organelle. Depending on the photosensitizer, PDT damage to the mitochondrial proteins may constitute the primary event in a chain leading to breakdown of the electron transport chain, disruption of the mitochondrial-membrane potential and mitochondrial swelling and, ultimately, cell death [177]. A direct consequence of mitochondria damage is the inhibition of proteins required to maintain the electrochemical gradient across the inner-mitochondrial membrane. Malate dehydrogenase, succinate dehydrogenase, and cytochrome *c* oxidase are inhibited by HpD-PDT. On the other hand, no inhibition of glucose phosphate isomerase, pyruvate kinase, and lactate dehydrogenase (all cytosolic proteins) is observed after HpD-mediated PDT [178]. Thus, cytosolic proteins are less susceptible to photo-oxidation than mitochondrial membrane bound proteins because the singlet-oxygen lifetime is reduced in aqueous environment. It has been demonstrated that the susceptibility of the protein to PDT correlates with the degree to which it is embedded into a membrane. Cytochrome *c* oxidase resides within the inner mitochondrial membrane. Succinate dehydrogenase is anchored in the inner mitochondrial membrane but protrudes out in the mitochondrial matrix. On the other hand, malate dehydrogenase floats free in the mitochondrial matrix [179]. Another mitochondrial protein complex - the permeability transition pore (PT pore) - [180] constituted by hexokinase, the peripheral-benzodiazepine receptor (PBR), the voltage-dependent anion channel, creatine kinase, the adenine nucleotide translocator and cyclophyllin D [181] has been proposed as a PDT target. Furthermore, cells expressing higher levels of PBR are more susceptible to Photofrin-PDT than cells expressing normal levels of PBR [182]. The activity of the adenosine triphosphatase, which extracts energy from the proton gradient across the mitochondrial membrane to form adenosine triphosphate (ATP), is reduced after *in vitro* HpD-PDT [183].

Mitochondrial swelling and leakage of markers from the mitochondria occurs only after oxidative phosphorylation inhibition due to photo-oxidation of mitochondrial proteins such as cytochrome *c* oxidase [177, 183]. As a result, and as will be discussed in Section 2.2.2, mitochondrion-localized photosensitizers are usually associated with apoptosis induction [184].

2.1.6.2 *LYSOSOME*

Photosensitizers may also localize in lysosomes [185]. Although lysosomal disruption may not be directly cytotoxic [186], acid hydrolases that leak out of the damaged lysosomes may degrade cellular components. However, PDT mediated by tetraphenylporphyrin (TPPS) which localizes mainly in the lysosomes, disrupts lysosomes but does not significantly decrease cell viability [185]. To relate the lysosomal localization and cellular insensitivity to lysosomal damage, Moan *et al.* suggested that lysosomes are a primary localization site but not the photodynamic target [187]. Upon illumination, lysosomes may rupture and the photosensitizer could relocalize to more susceptible organelles such as the mitochondrial and nuclear membranes. Dependent on the prevalent phenomenon, lysosomal localization can elicit either a necrotic or an apoptotic response as will be further discussed in Section 2.2.2.

Lysosomal subcellular localization is the basis for photochemical internalization, a novel PDT modality [188-189]. By photochemical internalization, lysosome-localized toxins, immune-response modulating molecules and DNA can be released into the cytoplasm of cells. Release of lysosome-localized fluorophores in the cytoplasm leads to an increase in the fluorescence intensity caused by deaggregation and has been demonstrated both *in vitro* and *in vivo* [190].

2.1.6.3 *MEMBRANES*

Many photosensitizers accumulate in the plasma membrane [174]. Photo-oxidation of cellular membranes is an efficient way to kill tumor cells [191]. Photodynamically active photosensitizers may have no inherent affinity for specific membrane protein but may partition into the surrounding lipid layers. Membranes, especially mitochondrial membranes, may thus act as localization sites for photosensitizers. Damage to cell membranes after PDT have been shown by a number of methods: ESR, electron microscopy, microscopic observation of blebs and cell expansion [192]. Although direct photo-oxidation of cell membrane lipids may not be lethal, it may still have an important role in low-dose PDT as peroxidized lipids may produce potent second messengers leading to cell death.[193].
Membrane effects also cause increased attachment to a substratum and intracellular matrix after PDT in adherent cells, and decreased attachment of suspended cells [194-195]**.** These membrane effects may be of great importance for reducing the metastatic potential of surviving tumor cells.

2.1.6.4 *NUCLEUS*

The nucleus is another organelle that may be sensitive to photodynamic damage. Since DNA encodes genetic information, any lesion that occurs in the genome creates an extremely dangerous situation for the cell. The mechanisms of DNA damage induced by photodynamic therapy are not well understood. PDT can cause guanine base oxidation, cross-linking of DNA strands or sister chromatid exchange [196-197]. As anionic photosensitizers localize outside the nucleus, they produce little direct DNA damage [198]. Only a small fraction of DNA, localized close to the nuclear membrane may thus be damaged by PDT [199]. However, a particular attention must be paid to cationic photosensitizers as they may interact with DNA negative charges. DNA damage can be observed after HpD- or cationic-porphyrin-mediated PDT *in vitro* [200]. However, when PDT-DNA damage and X-ray induced DNA damage are compared, data show that there is less DNA damage from PDT treatment after equitoxic doses [201]. Treatment with X-ray produced 80% more strand breaks, 5% more sister-chromatid exchanges, and more chromatid aberrations than PDT does. Furthermore, PDT-induced strand breaks are more efficiently repaired than those caused by X-ray irradiation [202]. Thus, the mutation potential of Photofrin and aluminium phtalocyanine-mediated-PDT is insignificant compared to that of X-ray irradiation [203]. Recently, the ability of HpD, m-THPC, and methylene blue to damage DNA *in vitro* was examined. No DNA damage was observed after m-THPC-PDT, while minor damage have been observed with HpD- and methylene blue-PDT. These damage are transient and resolved 4h after treatment [204]. In conclusion, DNA damages are not the major initial contributors to the PDT response but they can be a major factor during cell death.

2.1.6.5 *PHOTOSENSITIZER RELOCALIZATION*

Light exposure can also change the intracellular localization of a photosensitizer molecule, a process called photorelocalization [205-208]. It is significant after rather low exposures, or multiple exposures, where the first illuminations might contribute to a change in the mobility of the photosensitizer within the cell [187, 206]. For some hydrophilic sensitizers, photorelocalization from lysosomes to the nucleus occurs. The resulting damage to the DNA increases the quantum yield of cell destruction of these photosensitizers [187, 206, 208].

2.1.7 THE BASIS FOR TUMOR SELECTIVITY

As referred before, tumor selectivity is one of the major advantages of PDT. Several theories have been proposed for the mechanisms explaining why photosensitizing drugs are selectively taken up and/or retained in tumour tissues. These theories are based on special properties of tumours cells, or on physiological differences between tumours and normal tissues [209-214]. The reasons for selective uptake of photosensitizers in neoplastic and altered tissues may be of enzymatic, morphological or environmental character as will be presented below. The low tumour pH (related to poor vascularity of tumours leading to enhanced glycolytic activity followed by an increase in lactate levels) causes preferential accumulation of drugs that protonate and become more lipophilic as they enter acid tumours *via* the blood supply [215]. Tumours contain many macrophages that can ingest and monomerize aggregated photosensitizers as well as lipoprotein bound drugs [216]. Lipophilic photosensitizers preferentially bind to lipoproteins. More low-density lipoprotein (LDL) receptors are found on the surface of tumour cells as compared to normal cells [217]. Tumours have a poor lymphatic drainage and a leaky vasculature [216, 218]. Differences in water content and in other physiological parameters between tumours and normal tissue play a role for tumour localization of drugs. A large interstitial space is often found in tumours. When compared to normal tissues, a higher content of collagen seems to be present in several tumours [219].

Tumours are already deprived of oxygen, prior to PDT [220], and additional PDT-induced vascular damage in vascularized stroma may inactivate them selectively [221-225]. Alterations of metabolic steps in heme synthesis may be the main reasons for increased ALA-induced accumulation of PpIX in neoplastic cells and tissues. Thus, in some malignant cells and tissues, the porphobilinogen deaminase activity is increased [86, 226-229], while the ferrochelatase activity is reduced [86, 226, 228, 230]**.** Since ferrochelatase catalyzes the insertion of ferrous iron into the PpIX ring, the amount of the labile iron pool influences PpIX accumulation [231]. The importance of available iron on PpIX production was demonstrated using iron chelators [147, 232-234]. As mentioned above, tumours and normal tissues differ with respect to physiological structures. This may affect PpIX production and accumulation, and lead to tumour selectivity. Due to inflammation, many tumours may have a slightly elevated temperature [235-236]. The rate of biosynthesis of PpIX increases steeply with increasing temperature [237-239]. Stratum corneum is the main barrier for penetration of topically applied drugs from the skin surface into tumours and other tissues [240]. When ALA, or its derivatives, is applied topically on cutaneous tumours, some tumour selectivity is caused by a compromised stratum corneum [101, 212]. Differences between tumour and normal cells with respect to proliferation, differentiation, mitochondrial content, pH, *etc.* may lead to selective PpIX accumulation and retention [209, 241-247]. Interactions between these factors may exist depending on the nature of disease, its localization and stage, and on the photosensitizer or PpIX precursor used, as well as on its application mode and time [209].

2.1.8 LIGHT

Photodynamic therapy can be applied only to tumours and other lesions that can be reached by light, either directly or through optical fibers. The PDT of skin diseases is made easy by the accessibility of the skin to light application.

2.1.8.1 *PRINCIPLES OF LIGHT PENETRATION*

Light propagation through tissues implicates processes of refraction, reflection, absorption and scattering (Figure 2.10).

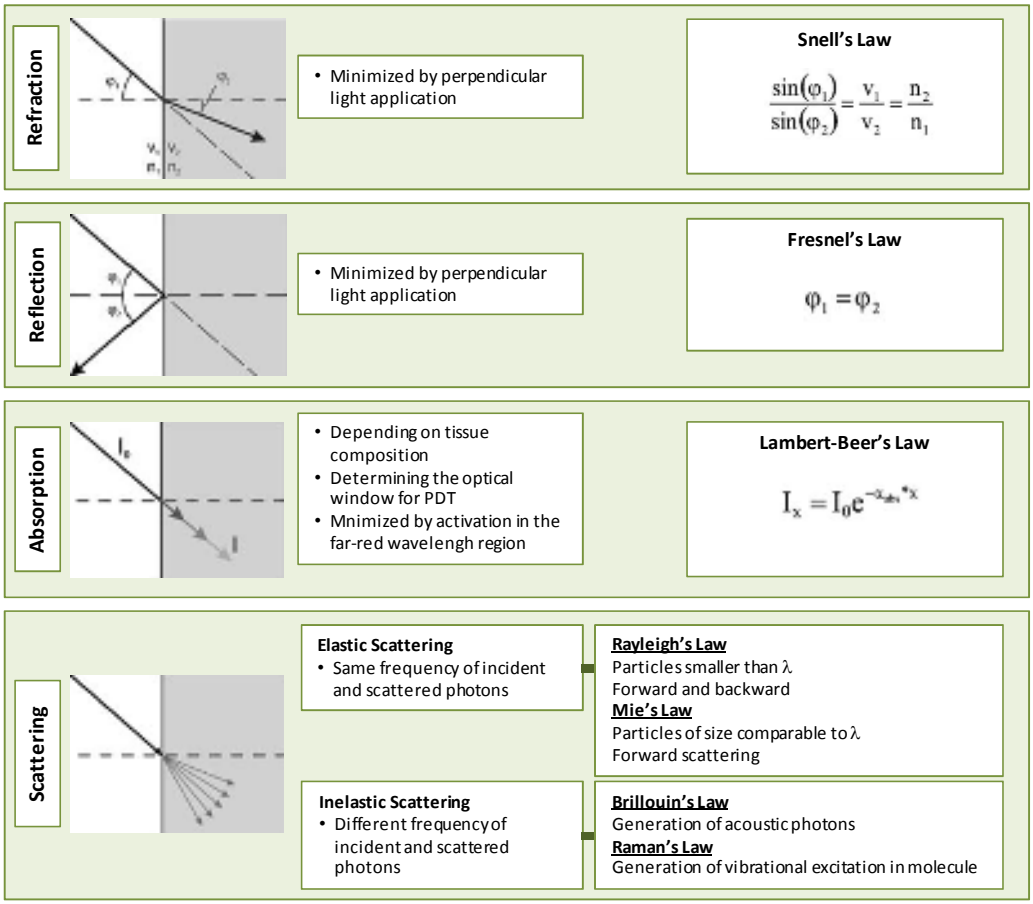

Figure 2.10 *Interaction between light and tissue [adapted from Plaetzer et al., 2009 [248]]*

Reflection from the interface between two media and refraction are governed by Fresnel's law and Snell's law, respectively, and their impact on the loss of intensity are determined by the relative values of their refractive indices [249]. Since both processes depend on the angle of incidence, they can be minimized by applying the light beam perpendicular to the interface between the two media. Scattering and refraction cause a widening of the light beam resulting in a loss of fluence rate (given as power per unit area of light in [$W.m^{-2}$]) and a change in the directionality of the light beam.

Scattering in tissue is ruled by quite complex variables (Figure 2.10). Inelastic scattering (Brillouin scattering and Raman scattering) does not seem to play an important role in this case. For elastic scattering, neither Rayleigh scattering nor Mie scattering completely describe the effects observed in tissue where photons are mainly scattered in the forward direction. The experimentally observed scattering shows weaker wavelength dependence than that predicted by Rayleigh's theory, but the effect is stronger than that given by Mie scattering [250-251]. Scattering of light in tissue has thus the most pronounced effect on light intensity and directionality. Besides scattering, absorption of light quanta is most relevant for the loss of light intensity with increasing penetration depth. The reduction in intensity caused

by both processes can be mathematically described by an exponential function similar to Lambert–Beer's law. The intensity at a given depth x can be calculated [252], by the equation:

$$I_x = I_0 e^{-(\alpha abs+\alpha sca)x}$$

with I_x being the intensity at depth x and I_0 the intensity at the media interface. The parameters α_{abs} and α_{sca} represent the absorption and scattering coefficients, respectively. Thus small changes in the attenuation coefficient lead to large changes in the fluence rate with depth. Therefore it is advantageous to have photosensitizers that absorb near 800 nm to maximize the treatment depth in many different tissues. The inverse of the attenuation coefficient is the attenuation depth which describes the depth that light entering tissue is reduced to 1/e (approximately 37%) of its initial intensity. Typical values of the attenuation depth range from 1 to 3 mm for non-pigmented tissues [253-254]. Dougherty has reported that the destructive effects of PDT extend to two attenuation depths or about 5 to 6 mm, indicating that as little as 10 percent of the entering light is required for a photodynamic effect [255].

2.1.8.2 *LIGHT INTERACTION WITH TISSUE IN PDT*

To be useful in PDT, a light source must emit wavelengths in the absorption spectrum of the photosensitizers. All porphyrin-like compounds have a strong absorption band around 400 nm (called the Soret band) and weaker satellite absorption bands (Q-bands) between 600 nm and 800 nm. The amount of photoactivation depends on the amount of absorbable light that reaches the photosensitizer in the target tissue.

Light entering tissue is absorbed by the dominant chromophores (hemoglobin, melanin and water), each of them absorbing light at different wavelengths. Depending on the absorption spectra of the chromophores, the penetration depth will change with the wavelength. The absorption spectra of these molecules define the optical window for PDT in tissue (Figure 2.11) [27, 54, 256], and determine how deeply the light will penetrate.

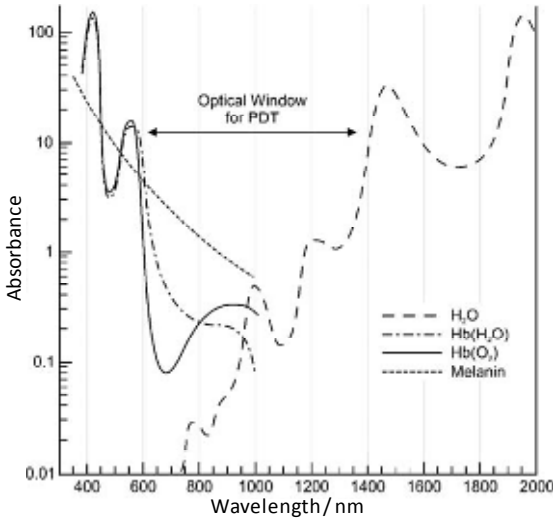

Figure 2.11 *The "optical window" for photodynamic therapy [adapted from Kohen et al., 2002 [29]]*

Long wavelengths penetrate more deeply into tissue, but this advantage is limited by how strongly the photosensitizer absorbs light at these long wavelengths. If absorption is low, time of exposure to light may be extended or the amount of deposited light energy may be increased to achieve photoactivation. There is a need for designing optimal combinations of photosensitizers, light sources and treatment parameters for each PDT application.

The so-called "optical window" of living tissue is between 600 nm (beyond the absorption of heme) and 1300 nm (below the absorption of water). Thus, to get optimal depths, photosensitizers absorbing in this region must be used, preferably at the highest possible wavelengths. One should keep in mind that hemoglobin (Hb) and HbO_2 show different absorption in the range of 600-700 nm, which is commonly used for PDT. The oxygen concentration changes during PDT because of vessel damage and direct consumption of oxygen in the photosensitizing process itself. *In vivo*, there might also be a significant difference in the amounts of HbO_2 and Hb between non-tumor and tumor tissue due to a possible lower oxygenation and pH of the latter [36]. This will lead to a change in the penetration spectrum and has to be taken into account [257].
Theoretically, photons up to 1240 nm (corresponding to the gap between the energy of ground state oxygen and that of singlet oxygen) might be used. However, photons above about 850 nm will hardly generate singlet. Indeed, one has to produce a triplet state whose energy level is high enough to allow an efficient energy transfer to molecular oxygen. For treatment of deep lesions it is desirable to apply a photosensitizer with a high absorbance in the red region. Many of the second generation photosensitizers absorb at longer wavelengths than the traditionally used 630 nm for HpD. For PDT of solid tumors, the

effective penetration depth, defined as the depth x, where I_x decreases to 37% of I_0 (see above) is of great relevance [27]. For clinical treatment with Photofrin, the penetration depth of the 630 nm excitation light is approximately 3–5 mm, depending on the tissue [258]. The use of photosensitizers with absorption peaks at wavelengths >700 nm (or even higher) should, at least, double the penetration depth thus enabling treatment of thicker tumors [253, 259].

Light absorption leads to heat generation. Generally, fluence rates above about 150 $mW.cm^{-2}$ would give hyperthermia [260]. Recent studies have shown that a low fluence rate is preferable since depletion of oxygen occurs at high fluence rates [224, 261-265]. At the same time, the exposure time needs to be considered. Thus, the fluence rate influences the direct photochemical oxygen consumption and, therefore, plays a critical role in clinical PDT [264-265].

2.1.8.3 *LIGHT SOURCES AVAILABLE FOR PDT*

Light sources available for PDT belong to two broad groups: non-coherent (broadband lamps and diode lamps) and coherent sources (lasers) [266-267]. Coherent light originates from photons emitted in a resonance mode and that are in phase. Their usefulness mainly depends on a few photophysical characteristics: the emission spectrum, irradiance, spatial distribution and constancy of the output.

a) *Lasers*

Lasers produce highly coherent monochromatic light that can be efficiently delivered by quartz fiber optics. With lasers, specific areas can be more easily targeted. Lasers permit to minimize exposure times at selected wavelengths. Pulsed gold vapor, continuous-wave argon pumped dye, copper vapor, potassium–titanium–phosphate (KTP) and pulsed-dye lasers have been used in dermatologic PDT.

Unlike lamps, lasers allow for the exact selection of wavelengths matching the absorption peak of the photosensitizer and provide a highly homogeneous light beam. This light can be led through optical fibers and focused directly on the target. Argon dye, KTP dye, metal vapour, copper and gold lasers have been used for clinical PDT [266-268]. Lasers emit continuous wave or pulsed light, with pulse lengths down to a few femtoseconds. It has been hypothesized that high-intensity pulsed light could penetrate deeper into tissues than continuous wave light by causing a transient decrease in the absorption of chromophores in

tissue by the first part of the pulse [269]. This process allows the rest of the pulse to pass through tissue with less attenuation. Whether a pulsed laser is better than a continuous-wave light source in PDT is still unclear. Most clinical studies have shown no significant differences in PDT efficacy of pulsed and continuous wave light [269-273]. Nevertheless, several studies have suggested that pulsed light therapy may be useful for treatment by topical PDT of acne, actinic keratosis and photorejuvenation. A controlled investigative study, performed in healthy human skin *in vivo* following microdermabrasion, showed that intense pulsed light sources (IPL) such as filtered broadband flashlamps, produced evidence of minimal activation of photosensitizer, with a dramatically smaller photodynamic reaction than seen with a conventional continuous wave broadband source [273].

Lasers allow shortening of the treatment time as they emit a high fluence of monochromatic light corresponding to the absorption peak of the photosensitizer. In addition, they keep damage to surrounding tissues to a minimum because they can be focused with great precision on very small target areas with sharp boundaries [266]. However, they are expensive, have low reliability and portability and can illuminate only small areas of the skin surface. In addition, their high output is unnecessary in clinical conditions because, during PDT, the light intensity is kept in the range of 150–200 mW/cm^2 to trigger photochemical reactions without producing ablative hyperthermic effects [274]. Lasers are necessary for the PDT of internal organs or the experimental investigation of 'second generation' photosensitizers, which have narrow absorption peaks in the far red and near-infrared regions. However, for porphyrin based PDT of dermatological conditions, lasers have not shown therapeutic advantages over the cheaper and more practical incoherent light sources.

b) *Non-coherent sources*

Non-laser sources such as broadband high-pressure lamps or fluorescent lamps spans the whole visible range, with large infrared and negligible ultraviolet emissions. For dermatology, they are superior than laser systems because of their large illumination field, low cost, small size, and simple construction [266, 275-277].

Metal halogen lamps are widely used because they are cheap and have a high power density that keeps light exposure times within practical limits. They can be used as sources of white light (e.g. slide projector lamps) or can be equipped with optical filters that allow a selection of a waveband of 100–200 nm while cutting-off shorter wavelengths that are not necessary for drug activation, and infrared wavelengths that can overheat the skin causing a burning sensation.

The only fluorescent lamp useful for PDT is the Blu-U® (Dusa) light system. Its emission peak in the Soret band is sufficient for an effective irradiation of porphyrin-sensitized skin. A blue

fluorescent lamp is routinely used in Levulan® ALA-PDT of AK in the U.S.A. There are now several reports that blue, green and red light can be effective in topical PDT of AK, but the more deeply penetrating red light is superior when treating BD and BCC [278].

Light emitting diodes (LEDs) are small solid-state semiconductors with a high and reliable emission with peak emission of 631nm and a narrow bandwidth of 20–50 nm without infrared emission. LEDs have a deeper PDT action in tissue than a filtered halogen lamp of 560–740 nm emission, and hence LED may be more effective in treating the deeper parts of tumours [279]. They can be arranged in grids or panels to give a broad field of illumination. The power output and the uniformity of the irradiation field of both broadband lamps and LED lamps must be carefully checked during any single exposure and at regular intervals with an appropriate radiometer or a spectroradiometer. They are simple to use and do not have special electrical requirements.

In dermatology, non-coherent halogen, xenon arc and metal halide lamps, fluorescent tubes, LED and IPL are the most frequently used light sources for PDT.

c) *Lasers versus non-coherent light sources*

Lasers and non-coherent light sources have been used for PDT and usually show similar efficacies [266, 280-281]. Since coherence is lost within a few tenths of a millimeter of penetration into human tissue, this property is not of any importance for PDT. Light doses are principally related to the emission spectrum of the light dose and the peak of absorption of the drug. After ALA sensitization, 37 J/cm^2 of light from an LED lamp peaking at 630 nm or 75–100 J/cm^2 of a filtered incoherent lamp centered in the red waveband gives similar biological effects [282].

Light exposure using a laser at a defined wavelength allows accurate light dosimetry at the surface of the lesion. For broad-band sources the depth of light penetration, the extinction coefficient of the photosensitizer, and the spectral intensity can all vary across the bandwidth of light used. Therefore, the light doses reported with the use of a laser, filtered light and white light are not directly comparable.

No single light source is ideal for every possible indication of PDT, even with the same photosensitizer. Choice of light sources should be based on: reliability, size, simplicity of maintenance, cost, photosensitizer absorption (fluorescence excitation and action spectra), disease (location, size of lesions, accessibility). In the last few years, LED sources have shown considerable development, with improvements in design making these relatively inexpensive sources convenient for wide area irradiation and popular for patient use, e.g. the AKTilite® 16 and 128 (Galderma) and the Omnilux® (Photo Therapeutics Ltd, Altrincham, U.K.). Furthermore, a report has recently introduced the concept of ambulatory PDT to

reduce hospital attendance for PDT [283]. In a pilot study of five patients with Bowen's disease, PDT was performed with ALA and a portable LED device, where low irradiance light exposure took place over 100 min (ALA 4 h, 637 nm, 75 J/cm^2, 12 mW/cm^2. Four of five patients were in clinical remission after a median of 9 months.

2.2 BIOCHEMICAL EFFECTS OF PHOTODYNAMIC THERAPY

In this second part of the introduction, I will review the biological effects induced by PDT with emphasis on:

- the direct cytotoxic effect of PDT on tissue and the role of vascularization
- the mechanisms of cell death in PDT
- the changes in cell signaling after PDT

2.2.1 DIRECT CYTOTOXIC EFFECT OF PDT ON TISSUE AND THE ROLE OF VASCULARIZATION

At the tissue level, the targets of PDT include tumor cells, the microvasculature of the tumor bed as well as normal microvasculature, and the inflammatory and immune host system. PDT effects on all these targets may influence each other, producing a cascade of responses (Figure 2.12).

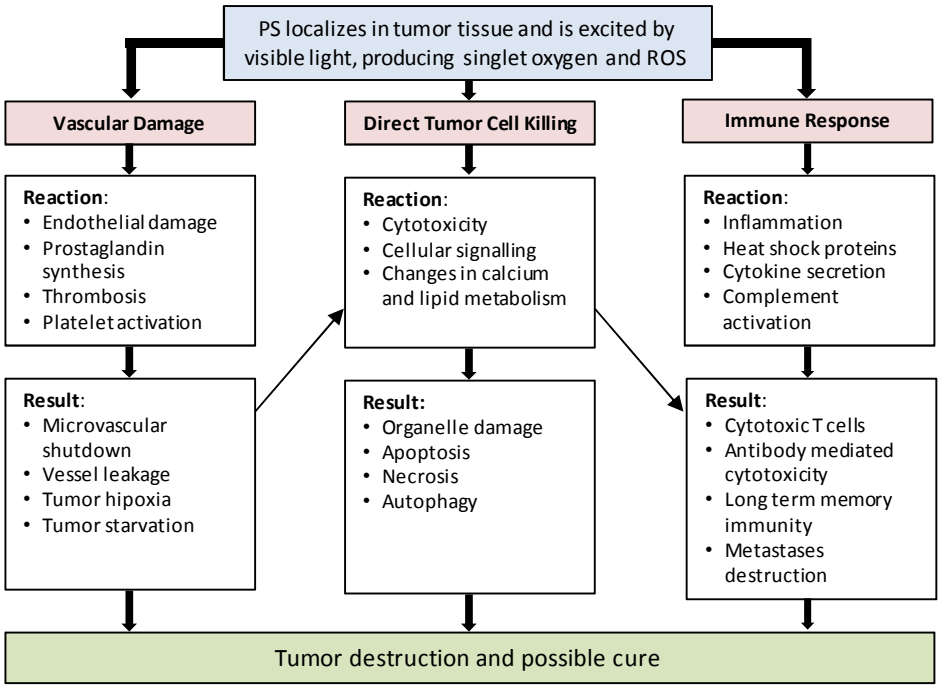

Figure 2.12 *Pathways of PDT-mediated tumor destruction illustrating possible contributions from direct tumor cell killing, vascular damage and host immune response.*

The relative importance of each for the overall tumor response has yet to be fully defined. It seems clear, however, that the combination of all these components is required for long-term tumor control [25].

2.2.1.1 DIRECT CYTOTOXIC EFFECTS OF PDT ON CANCER CELLS

It is generally accepted that PDT exerts a direct cytotoxic effect caused by the irreversible photodamage to vital subcellular targets such as the plasma membrane and intracellular membranes of the mitochondria, lysosomes, Golgi apparatus and endoplasmic reticulum. As I discussed previously in Section “Subcellular localization and relocalization”, the intracellular localization of the photosensitizer coincides with the primary site of photodamage [284-288]. This is because the photogenerated singlet oxygen has a very short lifetime and, thus, very limited diffusion in biological systems [153]. However, several studies have shown the relocalization of certain photosensitizers after irradiation [206, 289-290]. As a consequence, the photodamage can rapidly propagate to other subcellular locations than the primary site. Moreover, other reactive oxygen species resulting from the singlet oxygen attack may migrate at longer distances from the site of formation. Among them, hydrogen peroxide can be converted into the more reactive hydroxyl radicals.

Due to the high reactivity of singlet oxygen and hydroxyl radicals, virtually all macromolecular constituents, such as proteins, DNA and lipids, are directly affected by PDT. Proteins are prominent targets of singlet oxygen or free radical attack in cells subjected to photooxidative stress. Damage to proteins is often due to oxidation of essential methionine, tryptophan, histidine, or cysteine residues. It can thus cause protein modification resulting in enzyme inactivation, dysfunction of cellular membrane pumps, membrane and intra-cellular receptor damage and the modification of structural proteins. Since most dyes do not accumulate in cell nuclei, PDT induces much less DNA damage [291]. Finally, membrane lipids may also be important targets in cells subjected to a photooxidative stress, especially if the responsible photosensitizing agent is amphiphilic and localizes in the membrane bilayer. Singlet oxygen and other ROS can react with membrane lipids including unsaturated triacyl glycerols, cholesterol and phospholipids**.** The resulting intermediates of peroxidative reactions, such as lipid hydroperoxides, are potentially dangerous because they may propagate the initial peroxidative stress from one membrane to another one in cells. They may also participate in cell death pathway as will be discussed later. Whenever cellular detoxifying and antioxidant enzymes or agents are overwhelmed during PDT, the described oxidative stress leads to a

progressive failure of cellular machinery and ultimately to cell death as I will discuss in Section 2.2.2 and 2.2.3.

The early effects of PDT carried out with lipophilic sensitizers are detectable within a few hours after treatment and include biochemical changes such as inactivation of membrane enzymes, increased membrane permeability, formation of blebs, disruption of membranes, inhibition of cell division, breakdown of the respiratory process and cell lysis. On the other hand, hydrophilic photosensitizers photochemically inactivate cells through the release of lysosomal hydrolases or, alternatively, the photosensitizer may be released from the lysosomes before or during light exposure producing photochemical damage to other subcellular targets [42]. Such effects are related to the light and drug doses used [292]. An inverse relationship between these two doses has been found. Comparable biological effects can be produced by combining a relatively high photosensitizer dose with a low light dose or, conversely, a low drug dose with a high light dose. The cell genotype was also found to determine whether cell death occurs by apoptosis or necrosis [285, 293-297]. Indeed, apoptosis was the predominant mode of cell death when murine leukemia P388 cells were photosensitized with chloroaluminum phthalocyanine (AlPc), using low light doses, whereas necrosis was observed for higher light doses [293]. Similar results were obtained in studies where human bladder carcinoma HT1197 cells were subjected to 5-aminolevulinate (ALA)-induced PDT [298] and in CNE2 cells, TWO-1 cells (human nasopharyngeal carcinoma cells) and AY-27 cells (chemically-induced rat bladder carcinoma cells) photosensitized with hypericin [297, 299]. In addition, it has been found that biological effects can be modulated by different combinations of doses. With low light and drug doses, cell viability may be maintained while other traits (signaling activity, cytokine formation, receptor expression) may be altered. At higher doses of one or both components of PDT, the disruption of cell membranes and organelles causes necrosis, which contributes to the formation of an inflammatory state. At intermediate combinations of light and drug, cells may undergo apoptosis [292]. These findings indicate that the type of cell death switches from apoptosis to necrosis with the increase in the strength of the insult [300] as will be further detailed in the Section “Cell death pathways”.

As was just mentioned, exposure of tumors to PDT *in vivo* can reduce the number of tumor cells through direct photodamage. However this may be insufficient for tumor cure as it has been demonstrated in several studies on rodent tumor systems [61, 301-302]. After employing curative procedures with several photosensitizers, it was shown that the direct photodynamic tumor cell death was less than 2 logs and in most cases less than 1 log, i.e., far short of the 6–8-log reduction required for tumor cure. Non-homogenous

photosensitizer distribution within the tumor might be one of these limitations. Korbelik and Krosl [303] have also shown that both photosensitizer accumulation and tumor cell kill decrease with the distance of tumor cells from the vascular supply.

Another parameter that can also limit direct tumor cell kill is the availability of oxygen within the tissue undergoing PDT treatment. Two mechanisms can produce such limitations: the photochemical consumption of oxygen during the photodynamic process and the effects of PDT on the tissue microvasculature. Since oxygen in the tissue environment is consumed during PDT, rapid and substantial reductions in tissue oxygen tensions on illumination of photosensitized tissues were reported [304]. Photofrin–PDT produces very low levels of oxygenation in fractions of the tumor by decreasing the rate of oxygen diffusion from the capillaries and the radius of oxygenated tissue volume around them [305]. To minimize this phenomenon, the fluence rate can be adjusted downward to slow oxygen consumption sufficiently to facilitate the maintenance of (tumor) tissue pO_2 levels during treatment. Another approach toward maintenance of tissue oxygenation during PDT is the fractionation of light delivery [265, 305]. This consists of very short light and dark intervals, allowing reoxygenation during the dark periods. Generally, treatment regimens using a low fluence rate or intermittent light, show superior effectiveness in delaying tumor regrowth [306]. Recent clinical studies have shown that oxygen depletion also occur during PDT in patients. The kinetics for this depletion varied from very rapid (within seconds of light exposure) to slow (>10 minutes of light exposure) or no effect at all in basal cell carcinoma lesions in patients undergoing Photofrin (1mg/kg)–PDT at a light dose rate of 150 mW/cm^2 [225].

2.2.1.2 ROLE OF VASCULARIZATION

Along with oxygen consumption within the tissue undergoing treatment, the oxygen supply in the tissue can also be diminished by the damaging effects of PDT on the microvasculature [307]. Vascular shutdown can be readily observed following PDT [308] and can lead to severe and persistent post-PDT tumor hypoxia/anoxia [309]. The mechanisms underlying the vascular effects of PDT differ greatly with different photosensitizers. Photofrin–PDT leads to vessel constriction, vessel leakage, leukocyte adhesion and thrombus formation, all apparently linked to platelet activation and release of thromboxane [308, 310]. PDT with certain phthalocyanine derivatives causes primarily vascular leakage [311], while PDT with NPe6 results in blood flow stasis primarily because of platelet aggregation [312]. All these effects may include components related to damage to the vascular endothelium. PDT may also lead to vessel constriction via inhibition of the production or release of nitric oxide by the endothelium [313]. On the other hand, administration of agents inhibiting nitric oxide

synthase or scavenging nitric oxide appears to enhance tumor cure, apparently by enhancing the PDT induced disruption of vascular perfusion [314]. In preclinical experiments, the microvascular PDT responses can be partially or completely inhibited by the administration of agents that affect eicosanoid generation, such as indomethacin [223], various thromboxane inhibitors [223], and aspirin [315]. This inhibition can markedly diminish the tumor response [316]. Recent studies have also revealed important differences between PDT effects on normal and tumor vasculature [262, 317]. It has also been suggested that monitoring PDT-induced changes in tumor oxygenation may be a valuable prognostic indicator of photodynamic therapy effectiveness [318].

2.2.2 MECHANISMS OF CELL DEATH IN PDT

Although PDT can induce many cellular and molecular signaling pathway events in cells, its main purpose is to induce cell death [319]. The concentration, physical chemical properties and subcellular location of the photosensitizer, the concentration of oxygen, the appropriate wavelength and intensity of the light, as well as the specific properties of the cell type may all influence the mode and extent of cell death [248, 319-321].

Programmed cell death (PCD) is defined as a genetically encoded form of suicide occurring in a predictable place and time during embryonic development [322]. Three morphologically distinguished forms of PCD have been characterized during development. Type I PCD is characterized by phenotypic changes involving nuclear condensation and general cellular shrinkage. Type II PCD is distinguished by a lysosomal-dependent digestion of the cell and the presence of autophagic vacuoles (autophagosomes). Type III PCD is marked by cellular swelling and a rapid loss of plasma membrane integrity. These processes are defined as apoptosis, autophagic cell death and necrosis, respectively, and are cellular programs known to play a crucial role in normal development, tissue homeostasis and in eliminating abnormal and damaged cells (Figure 2.12) [323].

A presentation of the intervention of PCD in PDT is presented below whereas the detailed molecular mechanisms will be discussed in Section “Changes in cell signaling after PDT”.

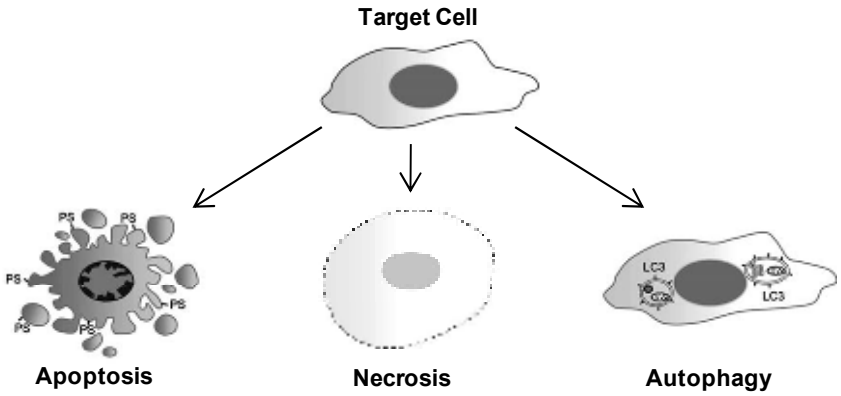

Figure 2.12 *Morphological characteristics of apoptosis and non-apoptotic cell death. Apoptosis is characterized by membrane blebbing, cytoplasmic shrinkage, chromatin condensation, exposure of phosphatidylserine on the cell surface and, in a later stage, the formation of apoptotic bodies. Death by autophagy is characterized by the double membrane vesicles containing cytosolic organelles. During necrosis, cells swell and loose their membrane integrity [adapted from Sun et al., 2009 [324]]*

2.2.2.1 *APOPTOTIC CELL DEATH IN PDT*

The word apoptosis (Greek: apo – from, ptosis – falling) is based on the morphology of the dying cells, which include cellular shrinkage, membrane blebbing and eventually fragmentation into membrane bound apoptotic bodies [325]. The major biochemical features of apoptosis are activation of intracellular proteases, especially caspases, and internucleosomal DNA fragmentation.

During apoptosis the cells shrink, the nuclear chromatin becomes pyknotic and condenses against the nuclear membrane. Eventually the cytoplasm and the nucleus break up into apoptotic bodies. Although the cytoplasmic organelles remain intact, DNA is digested at internucleosomal sites, giving rise to fragments that are multiples of 180–200 bp [326-327]. Simultaneously, the cell membrane loses its asymmetry and phosphatidylserine becomes exposed on the cell surface. These changes ensure that apoptotic cells are immediately recognized by neighboring cells and/or phagocytised with the result that many cells can be deleted from tissues in relatively short time [328]. It is believed that this type of cell death does not to trigger inflammation [329].

Several external signals may trigger two major apoptotic pathways, involving either activation of death receptors in response to ligand binding (extrinsic or death receptor pathway), or the

release of pro-apoptotic proteins from mitochondria to cytosol (intrinsic or mitochondrial pathway) [326-327]. The extrinsic pathway is activated by apoptotic stimuli comprising extrinsic signals such as the binding of death-inducing ligands to cell surface receptors. The extrinsic pathway is mainly activated by ligand-bound death receptors such as TNF-TNFR1, FasL-Fas and TRAIL-DR4 or -DR5. Activation of cell surface receptors from the tumor necrosis factor (TNF) gene family therefore activates the initiator caspase-8 via adaptor and scaffolding proteins.

In other cases, apoptosis is initiated following intrinsic signals including DNA damage induced by irradiation or chemicals, growth factor deprivation or oxidative stress. This process is triggered by disruption of mitochondrial function, which causes the release of cytochrome *c* to the cytosol [330]. Released cytochrome *c* binds Apaf-1 and induces its oligomerization, in the presence of dATP. This complex, termed apoptosome, recruits and activates the initiator caspase-9 [331-332]. Some evidence has indicated that the two pathways are linked and that molecules involved in one pathway can influence the other [333]. In both pathways, the activation of initiator caspases (caspase-8 or caspase-9) leads to the activation of effector caspases (caspase-3, -6 and -7) (Figure 2.13).

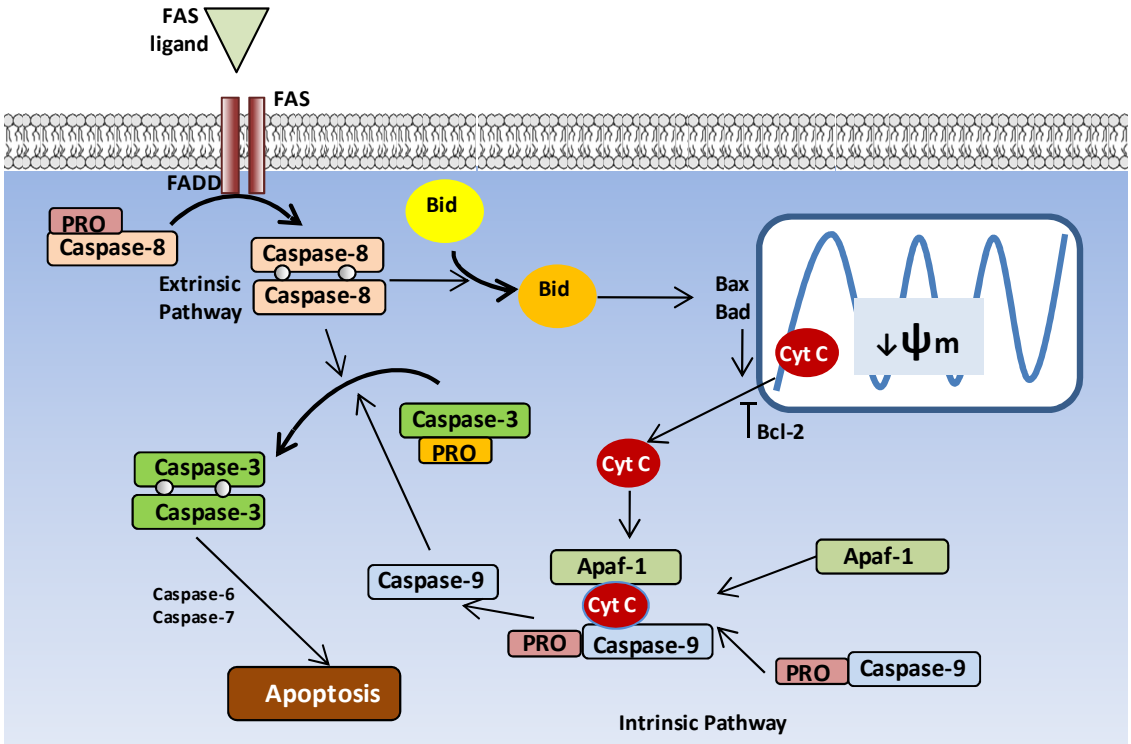

Figure 2.13 *Diagram of the apoptotic process. The two major apoptotic pathways, the death receptor-mediated, or extrinsic pathway, and the mitochondria-mediated-pathway are represented [adapted from Jin et al.,2005 [334]]*

a) *Extrinsic pathway*

The extrinsic pathway has been shown to be activated by photodynamic therapy. A transient increase in the protein levels of the surface death receptor Fas and of its ligand FasL occurred after photosensitization of human epidermoid carcinoma A431 cells with silicon phthalocyanine 4 (Pc 4). A multimerization of the Fas protein and its interaction with the adaptor molecule FADD was also observed [335]. Accordingly, caspase-8 cleavage was observed in the human epidermoid carcinoma A431 cells photosensitized with Pc 4, and pre-incubation of the cells with rhFas:Fc fusion protein partially inhibited cell death [335]. Antibodies against Fas or FasL also reduced apoptotic death of nasopharyngeal cells subjected to PDT with Hypocrellin A and Hypocrellin B [336]. In *in vivo* studies, in which NR-S1 tumor-bearing mice were treated by PDT with Photofrin, Fas-positive tumor cells were observed in the same area where many TUNEL positive tumor cells were found and expression of Fas and FasL was also observed in the tumor cells surrounding TUNEL-positive cells [337]. Activation of caspase-8 was found to mediate apoptotic death of human promyelocytic HL-60 cells photosensitized with Rose Bengal [338]. In this model, inhibition of caspase-8 impeded cytochrome *c* release from mitochondria and cleavage of procaspase-3, suggesting that caspase-8 acts upstream of these events. In fact, caspase-8 cleaves Bid (BH3-interacting domain death agonist), generating a truncated Bid fragment [339] that initiates mitochondrial outer membrane permeabilisation (MOMP) through the multidomain pro-death molecules Bax or Bak [340]. In turn, Bax/Bak translocation to mitochondria induces the release of cytochrome c into the cytosol and subsequent activation of the executioner caspases. Besides promoting death by activating the pro-apoptotic proteins Bax and Bak, Bid may also inactivate prosurvival proteins [341], thereby inducing the release of cytochrome *c* and connecting the extrinsic and intrinsic pathways. Bcl 2, on the contrary, impedes the cytochrome *c* release in the cytosol thereby inhibiting apoptosis.

Although the fast kinetics of caspase-8 activation in HL-60 cells subjected to PDT with Rose Bengal may suggest that singlet oxygen generated during photoactivation of the sensitizer directly induces multimerization-mediated activation of the Fas receptor, even in the absence of the FasL, a rapid upregulation of the Fas and FasL protein levels was observed in human epidermoid carcinoma A431 cells photosensitized with Pc4 [342]. By contrast, a direct effect of the photosensitizer on the activation of the Fas receptor is supported by studies showing that ultraviolet A radiation induces formation of the Fas–FADD–caspase-8 death complex in HL-60 cells in a FasL-independent manner [343]. Despite evidence indicating a role for the death receptor-mediated mechanism in apoptotic death of PDT treated cells it was found that FADD null mouse embryonic fibroblasts still undergo apoptosis when photosensitized with

Pc 4 [344]. These results indicate that in this case other mechanisms may be involved in apoptotic death induced by PDT.

b) *Intrinsic pathway*

Photosensitization of different cell types was also shown to stimulate the intrinsic pathway of apoptosis. This effect is more obvious with some sensitizers that target mitochondria [288], these organelles playing a central role in apoptosis. In this case, it is not surprising that PDT can induce apoptosis rapidly, both *in vivo* [337] and *in vitro* [345]. However, since photosensitizers may also be accumulated in other cellular compartments (e.g. lysosomes, endoplasmic reticulum, Golgi apparatus), local damage induced by photosensitization may be propagated to the mitochondria by various means [346-347].
Studies using different cell models and various sensitizers have shown that photosensitization induces a rapid release of cytochrome *c* from the mitochondria. The intracellular Ca^{2+} chelator BAPTA inhibited PDT induced cytochrome *c* release and caspase-3 activation, suggesting that the increase in the intracellular Ca^{2+} levels may trigger cytochrome *c* release from mitochondria [348]. A drop in mitochondrial membrane potential, concurrent with a drop in ATP levels and a decrease in cell respiration, was also observed in the early phase of the response of promyelocytic K562 cells to photodynamic treatment with hematoporphyrin [349]. Studies on human epidermoid carcinoma A431 cells suggested that PDT causes an up-regulation of glycolytic phosphorylation as a compensatory mechanism to overcome mitochondrial dysfunction and to provide energy equivalents required for apoptotic cell death [349]. Indeed, glycolytic ATP production constitutes a strict requirement during the initial events of the demise process [349].

2.2.2.2 *AUTOPHAGIC CELL DEATH IN PDT*

Autophagy (from the Greek, “auto” oneself, “phagy” to eat) refers to any cellular degradative pathway involving the delivery of cytoplasmic component to the lysosome. Autophagy is a physiological process that plays an important role in the turnover of cellular proteins and other macromolecules. Moreover, it is the major catabolic route for eukaryotic cells to salvage essential molecules, and to maintain an amino acid level sufficient to sustain protein synthesis during nutritional deprivation.

At least three forms have been identified— macroautophagy, microautophagy, and chaperone-mediated autophagy— which differ on the mode of intracellular component delivery to the lysosome and their physiological functions. Macroautophagy (herein referred

to as autophagy) is the most important regulated catabolic mechanism used by eukaryotic cells to degrade long-lived proteins and organelles. Unlike apoptosis, which relies on the activation of caspases that cleave several target proteins [350], autophagic cell death is caspase independent [351]. Indeed, autophagic cell death has been demonstrated in cells with defects in the apoptosis machinery [352] and in cells grown in the presence of caspase inhibitors [353]. Cells undergoing autophagic death look different from cells undergoing apoptosis. The characteristic cellular morphology of apoptosis results from caspase cleavage of cytoskeletal and other structural proteins [350]. In apoptotic cells, although early degradation of the cytoskeleton is observed, organelles are preserved until fairly late in the process. By contrast, autophagic cell death is characterized by the accumulation of large numbers of autophagic vesicles, in which organelles are degraded early in the process, while the cytoskeleton persists intact and functional until late in the process [354]. Morphologic changes, such as chromatin condensation or membrane blebbing, may also occur in autophagic cell death, but there is no DNA fragmentation or formation of apoptotic bodies [355].

Autophagy includes the delivery to the lysosome of cytoplasmic components sequestered inside double-membrane vesicles. The first steps are characterized by the formation (vesicle nucleation) and expansion (vesicle elongation) of an isolation membrane, the phagophore. The extremities of the phagophore then fuse (vesicle completion) forming the autophagosome, a double-membrane vesicle that sequesters the cytoplasmic material. Then, autophagosomes fuse with lysosomes to become autolysosomes, where sequestered cellular components, together with the inner membrane, are digested [356]. Amino acids and fatty acids generated by this process can be used for protein synthesis, or can be oxidized by the mitochondrial electron transport chain to produce adenosine triphosphate (ATP) for cell survival under starvation conditions [357].

Virtually all cells have autophagy at low basal levels to maintain homeostatic functions such as protein and organelle turnover. Autophagy can be rapidly activated whenever cells need to generate intracellular nutrients and energy, e.g. growth factor withdrawal, starvation, or high bioenergetic demands. Autophagy is also upregulated when cells need to discard damaged cytoplasmic components, for example, during oxidative damage or infection, or to undergo structural remodeling during developmental transitions. Nutritional status, hormonal factors, and other clues like temperature, oxygen concentrations, and cell density also play a role in the control of autophagy [358-360].

In most circumstances, autophagy is a stress adaptation pathway that promotes cell survival. Besides defending cells against metabolic stress, autophagy functions include the elimination of defective proteins and organelles, the prevention of abnormal protein aggregate accumulation and the removal of intracellular pathogens. These functions are critical for autophagy-mediated protection against cancer, aging, neurodegenerative diseases, as well as infection. However, in addition to promoting cell survival, autophagy can lead to cell death. In an apparent paradox, autophagy is also considered as a form of nonapoptotic programmed cell death called “autophagic” or “type II” cell death. Autophagy role in cell death pahway in different settings has been recently shown using knockdown of Bax/Bak and *Atg* genes. Wei *et al.* showed that exposure to a variety of apoptotic stimuli does not induce apoptosis in Bax/Bak-deficient mouse embryonic fibroblasts [361]. It has been revealed, by electron microscopy, that drug treated Bax/Bak-deficient cells contain numerous double membrane vesicles. These vesicles have been confirmed to be autophagosomes as they show a punctate distribution of GFP-LC3 (GFP-LC3 is specifically concentrated on autophagosomes during autophagy while is normally spread throughout the cytoplasm in basal conditions) [352]. This nonapoptotic form of cell death was shown to be inhibited by 3-methyladenine (3-MA) and wortmannin, which suppress autophagosome formation, or by silencing Atg5 and Atg6, using several different methods [352]. Thus, these results show that autophagosome formation has a role in cell death induced by certain cytotoxic drugs, suggesting the existence of an alternative death mechanism to apoptosis termed autophagic cell death. It was also shown that a pancaspase inhibitor induces nonapoptotic death in the presence of autophagic characteristics, which is inhibited by silencing of Atg5 and Atg7 [353].

Autophagy may not be simply the result of crossing a quantitative threshold of self-digestion. In fact, cells subjected to prolonged growth factor deprivation can lose the majority of their mass via autophagy and fully recover when placed in optimal culture medium [362]. The factors that regulate whether autophagy is cytoprotective or cytotoxic, and that determine whether cytotoxicity occurs by self-cannibalism or by specific degradation of cytoprotective factors, are not yet entirely understood. Although autophagy can independently determine life and death decisions of the cell, it has also been linked to apoptotic death pathways.

The understanding of the molecular basis of autophagic death is still limited. It is currently known that autophagy depends on proteins involved in the formation of autophagosomes such as PI3 kinase type I and III [352-353]. PI3 kinase type I may be activated by growth factors such as insulin. Autophagy inhibition by PI3 kinase type I is dependent on PDK1 and AKT which regulates mammalian target of rapamycin (mTOR). It is still unclear how the activation of mTOR inhibits autophagy. This mechanism may involve phosphorylation of

Atg13, which is part of a protein complex with Atg1, a serine/threonine kinase. As mTOR is regulated by many other proteins, it is assumed that the autophagy regulation is likely to be very complex. On the contrary, PI3 kinase type III, which includes Atg6 in its complex, promotes the nucleation of autophagic vesicles whose progression is mediated by two ubiquitin-like conjugation systems: the Atg12 and the Atg8 pathways (Figure 2.14).

There are a few recent reports on the induction of autophagic cell death by photodynamic therapy although most are dealing with apoptosis-deficient cells or cells whose caspase activity has been inhibited. Due to the high reactivity of photogenerated ROS it is possible that autophagy is initiated in an attempt to remove oxidatively damaged organelles or to degrade large aggregates of cross-linked proteins, produced by photochemical reactions, which cannot be removed by the ubiquitin–proteasome system. Alternatively, the function of autophagy could be orchestrated by dedicated signaling molecules and switched from a survival to a lethal pathway in some instances.

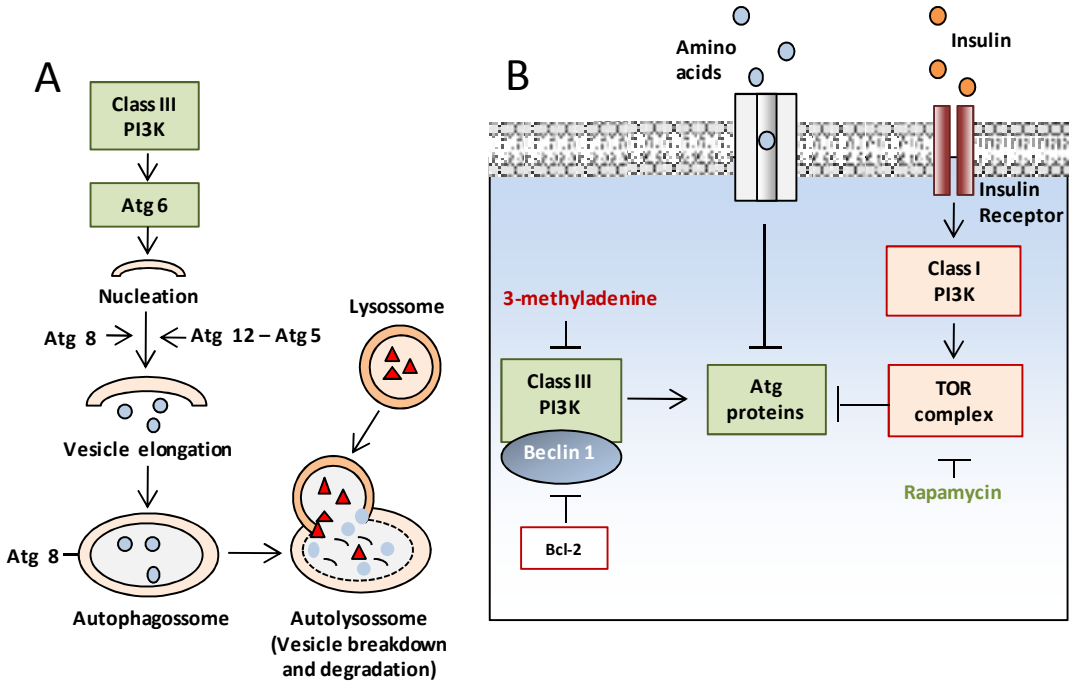

Figure 2.14 *Diagram of the autophagic process.* ***A****) The cellular events during autophagy are represented. Autophagy has distinct stages: 1) vesicle nucleation (formation of the isolation membrane/phagophore) regulated by Class III PI3K and Atg6, 2) vesicle elongation and completion (growth and closure to form the autophagosome) regulated by Atg 8 or Atg12-Atg5 complexes, 3) fusion of autophagosome with the lysosome to form an autolysosome followed by the autophagosome inner membrane lysis and breakdown of its contents.* ***B****) Shown here are some of the regulatory pathways that have been targeted pharmacologically for experimental or clinical purposes. Inhibitors and activators of autophagy are shown in red and green, respectively [adapted from Levine et al., 2008 [363]]*

Cell death modalities in hypericin-mediated PDT have been examined in wild type MEFs and in apoptosis-deficient Bax−/−Bak−/− MEFs. In these cells all the biochemical hallmarks of apoptosis are prevented while photokilling continues through the induction of a non-apoptotic cell death pathway associated with the ultrastructural and biochemical features of autophagy [364]. The blockade of autophagy by the PI3K class III inhibitor wortmannin, in apoptosis-deficient DKO cells results in a significant reduction of cell death, which evidences that PDT can stimulate an autophagic cell death pathway, at least under conditions of apoptosis inhibition**.** Further studies suggested that PDT-induced ER photodamage with a porphycene called CPO induces autophagy in both L1210 and DU145 cultures [365]. Both apoptosis and autophagy were shown to occur in L1210 cultures following PDT with CPO. In these cells there was an equilibrium between autophagy and apoptosis, with inhibition of either process leading to enhanced activity by the other. In the case of PDT with CPO it appears that the induction of autophagy leads to cell death. The basis for this death, in the context of PDT, possibly lies in the ability of CPO to photodamage Bcl-2 as its downregulation has been shown to induce/facilitate the development of autophagy [366-367]. This hypothesis is based on the observation that Bcl-2 and/or Bcl-xL can inhibit not only apoptosis but also Beclin 1-dependent autophagic cell death [368], through a direct interaction, which has been recently shown to require the BH3 domain in Beclin 1 [369]. Nevertheless, the induction of both apoptosis and autophagy occurs also in HeLa cells following hypericin-mediated PDT regardless of a reduction in the levels of expression of anti-apoptotic Bcl-2 proteins [370], thus suggesting that other molecular determinants can play a key role in this process.

Recent studies have suggested that the specific ROS-damaged subcellular site is a factor which could potentially influence the outcome of the autophagic process in PDT-treated cells. For instance, when ER is the main photo-damaged organelle and mitochondria are spared from major alterations as reported in Bax-deficient cells, autophagy could target the ER for extensive engulfment and degradation resulting in the activation of a cell death pathway [371].

2.2.2.3 *NECROTIC CELL DEATH IN PDT*

In contrast to apoptosis, necrosis has been considered as an uncontrolled form of cell death. Morphologically, necrosis is characterized by vacuolization of the cytoplasm, loss of membrane integrity and cellular swelling, as illustrated in Figure 2.12. The resulting release of intracellular components into the microenvironment can provoke an inflammatory response. Although necrosis is usually a consequence of pathological traumas such as

infection or ischemia, it can be induced by TNFα or Fas ligand *via* their respective death receptors [372]. The latter observation points to the fact that necrosis may not be such an uncontrolled form of cell death as initially suggested. Growing evidence supports a ‘‘sequence’’ of events that characterize necrotic cell death at both the morphological and biochemical levels, thereby reflecting a programmed course of events in the dying necrotic cell, and contributing to a definition of necrotic cell death. It is thus suggested that Type III PCD—programmed necrosis—is not due to a well described signaling cascade, but is the result of interplay between several signaling pathways.

The lack of caspase and lysosomal involvement distinguishes programmed necrosis from other types of PCD. Programmed necrosis is characterized by early swelling of intracellular organelles such as mitochondria, ER, and Golgi apparatus, followed by loss of plasma membrane integrity. After signaling or damage induced lesions, signs of controlled necrotic processes, such as mitochondrial dysfunction, enhanced generation of reactive oxygen species, ATP depletion, or proteolysis by calpains and cathepsins, can be observed [373]. In addition, programmed necrosis is also associated with nuclear degradation that is accompanied by the release of nuclear factors such as high mobility group box 1 (HMGB1) that triggers a potent inflammatory response [374]. Recent reports describe that this programmed necrosis is firmly regulated and, depending on the cell death system and/or PCD insult, implicates different proteins, such as TRAIL, TRADD, TRAF2, JNK1, RIP1, XRCC1, AIF, calpains, Bax, or Drp1 [375].

Death receptor-induced necrosis might depend on the kinase RIP1 (receptor-interacting protein 1). As a matter of fact, cells with downregulated RIP1 as well as RIP1-deficient Jurkat cells show partial resistance to Fas-induced cell death [376]. Receptor-interacting protein 1 likely targets the mitochondria resulting in excess formation of ROS [377]. ROS are considered to play a central role in necrosis, since the ROS scavengers efficiently prevent necrosis induced by several treatments [378-379].

Besides death receptor/triggered necrosis, DNA damage can result in necrosis as well. This necrotic death is mediated by PARP-1, a protein involved in DNA damage repair. Overactivation of this enzyme results in a drop of cellular NAD^+ and ATP, suggesting the connection with mitochondria [380]. In agreement with this hypothesis, PARP-1 activation has been shown to induce AIF translocation from the mitochondria to the nucleus, mediating a caspase independent death [381]. PARP-1-mediated necrosis has been shown to depend on the proteins RIP1, TRAF2 and JNK1 [382]. These observations altogether indicate that necrosis should no longer be exclusively viewed as an unregulated process. A regulated form of necrosis–also called necrosis-like programmed cell death – might be considered as a different type of cell death, besides accidental necrosis [383].

2.2.3 CHANGES IN CELL SIGNALING AFTER PDT

Several signal transduction pathways are activated by PDT [176]. PDT induces an acute stress reaction leading to changes in cellular metabolism which may result in cell death. Depending on certain conditions, cells subjected to PDT may die from necrosis, apoptosis or autophagy. Important signal transduction pathways determining the outcome of PDT imply mitogen activated protein kinases (MAPKs) expression, lipid metabolism effects, calcium intracellular levels, expression of transcription factors, cyclic nucleotides, cell adhesion molecules, as well as inflammatory cells and mediators (Figure 2.14). The understanding of the effect of PDT on signal transduction pathways may allow the improvement of PDT efficacy.

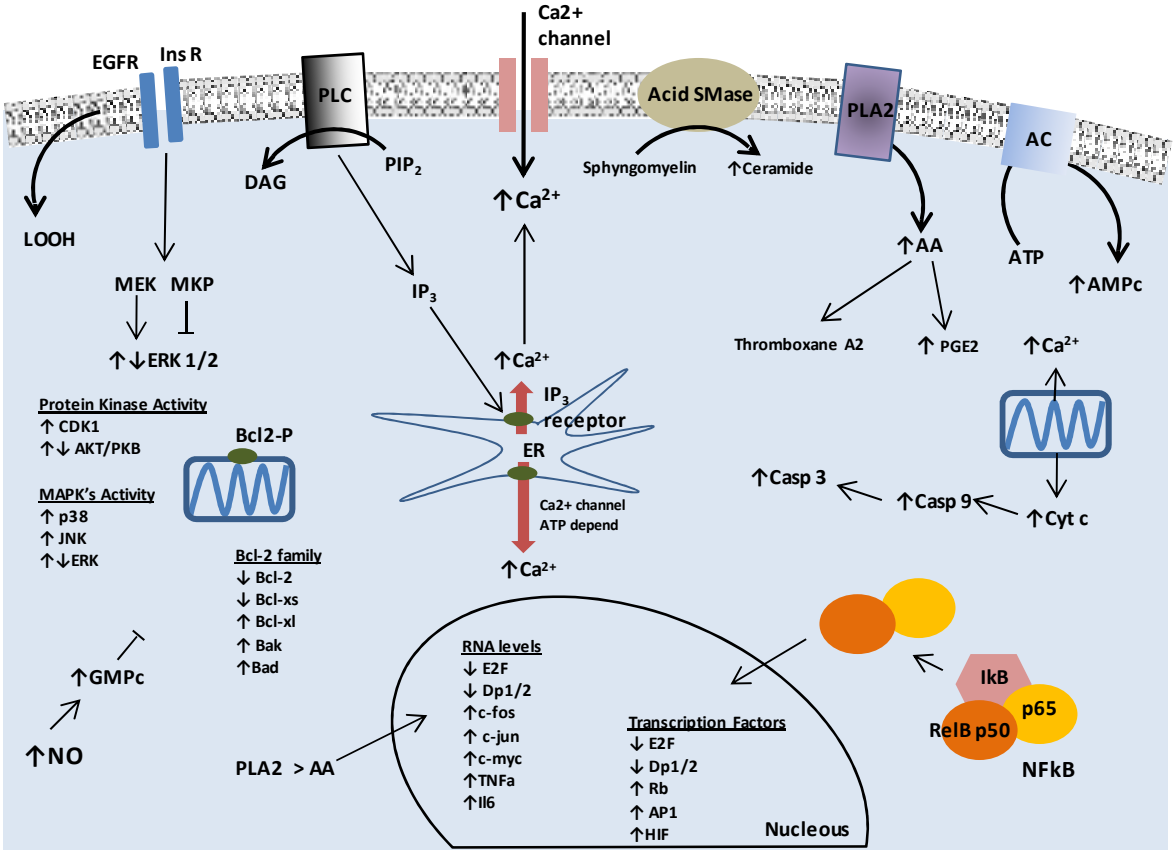

Figure 2.14 *Diagram representing some of signalling mechanisms activated in PDT-treated cells [adapted from Almeida et al., 2004 [384]]*

2.2.3.1 *ROLE OF MAPK'S MODULATION IN PDT*

The mitogen activated protein kinases (MAPKs) are a group of serine/threonine protein kinases, activated by dual phosphorylation on a tyrosine and a threonine residue. The MAPK pathway is a signaling cascade that plays a critical role in cell growth, differentiation, and cell survival through the activation of intracellular substrates including transcription factors, such as Elk-1, c-jun, and activating transcription factor 2 [385]. MAPKs are a superfamily of three related kinases that are activated by several extracellular stimuli. Three members of this family of kinases are the extracellular signal regulated kinases (ERKs), the c-Jun NH_2 terminal kinases/stress activated protein kinases (JNK/SAPKs), and the p38 MAPK. A variety of mitogenic or stress stimuli may activate ERKs leading to the production of proteins required for cell proliferation and/or differentiation [386]. In contrast, JNK and p38 are downstream members of two stress-signaling cascades. Their activation begins with autophosphorylation of a primary kinase (MAP3K), that acts on an intermediate kinase (MAP2K: M2K3/4/6 for p38; M2K4/7 for JNK) and ultimately activates the terminal MAPK [387-388]. Of the several known stress-activated MAP3Ks, apoptosis signal regulating kinase 1 (ASK1) is the best characterized in terms of regulatory mechanism. ASK1 is inactive when associated with reduced thioredoxin (Trx) or glutaredoxin (Grx), which acts as a redox sensor. Upon oxidative conversion from the dithiol to disulfide form, Trx or Grx dissociates from ASK1, thus permitting its activation and hence activation of downstream MAPKs [389-390]. JNK and p38 are activated primarily by environmental stresses such as UV light [391], heat shock [392], osmotic stress [393], hypoxia/anoxia [394] and other cellular stress [392], and participate in cell apoptosis in response to those insults [395]. Nonetheless, the role of each MAPK in cell death is dependent on the cell type and on the physiological context [385].

Reactive oxygen species induced by PDT have been shown to efficiently trigger a variety of cellular signaling pathways. The activation of MAPKs by PDT has been showed in different cell models using several photosensitizers [396]. While exposure of different types of cancer cell lines to PDT generally results in the activation of the stress-activated protein kinases JNKs and p38 MAPK, it usually causes inhibition or only transient activation of the ERKs. The activation patterns and functions of the MAPK after photochemical treatment are, however, strongly dependent of the cell type, photosensitizer, its cellular localization, and the light dose used as will be further discussed.

a) *Role of epidermal growth factor receptor/ ERKs / AKT*

One of the well-characterized MAPK signaling cascades is the pathway that induces mitogenesis upon stimulation by growth factors. The epidermal growth factor receptor (EGFR) is a tyrosine kinase involved in the initiation and progression of various cancers especially within their proliferative, angiogenic, invasive, and metastatic aspects [320]. The binding of growth factor to the receptor tyrosine kinase sequentially activates Ras and Raf. Raf then phosphorylates MEK, which in turn activates ERKs [385]. Activation of ERK has a critical role in cell proliferation and survival in many cell types. Blocking of the ERK pathway using dominant-negative mutants of ERK or using the MEK inhibitor PD98059 has been shown to abolish cell proliferation [397], enhance cell sensitivity to cisplatin treatment [398], and increase cytosine arabinoside-induced apoptosis [399]. Photodynamic therapy has been shown to exert an effect on EGFR and ERK phosphorylation. Hypericin-PDT of membrane fractions irreversibly inhibits phosphorylation of the EGFR, as well as the insulin receptor [400]. Similarly, there is an increased down-regulation of protein expression and phosphorylation of EGFR, after PDT which induces apoptosis causing a tumor regression state in metastases [401]. The true relevance of these findings on apoptosis induction must still be assessed because many non specific events might also take part in cell death at these high PDT doses. A downstream event in the mitogenic pathway is the activation of ERK, member of the MAPK family of kinases. It has been found that after PDT treatment of cells, ERK's expression is significantly decreased in relation to increased cell death [402]. Using hypericin as photosensitizer in various cell lines, Assefa *et al.* [403] showed an irreversible inhibition of EGF-induced ERK-2 activation with no direct relationship with cytotoxicity. On the contrary, in other studies it was shown that PDT has no influence on this member of the MAPK family. In this regard, Tao *et al.* [404] showed that in PAM212 cells, ERK activity is insensitive to BDP- PDT. A similar absence of effect on ERK-activation has been observed with 5-ALA based PDT in HaCaT cells [405]. Also Pc 4 - PDT in mouse lymphoma L5178Y-R cells and in CHO cells [406] did not induce ERK activation. Moreover, other recent studies shed new light on the effect of the duration of the ERK activation in the negative regulation of apoptosis. ERK activation following Photofrin-mediated PDT was functionally associated with survival of the PDT-resistant LFS087 cells, whereas ERK activation in the PDT-sensitive GM38A cells was found to be poor and very transient [407]. Hence, a rapid down-modulation of the ERK pathway which is observed with some photosensitizers may be implicated with the induction of apoptosis in photosensitized cells.

AKT is another important cell survival signal transducer that exerts its anti-apoptotic effects in a variety of ways, including phosphorylation of Bad, a pro-apoptotic protein, and inhibition of caspase-9. The phosphorylated Bad then associates with protein β−14.3.3, which sequesters Bad from Bcl-xL, thereby preventing cell death. An alternative mechanism whereby AKT promotes survival is through phosphorylation and activation of IκB kinase. The latter induces IκB degradation allowing NF-κB to enter the nucleus and to activate the transcription of anti-apoptotic genes [408]. In turn, proteins activated by phosphorylated AKT promote cell survival [409-410]. A few studies have shown that oxidative stress stimulates AKT phosphorylation. Singlet oxygen generated by Rose Bengal elicited AKT phosphorylation in mouse NIH 3T3 fibroblasts [409]. Bozkulak *et al.* also found that Photofrin-mediated PDT induced strong AKT phosphorylation while the PI3-K inhibitors blocked this response [411].

b) *Role of p38 / JNK*

Under similar conditions as those used for the study of the ERK pathway, PDT was able to activate the SAPK/JNK pathway, as well as the p38/HOG1 protein [405-406]. Activation of JNK and p38 MAPK, but not of ERK1 and ERK2, was observed for murine Pas 212 keratinocytes in response to the oxidative stress produced by photoactivation of benzoporphyrin derivative, at near cytotoxic levels [404]. Similar findings were reported for human HaCaT keratinocytes and for the hypopharyngeal carcinoma FaDu subjected to ALA-PDT [412], and in human adenocarcinoma HeLa cells treated with low hypericin-PDT doses [370, 406]. When this mode of sensitization was used, an increase in the phosphorylation (activity) of p38 MAPK was also observed in the human melanoma cell lines Bro and SkMel-23 [405]. Photoactivation of Pc 4 also increased the activity of JNK in murine LY-R leukemic lymphoblasts and CHO cells, whereas the activity of p38 MAPK was stimulated only in CHO cells. Simultaneously, a reduction in the phosphorylation of ERK2 was observed in CHO cells, but not in LY-R leukemic lymphoblasts [406]. In different models it has been shown that the SAPK/JNK pathway is involved in apoptosis induction, either *via* c-jun or *via* the phosphorylation (and thereby inactivation) of the anti-apoptotic Bcl-2 [413]. Taken together the results suggest that the role of MAPKs in PDT may depend on the cell type, the photosensitizer used and/or the light dose used. Recently, JNK activation, after pheophorbide-a based PDT, was shown to have an inhibitory effect on multidrug resistance by down-regulation of the P-glycoprotein in R-HepG2 cells [414].

c) *Role of cell line and/or photosensitizer*

As previously referred to, the available evidence suggests that the effect of PDT on the activity of MAPKs depend on the cell line and/or photosensitizer used. Tong *et al.* [407] compared the effect of Photofrin mediated PDT on the activation of MAPKs in immortalized Li–Fraumeni syndrome (LFS087) cells and in a normal human fibroblast cell line (GM38A). Immortalized Li–Fraumeni syndrome cells are more resistant to Photofrin-mediated PDT than normal human fibroblasts. They also showed a sustained activation of JNK1, p38 and ERK1/2 [415]. In contrast, photosensitization of the normal human fibroblast cell line GM38A induced a transient activation of the three MAPKs, followed by the reduction in ERK1/2 phosphorylation after the initial peak. The reduction of ERK1/2 phosphorylation was correlated with an up-regulation of mitogen-activated protein kinase phosphatase 1 (MKP-1) which dephosphorylates ERK1/2 [407]. The sustained activation of ERK1/2 in the LFS087 cell line is suggested to result from the low expression of MKP-1. Inhibition of ERK1/2 phosphorylation with PD098059 increased the sensitivity of LFS087 cells to Photofrin-mediated PDT, suggesting that this pathway protects the cells from cell death [407]. In contrast, blocking the p38 MAPK in LFS087 cells or in human adenocarcinoma HeLa cells had no effect on cell survival following Photofrin-mediated PDT [415].

Hypericin is probably the best characterized photosensitizer in terms of its effects on MAPK activity and the role of MAPKs in cell death. Photoactivated hypericin stimulated JNK and p38 MAPK activities and it produced an irreversible inhibition of the activity of ERK2 in A431 (human epidermoid carcinoma cells), human HaCaT keratinocytes, murine L929 fibroblasts and human adenocarcinoma HeLa cells [396]. The effect of photosensitization with hypericin on the activity of stress-activated kinases in human HaCaT keratinocytes was not affected by pretreatment with the antioxidant, N-acetylcysteine, [396], in contrast with the role of reactive oxygen species in the activation of JNK1 and p38 MAPK in photosensitized murine keratinocytes [404]. The biological functions associated with PDT-induced activation of MAPKs are thus controversial and complex [406].

2.2.3.2 *ROLE OF LIPID METABOLISM IN PDT*

Singlet oxygen and other ROS are powerful oxidants that can react with many biomolecules. These include unsaturated triacyl glycerols, cholesterol and phospholipids**.** Programmed cell death has been induced by a variety of oxidizing conditions, including H_2O_2 treatment [416], ionizing radiation [417], UVA radiation [418], and dye/visible light treatment [419]. Various studies have implicated lipid peroxidation in oxidant-induced programmed cell death by

showing, for example, that DNA laddering is inhibited by phenolic antioxidants [416]. Other studies have also shown that both exogenous and endogenous peroxides can trigger leukemia cell apoptosis. Similar results were obtained when HL-60 cells were photodynamically challenged using either Photofrin or aluminum phthalocyanine disulfonate as photosensitizer [419].

The extent of peroxidative injury in a photodynamically stressed cell may determine whether it ultimately survives or dies by apoptosis or necrosis [420]. This can be considered as a graded pattern of responses to membrane damage that increases in the following order: 1) no net damage when constitutive antioxidant capacity is sufficient to either prevent or repair peroxide lesions; relatively mild oxidative injury, which is sublethal and may trigger the induction of antioxidant proteins for increased cytoprotection [421-422]; 2) more extensive damage, which triggers apoptosis or autophagy after some undefined threshold has been reached, beyond which both constitutive and inducible repair capacity is exceeded; and 3) very extensive damage with membrane lysis, which abrogates any type of programmed metabolic response and leads to necrosis. In some cases, lipid peroxidation has been assigned a specific role in signal transduction based on various lines of evidence. Lipid metabolites such as arachidonate and diacylglycerol have been implicated in the upregulation of defense strategies against oxidative damage, such as heme oxygenase (HO-1) [422-423]. Lipid hydroperoxides (LOOHs) are also postulated to play an important role in cytoprotective as well as apoptotic signaling associated with the photooxidative stress. However, whether fatty-acid LOOHs or phospholipid-LOOH-derived, or by-products of chain reactions of lipid peroxidation such as 4-hydroxynonenal are also important still need clarification.

Beside inducing lipid peroxidation, PDT also modulates lipid metabolism by activating phospholipases. The rapid release of arachidonic acid metabolites has been observed in several cases after PDT and may result from the activation of phospholipase A_2, (a membrane enzyme activated by Ca^{2+}) subsequently leading to either apoptosis or survival [424]. Ceramides are other stress-induced secondary messengers that are generated from sphingophospholipids (which are part of the cell membrane) by sphingomyelinases. Ceramides may acts as secondary signal effectors molecules participating in the regulation of diverse cellular processes including apoptosis, cell senescence, cell cycle, and cellular differentiation [425]. In some *in vitro* systems, ceramide levels and apoptosis are both increased after PDT treatment. Ceramides have been shown to activate a number of enzymes involved in stress signaling cascades including both protein kinases and protein phosphatases. [320].

2.2.3.3 *ROLE OF INTRACELLULAR CALCIUM HOMEOSTASIS IN PDT*

Plasma membrane is one of the critical targets of PDT. Examination of the mechanism of cell lysis indicates that oxidative damage of membrane transport proteins induces a rapid impairment of ionic homeostasis of Na^+, K^+, Ca^{2+}, etc., while membrane integrity is still retained at this time [426]. As a result, PDT has been shown to raise the levels of total intracellular Ca^{2+} within *in vitro* cancer cells. This has been associated with cell death, or under certain conditions, with cell survival [80]. The calcium chelator BAPTA inhibited the release of cytochrome C, caspase-3 activation and apoptotic death of Chinese hamster V79 cells photosensitized with pheophorbide and of HeLa cells photosensitized with 2,4,5,7-tetrabromorhodamine indicating that Ca^{2+} plays a role in PDT-induced apoptosis [427]. However, in some cell types it was observed that elevation of the Ca^{2+} following photosensitization promotes cell survival and buffering of the intracellular Ca^{2+} enhanced cell death [428-429].

The increase in intracellular Ca^{2+} concentration after PDT treatment occurs via the influx of Ca^{2+} through ion channels, release of Ca^{2+} stored in the endoplasmic reticulum and mitochondria, and/or activation of ion exchange mechanisms [424]. Some of the differences between the stores of Ca^{2+} contributing to the Ca^{2+} rise may be due to the specificity of the photosensitizers, and particularly of their targets within the cells. As an example, phthalocyanine photosensitization was shown to cause a rapid depolarization of the plasma membrane (in less than 1 min) [426] and activation of phospholipase C [430]. Phospholipase C is a membrane bound enzyme that triggers the breakdown of phosphatidylinositol-4,5-bisphosphate leading to an intracellular release of inositol-1,4,5-trisphosphate ($I(1,4,5)P_3$) and consequent mobilization of Ca^{2+} from intracellular storage sites. Moreover, IP_3 in synergism with its phosphorylated product, $I(1,3,4,5)P_4$, enhances Ca^{2+} influx through receptor-operated Ca^{2+} channels (ROCCs) of the plasma membrane [431]. Membrane depolarization induced by PDT also contributes to stimulate the Ca^{2+} influx through voltage-operated Ca^{2+} channels (VOCCs) [426]. The plasma membrane Ca^{2+}-ATPase has a high Ca^{2+} affinity, and it was recently shown to be inactivated in cells undergoing apoptosis due to cleavage by caspases [432]. Since the effector caspases are rapidly activated in PDT, the inactivation of the plasma membrane Ca^{2+}-ATPases may also contribute to the rise in the Ca^{2+}, particularly in regions close to the plasma membrane.

An increase in intra-cytosolic Ca^{2+} activates a wide variety of cellular responses such as the release of arachidonic acid through an activation of phospholipase A_2, induction of the

protein kinase C dependent generation of superoxide radicals and condensation of chromatin around the nucleus. Increased Ca^{2+} together with the activation of protein kinase C and various clotting factors, such as PAF, convertin, Hageman and Christmas factor (Factor IX), contribute to the formation of intravascular thrombis. It has been clearly demonstrated that an increase in cytosolic Ca^{2+} stimulates the release of the von Willebrand factor [433], an adhesive glycoprotein synthesized by endothelial cells, which mediates the adhesion of platelets to the injured vessel walls. Since Ca^{2+} occupies a central role in excitation/contraction coupling in smooth muscle cells by initiating Ca^{2+}-calmodulin-dependent processes, illumination of blood vessels pretreated with a photosensitizing agent produces long-lasting contractions of the affiliated vascular smooth muscle cells [434]. Interestingly, these sustained contractions are primarily caused by an increase in the permeability of the plasma membrane to Ca^{2+} and not by an enhanced intracellular release or delayed sequestration of Ca^{2+} [434]. Chelation of extracellular Ca^{2+} with ethylenediaminetetraacetic acid (EDTA) completely inhibits the von Willebrand factor release [433] and relaxes the contracted smooth muscle cells within a few minutes [434]. All results indicate that extracellular and intracellular release of inorganic ions, such as Ca^{2+}, potentiates the cell killing effects of photosensitizing agents. Thus, Ca^{2+} is an important link between many of the pathways activated by PDT and plays a vital role in the effect of PDT.

2.2.3.4 *ROLE OF TRANSCRIPTION FACTORS EXPRESSION IN PDT*

Transcription factors are proteins which bind to enhancer regions of genes and interact such that transcription only occurs from a small group of promoters in any cell [176]. Transcription factors act as intracellular messengers between receptor-generated signals and the activation-associated changes in gene expression. They often form large transcriptional complexes with a variety of other transcription factors and accessory proteins, allowing them to participate in gene transcription modulation [320].

Activator protein-1 (AP-1) is a family of transcription factors that is activated by a variety of physical and chemical stresses. Activator protein-1 is a homo- or heterodimeric protein complex, composed of Jun (c-Jun, Jun-B, Jun-D), Fos (c-Fos, Fos-B, Fra-1, Fra-2), Maf (c-Maf, MafB, MafA, MafG/F/K and Nrl) and ATF (ATF2, LRF1/ATF3, B-ATF, JDP1, JDP2) – family proteins. Activation of AP-1 has been demonstrated for a number of tumour cell lines and for several photosensitizers [435-436]. Inhibition of protein kinases, with staurosporin, or of phospholipase A_2, with quinacrine, blocked the induction of c-fos mRNA in RIF-1 cells sensitized with Photofrin [435], suggesting that these pathways may participate in the signaling mechanisms leading to activation of early response genes contributing to cell death.

Another transcriptional factor shown to be modulated by PDT is NF-κB. Under resting conditions, the transcription factor NF-κB is present in the cytoplasm as homo- or heterodimers, formed by association of subunits belonging to a protein family that includes p50, p52, p65 (RelA), RelB and c-Rel. These complexes are sequestered in the cytoplasm by proteins belonging to the IκB family, including IκBα, IκBβ, IκBε, p100 and p105, inhibitors of NF-κB. Stimuli leading to NF-κB activation typically initiate a specific signal transduction cascade leading to phosphorylation of IκBs. Once phosphorylated, IκB is selectively ubiquitinated and degraded by the 26S proteosome, releasing NF-κB that is then translocated to the nucleus where it participates in the transcriptional activation. PDT has been shown to induce NF-κB activity in various cell models using different photosensitizers, but limited information is available concerning its role [437]. The expression of a dominant negative mutant of IκBα increased apoptotic death of HCT-116 cells photosensitized with APP, suggesting that NF-κB regulates the expression of gene(s) encoding proteins with an anti-apoptotic activity [438].

2.2.3.5 *ROLE OF CYCLIC NUCLEOTIDES IN PDT*

Nitric oxide (NO) plays an important role in tumor cell biology since it increases blood flow in the tumor, thereby promoting tumor growth and facilitating metastasis [439]. Photodynamic therapy induces NO production in the photosensitized tissues. Moreover, subcutaneous tumors generating low levels of NO were found to be more sensitive to PDT with Photofrin than those containing high levels of NO. The protective mechanism induced by NO was mediated by the activation of protein kinase G, and occurred upstream of the caspase-9 processing [440]. On the other hand, recent results indicate that the generation of NO increases the ALA-induced accumulation of protoporphyrin IX and subsequent photo-damage in cancerous cells by decreasing the levels of mitochondrial iron-containing enzymes. Based on the fact that the production of NO in some cancerous cells is elevated, NO in the cells may be responsible for the susceptibility to ALA-induced PDT [441].

Photosensitization of human bladder transitional carcinoma cells (clone T24) with HPD induced the intracellular accumulation of cAMP. This rapid and transient increase may be associated with the protective effect of cAMP against apoptotic death.

2.2.3.6 *ROLE OF CELLULAR ADHESION AND CELL COOPERATIVITY IN PDT*

Mammalian cells adhere to the extracellular matrix and to each other through specific membrane protein receptors [320]. These are classified into the following groups: selectins, cadherins, integrins and immunoglobulin G superfamily, such as intracellular cell adhesion molecule-1 (ICAM-1) and vascular cell adhesion molecule- 1 (VCAM-1). These specific membrane proteins work as signal transduction receptors triggering intracellular signaling pathways that regulate cell behavior, development, tissue inflammation as well as migration and penetration into underlying tissues. PDT was shown to induce alterations in the attachment of cancer cells to the substratum and between each other [442]. Photofrin PDT was shown to cause a dose-dependent decrease of enzymatic cell detachment by trypsin/EDTA in human glioma U251n and U87 cells [443]. These changes may be in part caused by the damage to adhesion molecules located within the cell membranes as well as the modulation of their expression. Several studies have shown that the modulation in cellular adhesion induced by PDT is directly correlated with the metastatic potential of cancer cells [444].

Another relevant aspect resulting from intercellular contact is cell cooperativity. It has been shown that cells subjected to PDT communicate [445]. This may be responsible for the formation of patches of damaged cells in PDT-treated monolayers. This observation is not due to clonal effects, but rather to “rescue” or “killing” factors transmitted between the cells. Such cooperativity, which has been demonstrated for a number of tumour cell lines and for several photosensitizers, almost certainly play a role for the efficiency of PDT and may explain the surprisingly deep necrosis sometimes observed after PDT [446].

2.2.3.7 *ROLE OF CYTOKINE EXPRESSION AND INFLAMMATORY MODULATION IN PDT*

PDT of tumors causes a rapid induction of an inflammatory response, characterized by the infiltration of leucocytes, mainly neutrophils, into the sensitized tumor. A PDT-induced generation of tumour-specific immune cells directed against both strongly and poorly immunogenic types of cancer has been reported [447]. PDT was less effective in the cure of tumours T-cell-deficient nude mice than in immune competent mice, providing evidence for the involvement of changes of the immune system in PDT-mediated tumour clearance [448].

PDT can modify the immune response and reduce the severity of experimentally induced immune diseases at doses below those that cause skin inflammation or erythema. This might result from altering the function of immune and nonimmune cell types [449-450]. Monocytes (CD14+), dendritic cells (CD83+) and Langerhans’ cells as well as activated lymphocytes bearing the interleukin-2 (IL-2) receptor (CD25) and HLA-DR are selectively sensitized by

5-ALA [451], HpD57 and verteporfin [452], whereas non-activated cells remain relatively unchanged [452]. In superficial basal cell carcinoma biopsies taken after ALA-PDT, mast cells were shown to slightly increase up to 72 h while polymorphonuclear phagocytes significantly increased at 4 h but decreased at 24 h. On the contrary, lymphocytes and macrophages gradually increased starting at baseline [453]. Photosensitized cells may undergo functional changes in receptor expression and in the release of cytokines. PDT with ALA was shown to upregulate IL-1α and downregulate the angiogenic IL-8 in nasopharyngeal carcinoma cells [454]. An upregulation of IL-6 and a decrease in IL-10 mRNA levels occurred in murine epidermal tumors treated with PDT and was accompanied by a dramatic increase in IL-10 expression in the skin [455]. It has been suggested that IL-6 has a role in the localized inflammatory effect produced by PDT and may modulate antitumour immunity [455].

PDT with ALA and other photosensitizers [456] of antigen presenting cells inhibit the immunologically mediated contact hypersensitivity response to topically applied haptens such as dinitrofluorobenzene. CHS response was also suppressed when the hapten was applied to a non-irradiated site, thereby suggesting a generalized suppression [457]. Finally, release of histamine, prostaglandin D2 and the platelet activating factor by mast cells, and release of the tumour necrosis factor by macrophages, can play a significant role in PDT effects [458].

2.3 CLINICAL APPLICATIONS OF PDT

Once limited to the treatment of superficial skin dysplasias, PDT is now utilized in broader applications. Four photosensitizing drugs have been approved in the European Union, the USA, Canada and/or Australia for the treatment of various malignancies, including cervical cancer, bladder cancer and cancers of the head and neck. Endoscopic light delivery in hollow organes has allowed PDT of advanced and early lung cancer, superficial gastric cancer and esophageal cancer. PDT has also benefited from technological advances in fiber optics, which allows precise interstitial light delivery to almost any internal tumor site in the body including large buried tumors in solid organs that would normally require extensive surgery for treatment. Now, with the appropriate optical technology, the expanded utility of PDT as a viable, broad-application treatment option for multiple types of localized malignancies and pre-malignant diseases largely depends upon improvement of the biological properties of the photosensitizers employed.

In this context, we have published two review articles (Annex II and III) in which the medical applications of PDT are discussed along with general physical principles.

2.3.1 APPROVED DERMATOLOGICAL APPLICATIONS

ALA (Levulan®) and MAL (Metvix®) have been approved by the Food and Drug Administration (USA) and by the European Community, respectively, for the photodynamic treatment of precancerous lesions [actinic keratosis (AK), Bowen's disease (BD)], superficial (sBCC) and nodular BCC (nBCC) in the skin. In accordance with international guidelines, the thickness of the tumour should not exceed 2 mm [100]. Topical PDT is particularly suitable for treatment of multiple skin lesions, extensive, often sun-exposed areas with multiple and recurring precancerous and cancerous lesions (field cancerization), areas where the cosmetic outcome is important, such as the face, neck and hands or where it is difficult to achieve a good cosmetic result using cryosurgery or excision surgery [459].
Their pharmacokinetic properties have been extensively studied and optimal treatment protocols have been defined. Levulan® (200 mg/g ALA) and Metvix® (160 mg/g MAL) are applied for 14-18 h and 3 h respectively, i.e. the time point of the highest ratio of porphyrin fluorescence depth to tumor depth, under an occlusive and light protecting dressing before irradiation with 75 J/cm^2 of red light from a high-pressure filtered lamp or 37 J/cm^2 of light from a diode lamp with an emission peak at 632 nm. Nevertheless, there are now publications reporting ALA efficacy when applied for 3 h, as with MAL [460].

Thin or moderately thick AK's are treated once. If after 3 months the effect is insufficient, the treatment is repeated with a later 3 month follow-up [461]. Hyperkeratotic AK, AK with histopathological severe atypia and AK in patients with immunosuppression are treated twice with a treatment interval of 1 week [462]. Bowen's disease and BCC are treated twice with a treatment interval of 1 week [459]. Photodynamic therapy can be repeated several times if required. Crusts and scales, if any, should be removed with keratolytic agents or curettage before applying ALA or MAL cream as the type of curettage may deeply influence results.

2.3.1.1 *ACTINIC KERATOSIS*

Actinic keratosis (AK) is a UV light–induced lesion of the skin that may progress to invasive squamous cell carcinoma. It is by far the most common skin lesion with malignant potential. The appropriate treatment of AK is generally chosen based on the number of lesions present and the efficacy of the treatment. Other variables to be consider include persistence of the lesions, age of the patient, previous history of skin cancer, and tolerability to the different

treatment modalities. Treatment consists in surgical destruction of the lesion or drug therapies, such as topical PDT, topical 5-fluorouracil (5-FU), 5% imiquimod cream and topical diclofenac gel. PDT has the advantage of allowing the treatment of large areas with many clinical and yet sub-clinical lesions.

Several randomized studies described clearance rates of 69-86% and 87-91% following a single treatment with PDT or two treatments 7 days apart, respectively. No significant difference in efficacy was evident on randomized comparison/control studies between PDT and 5-fluorouracil (5-FU) and cryotherapy. Significant superiority of cosmetic response was observed when comparing PDT with cryotherapy [463]. Thus, topical PDT is an effective therapy for thin and moderate thickness AK with a relatively poorer efficacy for acral lesions. A new stable nanoemulsion-based ALA formulation (BF-200 ALA) is currently in clinical development for PDT of AK. The efficacy and safety of PDT in the treatment of AK with BF-200 ALA have been evaluated indicating complete lesion clearance rates of 94,6% [146].

2.3.1.2 *BOWEN'S DISEASE*

Bowen disease is a squamous cell carcinoma (SCC) *in situ* with the potential for significant lateral spread. Topical PDT clears, on average, 86–93% of lesions of BD following one or two treatments. Topical MAL-PDT has recently been compared with cryotherapy or 5-FU in a multicentre randomized controlled trial (MAL 3 h, 570–670 nm, 75 J/cm^2, 70–200 mW/cm^2) [464]. Three months after last treatment, clearance rates were similar following MAL-PDT (86%), cryotherapy (82%) and 5-FU (83%). PDT gave superior cosmetic results compared with cryotherapy and 5-FU. After 24 months of follow up, 68% of lesions remained clear following PDT, 60% after cryotherapy and 59% after 5-FU. Topical PDT has been reported to be of particular interest in the treatment of BD in unusual sites (nipple, subungual) [465-466] and where it arises in a setting of poor healing (lower leg, epidermolysis bullosa and radiation dermatitis) [467-469]. It has further been shown to offer therapeutic benefit in erythroplasia of Queyrat [470].

In conclusion, topical PDT is an effective therapy for BD, with equivalence to cryotherapy and equivalence or superiority to topical 5-FU. Cosmetic outcome is superior to standard therapy. Topical PDT offers particular advantages for large/multiple patch disease and for lesions at poor healing sites. Overall, the studies on the use of ALA and MAL-PDT for the treatment of Bowen's disease have shown that PDT is at least as effective as cryotherapy and perhaps superior to 5-FU in overall clearance and response, with fewer side-effects and greater tissue sparing.

When primary cutaneous invasive SCC is considered, there is limited data on the efficacy of topical PDT. Clearance rates for superficial lesions of 54–100% have been observed following ALA and MAL-PDT but with recurrence rates ranging from 0% to 69% and reduced efficacy for the few nodular lesions treated [278]. The low efficacy of PDT on primary cutaneous invasive SCC is related to the limited depth of the therapeutic effect. In view of its metastatic potential, topical PDT cannot currently be recommended for the treatment of invasive SCC.

2.3.1.3 *BASAL CELL CARCINOMA*

Basal cell carcinoma (BCC) is the most common malignancy in humans. BCC is usually slowly growing, rarely metastasizes and has an excellent prognosis when properly treated. There are several clinical and histological subtypes, the two most frequent being the nodular and superficial BCC. Excisional surgery is conventionally regarded as the treatment of choice for BCC. Although effective, the cosmetic result following treatment is highly dependent on the anatomic site, lesion size, reconstruction method, and surgeon's expertise. BCCs being partial to head and neck need a high degree of cosmetic outcome in the therapy chosen for it.

Superficial BCCs have been reported to respond well to ALA-PDT with a clearance rate of 87%, compared with 53% for nodular lesions [278]. For nodular BCC, prior debulking curettage achieved a clearance rate of 92% compared with 0% in the control groups (curettage or PDT alone) [471]. Further attempts to increase the response rate of BCC - particularly of nodular lesions - have been performed using the more lipophilic MAL. A 5-year randomized trial compared clearance rates and cosmetic outcomes between a single session of MAL-PDT (MAL 3 h, 570–670 nm, 75 J/cm^2, 70–200 mW/cm^2) and double freeze-thaw cryotherapy in sBCC. Patients with partial response at 3 months were given 2 further MAL-PDT sessions or cryotherapy was repeated. Complete clinical response rates after 3 months' follow-up were 97% and 95% for for MAL-PDT and cryotherapy, respectively. The difference between these two treatments was not statistically significant. After 5 years' follow-up, clearance rates were similar for MAL-PDT (75%) and cryotherapy (74%). A superior cosmetic outcome was judged following PDT (87% vs. 49%) [472]. Recently, double MAL-PDT treatment cycles for 'difficult-to-treat' sBCC (large-sized lesions and/or those occurring on the mid-face or ears) were also reported. A single cycle of MAL-PDT (MAL 3h, 75J/cm^2, 570-670nm, 50-200mW/cm^2) involving 2 treatment sessions 1 week apart was performed. After a 3 months follow-up, a second cycle was performed for partially treated lesions. The complete clearance at 3 months was 85% for sBCC. After 2 years, the recurrence rate was 22% for sBCC. Ninety-four percent of patients were assessed to have a good to excellent

cosmetic outcome [473]. Another study with the same protocol examined efficacy, safety, and cosmetic outcomes in BCCs that were 'difficult-to-treat' and at high risk for surgical complications. After 3 months' follow-up, lesion complete response rate was 89% (93% sBCC and 82% nBCC). Fifteen percent of lesions had histologically confirmed recurrence within 2 years increasing to 20% within 4 years [474].

Other similar multicentre studies have focused on the PDT efficacy on nodular BCC treatment. Patients with nodular BCC received two sessions of either MAL-PDT or placebo cream plus light exposure in a randomized, double-blind controlled study. Before MAL application, lesions were surgically debulked. The overall complete response rates were 73% for MAL-PDT and 21% for placebo after 6 months [475]. MAL-PDT for nBCC was further compared with surgical excision. In patients with nBCC, two treatment sessions with MAL-PDT a week apart or surgical excision had similar overall cure rates after 3 months (91% vs. 98%). After 24 months, the recurrence rates were higher (10%) for MAL-PDT than for surgery (2%). The cosmetic outcome was good to excellent in 85% of the patients receiving MAL-PDT vs. 33% with surgery [473].

Based on these reports the British Photodermatology Group has recently concluded that topical ALA and MAL-PDT is effective for sBCC. Topical MAL–PDT is effective in nodular BCC, although with a lower efficacy than excision surgery, It may thus be considered in situations where surgery may be suboptimal. Gorlin's syndrome is a rare disease in which patients are prone to develop several lesions of BCC. Although the number of patients is small, PDT may be useful to treat patients with this disease as it leads to excellent healing and lack of scarring.

2.3.2 OFF-LABEL APPLICATIONS OF PDT WITH ALA OR MAL

The use of MAL or ALA in the photodynamic treatment of skin malignancies other than AK, BD and BCC, as well as for various infectious and inflammatory skin diseases, has been reported although they have not been approved by regulatory health authorities in Europe and USA.

2.3.2.1 *CUTANEOUS T-CELL LYMPHOMA*

Cutaneous T-cell lymphomas (CTCLs) are the largest group of cutaneous lymphomas, representing 65% of all cutaneous lymphomas. The goal of CTCL treatment is to induce remission, as there is currently no cure for this group of lymphomas. In the absence of remission, the goal is to reduce the tumor burden to some extent without compromising the already decreased immunity of the patient. Several palliative therapies have been used, with

variable efficacy rates. The choice of treatment depends on the stage of the disease, and the selected regimen must take into consideration toxicity, patient tolerance, and compliance, as well as potential benefits.

Several case reports and case series utilizing topical ALA-PDT and MAL-PDT for early stage CTCL have been published with multiple treatments usually being required for clearance [278]. Shanler *et al.* treated patch/plaque-stage cutaneous T-cell lymphoma with promising results and showed that protoporphyrin IX accumulated within lymphocytic infiltrates. Boehncke *et al.* using an argon laser at 630 nm showed inhibition of proliferation of malignant transformed T cells *in vitro* and *in vivo*. Wolf *et al.* have demonstrated the efficacy of PDT (20% 5-ALA) using a broad-spectrum source (40 J/cm^2 at 44 mW/cm^2) in two patients with CTCL who cleared after four and five PDT treatments, respectively. Complete remission is reported of four patients with CTCL IA–IIB treated with one to seven topical ALA-PDT treatments using an incoherent light source (ALA 6 h, 600–730 nm, 72–144 J/cm^2, 60–120 mW/cm^2) [476]. These patients had various histological types including two patients with CTCL, one CD30+ anaplastic large cell lymphoma and one CD8+ CTCL. Amman and Hunziker reported a poor response for an infiltrated plaque of CTCL to just one PDT treatment using an identical regimen suggesting that multiple treatments are required to obtain a complete histological response. Another report observed remission in four patients with unilesional CTCL and partial response in another following one to nine PDT treatments (MAL 3 h, 635 ± 18 nm, 37,5 J/cm^2, 86 mW/cm^2) [476]. Coors *et al.* showed a complete remission after PDT in patients with therapy-resistant lesions of CTCL. Therefore, PDT can have potential role in the treatment of localized CTCL, particularly as an additional treatment modality for patients with therapy-resistant lesions of CTCL.

2.3.2.2 *INTRAEPITHELIAL NEOPLASIA OF THE VULVA AND ANUS*

The use of topical PDT in the treatment of vulval intraepithelial neoplasia (VIN) indicates benefit with multiple treatments, with histological grade of VIN as a determinant of response. A retrospective review of different modalities for VIN observed a 48% relapse rate following PDT, comparable to rates of 42% following local excision and 40% after treatment by laser vaporization over 54 months [477]. Topical PDT has also been used to treat intraepithelial neoplasia of the anus with high recurrence rates in accordance with other tissue-preserving therapies for these indications [478].

2.3.2.3 *EXTRAMAMMARY PAGET'S DISEASE*

The use of topical PDT as monotherapy for extramammary Paget's disease (EMPD) is controversial as reports are mainly in combination with other therapies. However, clearance of EMPD lesions with ALA and MAL-PDT has been shown in several case reports [127]. In view of limited evidence and high recurrence rates, no recommendations are proposed concerning this indication.

2.3.2.4 *PHOTODYNAMIC THERAPY FOR INFECTIOUS AND INFLAMMATORY DERMATOSES*

The treatment of acne with PDT is based on the fact that *Propionibacterium acnes* contain endogenous porphyrins, in particular coproporphyrin III [479]. Therefore, visible as well as blue light phototherapy may be effective. Itoh *et al.* reported clinical benefit for several months after low-dose, single-course ALA-PDT [480]. A statistically significant reduction in inflammatory acne lesions after three courses of ALA-PDT performed within 3 weeks was also shown. However, no statistically significant reduction in P. *acnes* was observed. Therefore, it has been suggested alternative modes of action other than a mere bactericidal effect of ALA-PDT in acne [481].

Topical ALA and MAL-PDT has also been explored in nononcological indications other than acne. There is some limited evidence that inflammatory diseases such as psoriasis, sarcoidosis, localized scleroderma, as well as human papillomavirus dermatoses including condyloma acuminatum, epidermodysplasia verruciformis and verruca vulgaris may respond positively to topical PDT treatment.

2.3.2.5 *PHOTODYNAMIC THERAPY FOR SKIN CANCER PROPHYLAXIS AND SKIN REJUVENATION*

The use of PDT has also been associated with skin cancer prophylaxis and rejuvenation of the skin, namely changes in the signs of photodamage such as improvement in skin elasticity. Patients with AK who are also requesting a photorejuvenation process and organ transplant recipients are ideal candidates because they can benefit from combination treatment.

CHAPTER 3

MATERIALS AND METHODS

3.1 CHEMICALS AND BIOCHEMICAL REAGENTS

Meso-Tetrasulfonatophenylporphyrin (TPPS4) was supplied by Porphyrin Products (Logan, UT). L-Histidine (His), *meso*-tetraphenylporphyrin (TPP), hematoporphyrin, PPIX, folin reagent, 1,1',3,3'-tetraethoxypropane, thiobarbituric acid, butylated hydroxytoluene formaldehyde and protease inhibitor cocktail (P8340) were purchased from Sigma Chemical Co. (St Louis, MO). Reagents for cell culture, minimum essential medium with Earle's salts (EMEM), Hanks' balanced saline solution containing 20 mM Hepes (HBSS), Dulbecco's phosphate-buffered saline (DPBS), all without phenol red, fetal calf serum (FCS), trypsin, accutase and antibiotics were also provided by Sigma Chemical Co (St Louis, MO, USA). 1-Butanol, absolute ethanol, trichloroacetic acid, phosphoric acid, EDTA, ammonium phosphate, calcium chloride and sodium dodecyl sulfate (SDS) Triton X100 (TX100), toluene, and dimethylsulfoxide (spectroscopic grade solvents) were supplied by Merck (Darmstadt, Germany). Neutral Red (NR) was a Fluka (Saint-Quentin Fallavier, France) product. LysoTracker Green was obtained from Molecular Probes (Eugene, OR, USA). Inhibitors of p38 (SB203580) and JNK (SP600125) were purchased from Calbiochem (Darmstadt, Germany). Annexin V-FITC and specific antibodies against caspase-3, caspase-8, caspase-9 and p62/SQSTM1 were provided by Santa Cruz Biotechnology (Heidelberg, Germany) whereas those against total p38, phospho-p38, total JNK, phospho-JNK, total AKT, phospho-AKT, total ERK, phospho-ERK were purchased from Cell Signaling (Beverley, MA, USA). Mouse anti-cytochrome c antibody was purchased from BD Bioscience (Le Pont de Claix, France). Acetyl-Asp-Glu-Val-Asp-AMC (Ac- DEVD-AMC) for caspase-3, acetyl-Ile-Glu-Thr-Asp-AMC (Ac-IETD-AMC) for caspase-8 and acetyl-Leu-Glu-His-Asp-AMC (Ac-LEHD-AMC) for caspase-9 were purchased from AnaSpec, Inc (San Jose, CA, USA). All other chemicals used in this work were of the purest available grade and were used without further purification.

3.2 PORPHYRIN SYNTHESIS

Porphyrin conjugates (P-R) (Figure 1.1) have been synthesized by Professor Cavaleiro's group at the University of Aveiro (Portugal), as described by Tomé *et al.* [482-483]. The 500 μM stock solutions were prepared in water:DMSO (1:1 v/v) and stored at 0-4 °C. Since P-$(Lys)_n$ has no defined molecular weight (depending on the Lys chain polymerization and the degree of porphyrin linked) its concentration was determined assuming the same molar absorbance of the Soret band in 1% aqueous SDS for the parent porphyrin and the

conjugate P-$(Lys)_n$. Taking into account the weighed material and the spectrophotometrically determined concentration it is found that the degree of polymerization *n* is about 35.

3.3 BIOCHEMICAL AND PHYSICOCHEMICAL METHODS

3.3.1 Spectroscopic Equipment

UV/vis absorption measurements were performed with either a UVIKON 943 or a Shimadzu UV-2101PC spectrometer. Fluorescence spectra were recorded with an SLM Aminco-Bowman (series 2) (Bioritech, Chamarande, France) equipped with software for emission spectra correction. Solutions for fluorescence measurements were prepared with an absorbance ≤0.05 at the excitation wavelength (usually 407 nm). Fluorescence quantum yields (Φ_F) were determined using TPP as a reference (Φ_F = 0.12 in toluene). Porphyrin fluorescence lifetimes were measured in solutions whose absorbance was ~0.5 using optical cells whose light path was 5 mm. Lifetimes were determined with a Horiba-Jobin Yvon NanoLed single photon counting system using 200 ps laser pulses excitation at 373 nm and monitoring emission at 654 nm. The IBH software library provided the emission decay analyses.

3.3.2 Laser Flash Spectroscopy

3.3.2.1 *NANOSECOND LASER FLASH SPECTROSCOPY*

The nanosecond-laser flash spectroscopy equipment with photoelectric detection as built at the Institute of Technology of the Polytechnic University of Valence (Spain) is schematically shown on Figure 3.1.

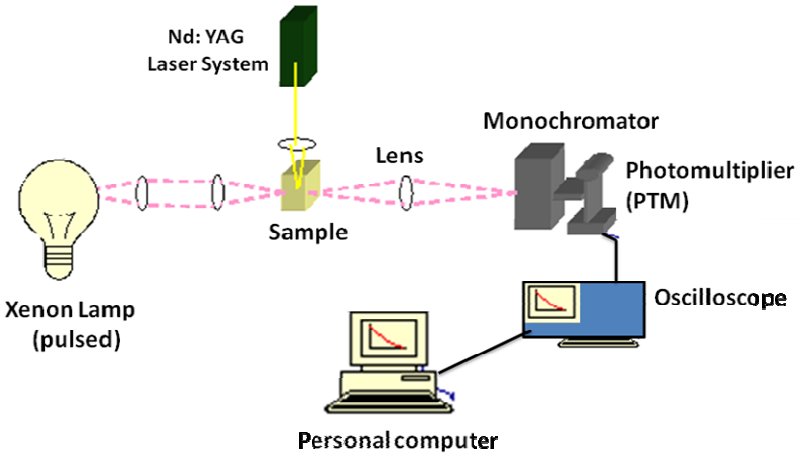

Figure 3.1 *Scheme of the nanosecond laser flash set-up.*

The analyzing light is constituted by a pulsed Lo255 Oriel xenon lamp emitting a quasi-stationary light fluence over about one millisecond. After focusing, the beam passes through the optical quartz cell (1 cm light-path) containing the solution of the photosensitizer at right angle to the path of the exciting laser pulsed beam. The third harmonic of a pulsed Nd: YAG SL404G-10 Spectrum Laser Systems is used for excitation at 355 nm. The single pulses have a ~10 ns duration (the approximate detection limit for the timescale) and the energy is ~ 10 mJ/pulse. The absorbance of the P-R samples was ~0.4 - 0.5 at the exciting laser wavelength. The short laser pulse results in the formation of transient species. At the output of the optical cell, the analyzing light is then focused on the entrance slit. The optical detection is achieved with an Oriel monochromator. The transmission of the sample before, during and after the laser pulse is thus measured by the photomultiplier which converts light into electrical signals which are acquired by a TDS-640A Tektronix oscilloscope. The output signal from the digital oscilloscope is transferred to a personal computer. Data are converted into absorbance and analyses are performed with the Kaleidagraph® software.

3.3.2.2 *FEMTOSECOND LASER FLASH SPECTROSCOPY*

While nanosecond laser flash spectroscopy deals with the study of triplet states in the µs time scale, the study of the photophysics of upper excited singlet states in tenths of picoseconds when no significant triplet state formation has taken place requires special equipment. While the basic principles are the same as those of nanospectroscopy, lenses are replaced by semi-transparent mirrors allowing the fine tuning of optical paths. Thus, the time delay between excitation and analysis is defined by the time of flight of the photons (velocity: 3×10^8 m/s) and geometry. We performed the femtosecond transient absorbance measurements at the Radiation Laboratory of the University of Notre Dame (Indiana, USA) using a Clark 6MXR 2010 laser system transient and an optical detection system provided by Ultrafast Systems (Helios). The source for the pump and probe pulses is the fundamental of the Clark laser system (775 nm, 1 mJ/pulse, FWHM = 130 fs, 1 kHz repetition rate). A second harmonic generator is introduced into the path of the laser beam to provide 387 nm (3.20 eV, 130 fs) laser pulses for the pump (excitation wavelength of the porphyrin solutions). 5% of the fundamental is diverted through a sapphire crystal whose dielectric properties allow creating a white light continuum. Before creating the white light probe, the fundamental is fed through a delay providing the experimental time window of 1.6 ns with a maximum step resolution of 7fs. The energy of the pump beam (2 mm diameter) is 5 µJ/pulse on the sample cell (2 mm light path, absorbance of the porphyrin solution: 0.3) where it merged with the

analyzing white light with an angle < 10°. Thus in contrast to nanosecond laser flash spectroscopy, the analyzing and excitation beams are nearly co-linear. It should be noted that these experimental conditions ensure that no stimulated emission is produced (see supporting information in article of Chapter 4). After passing through the cell, the white light is focused on a 200 µm core fiber connected to a CCD spectrograph enabling time-resolved spectra recording in the range 425 - 800 nm. Usually, 5000 excitation pulses are averaged to obtain the transient spectrum at a set delay time. Kinetics at appropriate wavelengths are obtained from the time resolved spectra.The 3D data are analyzed with the surface Xplorer lite software [484].

3.3.3 Measurement of Histidine degradation photosensitized by porphyrins under steady state irradiation.

The yield of singlet oxygen production by P-R under steady state irradiation was measured using histidine (His) as a specific type II photodynamic substrate [485]. Dioxygen-saturated 10 mM phosphate buffer solutions (pH 7.0) containing 500 μM His and 5 μM $TPPS_4$ (see below) or the porphyrin under study were irradiated with increasing light doses at 365 nm delivered by a filtered high-pressure mercury lamp [485]. Irradiations were performed in a 1 × 1 cm cuvette (2.5 mL). Histidine destruction was monitored by HPLC using a Whatman Partisil 10/25 SCX cation exchange column and 15 mM $NH_4H_2PO_4$ whose pH was adjusted to 2.3 by addition of phosphoric acid as a mobile phase. The TPPS4 was used as a reference photosensitizer producing singlet oxygen with a quantum yield of ~0.5. Chemical actinometry based on the photoreduction of ferrioxalate by the UV radiation was carried out according to Parker [486].

3.4 CELLULAR BIOLOGY METHODS

3.4.1 Cell line

We used in our study an immortalized NCTC 2544 human skin keratinocyte cell line purchased from ICN Flow (Fontenay sous Bois, France).

3.4.2 Cell line maintenance

The NCTC 2544 human skin keratinocytes are adherent cells which grow up to form monolayers after inoculation. A constant number of cells is reach at confluence as a result of contact cell cycle arrest. NCTC 2544 human skin keratinocytes are cultured, with passages

once a week (1:10 splitting ratio), at 37 ºC in a humidified sterile atmosphere with 95% air and 5% CO_2, using EMEM supplemented with 10% FCS, 100 U/mL penicillin and 100 µg/mL streptomycin without other additives. Just before reaching confluence, cells are washed twice with 10 ml of DPBS. Then, two ml of a solution of 0.05% trypsin containing 0.02% EDTA are added to culture flasks for 5 minutes at 37 ºC to detach adherent cells. As soon as cells are in suspension, trypsin is inhibited by adding 2 ml of 10% FCS-supplemented EMEM. The cell suspension is then divided into 10 culture flasks containing culture medium. Culture flasks are finally placed with loosened caps in an incubator at 37 ºC with a humidified sterile atmosphere with 95% air and 5% CO_2. NCTC 2544 human skin keratinocytes have a doubling time of about 1.5 days and there are approximately 1.5 x 10^7 cells per 75 cm^2 culture flask at the moment of culture division.
Stock samples of NCTC 2544 human skin keratinocytes are kept frozen in EMEM with 10% DMSO. CryoTubes are filled with the cellular suspensions and placed in a cell Cryo Freezing Container slowly frozen to -80 ºC at a cooling rate of -1 ºC/min for successful cell cryopreservation. Frozen cells are rapidly transferred to a liquid nitrogen container (-196 ºC) and stored. To maximize recovery of the cells when thawing, the cells are warmed very quickly by placing the tube directly from the liquid nitrogen container into a 37°C water bath with moderate shaking. As soon as the last ice crystal melts, the cells are immediately diluted into prewarmed 10% FCS supplemented EMEM.

3.4.3 Cell treatment

With the exception of fluorescence microscopy experiments, cells from trypsinized confluent monolayers were seeded in 35 mm diameter plastic Petri dishes at a density of about 8,000 cells/cm^2 (2.5 mL at about 30,000 cells/mL in EMEM supplemented with FCS) and were grown for 4 days reaching 60-80% of confluency. For fluorescence microscopy, cells were seeded on 30 mm diameter and 0.15 mm thick coverglass at a density of about 1,700 cells/cm^2 (2.5 mL at about 5,000 cells/mL) and were grown for 4 days.

The incubations were carried out with 1 ml of P-R at various concentrations and for various times in either HBSS or 10% FCS-supplemented EMEM, respectively for short (up to 3 h) or long incubations (up to 18h). In the case of endogenous PPIX synthesis, incubations were performed with 1ml of 0.2 to 0.8 mM ALA for 18 h in 10% FCS supplemented EMEM. After incubation with P-R or ALA, cells were washed twice with 4 mL of HBSS before measurements.

3.4.4 Irradiation

Cell monolayers were washed thoroughly with HBSS to remove any trace of photosensitizer. After washing, cells were covered with 1mL of HBSS without photosensitizer. Petri dishes were then irradiated with a broad band red light provided by a custom-built table consisting of two 300 watt tungsten- halogen lamps whose light was filtered with Balzers Y54 and Calflex 3000 optical filters [487]. Petri dishes were placed on a 30 x 25 cm thermostated (37 °C) glass table above the lamps. The present system allows the simultaneous irradiation of 15 Petri dishes (35 mm). During the irradiation period, control Petri dishes are kept in the dark under the same conditions as the irradiated cells.

Under these conditions, most of the light originates from wavelengths in the range 500 - 750 nm as determined with a CS 1000A Minolta spectroradiometer. The absolute calibration has been performed by chemical actinometry using the photodynamic degradation of 50 µM His by 20 µM hematoporphyrin in air saturated 50 mM phosphate buffer (pH 7.3). The quantum yield of His degradation is first measured under irradiation with 365 nm monochromatic light delivered by a filtered high-pressure mercury lamp as described above (section 3.3.3) [485]. Then, the His degradation is performed with red light. The relative absorbed light is equal to $S\int(\int I_\lambda(1-10^{-Abs\lambda})d\lambda)d_t$, where S is the surface of the Petri dish, Abs_λ the optical density at the wavelength λ and I_λ the relative light intensity at the wavelength λ, obtained from the radiometer. It is thus possible to calculate the absolute spectral distribution assuming that the His degradation quantum yield in the red range is similar to that at 365 nm. Presently, the integration over the wavelength range yields a light intensity of 5.0×10^{16} photon s^{-1} cm^{-2} corresponding to 15.2 mW cm^{-2}.

3.4.5 Cellular protein measurement

The protein concentration of cell extracts has been determined using the Lowry protocol. The "Lowry assay: Protein by Folin Reaction" [488] has been used to estimate the amount of proteins in biological samples. Under alkaline conditions the divalent copper (Cu^{2+}) ion forms a complex with peptide bonds in which it is reduced to a monovalent ion (Cu^{+}). Cu^{+} and the radicals of tyrosine (Tyr), tryptophan (Trp), and cysteine (Cys) react with the Folin reagent, a phospho-molybdic-phosphotungstic reagent yielding a blue color. As a result, the total concentration of protein in the sample can be deduced from the concentration of Trp, Tyr and Cys residues that reduce the Folin reagent.

Procedure:

After irradiation or sham irradiation, supernatants are collected. Cells are washed twice with 1ml of PBS, scrapped off in 400 µl of distilled water. Then, 60 µl of Tx100 (0.5%) are added. After homogenization, 150 µl of the homogenate is collected in which are added 100 µl of NaOH (0,1 N) and 2 ml of a reagent consisting of 100 mgl^{-1} of $CuSO_4.5H_2O$, 2 $g.l^{-1}$ of $C_4H_4KNaO_6.4H_2O$ and 20 $g.l^{-1}$ of Na_2CO_3. After 15 minutes, 100 µl of Folin reagent is quickly added and vortex immediately. The absorbance is measured using a multiwell plate reader at 750 nm after an incubation of 90 min at room temperature in the dark. Simultaneously, a standard curve is obtained using Human Serum Albumin.

3.4.6 Neutral Red uptake assay

The neutral red (NR) assay is based on the initial protocol described by Borenfreund and Puerner [489] that determines the active H^+ pump-dependent accumulation of the neutral red dye in the lysosomes of viable cells [490]. The incorporated dye is then liberated from the cells in an acidified ethanol solution. An increase or decrease in the number of cells or their physiological state results in a concomitant change in the amount of dye incorporated by the cells in the culture. The assessment of photocytotoxicity by the NR uptake assay has been validated by the European Union for the testing of phototoxic chemicals and for the classification and labelling of hazardous chemical (EU Commission Directive 2000/33/EC).

Procedure:

A day before the experiments, a stock solution of NR (1.4 x 10^{-2} $mol.l^{-1}$) is diluted to 1/80 in 10% FCS supplemented EMEM. This solution is placed overnight at 37 ºC in the humidified sterile atmosphere. The day of the experiment, the RN solution is centrifuged at 3000 *g* during 20 minutes to eliminate microcrystals. Three hours after treatment and/or irradiation, the culture medium is discarded by suction. Cell monolayers are then washed twice with PBS and 0.5 ml of the RN solution are added to each Petri dish. After 3 hours at 37 ºC in a humidified sterile atmosphere with 95% air and 5% CO_2 the medium is carefully removed. Cells are washed once with 1 ml of PBS and fixed with 0.5 ml of a solution of 0.4% formaldehyde and 10% $CaCl_2$. The fixative solution is removed and the incorporated dye is then solubilized in 1 ml of elution solution (acetic acid 19% and ethanol 50% (v/v) followed by gentle shaking for 10 min so that complete cell dissolution is achieved. Aliquots of the resulting solutions are transferred to 96-well plates (330 µl per well) and absorbance at 550 nm is recorded using a multiwell plate reader. The experiment is done in triplicate. Each test includes 3 blanks containing complete medium without cells to determine the background

absorbance. Results are analyzed and presented as percentage of control values. The average absorbance of untreated and un-irradiated cells is taken as 100% viability. The viability percentage after the various treatments is expressed taking this value as a reference.

3.4.7 Thiobarbituric acid reactive substances (TBARS) assay

The measurement of Thiobarbituric Acid Reactive Substances (TBARS) is a indirect method for screening and monitoring lipid peroxidation *in vitro*. Decomposition of the unstable peroxides derived from polyunsaturated fatty acids results in the formation of malondialdehyde (MDA), which can be quantified colorimetrically or fluorimetrically following its reaction with thiobarbituric acid under high temperature and acidic medium [491].

Procedure:

Immediately after irradiation or sham irradiation, 900 μl of supernatants are collected. After adding 90 μL of butylated hydroxytoluene (2% w/w in ethanol), samples are kept at -20 ºC in the dark until the day of the TBARS assay. A negative control is prepared with 900 μl of HBSS which are treated in the same way as the cell samples. Cells are scrapped on the remaining 100 μl of supernatants and collected for protein determination. The day of the TBARS assay, samples are defrosted and, again, 90 μL of butylated hydroxytoluene (2% w/w in ethanol) are added. One ml of the TBA reagent (TBA 0.375% (w/v) and TCA 15% (w/v) in hydrochloric acid 0.25 N) is, then, added to each sample. After incubation at 80 ºC for 15 min, sample solutions are placed on ice. Then, one ml of 1-butanol is added and the mixture is vigorously vortexed. The upper butanol phase is collected and centrifuged at 10000 rpm for 5 min. Finally, fluorescence intensity is measured (excitation = 515 nm, emission = 550 nm). TBARS are expressed as malondialdehyde equivalents using 1,1,3,3-tetraethoxypropane, a precursor of MDA, as a reference counpound. Results normalized to the sample protein content (pmol of MDA/mg of protein) are means ±SD of 3 experiments done in triplicate.

3.4.8 Fluorescence microscopy equipment for study of photosensitizer localization

Fluorescence microscopy is based on the phenomenon that certain cell components emit light of longer wavelengths upon irradiation with light of shorter wavelength. The cell fluorescence may arise from endogenous cell constituents (NAD(P)H, oxidized flavins, porphyrins....). Alternatively, the cell can become fluorescent after treatment with fluorescing chemicals. The basic task of the fluorescence microscope is to record the fluorescence

emission using a series of optical filters to make up the fluorescence image under excitation of cells with light of appropriate wavelength.

Procedure:

For fluorescence microscopy, sub-confluent cells (60-80% confluency) are cultured on 30 mm diameter and 0.15 mm thick coverglass. After incubation with 1 ml of P-R for 3 h in 10% FCS-supplemented EMEM cells are washed twice with 1 ml of PBS. Coverslips are incorporated into a custom-made open dish-type chamber that is compatible with fluorescence microscopy and cells are covered with 500 μl of PBS. Cell microfluorometry is then performed using an inverted fluorescence microscope (Nikon Eclipse TE 2000 DV) equipped with a CoolSNAPHQ™ detector cooled to – 30°C (Princeton Instruments; Division of Roper Scientific, Evry, France). This system is controlled by the Metaview/ Metamorph software, which is also used for image analyses. The fluorescence is recorded with a CCD camera (1392 × 1040 pixels, 8980 ×6700 μm) through a ×100 oil immersion Phaco 3 Nikon objective. A 2 × 2 binning is used to produce 696 × 520 images, corresponding to a field of about 110 × 80 μm. Fluorescence is collected through a filter block (UV2A Nikon) consisting of a dichroic mirror at 400 nm and an excitation filter in the range 330-380 nm. To record the porphyrin red fluorescence, the emission filter of the filter block is replaced by a 645AF75 filter (~610-700 nm) from Omega Optical (Brattleboro, VT, USA).

Double labeling experiments have been performed using LysoTracker, a fluorescent acidotropic probe for labeling and tracing acidic organelles, such as lysosomes in live cells. The LysoTracker dye stock solution is thawed at room temperature and protected from light. Dye solutions decompose rapidly if exposed to light. Thawed vials should not be refreezed as LysoTracker decomposes during freeze-thaw cycles. Because of the porphyrin red fluorescence, Lyso Tracker green is chosen to avoid fluorescence emission overlapping. After incubations with 1 ml of solution of 5 μM P-R for 3 h in 10% FCS-supplemented EMEM cells are washed twice with 1 ml of PBS. Coverslips are incorporated into a custom-made chamber and adherent living cells are covered with 500 μl of PBS. After LysoTracker green addition (final concentration of 125 μl), the chamber is immediately shaken to distribute the dye evenly and cells are incubated for 15 min at 37 ºC in the dark. A 535AF45 filter (~510-565 nm) from Omega Optical is used to record the LysoTracker green fluorescence. No porphyrin fluorescence is detected with the green emission filter while negligible fluorescence of the LysoTracker Green is recorded with the red emission filter. Background fluorescence obtained from cell-free areas is subtracted from all the acquired images.

3.4.9 Flow cytometry

Flow cytometry is a means of measuring certain physical characteristics, such as cell shape, size, and internal complexity, as well as chemical characteristics of cells or particles as they pass in a fluid stream through the use of a beam of laser light. Light scattering or fluorescence emission (if the particle is labeled with a fluorochrome) provides information about the particle properties. Therefore, the rapid morphological alterations that characterize the progression of programmed cell death can be monitored by flow cytometry. Apoptotic and necrotic cell death can thus be detected by flow cytometry after annexin V-FITC and propidium iodide staining.

Procedure:

At various times after photosensitization with P-R, adherent cells are washed twice in ice cold DPBS and gently detached with 500 μl of accutase. Cells are transferred to 15 mL conical tubes and gently washed with 10% FCS supplemented medium by low speed centrifugation at 1500 rpm for 5 minutes. Cell pellets are washed once with DPBS and then re-suspended in assay buffer (0.1 M HEPES/NaOH, pH 7.4; 140 mM NaCl; 25mM $CaCl_2$) at a concentration of $1x10^6$ cells/mL. Annexin V-FITC binding has been assessed using the Santa Cruz Biotechnology Apoptosis Kit (Santa Cruz Biotechnology, Heidelberg, Germany) according to the manufacturer's protocol as follows. An aliquot of the detached cell samples (100 μl) is transferred to a 5 ml culture tube. Annexin V-FITC (final concentration: 5 μg/mL) and propidium iodide (final concentration of 5 μg/mL) are then added. After 15 min of incubation in the dark at room temperature, 400 μl of assay buffer are added and cell fluorescence is measured in the spectral region 505-545 nm (FL1) for annexin V-FITC and 610-650 nm (FL3) for propidium iodide with a Cytomics FC 500 flow cytometer (Beckam Coulter, Villepinte, France). Data analysis has been performed using the Cytomics Analysis software. Untreated cells are analyzed and results displayed on a two-parameter histogram (forward-scatter on x-axis versus side-scatter on y-axis). All the living cells are gated while dead cells, subcellular debris and clumps are excluded from analysis. These are distinguished from single living cells as they have lower forward scatter and higher side scatter. Fluorescence compensation is then defined using negative control readings, e.g. no annexin V-FITC, no propidium iodide, Annexin V-FITC alone and propidium iodide alone. For annexin-FITC and propidium iodide, the spillovers are 7.4% on FL3 and 2.2% on FL1, respectively. Results are means ± SD of at least 3 independent experiments done in triplicate.

3.4.10 DNA fragmentation assay

DNA fragmentation has been assessed by determining cytoplasmic accumulation of histone associated DNA fragments using an enzyme-linked immunosorbent assay (Roche Diagnostics, Mannheim, Germany). This assay is based on the quantitative "sandwich enzyme immunoassay" principle using mouse monoclonal antibodies directed against DNA and histones. It provides specific determination of mono and oligonucleosomes in the cytoplasmic fraction of cell lysates.

Procedure:
Cells are incubated with P-R and irradiated as described above. Then, at different times after irradiation, the cell supernatant is removed and cells are washed twice with ice-cold DPBS. Both, adherent and floating cells are lysed with the kit buffer. After 30 min of incubation at room temperature, cell lysates are transferred to 2 ml Eppendorf tubes and centrifuged at 20,000 g for 10 min. The supernatant and cytoplasmic fractions are carefully removed. The pellet containing high molecular weight unfragmented DNA is discarded. The protein concentration is determined on 5 µl of the cytoplasm fraction using the method of Bradford (Bio-Rad Laboratories, Marne-la-Coquette, France). Equal amounts of protein (100 µg) from the cytoplasmic fraction are then transferred separately into an anti-histone precoated microtiter plate. After 90 min of incubation at room temperature, wells are rinsed 3 times with 300 µl of washing solution. After careful removal of the washing solution, 100 µl of conjugate solution (anti-DNA-peroxidase) are added to each well except for the blank. The conjugation solution is incubated for 90 min at room temperature after which each well is rinsed 3 times with the washing solution. The amount of peroxidase retained in the immunocomplex is determined with ABTS (2,2'-azino-di-[3-ethylbenzthiazoline sulfonate]) as a peroxidase substrate. Substrate solution is added and incubated on a plate shaker at 250 rpm until the color development is sufficient for photometric analysis (approximately 15 min). The content is homogenized by careful tapping of the plate and spectrophotometric determination is performed at 450 nm using a 96-microwell plate reader spectrophotometer. The substrate solution is used as a blank. Results are the average value of three independent experiments.

3.4.11 Caspase assays

The enzymatic activity of the caspase-3, -8 and -9 classes of proteases in P-R treated and irradiated cells has been determined by fluorometric reaction. Cells are first lysed to collect their intracellular content. The cell lysate can then be tested for protease activity by the addition of caspase-specific peptides that are conjugated to the fluorescent reporter molecule

aminomethylcoumarin (AMC). The cleavage of the peptide by caspases releases the fluorochrome that emits a fluorescence at 450 nm when excited with 350 nm light. The level of caspase enzymatic activity in the cell lysate is directly proportional to the fluorescence recorded with a fluorescent microplate reader.

Procedure:

Caspase activities are measured in cell lysates at various times after irradiation in the presence of P-R. To this end, adherent cells in 35mm Petri dishes are lysed in 50 µl of cold buffer (10 mM HEPES, pH 7.4, 2 mM EDTA, 0.1% CHAPS, 5 mM dithiothreitol and 1 mM phenylmethylsulfonyl fluoride, supplemented with 10 µg/mL pepstatin, aprotinin and leupeptin). After incubation for 10 min on ice, lysates are sonicated and centrifuged at 14000*g* for 5 min at 4°C. Supernatants are saved as representative cytosol extracts and kept on ice. The protein content of the cell lysates is estimated using the Pierce BCA assay (Thermo Fisher Scientific, Cergy Pontoise, France). We have determined that the enzymatic reaction for caspase activity is best carried out in a 96 well flat bottom microplate that can be read with a microplate reader equipped with fluorescence detection. The specific substrates stock solutions are kept as aliquots at -20 ºC. They are thawed at room temperature and freshly prepared as a 1:200 dilution in lysis buffer. Aminomethylcoumarin (AMC)-conjugated caspase substrates at a final concentration of 20 µM are then added to 40 µg of total cytosol protein and incubated for 30 min at 37 °C. The fluorescence of the coumarin dyes is measured with a 96-microwell plate reader under excitation at 360 nm and emission at 460 nm after incubation at 37°C for 90 min. The results are better expressed as the increase in caspase activity of apoptotic cells over that of non-induced cells. As the controls (substrate but no cell lysate and no substrate but cell lysate) give a substantial reading, these values are subtracted from the experimental results before calculating the increase in activity. The total reaction volume is kept constant and therefore distilled water is used to replace the volume normally occupied by either the cell lysate or the substrate reagent. The specific substrates used were: acetyl-Asp-Glu-Val-Asp-AMC (Ac- DEVD-AMC) for caspase-3, acetyl-Ile-Glu-Thr-Asp-AMC (Ac-IETD-AMC) for caspase-8 and acetyl-Leu-Glu-His-Asp-AMC (Ac-LEHD-AMC) for caspase-9.

3.4.12 Immunoblot analysis

Protein blotting is an analytical method that involves the immobilization of proteins on membranes before detection using monoclonal antibodies. In immunoblotting, sample proteins are separated using SDS polyacrylamide gel electrophoresis (SDS-PAGE) prior to protein immobilization on the nitrocellulose membranes. It provides information about

molecular weights and the potential existence of different isoforms of the proteins under study.

Procedure:

Before lysis, cells are washed twice with ice-cold DPBS. Then, they are lysed during 15 min at 4°C with 50 µl of RIPA buffer supplemented with 1% of the Sigma P8340 protease inhibitor cocktail and sonicated. After centrifugation at 14,000g for 2 min, the supernatants are saved as cell lysates and kept on ice. The protein concentration of cell extracts is determined using the Pierce BCA assay (Thermo Fisher Scientific, Cergy Pontoise, France). Equal amounts of proteins (40 µg) of the cell lysates are separated by 12% SDS – PAGE on a 10 lane cassete. After migration, the gel is carefully removed from the electrophoresis apparatus by separating the glass plates using a spatula as a lever. The stacking gel including the wells is cut off with a scalpel and discarded. The remaining separation gel is placed in a container containing transfer buffer. Great care must be taken to fully immerse the gel in the buffer. Besides, a nitrocellulose membrane, 2 Scotch Brite pads, 4 paper filters are soaked in a container containing the transfer buffer. Paper filters and the nitrocellulose membrane must be thoroughly wet. The transfer cassette is opened with the black end placed on the table. From the black side (negative electrode) to the red end, the transfer cassette is assembled in the following way: Scotch Brite pad - paper filter (Whatman) - gel - nitrocellulose membrane - paper filter (Whatman) - Scotch Brite pad. Air bubbles are squeezed out by pouring buffer and rolling after each addition. Then, the cassette is closed and placed in the transfer apparatus. After filling the transfer chamber with the transfer buffer almost to top, an ice pack and a stir bar are added, while the transfer apparatus is placed on a stir plate. Proteins are transferred onto nitrocellulose membranes at 140 V during 1 h. The transfer buffer is re-used twice.

After completion of the transfer, the membrane is removed and molecular weight bands marked using a ball-point pen. The entire membrane is submerged in Ponceau Red for 2 min until the membrane is completely red. The excess staining is then washed with deionized water long enough to detect bands. The efficiency of the migration/transfer is thus evaluated. After rinsing membranes with deionized water until the bands disappear, the nitrocellulose membranes are saturated with 5% skimmed milk in TTBS (25 mM Tris-HCl, pH 8.0, 125 mm NaCl, 0.05% Tween 20) on a shaker for 1 h at room temperature or overnight at 4 ºC. The skimmed milk solution is removed and the membranes washed 3 times with TTBS. Membranes are then immunoblotted in enough primary antibody solution (1:500 in in 5% skim milk in TTBS) to cover them and shaken for 1 h at 37 ºC. After washing 3 times with TTBS, primary antibodies are probed with their respective secondary antibody at the following dilutions: anti-goat-IgG-HRP (1:5000), anti-rabbit-IgG-HRP (1:5000) or antimouse

IgG-HRP (1:5000) for 1 h at room temperature. Secondary antibody solutions are made up in 5% skimmed milk in TTBS. Membranes are rinsed 3 times with TTBS and immunoblots are visualized using an enhanced chemiluminescence detection kit from Amersham (Saclay, France). Western blots are scanned and quantified using the software ImageJ (National Institutes of Health).

3.4.13 Cytochrome *c* immunofluorescent staining

Immunofluorescent staining consists of labeling antibodies with a fluorescent dye, allowing the labeled antibodies to react with their specific antigen. Then, the reaction product is observed under the fluorescence microscope. Several reaction sequences can be performed. The *direct* immunofluorescent staining consists in directly applying solutions of antibody labeled with a fluorescent dye (often fluorescein) to preparations containing the antigen. The *indirect* staining is carried out by first treating the preparation containing the antigen with an unlabeled specific antiserum. Then, the resulting antigen-antibody complex is revealed by treatment with a fluorescent-labeled antibody to the specific antibody. Immunofluorescent staining thus contributes to the understanding of cellular localization of specific antigens.

Procedure:

Coverslips seeded with semi-confluent cell monolayers are incubated for 3 hours with 5 µM P-OGal or for 18 h with 0.8 mM ALA. After two washings with 1 ml of PBS, coverslips are irradiated during 15 min. Depending on the protocol, coverslips are processed immediately or after addition of 2.5 ml complete culture medium. The Petri dishes are placed at 37 ºC in a humidified sterile atmosphere with 95% air and 5% CO_2. Then, cells are washed twice with DPBS, fixed for 30 min with 4% paraformaldehyde in DPBS (pH 7.4) and permeabilized with 0.1% TX100. After DPBS washing, cells are incubated with mouse anti-cytochrome c antibody (1:200) in a humidified chamber at 37°C for 30 min and then, after another washing with DPBS, incubated with Cy3- conjugated mouse anti–mouse antibody (1:100) for 30 min at room temperature. After rinsing in blocking buffer, cell nuclei are stained for 5 min with 50 µl of a 1 µg/ml solution of DAPI. The stained samples are rinsed and mounted in Mowiol (Calbiochem). All slides have been examined and photographed using a Nikon Eclipe TE2000-U fluorescence microscope equipped with a plan APO VC 60X / 1.40 objective under oil immersion. Images have been recorded with a Nikon DXM1200 CCD camera. For cytochrome c, the combination of a Nikon G-2A epifluorescence filter block and a Semrock Brightline® 617/73 emission filter has been employed, while for DAPI, a Nikon UV2A epifluorescence filter block and a Semrock Brightline® 457/50 emission filter has been used.

3.4.14 Cell transfection with GFP-LC3

The introduction of nucleic acids into eukaryotic cells by non-viral methods is defined as transfection. Several methods obviate the issue of introducing negatively charged molecules (e.g., phosphate backbones of DNA and RNA) into cells with a negatively charged plasma membrane. Chemicals like cationic lipid-based reagents (e.g. Lipofectamine 2000) coat the transfecting DNA thereby neutralizing or even creating an overall positive charge on the complex. As a consequence, the DNA transfection reagent complex can cross the membrane. Transfection can be either transient or stable. In transient transfection, foreign DNA is introduced and later eliminated by the cell prior to or during mitosis. Much more rarely, foreign DNA is introduced and enters the cell nucleus, adding to or replacing a portion of the cell's native DNA. This type of transfection, called stable transfection, transforms the cell so that the modified DNA is duplicated during mitosis. Transfection allows the study of gene function and protein expression in cells. Transient cell transfection with the microtubule-associated-protein-light-chain-3 (LC3) protein tagged at its N-terminus with green fluorescent protein (GFP), GFP-LC3, has been used to monitor autophagy through direct fluorescence microscopy.

Procedure:

The NCTC 2544 cells were grown on 18 mm coverslips and transiently transfected for 24 h with GFP-LC3 kindly provided by Drs. T. Yoshimori and N. Mizshima (Department of Bioregulation and Metabolism, The Tokyo Metropolitan Institute of Medical Science, Japan). Cells are transfected in the opti-MEM I medium supplemented with Glutamax, both agents provided by Gibco-Invitrogen (Cergy Pontoise, France), using Lipofectamine 2000 according to the supplier's protocol (Invitrogen). After 6 h of incubation, the medium is replaced by complete medium containing 10% serum and antibiotics. After transfection, cells are incubated for 3 hours with 5 µM P-OGal or for 18 h with 0.8 mM ALA and irradiated for 15 min. At various times after irradiation, cells are fixed with paraformaldehyde, rinsed and mounted on glass slides using Mowiol (Calbiochem). Cells are observed under the Nikon Eclipe TE2000-U fluorescence microscope equipped with a plan APO VC 60X / 1.40 objective under oil immersion described above for cytochrome c immunofluorescent staining but a Nikon B-2A epifluorescence filter block and a Semrock Brightline® 536/40 emission filter are used. Cells with active autophagy are defined as those displaying 3 or more puncta of GFP-LC3. Results are given under each experimental condition as percentage of cells with more than 3 puncta of GFP-LC3 over 500 cells expressing GFP-LC3

CHAPTER 4

STUDY OF THE PHOTOPHYSICAL AND PHOTOCHEMICAL PROPERTIES OF NEW TRI-CATIONIC PORPHYRIN DERIVATIVES

4.1 INTRODUCTION

Photodynamic therapy is inherently a dynamic process. At the most fundamental level the photodynamic process depends on the photosensitizer molecule itself. Notably, the behavior of the initial excited states of photosensitizers must be considered as a pre-requisite for a discussion on their photobiological activity. Thus, the first step of this study has consisted in the assessment of the photochemical and photophysical properties of the new tri-cationic porphyrin derivatives.

As it has been widely discussed in Section 1.2, several photophysical parameters may assist in fully characterizing the photosensitizers and in understanding their photobiological activities. The most relevant parameters are the excited singlet and triplet transient absorbance spectra, the singlet state lifetime (τ_S), the triplet-state lifetime (τ_T), the fluorescence quantum yield (Φ_F) and the triplet-state quantum yield (Φ_T).

4.2 OBJECTIVE

Based on the above considerations, a thorough study of the photochemical and photophysical properties of five water-soluble tricationic porphyrin conjugates has been undertaken. Their properties have been compared to those of the parent compound. Their structure is given in the General Introduction and below in Fig. 1 of Article I. The microenvironmental-dependent interactions of the various conjugated chains with the porphyrin ring in the singlet and triplet excited states have been investigated in buffer, ethanol, and negatively charged or neutral micelles. The rationale for such a study is that these solvents conditions may mimic many of the microenvironments sensed by these porphyrins upon incorporation into living tissues.

ARTICLE I

TRICATIONIC PORPHYRIN CONJUGATES: EVIDENCE FOR CHAIN-STRUCTURE-DEPENDENT RELAXATION OF EXCITED SINGLET AND TRIPLET STATE

J. Phys. Chem. B 2009, *113*, 16095–16704 16095

Tricationic Porphyrin Conjugates: Evidence for Chain-Structure-Dependent Relaxation of Excited Singlet and Triplet States

João Nuno Silva,[†,‡,||] Francisco Bosca,[⊥] João P. C. Tomé,[§] Eduardo M. P. Silva,[†] Maria G. P. M. S. Neves,[§] José A. S. Cavaleiro,[§] Larry K. Patterson,[▽] Paulo Filipe,[†] Jean-Claude Mazière,[○,◆] René Santus,[○] and Patrice Morlière*[○,◆]

Faculdade de Medicina de Lisboa, Hospital de Santa Maria, Clínica Universitária de Dermatologia, 1649-028 Lisbon, Portugal, INSERM, U histo, F-80054 Amiens, France, Université de Picardie Jules Verne, Faculté de Médecine et de Pharmacie, EA 4292, F-80036 Amiens, France, CIQU Amiens, Laboratoire de Biochimie, F-80054 Amiens, France, Universidad Politécnica de Valencia, Instituto de Tecnología Química, 46022 Valencia, Spain, Universidade de Aveiro, Departamento de Química, 3810-193 Aveiro, Portugal, University of Notre Dame, Radiation Laboratory, Notre Dame, Indiana 46556, and Muséum National d'Histoire Naturelle, RDDM, Photobiologie, F-75231 Paris, France

Received: August 17, 2009; Revised Manuscript Received: October 8, 2009

Conjugates of 5-(4-carboxyphenyl)-10,15,20-tris(4-methylpyridinium-4-yl)porphyrin (P—H) are promising photoactive agents for medical applications. As their ultimate efficacy will depend on the behavior of initial excited states, photophysical parameters have been determined with conventional steady-state absorption and fluorescence as well as time-resolved femto- and nanosecond spectroscopies. The fluorescence quantum yield of P—H and P—H conjugated to uncharged groups increases from ~0.03 in pH 7 buffer to ~0.05 in Triton X100 micelles (TX100) and in ethanol and to 0.12 in sodium dodecyl sulfate (SDS) micelles. Corresponding $^1S_1$ lifetimes are ~5–10 ns. In buffer, an equilibrium between P—H monomers and small-size aggregates is observed. Conjugation with poly-*N*-lysine (P—(Lys)$_x$) results in fluorescence quenching in all solvents. Structural reorganization of conjugates bearing a 1,2-*O*-isopropylidene-α-D-galactopyranosyl or a 1,2,3,4-di-*O*-isopropylidene-α-D-galactopyranosyl group occurs in ethanol (k_r ~0.15 ps^{-1}) after ^1S state solvation (~700 fs). Relaxation of bulky P—(Lys)$_x$ polypeptide chains takes place on a longer time scale in all solvents ($k_r \leq 0.01$ ps^{-1}) with enhanced internal conversion. Triplet state (^{3}T–T) transient spectra of all derivatives in PBS, SDS, TX100, and ethanol exhibit a strong absorbance with a broad maximum in the 460–475 nm region and minor maxima at ~540, 630, and 690 nm. In ethanol, energy transfer from the P—H $^3T_1$ state to β-carotene provides an estimate of ε ~40 000 M^{-1} cm^{-1} at 460 nm for the P—H $^3T_1$ state. Using triplet *meso*-tetraphenylporphyrin as an actinometer, the P—H triplet quantum yield (Φ_T) is estimated to be ~0.50 in all solvents. This high Φ_T leads to effective singlet oxygen production in buffered solutions.

1. Introduction

Tetrapyrrolic derivatives are ubiquitous in nature. Owing to their ability to complex a large variety of metal ions and to their extended and intense absorbances over the whole range of solar light, they have stirred numerous basic and applied studies over several decades.[1] Currently, they are the focus of ongoing investigations in several domains of public concern, in particular that of solar energy conversion as components of photochemical solar cells[2] as well as in biomedical applications.[3] Consequently, extensive research is currently under way to synthesize new derivatives and to characterize structural factors which confer unique spectroscopic and photochemical properties under differing microenvironmental conditions, e.g., those encountered in nanostructures[4] and in microheterogeneous assemblies of biological interest.[5] Our research focuses on the development of new photoactive substances suitable for therapeutic applications in dermatology. Regulatory approval has already been obtained for the treatment of malignant diseases by photodynamic therapy (PDT) involving porphyrin derivatives.[6,7] In dermatology, 5-aminolevulinic acid and its methyl ester (Metvix) the precursors of protoporphyrin IX, a potent natural photosensitizer—are currently used topically as eye-drops in the clinical treatment of various benign or malignant cutaneous lesions. These prodrugs are rather hydrophilic in nature.[8] To counter this disadvantage, the synthesis of water-soluble derivatives of porphyrins and chlorins has been undertaken. In addition to enhancing water solubility, conjugating amino acids, peptides, and sugars to porphyrins is of interest since such groups play a key role in cell metabolism and recognition, thereby facilitating specific targeting of photosensitizers to diseased cells or microorganisms.[9] Along these lines, a few new photosensitizers have been synthesized, whose water solubility is improved by conjugating polypeptide, dioxolanoxylene, and galactopyranosyl side chains at cationic *meso*-tetrasubstituted porphyrins.[5,10] Among these are examples in which a poly-*N*-lysine chain, a dioxolanoxylene group, or a 1,2-*O*-isopropylidene-α-D-galactopyranosyl moiety has been conjugated to the 5-(4-carboxyphenyl)-10,15,20-tris(1-methylpyridinium-4-yl)porphyrin (P—H) skeleton. The

* Corresponding author. Mailing address: INSERM ERI 12, Laboratoire de Biochimie, CHU Amiens—Hôpital Nord, place Victor Pauchet, 80054 Amiens Cedex 1, France. E-mail: morliere.patrice@wanadoo.fr.
† Faculdade de Medicina de Lisboa.
‡ INSERM.
§ Universidade de Aveiro.
|| CLU Amiens.
⊥ Universidad Politécnica de Valencia.
▽ University of Notre Dame.
○ Muséum National d'Histoire Naturelle.

10.1021/jp907910w CCC: $40.75 2009 American Chemical Society
Published on Web 10/27/2009

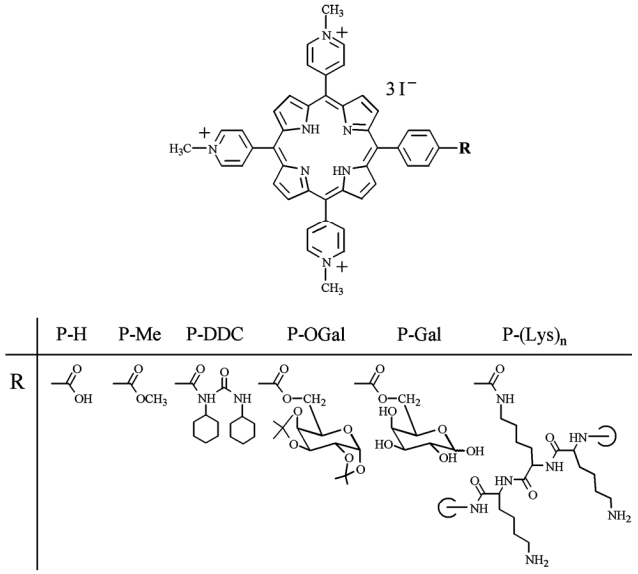

Figure 1. Names and chemical structures of 5-(4-carboxyphenyl)-10,15,20-tris(*N*-methylpyridinium-4-yl)porphyrin derivatives under study. P−H: 5-(4-Carboxyphenyl)-10,15,20-tris(*N*-methylpyridinium-4-yl)porphyrin Tri-iodide. P−Me: 5-(4-Methoxycarbonylphenyl)-10,15,20-tris(*N*-methylpyridinium-4-yl)porphyrin Tri-iodide. P−DDC: 5-[4-(*N*,*N*′-Dicyclohexylureidooxycarbonyl)phenyl]-10,15,20-tris(*N*-methylpyridinium-4-yl)porphyrin Tri-iodide. P−OGal: 5-[4-(1,2:3,4-Di-*O*-isopropylidene-α-D-galactopyranosyl-6-oxycarbonyl)phenyl]-10,15,20-tris(*N*-methylpyridinium-4-yl)porphyrin Tri-iodide. P−Gal: 5-[4-(α-D-Galactopyranosyl-6-oxycarbonyl)phenyl]-10,15,20-tris(*N*-methylpyridinium-4-yl)porphyrin Tri-iodide. P−(Lys)$_n$: Poly-L-lysine-poly-5-lysine conjugate.

resulting molecules have recently been shown to be of potential interest in dermatology and PDT, as they are able to be active in treating rapidly proliferating human skin cells in vitro (ref 11 and unpublished observations). To elucidate the markedly differing photobiological effectiveness of the water soluble tricationic porphyrin conjugates compared to the parent compound or its methyl ester, a study of their photophysical properties has been carried out. The microenvironments dependent interaction of the various conjugated groups with the porphyrin ring in singlet and triplet excited states has been investigated in both electrically neutral or negatively charged micellar media in which the first excited singlet and triplet states are formed in significant yield. Special attention has been paid to buffered aqueous solutions in which the positively charged P−H skeleton facilitates solubility. Additionally, such charge may alleviate stacking interactions between hydrophobic porphyrin macrocycles as well as static quenching of the excited states which is frequently encountered with tetrapyrrole derivatives. Indeed, a yield of at least 0.5 for $^1O_2$ formation has been obtained in buffered aqueous solutions. The species $^1O_2$ is the major cytotoxin produced by PDT.

2. Materials and Methods

2.1. Chemicals. The synthesis of P−H and of the five derivatives (P−R) under study (Figure 1) has been previously described.[9,10] Stock solutions of porphyrins (500 μM) were prepared in a water−ethanol−dimethylsulfoxide mixture (7:1:2 v/v). The concentration of the polylysine conjugate stock solution was determined in 0.1% SDS assuring the same molar absorbance as that of the parent compound at the absorbance maximum of the Soret band ($\varepsilon_{424} = 3.5 \times 10^5$ M^{-1} cm^{-1}). Tetrasulfonatophenylporphyrin (TPPS$_4$) was supplied by Porphyrin Products (Logan, UT). L-Histidine (His) and meso-tetraphenylporphyrin (TPP) were purchased from Sigma Chemical Co. (St Louis, MO). Triton X100 (TX100), sodium dodecyl sulfate (SDS), absolute ethanol, toluene, and dimethylsulfoxide (spectroscopic grade solvents) were supplied by Merck (Darmstadt, Germany). All other chemicals used in this work were of the purest available grade and were used without further purification. The phosphate buffer (10 mM, pH 7) or phosphate buffer saline (PBS) were prepared in water purified with a reverse osmosis system from Ser-A-Pure Co.

2.2. Spectroscopic Equipment. UV/vis absorption measurements were performed with either a UVIKON 943 or a Shimadzu UV-2101PC spectrometer. Fluorescence spectra were recorded with an SLM Aminco-Bowman (series 2) (Bioritech, Chamarande, France) equipped with software for emission spectra correction. Solutions for fluorescence measurements were prepared with an absorbance ≤0.05 at the excitation wavelength (usually 407 nm). Fluorescence quantum yields (Φ_F) were determined using TPP as a reference ($\Phi_F = 0.12$ in toluene).[14] Porphyrin fluorescence lifetimes were measured in solutions whose absorbance was ~0.5 and in optical cells whose light path was 5 mm. Lifetimes were determined with a Horiba-Jobin Yvon NanoLed single photon counting system using 200 ps laser pulses excitation at 373 nm and monitoring emission at 654 nm. The IBH software library provided emission decay analysis.

2.3. Laser Flash Spectroscopy. Femtosecond transient absorbance measurements were conducted at the Radiation Laboratory of the University of Notre Dame (Notre Dame, IN) using a Clark MXR 2000 laser system and an optical detection system provided by Ultrafast Systems (Florida). The source for the pump and probe pulses is the fundamental emission at 775 nm (1 mJ/pulse, fwhm = 130 fs, 1 kHz repetition rate). A second harmonic generator provides laser pump pulses at 387 nm (3.20 eV, 140 fs, 5 μJ/pulse, 2 mm diameter beam). Five percent of the fundamental is diverted through a sapphire crystal to create a white light continuum (λ = 450−750 nm) for monitoring transient absorbance changes after the pump pulse, determined by an optical delay. Measurements are carried out in a magnetically stirred sample cell (2 mm light path). A time window of 1.6 ns with a maximum step resolution of 7 fs for transient observation was used.[5] Nanosecond laser flash experiments were performed with the third harmonic (λ_{exc} = 355 nm) of a Quantel pulsed Nd:YAG spectrum laser system. Samples were contained in 10 mm × 10 mm light path cells made of Suprasil quartz and were deaerated for at least 30 min with dry nitrogen, when required. Unless otherwise stated, oxygen-free solutions were used in the experiments. Decays were generally recovered automatically averaging 5−8 shots, whereas for transient spectrum acquisition absorbance (generally 5 nm intervals) resulted from averaging 3−4 data at each wavelength. All laser spectroscopic measurements were conducted at room temperature with solutions of the porphyrins whose absorbance was ca. 0.3 (387 nm) and 0.4 (355 nm).

2.4. Photosensitized Histidine Degradation. Oxygen-saturated 10 mM phosphate buffer solutions (pH 7) containing 500 μM His and 5 μM TPPS$_4$ or the porphyrin under study were irradiated with increasing light doses at 355 nm. Histidine decay was monitored by HPLC using a Waters Partisil 10/25 SCX cation exchange column and 15 mM $NH_4H_2PO_4$ whose pH was adjusted to 2.7 by addition of phosphoric acid as a mobile phase.[16] Irradiations in a 1 cm cuvette (2.5 mL) were performed as detailed before.[16] Chemical actinometry was run on the photochemistry of ferrioxalate by the UV−vis method carried out according to Parker.[17]

TABLE 1: Absorbance (Absorption Maxima and Extinction Coefficients) and Fluorescence (Emission Maxima, Quantum Yield, and Lifetime) Parameters of P−R

		absorbance			fluorescence			
	solvent	λ_{max} (nm)	$10^{-3} \times \varepsilon$ (M^{-1} cm^{-1})		λ_{max} (nm)	λ_{max} (nm)	Φ_f	τ_f (ns)
P−H	ethanol	422 (0.0)	518 (4.7)	552 (5.9)	602 (5.7)	658 (2.2)	0.07	7.9
	buffer	431 (4.4)	515 (4.3)	592 (5.5)	638 (6.5)	699 (2.7)	0.07	9.9
	CTAC(1.0)	422 (5.5)	516 (4.8)	552 (5.9)	594 (7.5)	651 (2.2)	0.07	8.1
	SDS	426 (5.0)[a]	518 (4.6)[a]	556 (5.9)	603 (6.7)	658 (2.0)	0.09	8.7
	PBS	431 (3.6)	512 (4.3)	592 (5.2)	638 (6.5)	699 (2.7)	0.07	
P−Me	ethanol	425 (4.6)	518 (4.4)	553 (6.1)	602 (5.7)	648 (1.6)	0.07	7.7
	buffer	431 (2.0)[a]	516 (3.6)	594 (3.8)	643 (6.2)	693 (1.5)	0.04	1.6
	CTAC(1.0)	435 (3.9)	517 (3.6)	593 (6.2)	642 (5.2)	695 (1.7)	0.04	0.5
	SDS	425 (4.8)[a]	518 (4.6)[a]	555 (6.1)	595 (5.6)	650 (2.1)	0.07	3.0
	PBS	431 (2.0)[a]	512 (3.1)	593 (3.8)	643 (6.2)	693 (1.5)	0.04	
P−DDC	ethanol	425 (3.9)	518 (4.2)	554 (5.8)	602 (6.1)	648 (2.4)	0.06	7.6
	buffer	421 (4.9)	518 (4.2)	555 (5.9)	595 (7.1)	650 (2.2)	0.06	4.5
	CTAC(1.0)	435 (3.9)	517 (4.0)	593 (7.1)	638 (8.5)	694 (2.2)	0.07	10.5
	SDS	425 (3.7)	520 (3.2)	556 (5.9)	595 (7.1)	650 (2.4)	0.07	7.9
	PBS	431 (2.0)[a]	512 (3.1)	593 (3.8)	643 (6.2)	693 (1.5)	0.04	
P−OMe	ethanol	435 (3.7)	517 (4.7)	553 (7.6)	602 (6.1)	648 (2.5)	0.07	7.7
	buffer	421 (4.8)	518 (5.0)	556 (6.8)	595 (7.6)	650 (2.4)	0.06	4.0
	CTAC(1.0)	435 (3.9)[a]	517 (5.3)	593 (7.5)	642 (8.6)	695 (2.5)	0.08	10.6
	SDS	426 (5.1)	518 (5.0)	555 (7.6)	594 (8.5)	649 (2.7)	0.07	7.7
	PBS	422 (4.9)	516 (5.2)	552 (5.9)	593 (7.2)	649 (2.4)	0.07	8.1
P−CH3	ethanol	435 (3.9)[a]	517 (5.7)	551 (7.6)	599 (8.1)	648 (2.6)	0.08	7.8
	buffer	421 (5.8)	518 (5.8)	556 (6.8)	595 (7.1)	649 (2.7)	0.06	4.0
	CTAC(1.0)	422 (4.9)	518 (4.2)	554 (5.9)	594 (7.5)	650 (2.4)	0.06	10.4
	SDS	426 (5.0)	518 (5.0)	556 (6.8)	595 (7.1)	649 (2.7)	0.07	7.8
	PBS	421 (5.6)	516 (5.8)	556 (6.8)	595 (7.1)	649 (2.7)	0.06	8.0
P(py)4	ethanol	436 (3.8)[a]	516 (3.9)	551 ([illegible])	599 ([illegible])	649 (2.8)	0.08	8.1 (0.96), 8.1 (0.04)
	buffer	435 (4.0)	517 (3.4)	594 (5.0)	638 (8.1)	696 (2.7)	0.06	4.5 (0.96), 8.5 (0.04)
	CTAC(1.0)	422 (4.7)	522 (3.2)	552 (4.6)	595 (6.4)	650 (2.4)	0.06	4.2 (0.75), 8.2 (0.25)
	SDS	432 (3.9)[a]	519 (3.2)	594 (5.0)	638 (8.1)	696 (2.7)	0.07	7.7 (0.96), 8.6 (0.04)
	PBS	435 (4.0)	517 (3.4)	594 (5.0)	638 (8.0)	648 (2.7)	0.07	8.1

[a] Main emission band. [b] Minor emission band. [c] S$_1$ lifetime measured by fluorescence decay. [d] pH 7.10 mM phosphate buffer. [e] 0.5% Triton X100 in pH 7.0, 10 mM phosphate buffer. [f] 2% SDS in pH 7.0, 10 mM phosphate buffer. [g] 150 mM NaCl in pH 7.0, 10 mM phosphate buffer.

3. Results and Discussion

3.1. Properties of the First Singlet Excited State for P−H and Conjugates. *Steady-State Results.* Table 1 gives the main parameters for absorbance spectra of P−R in ethanol, pH 7 phosphate buffer, CTAC and PBS. Additionally, data from anionic (SDS) and neutral (TX100) buffered (pH 7) micellar solutions are included, as these systems provide microheterogeneous media where hydrophobic microenvironments polarity, solvent, or specific interactions between photosensitizers and biological structures. The large excess micelle concentration used here (1% SDS and 0.1% TX100) ensures that the porphyrins (5 μM) were essentially present as monomers.[18,19] In all solvents, the absorbance spectra show the characteristic features of porphyrins with strong Soret band (S$_0$ → S$_2$ transition) maxima at ≈420 nm ($\varepsilon \approx 250\,000$−$300\,000$ M^{-1} cm^{-1}) and four Q bands, with the weakly absorbing first Q$_y$ band of the S$_0$ → S$_1$ transition ($\varepsilon \approx 20\,000$ M^{-1} cm^{-1}) at ≈650 nm (Figure 2A). In all solvents, the absorbance follows the Beer−Lambert law up to concentrations of at least 10 μM. Comparison of data in Table 1 demonstrates that the absorbance maxima are less sensitive to conjugation than molar absorptivity. However, for all derivatives, absorbance maxima are shifted to the blue by a few nanometers in buffer as in PBS.

Fortunately, more specific information concerning solvent and conjugation effects on electronic states of the porphyrin can be obtained by fluorescence spectroscopy. In ethanol, the P−H fluorescence spectrum for Q derivatives is composed of two distinct bands corresponding to the S$_1$ → S$_0$ transition with the prominent emission at $\lambda_{max} \approx 650$ nm, as is generally observed with monomeric porphyrins in organic solvents (Figure 2B). The 350 cm^{-1} Stokes shift is rather large as compared to unchanged porphyrins or chlorins for which values of ≈150 cm^{-1} are generally observed in short-chain alcohols.[20] These strongly basic ethanol solutions obey the Kasha rule with two S$_2$ → S$_0$ emissions expected from substituted meso-tetraphenylporphyrins.[20,21] By contrast, a broad emission spectrum with a long emission tail extending beyond 800 nm is observed in buffer (i.e., PBS with a composition except for the solubilizing porphyrin). The fluorescence λ_{max} is shifted to the red by ≈50 nm, whereas the higher energy emission band attributed to monomers appears as a shoulder, independent of ionic strength (Table 1 and Figure 2B). However, the excitation spectra for fluorescence of all the conjugates in buffer are independent of emission wavelength and quite similar to their corresponding ground-state absorbance spectra. It is of note that the closely related 5-(4-(5-carboxy-1-butoxy-phenyl)-10,15,20-tris(1-methyl-pyridinium-4-yl)porphyrin does not exhibit such dramatic changes in fluorescence spectral shape and in Stokes shift under aqueous conditions.[22] The marked changes in the P−H fluorescence emission of all compounds except P−H (Table 1), in changing solvent from ethanol to buffer is consistent with the presence of an equilibrium between monomers and presumably small π−π porphyrin aggregates and/or nonconjugated dimers. Such behavior has been observed in neutral buffered aqueous solutions with this class of positively charged porphyrins.[23] The solvation shell of highly polar water molecules around the positive charges of the *N*-methylpyridinium side chains may not support sufficient charge−charge electrostatic repulsion between involved macrocycles to prevent hydrophobic interactions, despite the good water solubility of the tricationic porphyrins and overall compliance with the Beer−Lambert law. Altogether, the results here support to the contention that aggregation of cationic porphyrins involves both electronic and structural components.[23] Such loose stacking interactions would perturb singlet state energy levels enough to favor radiationless conversion processes. As a result, a shortening of the S$_1$ lifetime and a lower fluorescence quantum yield may be observed, as is commonly

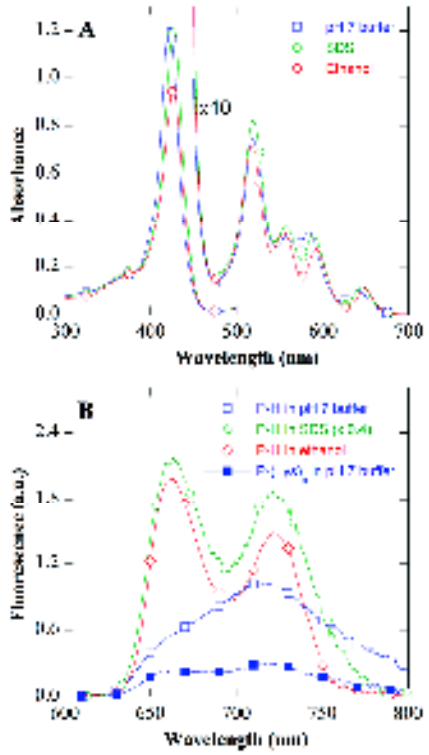

Figure 2. (A) Absorbance spectrum of 5 μM P−H in solution in 10 mM phosphate buffer (pH 7) (open blue squares), in 5% SDS containing 10 mM phosphate buffer (pH 7) (open green circles), and in ethanol (open red diamonds). Spectra were recorded at 22 °C in a 1 cm path length optical cell. (B) Fluorescence spectra of 0.1 μM P−H in 10 mM phosphate buffer (pH 7) (open blue squares, λ_{exc} = 421 nm), in 5% SDS containing 10 mM phosphate buffer (pH 7) (open green circles, λ_{exc} = 426 nm), and in ethanol (open red diamonds, λ_{exc} = 426 nm). The fluorescence of P−H in SDS is multiplied by 0.5. Fluorescence spectrum of 0.1 μM P−Lys$_{10}$ in 10 mM phosphate buffer (pH 7) (solid blue squares, λ_{exc} = 421 nm). Optical paths were 1 and 0.2 cm in excitation and in emission, respectively. Spectra were recorded at 22 °C with 1 nm slit in both light paths. The absorbance of the solutions was 0.02−0.05 at the excitation wavelength.

the case with porphyrin aggregates.[34] In the P−(Lys)$_{10}$ conjugate, however, the strong electrostatic repulsion between the heavily positively charged polylysine side chains appears large enough to electrostatically weaken interactions which lead to stacking of the saturated porphyrin rings. Both shorter spectral resolution and increased τ_F are observed (Figure 2B and Table 1). Similarly, in micellar SDS solutions, the strong electrostatic interaction of the polylysine chain with SDS micelle head groups and the large micelle excess concentration should serve to suppress ring−ring interactions, allow solubilization of P−(Lys)$_{10}$ in the aqueous phase, and lead to a higher fluorescence quantum yield (Φ_F = 0.05) (Figure S1 in the Supporting Information and Table 1). It is observed that the Φ_F of the other cationic porphyrins in SDS is twice that of P−(Lys)$_{10}$. This is probably due to the nonionic character of their conjugates' side chains allowing easier access of the macrocycle into the Stern layer as opposed to P−(Lys)$_{10}$ where the polylysine chain would tend to localize the porphyrin at the water−Stern layer interface.[35] Additionally, the enhanced water solubility of P−(Lys)$_{10}$ may cause the micelle−water distribution of this molecule to favor the water phase more than do the other conjugates. However, the positive (Lys)$_{10}$ group will interact electrostatically with the SDS micellar surface, causing stabilization. In TX100 micelles (Figure S2 in the Supporting Information), there are two possible scenarios for the incorporation of amphiphilic molecules.[36] The long hydrophilic tail of P−(Lys)$_{10}$ must extend into the aqueous phase, maintaining the porphyrin ring in the region of the micellar surface, while the other conjugates—depending on the hydrophobic character of their side chains—are probably distributed at different depths among the extended hydrophilic polyoxyethylene glycol headgroups of the TX100 palisade layer whose thickness is ~1.5 nm.[29] This region exhibits a much higher viscosity, due to the chain restriction in which the Stern layer is only a fraction of a nanometer thick.[37] This may explain the variable fluorescence lifetimes and yields in TX100 micelles. It should be noted that P−OGal and P−Gal are very sensitive to microenvironmental changes. The fluorescence of P−Gal is more markedly quenched in neutral TX100 micelles as compared to anionic SDS micelles in which the positive charges of the monosaccharide favor distribution at the micelle−water interface. By contrast, the 1-(α/β-D-galactopyranosyl-6-oxy)carbonyl tail favors incorporation into the neutral TX100 micelles. On the other hand, the replacement of adjacent OH groups by more rigid and less hydrophilic *O*-isopropylidene bridges strongly enhances the $^1S_1$ lifetime of P−OGal in both micellar systems. This heterogeneity of the microspatial polylysine chain[7] is probably responsible for the complex fluorescence decay of P−(Lys)$_{10}$ in micelles (see below). At this stage, ultrafast spectroscopic investigation may lead to a better understanding of the distinct properties of excited singlet states of conjugates in the various solvents.

Study of Excited Singlet States by Ultrafast (Femtosecond) Spectroscopy. Time-resolved ultrafast absorption spectroscopy of the lowest excited singlet state of P−H and its conjugates is of practical interest since it may reveal specific interactions of the different conjugated groups with the positively charged porphyrin ring in the $^1S_1$ state or with solvent molecules. Given that the fluorescence lifetimes of these derivatives in most solvents are of the order of several nanoseconds, there exists a spectroscopic window extending to tens of picoseconds following light absorption during which a quasi stable $^1S_1$ state is reached. During this interval, trans-ient absorption from the $^1S_1$ state to upper excited singlet states (^1S_n) of the molecules may be examined to obtain information on the type of interactions mentioned above.

Figure 3A presents transient absorbance difference spectra observed for P−H in buffer, ethanol, SDS, and TX100 micelles ~2 ps after excitation in the Soret band with a 0.15 ps, 387 nm laser light pulse. The spectral shapes of the initial absorbance difference spectra are practically independent of solvent and are very similar for unmetalated species obtained with P−Me, P−DPC, P−OGal, and P−Gal (Figure S3 in the Supporting Information). This is consistent with rather similar absorbance cross sections of these porphyrins not only for the $^1S_0 \rightarrow {}^1S_1$ (Table 1) but also for the $^1S_1 \rightarrow {}^1S_n$ transitions. An apparent absorbance maximum is observed at ~650 nm because of the strong contribution of bleaching in the Soret band resulting from the depletion of ground state molecules by the femtosecond laser pulse. In the case of the polylysine conjugate, the transient absorbance is also solvent-independent though somewhat less so, but its maximum is shifted to 475 nm (Figure 3B). In Figure 3A (cf. B), the strong negative absorbance changes in the 520−680 nm region are due to the contribution of the $^1S_1 \rightarrow {}^1S_0$ laser-induced fluorescence arising from the so-called Q_x bands of the porphyrin ring[27,28] on which is superimposed the bleaching of the weak Q_x bands and the appearance of excited singlet $S_1 \rightarrow S_n$ absorbance. It may be noted that the order of increasing intensity of the negative bands in the various solvents is qualitatively the same as that of Φ_F given in Table 1. The 387

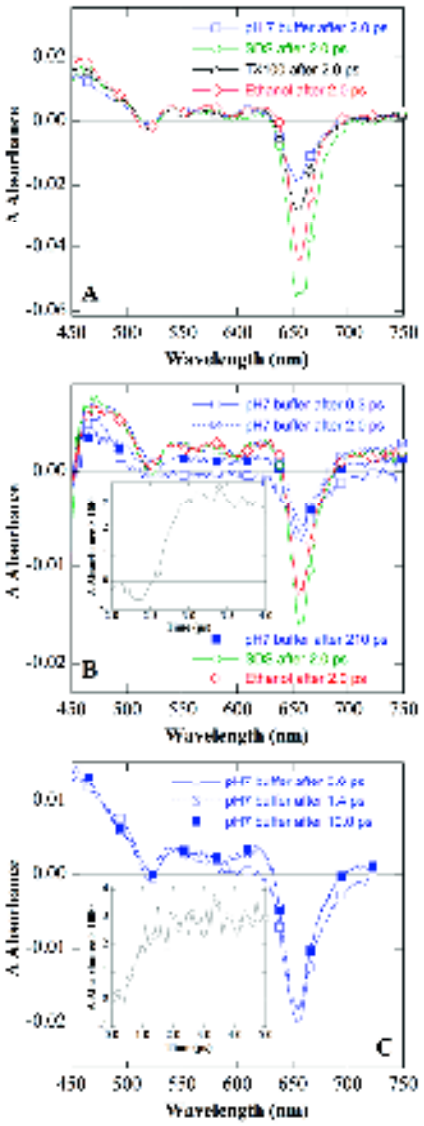

Figure 3. (A) Transient absorbance difference spectra obtained ~2 ps after femtosecond 387 nm laser flash photolysis of air-saturated solutions of P−Lys in 10 mM phosphate buffer (pH 7) (open blue squares), 1% SDS containing 10 mM phosphate buffer (pH 7) (open green circles), 0.5% TX100 containing 10 mM phosphate buffer (pH 7) (open black triangles), and ethanol (open red diamonds). (B) Transient absorbance difference spectra observed after femtosecond 387 nm laser flash photolysis of air-saturated solutions of P−Lys in 10 mM phosphate buffer, pH 7, ~0.3 ps (open blue squares), ~2 ps (open squares with + in middle), and 310 ps (solid blue squares) after laser flash, and in 1% SDS in 10 mM phosphate buffer (pH 7) (open green circles) and ethanol (open red diamonds), ~2 ps after laser flash. Inset: kinetics of growth of absorbance difference at 625 nm in buffer. (C) Transient absorbance difference spectra observed with air-saturated solutions of P−Lys in 10 mM phosphate buffer (pH 7) at ~0.9 ps (open blue squares), ~1.1 ps (blue squares with + in middle), and 10 ps (white open squares) after laser excitation. Inset: kinetics of growth of transient absorbance at 605 nm in buffer.

an light pulse directly populates high-lying vibronic states in the $^1S_2 - {}^1S_1$ region. Their relaxation leads to $^1S_1$ within ~200 fs, as previously estimated for dye molecules.[9] Hence, the negative absorbance in the 660 nm region due to the $^1S_1 \rightarrow {}^1S_0$ fluorescence appearing within the experimental time response (data not shown). In contrast to the steady-state emission spectrum, where the fluorescence λ_{max} of P−H in buffer is shifted by ~50 nm, the fluorescence λ_{max} observed by femtosecond spectroscopy is similar to that found in the three other solvents in which the fluorescence originates from the porphyrin monomer $^1S_1$ state. This λ_{max} remains constant during the experimental time window (~6 ns) (Figure 3B and C). Similar results are obtained with the other derivatives (Figure S2 in the Supporting Information). It would indicate that the formation of small aggregates of porphyrins favors effective internal conversion or migration of the excitation energy competing with [illegible] in the $^1S_1$ state of type excitonic states.

Figure 3C demonstrates that transient spectral changes are observed within 1 ps following the 0.11 ps laser flash in buffer. The narrowing of the $^1S_1 \rightarrow {}^1S_0$ emission decreases, while absorbance growths are observed in the 440−460 nm (see also initial part of kinetics in Figure 4A) and 580−750 nm regions with the appearance of a new band exhibiting a maximum at about 515 nm. Assuming monomolecular processes, a first-type rate constant $k_r = 1.5 \pm 0.3$ ps^{-1} can be estimated by kinetic analysis of data such as those shown in the inset of Figure 3C. No further change in the spectral shape is observed 1 ns after excitation. In the region of negative absorbance (e.g., ~660 nm), after the instantaneous fluorescence burst, a decrease of the negative absorbance following similar kinetics is observed due to the overlapping $^1S_n \leftarrow {}^1S_0$ transitions induced by the probe beam (data not shown). Similar results are observed with all the derivatives in all solvents (see other examples with P−dLys), and P−OGal in the insets of Figure 3B and of Figure S3 in the Supporting Information, respectively). These early spectral changes can be explained by the change of the dipole moment upon excitation of the porphyrin ring. The new local electric field generated by the excited porphyrin ring induces a reorientation of the surrounding polar solvent molecules, thereby creating a new H-bonding network surrounding the excited porphyrin-conjugated chain construct. This solvent relaxation decreases the energy of the $^1S_1$ state and produces the change observed in the transient absorbance with a rise time τ_r. In support of this explanation, it may be suggested that the $1/k_r$ value is consistent with literature values for dielectric motion of water molecules in response to charge in solute charge distribution.[9]

The same transient absorbances is observed with P−Me, P−DDC, P−OGal, and P−Gal after excitation in the Soret band. However, Figure 4A and B demonstrates that the structure of the conjugated group and the nature of the solvent can influence the decay of these transient species within a few picoseconds. In ethanol and so far, no transient decay is observed for P−H, P−Me, and P−DDC on a ~0 ps time scale (Figure 4A and B). On the other hand, in ethanol, transients from P−OGal and P−Gal conjugated to P−H by a longer and more flexible chain bearing a β-galactopyranosyl group decay by about 20% within 10 ps by a first-order process (decay rate constant ~0.15 ps^{-1}). These decays are wavelength-independent and are essentially absent in SDS and TX100 micelles (Figure 4A and B). It may be noted that conjugation with the polylysine chain increases an ultrafast decay of the singlet excited state species in all of the investigated solvents (Figure 4C). This decay occurs on a longer time scale than that observed with the conjugates P−OGal and P−Gal. It also follows more complex kinetics presumably due to the presence of a mixture of conjugates with the variable poly-ε-lysine chain length. The contribution of main first-order processes characterized by rate constants varying from ~0.01 ps^{-1} in TX100 to ~0.006 ps^{-1} in ethanol and SDS and to 0.006 ps^{-1} in buffer can be determined from the data of Figure 4B. Despite marked decay of the transient spectra originating from P−dLys, within 200 ps (Figure 3B), no major change in the transient absorbance spectra are observed for other derivatives

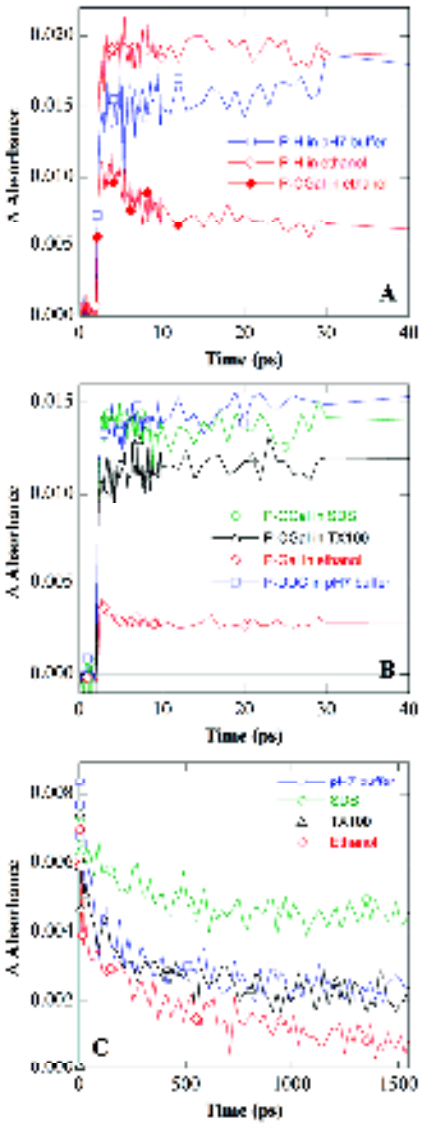

Figure 4. (A) Decays of transient absorbance at 454 nm after laser excitation (387 nm, laser fluence) of air-saturated solutions of P−H in 10 mM phosphate buffer (pH 7) (open blue squares) and ethanol (open red diamonds) and of P−OGal in ethanol (solid red diamonds). (B) Decays of transient absorbance (same following the recovery) 25 ns after laser flash photolysis of air-saturated solutions of P−OGal in 1% SDS containing 10 mM phosphate buffer (pH 7) (open green circles) and in 0.3% TX100 containing 10 mM phosphate buffer (pH 7) (open blue squares). Decays for P−H in ethanol (open red diamonds) and of P−OGal in 10 mM phosphate buffer (pH 7) (open blue squares). Decays for P−OGal and P−OGal were measured at ~450 nm, the region of apparent transient absorbance maximum for all compounds measured. For clarity of presentation, the P−Gal decay is given at 500 nm. (C) Decays of transient absorbance observed at ~435 nm after laser flash excitation of air-saturated solutions of P−(Lys)$_{20}$ in 10 mM phosphate buffer (pH 7) (open blue squares), in 1% SDS in 10 mM phosphate buffer (pH 7) (open green circles), in 0.3% TX100 in 10 mM phosphate buffer (pH 7) (open black diamonds), and in ethanol (open red triangles).

in buffer or other solvents (data not shown). In ethanol, about 80% of the P−(Lys)$_{20}$ transient species disappear within 1.5 ns, consistent with the low fluorescence quantum yield ($\Phi_f = 0.01$) reported in this solvent (Table 1).

The absence of spectral changes during the decay of the transient species originating from the original $^1S_1$ fluorescent state of P−OGal and P−Gal in ethanol suggests that these decays are not induced by photochemical changes in the porphyrin ring in the S$_1$ state. In this less polar solvent, water forms weaker hydrogen bonds as compared to water—lower excitation induces a more marked restructuring of the solvent comprised of the first solvent shell and the excited porphyrin-conjugate charge transfer. The orientation of water molecular (within the excited porphyrin ring−side chain exciplex) and/or intermolecular (within the spherical hydrogen bound networks may explain the longer lifetime of the hydrophobic bound state obtained, leading to increased energy loss by enhanced internal conversion to the ground state. In the case of P−(Lys)$_{20}$, an effective excited singlet state quenching is observed on a much longer time scale in all of the solvents. It may be suggested that full structural reorganization of the excited porphyrin ring−polylysine construct subsequent to the solvation change could require more time and consume more energy. The long poly-S-lysine chain adopts a bulky random coil conformation in buffer and a helical conformation in ethanol.[31] In micellar solutions, the bulky poly-S-lysine chain probably favors distribution of the charged porphyrin ring in the region of the water−micelle interface. However, the faster relaxation of the excited porphyrin−polylysine conjugate in TX-100 micelles suggests interaction of the Lys residues with the micelle possibly via hydrogen bonding with the oxyethylene glycol groups of the detergent molecules (Figure 4C).

3.2. Triplet State Properties of the Trientionic Porphyrins. Porphyrins can type II photodynamic agents through activation of dioxygen molecules by energy transfer from their lowest excited triplet state ($^3T_1$) to the oxygen triplet ground state giving singlet oxygen ($^1O_2$). Type I electron transfer reactions, although much less frequent, are also possible because tetrapyrroles can donate electrons to various substrates such as nitroreductases.[32] In previous studies,[17] we have shown that P−H and P−(Lys)$_{20}$ can generate $^1O_2$ and the photodynamic activity of the other conjugates toward photosensitization of human keratinocytes was found to be rather variable (unpublished observations). The characterization of triplet state parameters—such as transient absorbance spectra, lifetimes, $^3T_1$ quantum yields, and rate constants for $^3T_1$ interaction with oxygen—may assist in understanding the corresponding photobiological activities of the conjugates under study. The $^3S_1$ lifetimes of the order of ~5 to ~20 ns (Table 1) suggest that the triplet states of these trientionic porphyrins are populated with rate constants of ~10^8 s^{-1}, consistent with a $^1S_1(\pi\pi^*) \rightarrow {}^3T_1(\pi\pi^*)$ process.

Triplet State Transient Spectra. Figure 5A gives the transient absorbance difference spectra recorded ~2 μs after 355 nm laser excitation (laser flash photolysis) of P−H in ethanol, 1% SDS, and ethanol solutions. All transient species show strong absorbance with broad maxima in the 450−475 nm region and minor maxima at about 540, 580, and 660 nm corresponding to transitions between $^3T_1$ and higher triplet levels ^3T_n. Such behavior is generally observed with this class of molecules.[16,18] The strong negative absorbance observed in the region of the Soret band results from the depopulation of ground state molecules by the pulsing laser flash to produce molecules in the $^3T_1$ state. The spectral shape is practically independent of solvents, conjugation, and time delays after the laser pulse. This behavior is exemplified with P−H (Figure 5A) and the poly-S-lysine conjugate in buffer (Figure 5B). The quenching of the transient absorbance by dioxygen through second-order kinetics is consistent with its triplet nature (Table S1 and Figure S4 in the Supporting Information).

By contrast, the decay of the transient triplet absorption in N$_2$-saturated solutions strongly depends on solvent and conjugation (Table 2). One may note the rather long triplet state lifetimes

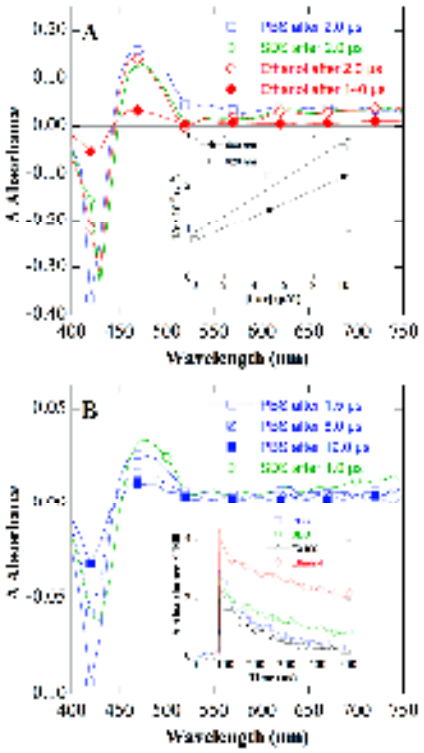

Figure 5. (A) Transient absorbance difference spectra observed 5 μs after 355 nm laser flash photolysis of N2-saturated solutions of P−H in PBS (open blue squares), 10 mM SDS containing 10 mM phosphate buffer (pH 7) (open green circles), and ethanol (open red diamonds). The transient spectrum in ethanol 450 ns after the laser flash (solid red diamonds) is included. The porphyrin concentration was 7.5 μM in all of the solutions. Inset: Reciprocal of the triplet lifetime of P−H measured at 520 nm (open black squares) and 480 nm (solid black circles) in ethanol as a function of the β-carotene concentration. Straight lines are the linear least-squares fits of the data with $y = 0.6655 + 1.9830x$ with $R = 0.97223$ at 520 nm and $y = 0.9263 + 1.1625x$ with $R = 0.99997$ at 480 nm. The porphyrin concentration was 15 μM in all solutions. (B) Transient absorbance difference spectra observed after 355 nm laser flash photolysis of N2-saturated solutions of P−(Lys)4 in PBS, 5 μs (open blue squares), 8 μs (blue squares with + in middle), and 10 μs (solid blue squares) after laser flash, and in N2-saturated solutions of 10 mM SDS containing 10 mM phosphate buffer (pH 7) (open green circles), 1 μs after laser flash. Time decays of transient absorbance at 460 nm in ethanol (open red diamonds), PBS (open blue squares), 10 mM SDS containing 10 mM phosphate buffer (pH 7) (open green circles), and 0.03% TX100 containing 10 mM phosphate buffer (pH 7) (open black triangles). The concentration of P−(Lys)4 was 2.5 μM in all solutions.

TABLE 2: Triplet State Lifetimes of P−R in Various Solvents at 20 °C

	τ_T^a (μs)			
compound	ethanol	PBS[b]	SDS[c]	TX100[d]
P−H	14.0	25.0	8.4	8.9
P−Me	4.7	56.8	45.1	30.
P−DDC	5.4	28.1	7.0	21.3
P−αGal	2. 5	1. 0	5.5	6.0
P−βGal	8.6	60.1	57.3	83
P−(Lys)4[e]	13.8−35.0	77.8−107.7	18.8−27.0	83.1−106.5

[a] Standard error on lifetimes: 10%. [b] 150 mM NaCl in pH 7, 10 mM phosphate buffer. [c] 3% SDS in pH 7, 10 mM phosphate buffer. [d] 0.03% Triton X100 in pH 7, 10 mM phosphate buffer. [e] Complex decay kinetics (see text).

in all the cases values in PBS. In all the solvents, the shortest lifetime is observed with P−OGal bearing a di-O-isopropylidene-β-galactosyl-oxyphenyl group. As mentioned above for the femtosecond spectroscopic data, such a side chain increases electronic energy loss by imposing a rigid conformation of the porphyrin ring at least in the excited states. Because of its intrinsic molecular heterogeneity, the transient originating from the poly-*S*-lysine conjugate shows complex decay kinetics illustrating the influence of structural factors in triplet state stabilization (inset of Figure S8). In all solvents, a component with a very long lifetime is observed. Very long lifetimes of 500−600 μs may be expected in micelles where binding and conformation at the water−micelle interface may slow down triplet state deactivation, such very long lived components are also recorded in ethanol and PBS. This behavior strongly suggests that the bulky conformation of the poly-*S*-lysine chains[37] hinders fast collisional processes contributing to an increased rate of return from the $^3T_1$ to the S_0 state.

These long lived triplet states, coupled to their diffusion controlled O_2 quenching rate, make possible prediction of photodynamic reactivity for the tricationic porphyrins in aqueous environments.

Determination of Molar Extinction Coefficients. Triplet identification was confirmed using 7.5 μM concentrations of P−H and conjugates. In ethanol, the $^3T_1$ states of these molecules exhibit an energy closure with β-carotene (Car) whose lowlying $^3T_1$ state energy is ≈7500 cm^{-1}. The intersystem crossing yield of Car is exceedingly small, but the β-carotene $^3T_1$ state (^{3}Car*) can be populated by energy transfer from molecules with $^3T_1$ states of energy higher than that of ^{3}Car*.[38] By this means, using the so-called comparative method, a molar extinction coefficient of ≈ 66,000 M^{-1} cm^{-1} has been determined for ^{3}Car* at 520 nm in toluene. This wavelength has two advantages, since it is close to the absorbance maximum of ^{3}Car* and the Car ground state molar absorbance at 520 nm is very low.[39] The present data have been obtained in ethanol, the only solvent common to Car and the conjugates. However, as a result of a 10 nm bathochromic shift of the Car transient spectrum in ethanol, the molar absorbance of the ^{3}Car* at 520 nm in this solvent can be estimated to be 75,000 M^{-1} cm^{-1} (Figure S8C in the Supporting Information). The demonstration of selective triplet energy transfer from the $^3T_1$ state of P−H and the most photocytotoxic conjugates P−DDC and P−OGal to ground state Car is provided in Figure S8A and S8B in the Supporting Information, showing the growth of the ^{3}Car* absorbance in the presence of 10 μM Car. The inset of Figure 5A illustrates quenching of the $^3T_1$ state of P−H by Car. The rate constants for the quenching of these ^3T states are given in Table S2 in the Supporting Information. It can be seen that the energy transfer is near equal for the P−DDC conjugated with the amphiphilic *N,N*-dicyclohexylamide tail. Considering that saturation and inner filter effects are negligible (see Supporting Information) and assuming a collisional quenching efficiency of unity for the transfer from the long lived $^3T_1$ state of P−H to produce the Car triplet, the concentration of molecules in the first excited triplet state of P−H can be obtained from which molar extinction coefficients (ε_T) are determined. By this method, the molar extinction coefficient of the $^3T_1$ state of the parent compound P−H at 480 nm, the wavelength of maximum absorbance, can be estimated to be ≈40,000 M^{-1} cm^{-1} (see Supporting Information). This is comparable to molar extinction coefficients previously reported for other porphyrins.[32,33]

Triplet Quantum Yield of P−H. With the $^3T_1$ state molar absorbance of P−H in hand, it is possible to estimate the $^3T_1$ formation quantum yield (Φ_T) by the comparative method.[39] *meso*-Tetraphenylporphyrin (TPP) can be used as an efficient standard as its Φ_T is 0.8 in toluene for which $\Delta\varepsilon_{520}$($^3T_1$)

TABLE 3: Triplet Formation Quantum Yields of P−H, P−TDDC, and P−OGal in Various Solvents at 20 °C

	Φ_T[a]			
compound	ethanol	PBS[b]	SDS[c]	TX100[d]
P−H	0.55	0.58	0.55	0.59
P−TDDC	0.56	0.59	0.55	0.62
P−OGal	0.55	0.59	0.56	0.59

[a] Φ$_T$ are given relative to that of P−H in ethanol taken as 0.55 (see text). [b] 150 mM NaCl in pH 7.4, 10 mM phosphate buffer. [c] 1% SDS in pH 7.4, 10 mM phosphate buffer. [d] 0.5% Triton X-100 in pH 7.0 10 mM phosphate buffer.

of S_0) = 35 400 M^{-1} cm^{-1} at 450 nm (data not shown).[34] To this end, a solution of TPP with an absorbance corresponding to that of 7.5 μM P−H at 488 nm was prepared in toluene. An equal population of singlet states of P−H and TPP under excitation with the same laser energy was assumed in the two solvents. The Φ_T of P−H can subsequently be estimated as the ≈0.55 in ethanol based on the maximal transient absorbance difference of TPP at a P−H in plots and a Δε value for P−H (≈40 000 M^{-1} cm^{-1} at 460 nm. Similar transient triplet absorbance spectra are observed with all of the derivatives in ethanol. As a result, P−H can be used as a secondary actinometer for the other derivatives. A Φ$_T$ value of 0.55 is probably valid for the other cationic porphyrins except for the P−Lys$_{16}$ conjugate. For the latter, an estimate of Φ_T ≈ 0.25 can be determined from data in the case of P−Lys$_{16}$ after taking into account that, under the concentration conditions used, [P−H] ≈ 2.8 [P−(Lys)$_{16}$].

Similar spectra and bandwidths are observed in all the solvents. It may thus be concluded that the absorption coefficient of the triplet does not depend markedly on the solvent and is the same (≈20 000 M^{-1} cm^{-1}). Given this assumption, the comparative method, with P−H in ethanol as the reference, allows an estimate of Φ_T for all the studied solvents.[29] No significant differences among Φ$_T$ values are observed with P−H and P−TDDC and P−OGal—the most photodynamic conjugates—given the expected experimental errors in such determinations (Table 3).[29] It is assumed that the $^3T_1$ state of P−H monomers is highly populated in buffer aqueous solutions despite the existence of monomer−aggregate equilibria.

It can be seen that in all the cases Φ$_T$ + Φ$_F$ is ≤1, suggesting the occurrence of internal conversion to S_0 state deactivation of the cationic porphyrins. This is consistent with observations from the time-resolved spectroscopy above. The contributions of solvent and conjugation effects to the nonradiative $^1S_1$ deactivation pathways can be assessed from knowledge of Φ$_T$ in Table 3 and Φ$_F$ and τ_S in Table 1. The measured mean $^1S_1$ lifetime τ_S is the reciprocal of the sum of the rate constants (k_i) for competing first-order radiative (in the presence of O_2) and nonradiative (intersystem crossing (ISC) to $^3T_1$ and internal conversion (IC) to S_0) deactivation processes, e.g., $1/\tau_S(k_{ic} + k_{isc}) = k_F + k_r$.[31,32] With P−H, P−TDDC, and P−OGal, straightforward calculations clearly show that nonradiative processes are faster in aqueous solutions (Table 4). The interaction with the Stern layer of SDS micelles restores values close to those observed with less polar ethanol, consistent with the role of the hydrogen bond network on the excited state energy dissipation. It may be noted that the contribution of the conjugate chain to the rate of nonradiative pathways is much less apparent at longer time scales, after thermal equilibration and solvation of the $^1S_1$ state. On the other hand, in ethanol, k_{ic}, k_{isc}, and k_F values for P−Lys$_{16}$ are 8.7×10^7, 3.1×10^7, and 1.7×10^7 s^{-1}, respectively. Since comparable values are obtained for P−Lys$_{16}$ in buffered solutions assuming Φ$_T$ ≈ 0.25, the almost coincident k_{ic} values suggest that preferential interaction of the bulky poly-*S*-lysine chain of random coil with the hydrophobic porphyrin ring impedes the ISC pathway in these media.

3.3. Quantum Yield of $^1O_2$ Formation by Tricationic Porphyrins in Buffered Aqueous Solutions. The formation of long-lived triplet states, quenched at a diffusion-controlled rate by oxygen (Table S1 in the Supporting Information) in surfactant aqueous solutions, suggests the production of $^1O_2$. The $^1O_2$ generation was detected using His as a specific O_2 probe, since its photosensitized oxidation occurs via a type II photodynamic mechanism in buffered aqueous solutions.[17,35] The quantity of $^1O_2$ produced was assessed using a comparative method with meso-tetrasulfonatophenylporphyrin (TPPS$_4$) as a reference water-soluble photosensitizer for which the quantum efficiency of $^1O_2$ generation in pH 7 buffer has been reported.[36,37] The 365 nm light dose-dependence of His consumption, which at low light doses follows first-order kinetics, has been monitored by HPLC analysis of irradiated solutions containing TPPS$_4$ or P−H or one of the five conjugates as a photosensitizer. The rate constants of His consumption have been normalized to the fraction of light absorbed at 365 nm, i.e., (1 − $10^{-A_{365}}$), with

TABLE 4: Calculated Rate Constants for the Nonradiative and Radiative Pathways of Deactivation of the First Singlet Excited States of P−H, P−TDDC, and P−OGal in Various Solvents at 20 °C[a]

	k_{ic} (10^7 s^{-1})			k_{isc} (10^7 s^{-1})			k_F (10^7 s^{-1})		
compound	ethanol	buffer[b]	SDS[c]	ethanol	buffer[b]	SDS[c]	ethanol	buffer[b]	SDS[c]
P−H	4.6	12.0	8.7	6.0	15.0	5.8	0.55	0.77	1.7
P−TDDC	4.3	8.0	8.5	5.9	10.4	4.5	0.49	0.66	1.7
P−OGal	5.1	11.6	8.3	6.2	11.0	5.5	0.41	0.62	1.1

[a] pH 7.4, 10 mM phosphate buffer. [b] k_F is assumed to be the same in buffer and PBS (150 mM NaCl in pH 7.4, 10 mM phosphate buffer). [c] 1% SDS in pH 7.4, 10 mM phosphate buffer.

TABLE 5: Quantum Yields of O_2 Mediated His Oxidation via the Photodynamic Action of P−H and of meso-Tetrasulfonatophenylporphyrin, at 20 °C, in PBS[a]

	$10^2 \times \Phi_{His}$[b]						
condition	P−H	P−Me	P−TDDC	P−OGal	P−Gal	P−(Lys)$_{16}$	TPPS$_4$
Ar/H_2O	0.03	0.05	0.35	0.3	0.03	0.17	
O_2/H_2O	8.6	8.0	9.0	7.6	8.1	3.6	4.4
O_2/H_2O + 0.1 M N_3^-	0.03	0.8	0.4	0.7	0.13	0.05	
O_2/D_2O	14	18	45	14	42	5.5	

[a] 150 mM NaCl in pH 7.4, 10 mM phosphate buffer. [b] The standard error is ≤10%. [c] Buffer was prepared with D_2O instead of water.

A being the absorbance of the solution at 365 nm. The presence of $^1O_2$ in these solutions has been ascertained using the classical tests.[7] Little H_2O_2 destruction is observed in Ar-saturated solutions and in O_2-saturated solutions in the presence of N_3^- ions which are effective $^1O_2$ quenchers. On the other hand, replacing H_2O by D_2O leads to an approximately 4-fold increase in the rate of H_2O_2 consumption. The quantum yields of H_2O_2 production ($\Phi_{H_2O_2}$) under various experimental conditions are reported in Table 5. It may be noted that the lower $\Phi_{H_2O_2}$ determined with P-DMC (χ_{Cl}) is consistent with its lower Φ_T. The value of $\Phi_{H_2O_2}$ with TPPS$_4$ as a photosensitizer is also provided in Table 5. As a consequence, an estimate of $\Phi_T(^1O_2)$ for all of the studied tricationic porphyrins can be determined, although there is some uncertainty in the literature concerning the $\Phi_T(^1O_2)$ of TPPS$_4$ in aqueous media. Divergent values of 0.8 and 0.4 have been reported for $\Phi_T(^1O_2)$ of TPPS$_4$ in PBS.[8,9] The $\Phi_T(^1O_2)$ obtained here with derivatives other than the poly-*N*-lysine conjugate are higher than expected in view of a Φ_T of 0.65 in buffered solutions. The uncertainty inherent to the comparative methods used for the determination of Φ_T (see above) added to that of $\Phi_T(^1O_2)$ may well explain such differences. Nevertheless, these experiments tend to show that the tricationic porphyrins under consideration very efficiently generate $^1O_2$ in aqueous media.

4. Conclusions

This work was undertaken to understand the photophysical basis for the photobiological effectiveness of P-R as photosensitizers. In the singlet excited states, these derivatives are quite sensitive to the solvation shell of both the polycationic tetrapyrrolic ring and the nature of the conjugated chain in short chain alcohols and aqueous solutions. It appears that, despite an excellent solubility in an aqueous medium, small-size oligomers like monomers and dimers of the studied tricationic porphyrins can form nonemissive intramolecular singlet state energy levels, favoring nonradiative conversion processes which result in shortening of the fluorescence lifetime and a diminished fluorescence quantum yield. In neutral aqueous solutions of the poly-*N*-lysine conjugate, strong electrostatic repulsion between the heavily positively charged polylysine side chains and the fairly positively charged porphyrin ring systems large enough to limit stacking and oligomer formation. In these latter solutions, femtosecond spectroscopy demonstrates that in the $^1S_1$ state, the conformational reorganization of guanidinium and poly-*N*-lysine conjugates induced by the change in the solvation state is very sensitive to microenvironmental factors. This behavior may be seen as a reflection of their amphiphatic character. The solvent-dependent flexibility of these conjugated chains demonstrated in the $^1S_1$ state may exist in the ground state as well. This may contribute to favored transport to and specific entrapment in intracellular sites. Such characteristics may confer peculiar photobiological activity on these conjugates. With the exception of the poly-*N*-lysine conjugate, the first excited triplet state of all the conjugates can be highly populated in a variety of microenvironments including PBS, thereby generating $^1O_2$ with a near unity quantum yield. Previous photobiological studies have shown that the P-DMC and P-OGs conjugates bearing a 4,4′ dihydroxybenzophenone-4-oxycarbonyl-1,2-butanediyl-3-oxycarbonyl chain (*O*-isoacetylidene-D-galacto-pyranosyl-6-oxycarbonyl chain, respectively, were the most effective cell photosensitizers. The present work suggests that their superior photocytotoxic activity cannot be explained in terms of a higher photodynamic efficiency. Besides promoting better penetration of the conjugates P-DMC and P-OGs (resulting from the hydrolytic, full or partial removal of the conjugated chains by cell metabolism may concurrently provide an effective way of modulating the porphyrin intracellular localization/partition within hydrophilic cytosolic sites or cell membranes, thus developing an effective photo-oxidative stress at multiple sites.

Acknowledgment. This work has been supported by a Luso-French PAUILF program (cooperation agreement between J.N.S.'s Ph.D. thesis. J.N.S., P.F., and R.S. are grateful to Prof. P. Kamat (Radiation Laboratory, University of Notre Dame) for providing access to the femtosecond laser flash spectroscopic setup and to Dr. T. Rubel of his laboratory for his advice regarding experimental details. P.F. and J.N.S. thank the Portuguese Society of Dermatology for several travel grants to the U.S. and France during the course of this study.

Supporting Information Available: Absorbance and fluorescence of conjugates. Calculation of the micelle occupancy for P-R. Additional data for femtosecond laser flash photolysis. Determination of the percent of P-R molecules excited by the femtosecond laser flash. Stern-Volmer plots of triplet quenching by dioxygen. Quenching of triplet P-R by dioxygen and β-carotene. Determination of triplet molar extinction coefficients. The numbers for tables and figures of the Supporting Information are preceded by "S". This material is available free of charge via the Internet at http://pubs.acs.org.

References and Notes

(1) *The Porphyrin Handbook*; Kadish, K., Smith, K. M., Guilard, R., Eds.; Academic Press: San Diego, CA, 1999; Vol. 1–10, pp 1–3069.
(2) Sankar, P. V. *J. Phys. Chem. C* **2007**, *111*, 2831–2860.
(3) [illegible]. *Photochem. Photobiol.* **1999**, *58*, 935–941.
(4) Majjesson, P.; Bonneau, S.; Brault, D. *Eur. Biophys. J.* **2007**, *36*, 943–953.
(5) Juzeniene, A.; Peng, Q.; Moan, J. *Photochem. Photobiol. Sci.* **2007**, *6*, 1234–1245.
(6) Sibata, C. H.; Colussi, V. C.; Oleinick, N. L.; Kinsella, T. J. *Expert Opin. Ther. Targets* **2000**, *4*, 919–934.
(7) Juzeniene, A.; Juzenas, P.; Ma, L. W.; Iani, V.; Moan, J. *Lasers Med. Sci.* **2004**, *19*, 139–149.
(8) Ito, H.; Kamibayashi, M.; Sato, K.; Ohkubo, K.; Kawabata, Y.; Kawabata, M.; Fukuzumi, S.; Miyatake, T.; Yuasa, T.; Matsui, K.; Saitadi, T.; Hamada, H. *Cancer* **2003**, *97*, 1097–1103.
(9) Chen, X.; Pan, L.; Pottier, R. A.; Truscott, T. G. *Photochem. Photobiol.* **2004**, *79*, 501–504.
(10) Tasler, S.; Baumann, D.; Mayer, T.; Spiegel, M.; Boche, G. *J. Am. Chem. Soc.* **2003**, *125*, 1518–1524.
(11) Martin, R. R.; Denyer, C. V.; Somerville, I. C. *Photochem. Photobiol.* **1994**, *59*, 171–178.
(12) Ochsner, M. *Photochem. Photobiol.* **1997**, *65*, 1053–1060.
(13) Bonnett, R.; Charlesworth, P.; Djelal, B. D.; Foley, S.; McGarvey, D. J.; Truscott, T. G. *J. Chem. Soc., Perkin Trans. 2* **1999**, 325–328.
(14) Matsuzaki, Y.; Tobita, S.; Tanaka, M.; Shizuka, H. *J. Chem. Soc., Faraday Trans.* **1995**, *91*, 3361–3368.
(15) Ito, H.; Kamibayashi, M.; Sato, K.; Ohkubo, K.; Kawabata, Y.; Kawabata, M.; Fukuzumi, S.; Miyatake, T.; Yuasa, T.; Matsui, K.; Saitadi, T.; Hamada, H. *Cancer* **2003**, *97*, 1097–1103.
(16) Chen, X.; Pan, L.; Pottier, R. A.; Truscott, T. G. *Photochem. Photobiol.* **2004**, *79*, 501–504.
(17) Tasler, S.; Baumann, D.; Mayer, T.; Spiegel, M.; Boche, G. *J. Am. Chem. Soc.* **2003**, *125*, 1518–1524.
(18) Martin, R. R.; Denyer, C. V.; Somerville, I. C. *Photochem. Photobiol.* **1994**, *59*, 171–178.
(19) Ochsner, M. *Photochem. Photobiol.* **1997**, *65*, 1053–1060.
(20) Bonnett, R.; Charlesworth, P.; Djelal, B. D.; Foley, S.; McGarvey, D. J.; Truscott, T. G. *J. Chem. Soc., Perkin Trans. 2* **1999**, 325–328.
(21) Matsuzaki, Y.; Tobita, S.; Tanaka, M.; Shizuka, H. *J. Chem. Soc., Faraday Trans.* **1995**, *91*, 3361–3368.

(22) Nikolaeva-Dimitrova, M.; Pennisi, C.; Radicki, S. *J. Agric. Food Chem.* **2008**, *56*, 168–172.
(23) Kozai, K.; Fukuda, S.; Wakami, L.; Nishiwaki, R.; Yamamoto, R. *J. Am. Chem. Soc.* **2001**, *123*, 7494–7502.
(24) Sarvikas, P.; Antikainen, M.; Hynninen, K.; Sievänen, K. *Photochem. Photobiol.* **1996**, *83*, 477–482.
(25) Torres, N. L.; Orozco, M.; Braun, A. M. *Angew. Chem., Int. Ed.* **1980**, *19*, 535–536.
(26) Dutta, D.; Mishra, S.; Dutta, A. *J. Phys. Chem. B* **2007**, *111*, 1648–1656.
(27) deLuis, C.-P.; Bettencourt, L. *J. Adol. Nurse.* **2001**, *566*–*566*, 113–116.
(28) Pennisi, C.; Kozai, K.; Wang, K.; Zhiqiang, C. *Acta Hortic.* **1999**, *47*, 84–97.
(29) Janzen, W.; Walker, G. C.; Johnson, A. T.; Kahen, M. A.; Barbara, P. F. *J. Phys. Chem.* **1988**, *92*, 7039–7041.
(30) Arunkumar, A. I.; Kumar, T. K. S.; Yu, C. *Biochem. Biophys. Acta* **1997**, *1338*, 68–76.
(31) Kitaev, A.; Sorokin, R.; Hussain, I. G. *Photochemistry*; Academic Press: New York, 1984; pp 54–58.
(32) Sánchez, A.; Kasselouri, A.; Desmettre, N.; Walrant, P.; Maillard, J.; de Oliveira, D. M.; Tedesco, A. C.; Prognon, P.; Delaite, J. *J. Photochem. Photobiol. B* **2005**, *81*, 151–162.
(33) Harman, A. *J. Chem. Soc., Faraday Trans.* **1981**, *77*, 381–391.
(34) Salmon, G. A.; Woodhall, W. H.; Halpern, M. A. *J. Photochem. Photobiol.* **1981**, *33*, 775–777.
(35) Stocker, J. A.; Lindmayer, K.; Stabstedt, L. *J. Photochem. Photobiol., A* **1988**, *107*, 133–144.
(36) Henderson, B. W.; Dougherty, T. J. *Photochemistry and Photobiology of Tumor Tissues. Contributions to the Chemistry of Biology and Medicine*; Pergamon Press: New York, 1983; pp 11–14 and 61–62.
(37) Jori, G. *Photodynamic Photochemistry*; Benjamin, W. A.: Inc: New York, 1987; pp 5–21.
(38) Kimel, S.; Tromberg, B. J.; Roberts, W. G.; Berns, M. W. *Photochem. Photobiol.* **1989**, *50*, 175–183.
(39) Aggarwal, L. P. S.; Baptista, M. S.; Borissevitch, I. E. *J. Photochem. Photobiol., A* **2007**, *189*, 181–185.

JP9076558

Tri-Cationic Porphyrin Conjugates: Evidence for Chain Structure-Dependent Relaxation of Excited Singlet and Triplet States

João Nuno Silva, Francisco Bosca, João P. C. Tomé, Eduarda M. P. Silva, Maria G. P. M. Neves, José A. S. Cavaleiro, Larry K. Patterson, Paulo Filipe, Jean-Claude Mazière, René Santus and Patrice Morlière

Supporting Information

1. Fluorescence of 5-(4-carboxyphenyl)-10,15,20-tris(4-methylpyridinium-4-yl)porphyrin conjugates (P-R) in micelles.

Absorbance spectra of P-H, P-Me, P-DOC, P-OGal, P-Gal and P-$(Lys)_3$ have been recorded either in plain solvents or in micellar solutions. Absorbance data regarding the conjugates are given in Table S1. In the case of micellar solutions it is important to determine the micelle occupancy for the porphyrin to make sure we deal with monomeric porphyrins. The critical micellar concentration (cmc) and aggregation number (N) are cmc = 8.0 mM, N = 62 and cmc = 0.5 mM, N = 143 for SDS and TX-100, respectively.[1,2] Under the conditions of this study ~1% SDS (35 mM) and 0.8% TX100 (~6 mM) the micelle concentration ([M]) is found to be 430 μM and 30 μM for SDS and TX100, respectively. Solubilization of aromatics in micelles is described by a Poissonian distribution. As a consequence, the fraction (y) of micelles with n conjugate molecules (Conj) is given by $f(n) = (Q^n/n!) \times \exp(-Q)$ with $Q = [Conj]/[M]$.[3] As an example, absorbance spectra were recorded with 5 μM of conjugates. The calculation shows that only 0.06% of SDS micelles contain 2 or more conjugate molecules. In the case of TX100, the proportion becomes 8%. Hence, it may be concluded that absorbance and fluorescence data (Table 1 in the article and Table S1) and fluorescence spectra (Figs. S1A and S1B) obtained from micellar solutions reflect the behavior of monomeric porphyrins.

2. Additional data for femtosecond 387 nm - laser flash photolysis of the parent compound and conjugates

Transient absorption spectra were recorded with conjugate concentration of ~25 μM. The Poissonian distribution here demonstrates that only 0.6% of SDS micelles contain 2 molecules of conjugates. In the TX-100 micelles, the same calculation shows that 32%, 24% and 12% of micelles contain 1, 2 or 3 conjugate molecules respectively. Owing to the large micellar size (diameter, 5.6 nm), the limited dimensions of the porphyrin (~1 nm) and the electrostatic repulsion between porphyrin rings it is likely that in TX-100 micelles the porphyrins are largely present as monomeric form.[4] Examples of transient spectra of P-Me in pH 7 buffer and SDS are shown in Fig. S2 while decay kinetics are presented in the insert of Fig. S2. Similarly spectral and/or kinetic data relevant to P-DOC, P-OGal and P-Gal are provided in Figs. S3 and S4, respectively. From experimental details provided in "materials and methods" it is relatively easy to determine the number of P-R molecules excited by the ~30 fs 387 nm laser flash.[5] The irradiated volume (2π mm^3) contains ~2 × 10^{17} molecules. The number of photons delivered per 8 μJ pulse is ~10^{13}. With a solution absorbance being ~0.3, 70% of the incident photons are absorbed producing a ~3.5% population of excited P-R. The repetition rate of the laser is 1 kHz and the fluorescence lifetime of the excited P-R is of the order of, or less than, 10 ns, it may be concluded that no excited state saturation occurs. It follows that there is no contribution of stimulated emission to fluorescence emission.

3. Experimental data to establish the general properties of the first triplet state in tri-cationic porphyrins

3.1. Stern-Volmer plots of triplet quenching by dioxygen. Figure S5 illustrates the excellent Stern-Volmer behavior for collisional quenching of ^{3}P-H and ^{3}P-DOC and P-OGal by dioxygen in neutral and O$_2$-saturated ethanol. SDS and FDS solutions. Oxygen quenching data for the triplet state of P-H and all the conjugates are given in Table S2.

3. 2. Determination of triplet molar extinction coefficients. With $^3T_1$ and $^1S_0$ symbolising the first excited triplet and ground state of a tri-cationic porphyrin, the sequence of reactions involved in determining triplet molar extinction coefficients may be given.

$^3T_1 \rightarrow {}^1S_0$; decay to ground state, rate k_1

$^3T_1$ + Car $\rightarrow$ Car + $^1S_0$ (energy transfer), rate k_2

^{3}Car$_1 \rightarrow$ Car; decay to ground state, rate k_3

Stern-Volmer kinetics apply to the $^3T_1$ decay of P-R, to yield k_2 values varying from ~1.6 to 3 × 10^9 M^{-1} s^{-1} indicating that this transfer is a diffusion control process (see Table S3 and insert Fig. 5A in article). The energy transfer from $^3T_1$ to ground state Car given in Fig. S6A and S6B illustrates the growth of the characteristic ^{3}Car$_1$ absorbance measured at 520 nm in ethanol. Figure S6A and the insert in Fig. S6A provide typical experimental data used for triplet molar extinction determination. The maximal ^{3}Car$_1$ transient absorbance ($Abs_{t,\lambda}$) for the transfer from the $^3T_1$ state of P-H to Car is reached about 10 μs after the photolytic laser flash. The inner filter effect of Car is maximal at ~430 nm (ε = 320,000 M^{-1} cm^{-1}) while at the excitation wavelength (355 nm), ε is only 16,500 M^{-1} cm^{-1}. It may be noted that saturation resulting from inner filter effect was negligible given that production of the $^3T_1$ transient at 480 nm essentially obeyed the Beer-Lambert law (see insert in Fig. S6A and legend). It is also of note that the ^{3}Car transient spectrum is shifted to the blue in ethanol as compared to toluene (Fig. S6C). Data in Fig. S6A allow an estimate of the molar extinction coefficient at 400 nm for the $^3T_1$ state. At the maximum, Abs_{max} for ^{3}Car$_1$ reaches ~0.345 at 520 nm. However due to its short lifetime (k_3 = 1.4 × 10^5 s^{-1}, τ = 6-7 μs in ethanol), ^{3}Car$_1$ undergoes substantial decay during the energy transfer process. Hence, $Abs_{t,\lambda}$ must be corrected to determine the true yield of [^{3}Car$_1$] produced by the transfer. Abs_{max} is given by the relationship: $Abs_{max} = Abs_t \times \exp[(k_3/k_2)\ln(1-k_2/k_3)]$ (equation 1) where Abs is the ^{3}Car$_1$ transient absorbance that would be observed in the absence of decay and $k_2 = k_2 \times [Car]$.[6] Application of equation 1 yields [^{3}Car$_1$] = ~3 μM at plateau. Taking into account the transfer yield $k_2[Car]/k_2 = 0.7$ at [Car] = 15 μM, the initial [$^3T_1$] is found to be 1.9 μM. The initial transient absorbance difference at 480 nm (ΔA = 0.28, see insert in Fig. S6A) after the laser pulse is due to both the long-lived $^3T_1$ absorbance and the ground state absorbance depletion by ^{3}Car$_1$ at a time when [^{3}Car$_1$] is still negligible. Since the molar extinction coefficient of ground state P-H in ethanol is ~1,000 M^{-1} cm^{-1} at 480 nm, the molar extinction coefficient of the $^3T_1$ state of P-H at this wavelength can be estimated from ΔA to be ~40,000 M^{-1} cm^{-1}.

(1) Aboagye, M.; Gibson, E. ... Int. J. ... Chem. Acta 1979, ... 279-281.

(2) Rowen, K. J.; Dennis, E. A. J. Phys. Chem. 1977, 81, 1025-1028.

(3) Kalyanasundaram, K. Photochemistry in Microheterogeneous Systems; Academic Press: San Diego, 1995; p 2-28.

(4) Fessenden, R. W.; Hoffman, M. Z.; Bunnett, J. F.; Gilbert, E. E.; Nist, B. J. Photochemistry and Radiation Biochemistry: Proceedings of the Symposium on Biochemical Problems Involving Radiation and Photochemical Reactions; Gatlinburg, Tennessee, 1962; Nuclear Science Series; National Academy of Sciences-National Research Council: Washington, DC, 1962; Vol. 1145, p 11-14.

(5) Burkinshaw, S. M.; Salthouse, J. A. Photochemistry of Porphyrins and Metalloporphyrins; Academic Press: London, 1998; Vol. 2, p 127-166.

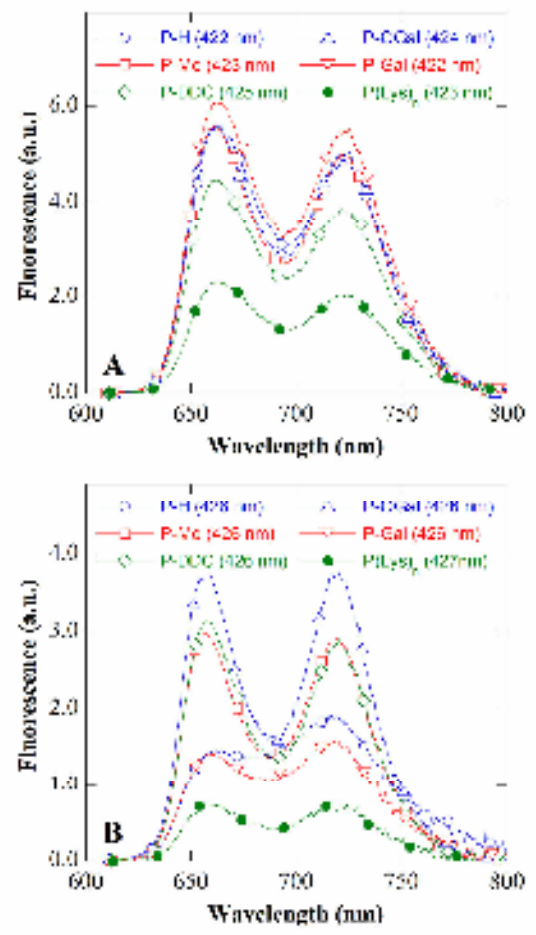

Figure S1. (A) Fluorescence spectra of 0.1 mM corr. units in 1% SDS containing 10 mM phosphate buffer (pH 7). Optical paths were 1.0 and 0.1 cm for excitation and emission respectively. Spectra were recorded at 22°C with 1 nm slits in both field paths. The excitation wavelength is indicated on the graph for each conjugate. The absorbance of the solutions was 0.02-0.03 at the excitation wavelength. (B) As in (A) but the fluorescence spectra of conjugates were recorded in 0.3% TX100 containing 10 mM phosphate buffer (pH 7).

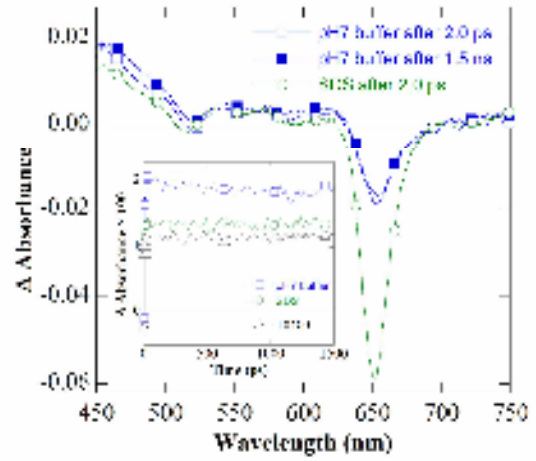

Figure S2. Transient absorbance difference spectra obtained ~2 ps (L, ○) or 1.5 ns (■) after femtosecond 387 nm laser flash photolysis of air saturated solutions of P-Gal in 10 mM phosphate buffer (pH 7) (■) and in 1% SDS containing 10 mM phosphate buffer (pH 7) (○). Insert: transient absorbance decays at 450 nm from air-saturated solutions of P-Gal in 10 mM phosphate buffer (pH 7) (L). 1% SDS containing 10 mM phosphate buffer (pH 7) (○) and 0.3% TX100 containing 10 mM phosphate buffer (pH 7) (△).

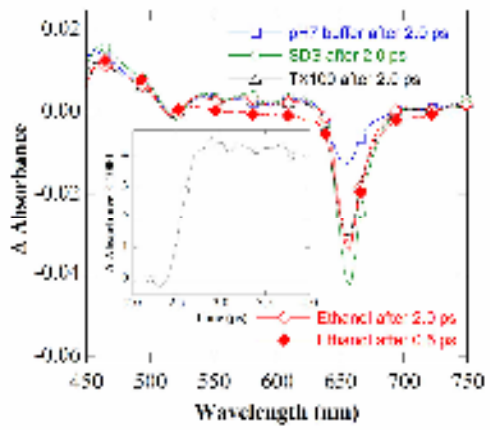

Figure S3. Transient absorbance difference spectra obtained ~2 ps after 0 ns absorption of 387 nm laser flash photolysis of air saturated solutions of P-OGal in 10 mM phosphate buffer (pH 7) (L). 1% SDS containing 10 mM phosphate buffer (pH 7) (○) 0.3% TX100 containing 10 mM phosphate buffer (pH 7) (△) and ethanol (◇). The spectrum in ethanol after ~0.5 ps is increased (◆) to show growth of absorbance at 540 nm in ethanol.

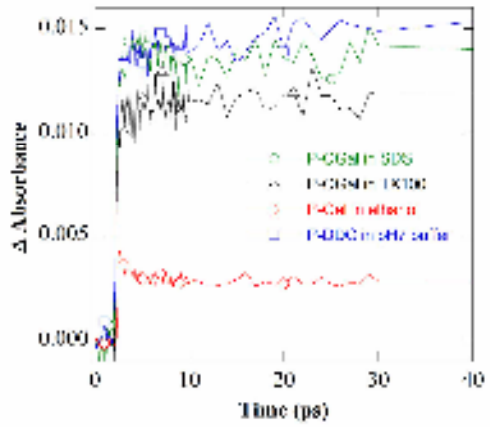

Figure S4. Transient absorbance decay following femtosecond 387 nm laser flash photolysis of air saturated solutions of P-OGal in 1% SDS containing 10 mM phosphate buffer (pH 7) (○) and in 0.3% TX100 containing 10 mM phosphate buffer (pH 7) (△), of P-Gal in ethanol (◇) and of P-DDC in 20 mM phosphate buffer (pH 7) (L). Decays for P-OGal and P-DDC were measured at 540 nm, the region of apparent transient absorbance maximum for all compounds measured. For clarity of presentation, P-Gal decay is given at 500 nm.

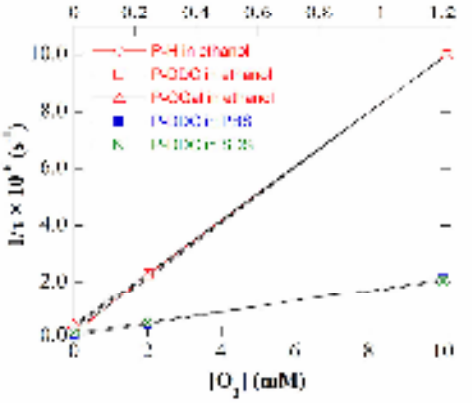

Figure S5. Reciprocal of τ1 lifetimes (τ) for P-H (○), P-DDC (□) and P-OGal (△) as a function of the O_2 concentration in ethanol (open symbols and ◇ for P-DDC in PBS (■) and in 1% SDS containing 10 mM phosphate buffer (pH 7) (□) (upper abscissa scales). τ_1 decays were recorded at 540 nm in 2.5 μM solutions of photofrin.

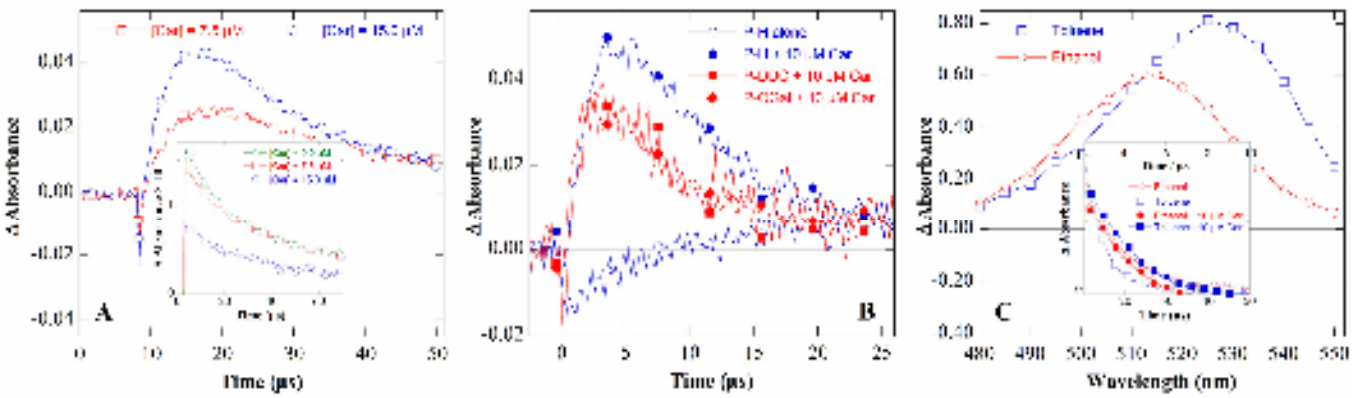

Figure S6. (A) Growth and decay of β-carotene triplet state absorption at 520 nm following 355 nm laser flash photolysis of a mixture of 15 μM P-H with either 7.5 μM (□) or 15 μM (○) β-carotene in N_2-saturated ethanol solutions. Insets: Decay of the triplet state absorption of P-H at 460 nm in the absence (○) or in the presence of 7.5 (□) or 15 μM (◇) β-carotene, illustrating the β-carotene inner filter effect at this wavelength. The corresponding absorbance values at 355 nm were 0.17, 0.33 and 0.45, respectively. Note that the experimental ΔAbsorbance (0.05) observed with 15 μM Car is slightly lower than the theoretical value (0.09). **(B)** Growth and decay of the transient absorbance for the β-carotene triplet measured at 520 nm after 355 nm-laser flash photolysis of N_2-saturated solutions of P-H (●), P-DDC (■) and P-OGal (◆) in ethanol in the presence of 10 μM Car. Porphyrin concentration was 15 μM. Note in the absence of Car the bleaching of the absorbance of P-H followed by recovery is due to decay of its triplet state (○). **(C)** Transient absorbance spectra of β-carotene triplet molecules in toluene (□) and ethanol (○) after energy transfer from anthracene triplet molecules to ground state β-carotene. Spectra were recorded ~2 μs (corresponding to maximum transient absorbance at 520 nm of Car triplet) after 355 nm laser flash photolysis of a mixture of 10 μM anthracene and 10 μM of Car in N_2-saturated solutions as described by Nielsen *et al.*[5] Insert: Decay of anthracene triplet absorbance measured at 420 nm in ethanol (○,●) and at 430 nm in toluene (□,■) in the absence (lower time scale, ○,□) and in the presence (upper time scale, ●,■) of 10 μM Car showing comparable energy transfer efficiency in ethanol (42%) and toluene (50%).

TABLE S1. Absorbance (Absorption Maxima and Extinction Coefficients) and Fluorescence (Emission Maxima, Quantum Yield and Lifetime) Parameters of Tri-Cationic Porphyrin Conjugates in Various Solvents

Compound	Solvent	Absorbance						Fluorescence			
		λ_{max} / nm [10^{-3} ε / $M^{-1}cm^{-1}$]						λ_{max} / nm	λ_{max} / nm	Φ	τ / ns
P-DDC	EtOH	425 [384]	517 [14.0]	553 [5.1]	592 [5.1]	648 [1.8]		659	720	0.041	9.7
	Buffer[a]	421 [327]	518 [13.8]	556 [5.8]	593 [4.2]	649 [1.8]		660	658 (sh)	0.029	4.6
	TX100[b]	423 [339]	517 [15.6]	553 [6.2]	587 [5.0]	643 [1.9]		657	718	0.061	9.3
	SDS[c]	426 [329]	518 [15.6]	555 [6.1]	590 [5.0]	647 [1.7]		658	719	0.135	10.6
	DPS[d]	422 [229]	519 [14.2]	557 [5.8]	593 [4.2]	650 [1.8]		660	655 (sh)	0.03	
P-DDC	EtOH	425 [249]	517 [18.2]	554 [7.8]	592 [6.2]	648 [2.4]		660	721	0.038	9.4
	Buffer	422 [268]	518 [16.7]	556 [6.8]	593 [5.2]	650 [2.3]		661	660 (sh)	0.030	7.5
	TX100	425 [335]	517 [15.0]	553 [8.1]	586 [7.2]	644 [2.7]		658	719	0.069	10.5
	SDS	426 [257]	520 [17.2]	556 [7.8]	589 [7.1]	646 [2.4]		661	72	0.1 8	9.9
	DPS	423 [257]	519 [15.5]	555 [6.1]	591 [5.2]	648 [1.9]		7 6	652 (sh)	0.027	
P-OGal	EtOH	425 [217]	517 [16.2]	553 [7.6]	592 [6.1]	648 [2.2]		659	721	0.036	8.7
	Buffer	421 [348]	518 [13.8]	556 [6.8]	593 [5.3]	649 [2.4]		660	658 (sh)	0.027	4.4
	TX100	424 [3 5]	517 [18.4]	554 [7.5]	587 [6.3]	644 [2.3]		658	719	0.068	10.1
	SDS	426 [251]	518 [17.0]	555 [7.6]	589 [6.8]	647 [2.2]		661	722	0.110	10.1
	PBS	422 [258]	519 [16.5]	554 [6.8]	592 [5.3]	649 [2.]		7 7	6 5 (sh)	0.034	
P-Oct	Ethanol	425 [231]	517 [17.7]	554 [7.6]	593 [6.3]	648 [2.4]		659	721	0.037	7.8
	Buffer	422 [258]	518 [15.8]	556 [6.7]	593 [5.1]	650 [2.]		7 9	658 (sh)	0.03	7.5
	TX100	422 [273]	518 [17.1]	554 [7.3]	584 [7.3]	640 [2.2]		7 9	659	0.033	10.5
	SDS	426 [244]	519 [16.4]	556 [7.4]	588 [6.7]	646 [2.4]		663	724	0.132	10.5
	PBS	423 [255]	518 [15.8]	556 [6.8]	592 [5.1]	649 [2.2]		7 7	657 (sh)	0.030	
P-Lysin	Ethanol	426 [245]	518 [20.0]	554 [14.0]	592 [2.5]	649 [6.2]		660	722	0.014	2.5 (98%) - 8.1 (2%)
	Buffer	423 [200]	521 [17.1]	556 [9.0]	588 [8.3]	646 [3.2]		723	662	0.011	1.7 (35%) - 6.3 (81%)
	TX100	422 [317]	520 [19.5]	556 [13.0]	588 [9.1]	647 [3.7]		6 9	7 9	0.0 9	1.3 (15%) - 9.1 (85%)
	SDS	427 [264]	520 [2 .2]	556 [10.7]	590 [8.1]	648 [3.5]		662	72	0.053	1.7 (13%) - 8.8 (87%)
	PBS	424 [194]	521 [17.0]	556 [9.0]	589 [6.9]	648 [3.3]		7 8	6 5	0.0 0	

[a] 100 mM phosphate buffer at pH 7. [b] 0.1% Triton X100 in pH 7.0, 10 mM phosphate buffer. [c] 0.5% SDS in pH 7.0, 10 mM phosphate buffer. [d] 150 mM NaCl in pH 7.0, 10 mM phosphate buffer.

TABLE S2. Bimolecular Rate Constants of Dioxygen Quenching of the Triplet State of 5-(4-carboxyphenyl)-10,15,20-tris(4-methylpyridinium-4-yl)porphyrin tri-iodide and of Conjugates in Various Solvents at 20 °C

Compound	$k_q(O_2) \times 10^{-9}$ (M^{-1} s^{-1})			
	Ethanol	PBS[a]	SDS[b]	TX100[c]
P-H	1.7 ± 0.3	1.6 ± 0.1	1.8 ± 0.2	1.5 ± 0.1
P-Cl	1.1 ± 0.3	2.1 ± 0.1	1.9 ± 0.1	1.9 ± 0.3
P-DDC	1.0 ± 0.3	1.7 ± 0.2	1.5 ± 0.1	0.95 ± 0.05
P-GGa	0.9 ± 0.3	1.4 ± 0.1	1.1 ± 0.1	0.75 ± 0.10
P-Ga	1.1 ± 0.3	2.1 ± 0.2	1.9 ± 0.1	1.5 ± 0.1
P-Lys(A)	0.9 ± 0.2[d]	2.1 ± 0.1	2.1 ± 0.2	1.8 ± 0.3

[a] O_2-solubility in ethanol: 20.1 mM. O_2-solubility in SDS and TX100 buffered solution is assumed to be the same as in buffer (~2 mM at 20 °C). [b] 50 mM NaCl at pH 7, 10 mM phosphate buffer. [c] 0.2% Triton X-100 at pH 7.0, 50 mM phosphate buffer. [d] Biexponential decay (see text). [e] Average value due to complex kinetics in deaerated solutions.

TABLE S3. Bimolecular Rate Constants for Quenching of the Triplet State of 5-(4-carboxyphenyl)-10,15,20-tris(4-methylpyridinium-4-yl)porphyrin tri-iodide (P-H), of P-DDC and of P-GGa Conjugates by β-Carotene in Ethanol at 20 °C

Compound	P-H	P-DDC	P-GGa
k_q	10^{10} M^{-1} s^{-1}	1.5 ± 0.3	2.5 ± 0.3	1.6 ± 0.3

[a] k_q are the means ± SD of two values resulting from lifetime determinations performed at 4 °C and at 20 °C.

4.3 MAIN RESULTS AND DISCUSSION

4.3.1 ABSORPTION SPECTRA AND EXTINCTION COEFFICIENTS

The absorption spectrum of P-H is presented in Fig. 2A (Article I) and the characteristics for all compounds are given in Table 1 (Article I). Depending on solvent conditions (ethanol, buffer, TX100, SDS and PBS) the absorbance spectra of all derivatives exhibit the well know absorption spectra characteristic of porphyrins with a Soret band (strong UV absorbance band at ~420 nm) and 4 minor absorbance maxima at ~520, 550 and 630- 650 nm.

Extinction coefficients are provided in Table 1 (Article I). As can be seen, no major differences are observed with solvents reproducing various microenvironmental conditions. As to the comparison between P-R, no major difference in their absorption properties is observed suggesting that all are potentially interesting photosensitizers in terms of ability to absorb light. When compared to the presently used PPIX in oncological dermatology, the absorbance of the photosensitizers better matches the therapeutic window beyond 650 nm, where light penetration is higher (see Section 2.1.8).

4.3.2 FLUORESCENCE SPECTRA AND QUANTUM YIELDS

Spectra are presented in Fig. 2B (Article I) and the characteristics for all compounds are given in Table 2 (Article I). All the compounds have rather similar fluorescence quantum yields with the exception of P-$(Lys)_n$ whose fluorescence quantum yield is slightly lower. The P-R fluorescence quantum yields are mostly independent of the solvent conditions except for SDS micellar solutions where they are significantly higher. Despite an excellent solubility in an aqueous medium, the formation of small-size oligomer-like or noncovalent dimer favoring nonradiative conversion processes is observed which result in the shortening of the fluorescence lifetime and a diminished fluorescence quantum yield of most conjugates.

The existence of fluorescence is particularly interesting in the context of this work because the sensitivity of fluorescence measurements allows: 1/ quantitative measurements of P-R concentration in cell systems, and 2/ the study of the P-R intracellular localization. As noted above, all conjugates possess a good fluorescence quantum yield in micellar solutions allowing a possible detection in living tissues.

Furthermore, in the event of a future clinical use of P-R, fluorescence is useful for the diagnosis/delineation of tumor tissue, the fluorescence-guided adjustment of the irradiation

area [492] and the assessment of the treatment success by checking the fluorescence quenching after PDT related to the porphyrin photobleaching in the irradiated area [493]. However, the use of P-R for this purpose may not be easy because of moderate fluorescence quantum yields.

The modest P-R fluorescence quantum yields and the fluorescence lifetimes indicate that non-radiative pathways are involved in the deactivation of the $^1S_1$ state of P-R with return to the $^1S_0$ ground state. Thus internal conversion (heat exchange with the surrounding solvent molecules) and/or "intersystem crossing" with triplet state formation are likely to occur.

4.3.3 FEMTOSECOND SPECTROSCOPY

The femtosecond experiments were conducted at the Radiation laboratory of the University of Notre Dame (USA). The results are detailed in Fig. 3 and 4 of Article I published in the Journal of Physical Chemistry B.

The laser flash photolysis in the femtosecond time scale allows to study the photophysical events taking place before the formation of the triplet state, namely the behavior of the excited singlet states (S_1, S_2, …, S_n). We have observed that in some cases the strong flexibility brought by the structure of the conjugated chain is responsible for the ultra-fast occurrence of an interaction between the side-chain and the porphyrin ring. Although these parameters are important in understanding the physical-chemical processes leading to the population of the $^1S_1$ state of P-R, they do not give access to those characterizing their triplet state, the essential excited state regarding their photosensitizing ability.

4.3.4 TRANSIENT ABSORBANCE SPECTRA AND PROPERTIES OF THE TRIPLET STATE

Spectra are presented in Fig. 5 (Article I). The time dependence of the absorbance allows the measurement of triplet state lifetimes reported in Table 2 (Article I). All are in a time range extending from a few µs to 50 µs. They are longer in PBS than in the other solvents. The P-$(Lys)_n$ triplet has the longest lifetime. This may be due to the bulky conformation of the poly-lysine chains that may hinder fast collisionnal processes contributing to an increased rate of return from the $^3T_1$ to the $^1S_0$ state. These long-lived triplet states make it possible to predict a photodynamic activity of P-R in aqueous environments.

Another important parameter regarding the triplet state is its formation quantum yield. The triplet state quantum yield (ϕ_T) may be calculated from the absorption spectra of the triplet

state, provided we know its extinction coefficient (ε_T). Extinction coefficients are obtained by classical methods involving an energy transfer to β-carotene singlet ground state to produce the β-carotene triplet whose molar absorbance has been determined rather accurately. Such a transfer is very efficient because of the low-lying triplet state energy of β-carotene. As a consequence, the concentration of β-carotene triplets formed is assumed to be equal to that of the P-R triplets, thus allowing the calculation of the molar absorbance (ε_T) of the P-R triplets. The details of the calculation are mentioned in the supplemental data of Article I. The determination of the extinction coefficient of triplet state allows the determination of the P-R triplet concentration.

Simultaneously, actinometry of the laser beam can be achieved with a molecule whose triplet state quantum yield and extinction coefficient are well known. Here *meso*-tetraphenylporphyrin (TPP) has been used as an actinometer. Thus, the unknown triplet state quantum yield (ϕ_T) can be calculated by comparing the triplet concentrations of P-R and TPP obtained with solutions of P-R and TPP having the same absorbance at 355 nm, the exciting laser wavelength (see Chapter 3) [494].

A summary of all these properties appears in Table 4 (Article I) which also reports the calculated rate constants for the non-radiative (internal conversion and intersystem conversion) and radiative (fluorescence) deactivation processes characterizing the P-R. The triplet state quantum yield of P-R but P-$(Lys)_n$ is rather high (0,5 – 0,6) whatever the solvent. This suggests that P-R may be efficient photosensitizers in most environments.

4.3.5 SINGLET OXYGEN FORMATION

The above data strongly suggest that singlet oxygen can be produced with an efficient quantum yield. Singlet oxygen formation can be probed by measurement of the histidine (His) oxidation which only occurs through a type II photodynamic process. The quantum yield of singlet oxygen mediated-His oxidation is reported for all the P-R in Table 5 (Article I). Quantum yields of about 0.08 are obtained with all P-R but P-$(Lys)_n$ for which the quantum yield is about 0.02 consistent with its lower ϕ_T. As expected, no His oxidation occurs in the absence of O_2. The formation of $^1O_2$ is supported by adding N_3^- which inhibits His oxidation by reducing the $^1O_2$ lifetime. On the other hand, replacing H_2O by D_2O, which enhances $^1O_2$ lifetime, leads to an increase in the rate of His consumption definitely demonstrating singlet oxygen formation.

Using *meso*-tetrasulfonatophenylporphyrin ($TPPS_4$) whose singlet oxygen formation quantum yield is known [495], we are able to calculate the quantum yield of singlet oxygen formation via the photodynamic action of P-R. These values are close to 0.8 for P-H, P-Me, P-DCC, P-OGal and P-Gal, and close to 0.2 for P-Lys. The values obtained here are slightly higher than the triplet state quantum yield values mostly because of uncertainty in the comparative standard we used. Nevertheless, these results demonstrate that the transfer from P-R triplet state to molecular O_2 is very efficient in generating $^1O_2$ in aqueous media.

4.4 CONCLUSIONS

This work was undertaken to establish the photophysical properties underlying the effectiveness of P-R as cell photosensitizers. Considering the results described above we can conclude that:

1- All compounds are potentially interesting considering their efficacy in singlet oxygen formation. The poly-*S*-lysine conjugate might be considered *a priori* as the less interesting, due to its lower quantum yield of singlet oxygen production. However, it will be shown in the next chapter that its photocytotoxic activity in cells cannot be solely inferred from the photophysical study.

2- The fluorescence properties of all compounds permit their use for further fluorescence studies in cell systems *in vitro* and, possibly, for the clinical diagnosis of tumor tissue.

3- The present work suggests that the eventual differences in the photocytotoxic activity of all compounds, other than the poly-*S*-lysine conjugate, could not be explained in terms of different photodynamic efficiencies. Other factors might be implicated such as modulation of cellular uptake and of intracellular localization/partition within cytosolic sites and cell membranes.

CHAPTER 5

STUDY OF THE PHOTOBIOLOGICAL PROPERTIES OF NEW TRI-CATIONIC PORPHYRIN DERIVATIVES

5.1 INTRODUCTION

In Chapter 4, we have demonstrated that the excited triplet state of the tricationic conjugates is highly populated. We have further established that all the conjugates under study are effective type II photodynamic agents producing singlet oxygen - a cytotoxin - at comparable and high yields except P-$(Lys)_n$.

The photobiological properties of a photosensitizer depend on its structural features (nature of peripheral groups, coordinated metal ion and accompanying axial ligands), which determine the electronic charge, the hydrophobic character, the aggregation state, and ultimately, the affinity for binding sites [38, 496]. As reported in Section 2.1.3.5 and section 2.1.6, these structural features determine several key factors for the outcome of photodynamic therapy, such as cellular uptake and subcellular localization of the photosensitizer [174]. This is of particular interest in this study, as it has been previously showed that all photosensitizers have similar intrinsic $^1O_2$ production capacity. As a hypothesis, the cell photosensitization effectiveness of P-R may primarily depend on photosensitizer uptake and localization and, thus, may be chain-dependent.

When studying new photosensitizers, their photocytotoxicity effectiveness and their capacity to induce an oxidative stress must be determined. Most PDT sensitizers may also trigger a variety of responses ranging from antioxidant response to programmed cell death. There is considerable interest in elucidating the signaling pathways leading to these responses in order to better understand how PDT operates at the cellular and molecular levels. These include the modulation of the cell survival and cell death pathways and activation of signal transduction pathways [173].

5.2 OBJECTIVE

This chapter can be divided in two complementary parts with the following objectives:

Objective of Part I.
The first part concerns the assessment of the uptake kinetics and subcellular localization, as well as the mechanisms of the photocytotoxicity of five new tri-cationic porphyrin derivatives in a proliferating human skin keratinocytic cell line (NCTC-2544). Such a study allows a comparison of the different biological effects of molecules belonging to the same class of compounds but endowed with different chemical and physical properties reported in chapter

4. Their photobiological properties will be compared to those of the parent compound. The rationale for such a study is that the different substituents of the tri-cationic porphyrin derivatives may affect their cell uptake and intracellular distribution pattern. As a result, some structure-photocytotoxic activity relationship for these new tri-cationic porphyrin derivatives can be established. Furthermore, it is a pre-requisite for further study on their mechanism of action and the prevailing form of cell death they induce.

Objective of Part II.

The second part is devoted to the study of these prevailing forms of cell death and the involved signaling pathways. The elucidation of the signaling pathways leading to these responses is of interest since it provides clues to better understand how PDT operates at the cellular and molecular levels.

As deduced from Part I, it turns out that the P-OGal conjugate is the most photocytotoxic tri-cationic porphyrin conjugate. As a result, we have more extensively investigated the oxidative signaling events associated with the cell killing induced by the P-OGal-PDT. There are only a few studies regarding the MAPKs involvement in the PDT stress, especially those concerning cationic porphyrins. We have thus examined the role of MAPK's. We provide evidence for the modulation of p38, JNK, ERK and AKT expression during the PDT mediated cell death in the NCTC 2544 cell line.

ARTICLE II

ENHANCEMENT OF THE PHOTODYNAMIC ACTIVITY OF TRI-CATIONIC PORPHYRINS TOWARDS PROLIFERATING KERATINOCYTES BY CONJUGATION TO POLY-S-LYSINE

PAPER www.rsc.org/pps | Photochemical & Photobiological Sciences

Enhancement of the photodynamic activity of tri-cationic porphyrins towards proliferating keratinocytes by conjugation to poly-S-lysine

João Nuno Silva,[a] Josiane Haigle,[b] João P. C. Tomé,[c] Maria G. P. M. S. Neves,[c] Augusto C. Tomé,[c] Jean-Claude Mazière.[d,e,f] Cécile Mazière.[d,e,f] René Santus.[b,g] José A. S. Cavaleiro.[c] Paulo Filipe[a] and Patrice Morlière*[d,e,f]

Received 9th September 2005, Accepted 17th October 2005
First published as an Advance Article on the web 25th November 2005
DOI: 10.1039/b512841b

A fast uptake of the tri-cationic 5-[4-(carboxyethoxy)phenyl]-10,15,20-tris(4-methylpyridinium-4-yl) porphyrin tri-iodide (P-H), independent of the presence or absence of proteins in the culture medium, occurs during incubation of NCTC 2544 human keratinocytes with this porphyrin. By contrast, the uptake of the poly-S-lysine conjugate (P-(Lys)$_n$) is faster in serum-free medium than in the supplemented medium suggesting that P-(Lys)$_n$ interacts with serum proteins. The P-(Lys)$_n$ uptake is at least an order of magnitude greater than that of P-H in serum-free or supplemented culture medium. With histidine as a specific probe of type II photodynamic reactions, the relative photosensitizing effectiveness of the conjugate is only one fourth that of P-H. Nevertheless, the photocytotoxicity of the conjugate is strongly enhanced as compared to that of P-H as a result of its larger uptake. Thus, the doses achieving 50% of photocytotoxicity after incubation with 5 μM of the conjugate and its parent cationic porphyrin are about 20 mJ cm^{-2} and 1 J cm^{-2}, respectively. Similarly, the initial rate of the cell lipoperoxidation induced by photosensitization with P-(Lys)$_n$ is about 8 times higher than that obtained with P-H. Fluorescence microscopy reveals that P-H is more diffusely located in the cytoplasm than P-(Lys)$_n$, which seems to accumulate in lysosome-like structures. Little if any staining of the nucleus is observed with both photosensitizers.

Introduction

Photodynamic therapy (PDT) is an interesting alternative treatment in several domains of oncology and ophthalmology.[1–4] In dermatological oncology, PDT is presently used in the treatment of basal and squamous cell carcinomas or of pre-cancerous states such as solar keratoses. Presently authorized photoactive substances are tetrapyrrolic derivatives such as the historical reference photosensitizer, Photofrin®, a mixture of photosensitizing porphyrin oligomers or more recently, *meso*-tetrakis(*m*-hydroxyphenyl)chlorine (Foscan®) used in palliative treatments of head and neck cancers. In dermatology, the precursor of the powerful photosensitizer protoporphyrin IX, *e.g.* 5-aminolevulinic acid (ALA) or its methyl ester are currently topically used as a pro-drug to treat cutaneous intraepithelial cancers.[5] With the exception of Photofrin®,[6] all these photosensitizers are rather insoluble in water. Their use implies the tedious preparation of special formulations for their systemic or topical administration.

As a result, workers in the field of PDT have carried out the synthesis of water-soluble derivatives of porphyrins and chlorins.[7] Thus, the water-soluble *meso*-tetra(*m*-aspartylchlorin), undergoes advanced clinical trials in Japan to treat lung cancer.[8] Along these lines, poly-S-lysine-porphyrin and chlorin conjugates have also been synthesized. Their water solubility has been further improved by conjugating the polypeptide side-chain to cationic *meso*-tetra-substituted porphyrins.[9,10] These derivatives are effective in the photoinactivation of both Gram (+) and Gram (−) bacteria.[9] In view of other potential medical applications of poly-S-lysine conjugates, especially in dermatological oncology, effective PDT activity towards rapidly proliferating cells cannot be anticipated since the structure of bacterial cells is quite different from that of mammalian cell membranes.[1] As a consequence the response of mammalian cells to PDT with the cationic porphyrin and its polylysine conjugate has been investigated. With the immortalized NCTC 2544 human skin keratinocytes as model of proliferating cutaneous epithelial cells, we have compared the intracellular localization and the photocytotoxicity of a tri-cationic porphyrin, with those of the poly-S-lysine conjugate.

Materials and method

Chemicals, culture media and routine spectroscopic equipment

Reagents for cell culture, minimum essential medium with Earle's salts (EMEM), Hanks' buffered saline solution containing 20 mM Hepes (HBSS), Dulbecco's phosphate-buffered saline (PBS), all without phenol red, fetal calf serum (FCS), trypsin and antibiotics were purchased from Gibco (Cergy-Pontoise, France). The Folin

[a]*Hospital de Santa Maria, Clínica Universitária de Dermatologia, 1600 Lisboa, Portugal*
[b]*Muséum National d'Histoire Naturelle, RDDM, Paris-Nanterre, F 75231 Paris, France*
Universidade de Aveiro, Departamento de Química, Campus Universitário de Santiago, 3810-193, Aveiro, Portugal
[d]*INSERM, ERI12, Laboratoire de Biochimie, CHU Amiens-Hôpital Nord, place Victor Pauchet, 80054 Amiens Cedex 1, France. E-mail: morliere.patrice@chu-amiens.fr*
[e]*CHU Amiens, Laboratoire de Biochimie, F-80054 Amiens, France*
[f]*Université de Picardie Jules Verne, Faculté de Médecine et de Pharmacie, EA 2087, F-80054, France*
[g]*INSERM, U697, F-75475, Paris, France*

reagent. 1,1′,3,3′-tetraethoxypropane and Triton (Tris) were supplied by Sigma Chemical Co. (St Louis, MO, USA). Neutral Red (NR) was a Fluka (Saint-Quentin Fallavier, France) product whereas 1-butanol, Triton X100 (TX100), sodium dodecyl sulfate (SDS) and Hepes were supplied by Merck (Darmstadt, Germany). LysoTracker Green was obtained from Molecular Probes (Eugene, OR, USA). The synthesis of the tri-cationic 5-(4-carboxyphenyl)-10,15,20-tris(1-methylpyridinium)porphyrin (P-H) and of the poly-S-lysine conjugate (P-Lys) have been described by Toner *et al.*[9] Since P-Lys, has no defined molecular weight (depending on the Lys chain polymerization and the degree of porphyrin linked) its concentration was determined assuming the same molar absorbance in the Soret band for the parent porphyrin (P-H) and the conjugate P-(Lys), in the aqueous SDS. Taking into account the weighed material and the spectrophotometrically determined concentration it is found that the degree of polymerization n is about 35. Stock solutions of the porphyrins (500 μM) were prepared in water–DMSO mixture (1 : 1 v/v) and stored at 4 °C. The optical absorption spectrophotometry was carried out with an UVIKON 943 spectrophotometer provided by Kontron Instruments (Montigny-le-Bretonneux, France). An SLM AMINCO BOWMAN (series 2) (Rochester, Champs-sur-Marne, France) equipped with correction of excitation and emission spectra was used for fluorescence measurements. Gel exclusion chromatography was performed with Bio-Gel P-100 (Bio-Rad, Ivry-sur-Seine, France, Marnes-la-Coquette, France) packed with Bio-Gel P-5100. Solutions of P-H and P-(Lys)$_{35}$ at 1 μM in EMEM with or without 10% FCS were used for loading the column and elution was carried out with PBS.

Cell culture and treatment

The NCTC 2544 immortalized human skin keratinocyte cell line was purchased from ICN Flow (Thiverval-sous-Bois, France). Cultures were propagated in BMEM supplemented with 10% FCS, 100 U mL^{-1} penicillin and 100 μg mL^{-1} streptomycin without other additives (weekly passages, 1 : 10 splitting ratio). Cells from trypsinized confluent monolayers were seeded at about 75 000 cells per 35 mm diameter plastic Petri dish containing 2.5 mL of EMEM supplemented with FCS. They were grown for 4 days at 60–80% of confluency. Cells were washed for various times with Hanks' balanced salt medium (HBSS) or 10% FCS-supplemented EMEM containing the desired concentration of photosensitizer. After incubation, cells were thoroughly washed twice with 2 mL of HBSS before irradiation (photosensitizer uptake is not stopped by hypothermic conditions, photocytotoxicity or fluorescence microscopy). Irradiations were carried out with 1 mL of HBSS, devoid of photosensitizer, covering the cell monolayers. Sham-irradiated cells, used as controls, consisted of cells kept in the dark for the same duration and under the same environmental conditions as the irradiated cells.

Cellular uptake of photosensitizers

Immediately after washing, cells were mechanically scraped in 1 mL of water. After collection, 100 μL of an 11% SDS solution in 10 mM, pH 7.0 phosphate buffer were added to the cell suspension. Fifty μL of this solution were saved for protein determination using the method of Lowry *et al.* with the Folin reagent.[12] The rest was used for fluorometric measurement of the photosensitizer concentration, using standard photosensitizer solutions for calibration with excitation and emission wavelengths respectively set at 427 and 655 nm. The photosensitizer concentration was normalized to the protein content and the data are the mean ± standard deviation (SD) of at least three independent experiments, each performed in triplicates.

Irradiation

Irradiation of cell monolayers with broad band red light was carried out with a custom-built table consisting of two 500 W tungsten-halogen lamps whose light was filtered with Balzers VS4 and calflex 2000 optical filters. The lamps were placed below the 30 × 25 cm table thermostated at 37 °C. Under these conditions, most of the light arises from wavelengths in the range 500–750 nm as determined with a CS 1000A Minolta spectroradiometer. Absolute calibration of the light fluence rate was carried out using the photosensitizer concentration of 50 μM His (see below) by 20 μM benzoporphyrin in air saturated 50 mM pH 7.4 phosphate buffer as actinometer. The quantum yield of His degradation was first measured under irradiation with 365 nm monochromatic light collimated by a filtered high pressure mercury lamp as described in ref. 13. Then, the photodynamic His degradation was performed with the red light. The relative absorbed light is equal to $S(1/\lambda)(1 - 10^{-A\lambda})/Ab\lambda$, where S is the surface of the Petri dish, $A\lambda$, the optical density at the wavelength λ and I_λ the light intensity at the wavelength λ, obtained from the radiometer. It is thus possible to calculate the absolute spectral distribution assuming that the His degradation quantum yield in the red range is similar to that at 365 nm. The integration over the wavelength range yields a light intensity of 5.0×10^{-6} photon s^{-1} cm^{-2} corresponding to 1.5.2 mW cm^{-2}. For the sake of comparison with other reports it may be estimated that this intensity is equivalent to monochromatic light intensities I_λ of 4.9×10^{-6} photon s^{-1} cm^{-2} (= 1.9 mW cm^{-2}) and 4.7×10^{-6} photon s^{-1} cm^{-2} (= 1.6 mW cm^{-2}) for P-(Lys)$_{35}$ and P-H respectively at the maximum of the first visible absorption band, namely at 648 nm for P-(Lys)$_{35}$ (ε = 4000 mol^{-1} L cm^{-1}) and at 650 nm for P-H (ε = 1900 mol^{-1} L cm^{-1}). These estimates have been calculated by the relations $\int I_\lambda(\varepsilon/\ln 10)\,d\lambda = I_{\lambda_0}\varepsilon_{\lambda_0}$, where I_λ is the incident light intensity, ε_λ the molar absorbances in PBS at wavelength λ. This calculation is valid for weakly absorbing solutions.

Neutral Red uptake assay

As established earlier,[4] the photocytotoxic effect was determined by the NR uptake assay performed according to Lassarre *et al.*[14] Stained challenged cells were washed and further incubated at 37 °C for 2 h with the supplemented culture medium before loading with NR. This 2 h lag was chosen to allow the initial damage to propagate but was short enough to avoid important proliferation of undamaged cells (population doubling time is about 1 day) which may alter data. The NR uptake is a widely used assay for evaluating the photocytotoxicity of exogenous drugs or hazardous compounds. It has been validated by the European Union for testing phototoxic chemicals and for the classification and labelling of hazardous chemical (EU Commission Directive

2000/A571.C).[24] As reported earlier,[17] in the case of NCTC 2544 keratinocytes the cell injury measured with the NR uptake closely parallels that obtained by the well-known Trypan Blue exclusion test. Data are presented as the percentage of NR uptake with respect to that of a control consisting of sham-irradiated untreated cells. The data are the mean ± SD of at least three independent experiments, each performed in triplicates.

Thiobarbituric acid reactive substances (TBARS) assay

Immediately after irradiation or sham irradiation, cell supernatants (0.9 mL) were collected for TBARS assay used as an index of lipid peroxidation. TBARS were fluorometrically assayed in terms of malondialdehyde (MDA) equivalent as earlier described[16] using 1,1',3,3'-tetramethoxypropane for calibration. Cells were washed twice with PBS, scraped and collected for protein determination. The TBARS values were normalized to the cell protein content. Data are the mean ± SD of triplicates.

Photosensitized His degradation

Dioxygen-saturated solutions containing 5 μM P-H or P-(Lys)$_n$ and 500 μM His in PBS were irradiated with increasing light doses at 365 nm. Histidine was monitored by HPLC using a Whatman Partisil 10/25 SCX cation exchange column and 50 mM $NH_4H_2PO_4$ whose pH was adjusted to 2.3 by addition of phosphoric acid as mobile phase, as earlier described.[13] Irradiations, in a 1 × 1 cm cuvette (2.5 mL), were performed with an OSRAM HBO 200 W high pressure mercury lamp whose 365 nm Hg emission line was isolated as detailed before.[13] Chemical actinometry based on the photoreduction of ferrioxalate by the UV radiation was carried out according to Parker.[19]

Fluorescence microscopy

An inverted fluorescence microscope (Eclipse TE 3000 DV Nikon) equipped with a CoolSNAP$_{HQ}$™ detector cooled at −30 °C (Princeton Instruments; Division of Roper Scientific, Evry, France) was used for cell microfluorometry. This system is controlled by the Metaview/Metamorph software, which is also used for image analyses. The fluorescence was recorded with a CCD camera (1392 × 1040 pixels, 8980 × 6700 μm) through a ×100 oil immersion Phaco 3 Nikon objective. A 2 × 2 binning was used yielding 696 × 520 images corresponding to a field of about 110 × 80 μm. The exposure time was 2 s. The cytosolic fluorescence obtained from cell-free areas was subtracted from all acquired images. Fluorescence was collected through a filter block (UV2A Nikon) consisting of a dichroic mirror at 400 nm, an excitation filter in the range 330–380 nm. The emission filter of the filter block was removed and the red fluorescence of the porphyrin derivatives was collected through a 645AF75 filter (>645 @ 75 nm) from Omega Optical (Brattleboro, VT, USA). In the case of cytosol labeling with LysoTracker Green, the green fluorescence was collected through a 535AF45 filter (~510–565 nm) from Omega Optical. We checked that no porphyrin fluorescence was collected through the green emission filter and that negligible fluorescence of the LysoTracker Green was recorded through the red emission filter. The displayed images are scaled as 256 gray levels between the minimum and maximum fluorescence.

Results and discussion

P-H and P-(Lys)$_n$ uptake and retention

NCTC 2544 keratinocytes were incubated for increasing times with increasing concentrations of the porphyrin derivatives (Fig. 1) in FCS-supplemented EMEM. As shown in Fig. 2A, an extremely fast uptake of P-H is observed, a plateau being reached less than half an hour after the beginning of the incubation. For P-(Lys)$_n$, the initial uptake rate is faster, but it takes longer to reach the plateau, i.e. about 2–3 h after the beginning of the incubation. Once the plateau is reached, no major changes occur at longer incubation times (up to 18 h, data not shown). The most striking difference between P-H and P-(Lys)$_n$ resides in the cell porphyrin contents (Fig. 2A). There is about an order of magnitude between the uptake of P-(Lys)$_n$ and that of P-H.

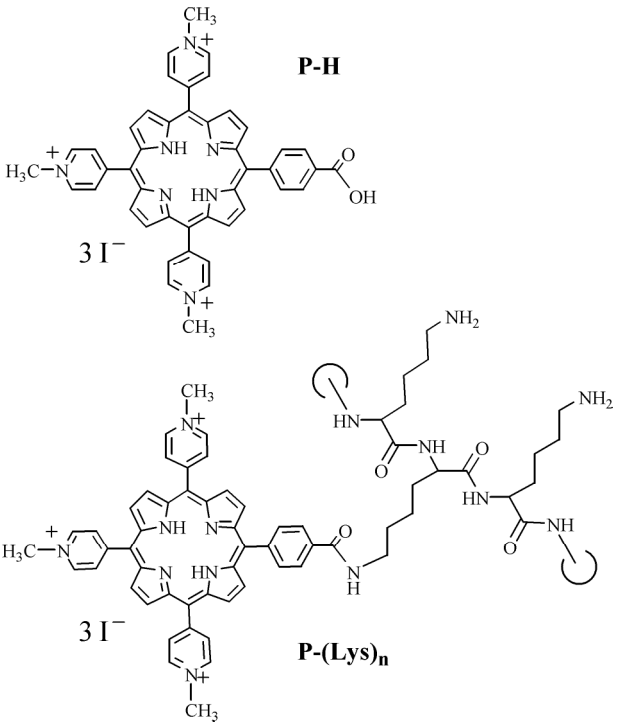

Fig. 1 Chemical structures of P-H and P-(Lys)$_n$.

The uptake was also measured as a function of the porphyrin concentration after a 2 h incubation in FCS-supplemented EMEM, at times for which maximum uptakes have been observed above. As shown in Fig. 2B, the uptake is practically proportional to the incubation concentration. This figure also confirms the lower uptake of the polylysine derivative. It is noteworthy that enhanced uptake associated with the conjugation of polylysine to photosensitizers was already reported by Hamblin *et al.*, in the case of chlorins.[20]

A significant difference was noted in the clearance of P-H and P-(Lys)$_n$ as shown by chase experiments performed after loading cells for 18 h with 5 μM of P-H or P-(Lys)$_n$ in FCS-supplemented EMEM followed by washing. About 65% of P-H and only about 10% of P-(Lys)$_n$ were released during the first hour of incubation with porphyrin-free FCS-supplemented EMEM. In both cases, no further loss was observed up to 6 h of incubation with the porphyrin-free medium.

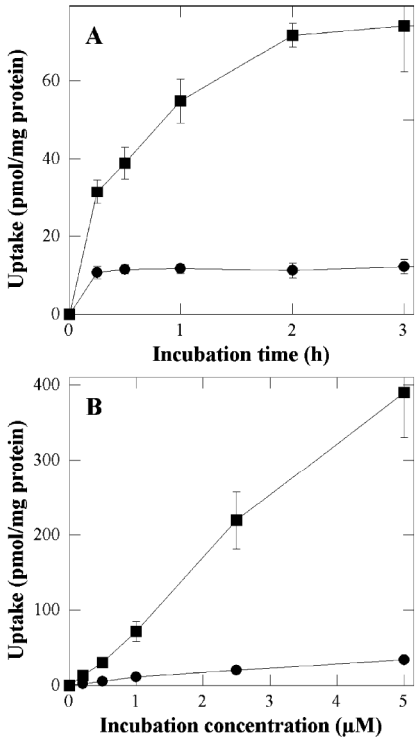

Fig. 2 Uptake of P-H (●) and P-(Lys)$_n$ (■) as a function of the incubation time (A) and of the incubation concentration (B). In A, cells were incubated with 5 μM of porphyrin in FCS-supplemented EMEM in 8-well chambered coverglass for 3 h with FCS-supplemented DMEM. Data are the mean of at least three independent experiments performed in triplicates.

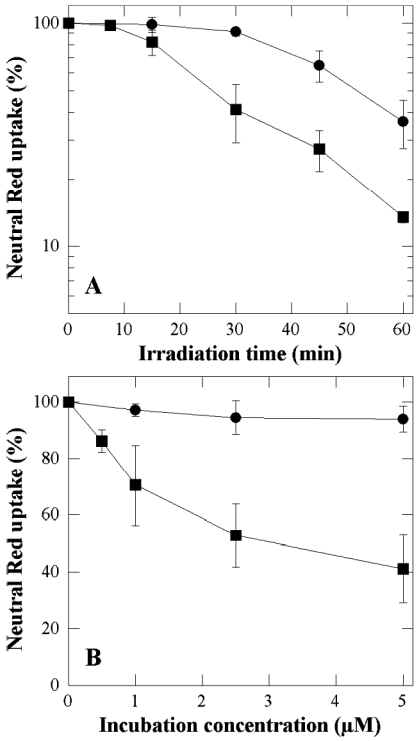

Fig. 3 Cytotoxic effect photosensitized by P-H (●) and P-(Lys)$_n$ (■) as a function of the irradiation time (A) and of the incubation concentration (B). In A, prior to irradiation, cells were incubated for 3 h with 5 μM of porphyrin in FCS-supplemented DMEM. In B, cells were incubated for 3 h with the porphyrin in FCS-supplemented DMEM, and then irradiated for 30 min. A Neutral Red uptake of 100% corresponds to sham-irradiated untreated cells. Data are the mean of at least three independent experiments performed in triplicates.

Photocytotoxicity of P-H and P-(Lys)$_n$

As detailed in the experimental section, Photocytotoxicity was estimated by the NR uptake assay. Prior to irradiation, cells were incubated with 5 μM P-H or P-(Lys)$_n$ for 3 h in FCS-supplemented EMEM in order to reach maximum uptakes. Then cells were irradiated with increasing light doses (Fig. 3A). Control experiments were carried out with cells incubated with up to 0.3% DMSO or the incubation medium but in the absence of porphyrins and then, shamed-irradiated. Control experiments were also performed with cells incubated with porphyrins but not irradiated (up to 60 min). No alteration of the NR uptake was observed with both types of control cells compared to untreated cells. It could also be determined that neither P-H nor P-(Lys)$_n$ exhibited any cytotoxic effect in the dark at incubation concentrations up to 5 μM (data not shown). No photocytotoxicity was observed with up to 5 μM P-H and irradiation times up to 30 min (Fig. 3B). Fig. 3A also shows that the irradiation time must be increased to 60 min to observe a noticeable photocytotoxic effect with 5 μM P-H. On the other hand, after incubation with 5 μM P-(Lys)$_n$, a marked photocytotoxic effect occurs at much shorter irradiation times (Fig. 3A). Thus, the light doses corresponding to a 50% loss of NR uptake are 20–25 min and 50–60 min for P-(Lys)$_n$ and P-H, respectively. The much greater photocytotoxicity of P-(Lys)$_n$ is also evidenced by Fig. 3B, showing that incubation with 2.5 μM of the conjugate is sufficient to produce a 50% loss of NR uptake after 30 min of irradiation.

The greater photocytotoxic effect of P-(Lys)$_n$ as compared to that of P-H may be the consequence of three parameters: e.g. a larger concentration of P-(Lys)$_n$ in the cells or a stronger molar absorbance or an intrinsic greater photosensitizing efficiency. To assess the relative intrinsic photosensitizing efficiency of these two porphyrins the quantum yield of the photosensitized degradation of DHA which occurs via a type II photosensitized mechanism was determined upon monochromatic irradiation as detailed in the experimental section.[4] The DHA degradation quantum yield was found to be 0.66 and 0.60 using respectively P-H and P-(Lys)$_n$ as photosensitizers, indicating that the intrinsic photosensitizing ability is not altered in the porphyrin conjugate. Using polychromatic light, the rate of absorbed light (einstein concentration) is equal to $\int I_0(\lambda)[1-10^{-A(\lambda)}]d\lambda = \int I_0(\lambda)(1-10^{-\varepsilon(\lambda)lc})d\lambda$, where I_0 is the incident intensity, $\varepsilon^{P\text{-}H}$ and $\varepsilon^{P\text{-}(Lys)_n}$ the molar absorptivities at wavelength λ of P-(Lys)$_n$ and P-H, respectively. These molar absorptivities are unknown in the investigated microenvironments. However a reasonable estimate can be obtained by using those determined in PBS, a polar solvent and in 0.3% Triton X100 non-polar micelles. As compared to the parent compounds, the visible absorption bands exhibit a hyperchromic effect and the two last visible absorption bands of P-(Lys)$_n$ undergo a few nanometers bathochromic shift. Combined with the increase of the spectral output of the lamp in the concerned wavelength range, this yields ratios in favor of P-(Lys)$_n$ equal to about 2.6 and 2.8 in PBS and 0.3% Triton

A. [illegible] respectively. They are not large enough to explain alone the greater efficiency of the polylysine derivative. In view of the lower photodynamic effectiveness of P-(Lys)$_n$, it may be suggested that its larger uptake or its better retention than those of P-H strongly contributes to its greater photocytotoxicity. The enhancement of the phototoxic response due the conjugation to polylysine was also reported by Hamblin *et al.*, in the case of related chlorin e$_6$ conjugates.[29]

P-H and P-(Lys)$_n$ photo-induced oxidative stress

The photo-induced lipid peroxidation was used as an overall index of the intensity of the photo-induced oxidative stress induced in keratinocytes by the studied porphyrins. Lipid peroxidation was assayed by measuring TBARS formation. No TBARS formation was detected in the photosensitized cells in agreement with previous studies dealing with photosensitization by endogenous[22] or exogenous photosensitizers.[23] Then, we focused our attention on the TBARS released in the supernatant. No significant TBARS release can be observed with all the above described controls. As shown in Fig. 4, the ability of P-H and P-(Lys)$_n$ to trigger lipid peroxidation parallels their photocytotoxic effects. Furthermore it can be seen that P-(Lys)$_n$ produces much more TBARS than P-H. However it must be pointed out that this does not demonstrate that membrane damage are responsible for the observed cytotoxic effects. It simply suggests that the photocytotoxic effect of the studied derivatives is correlated to their overall ability to trigger an oxidative stress, whatever the targets.

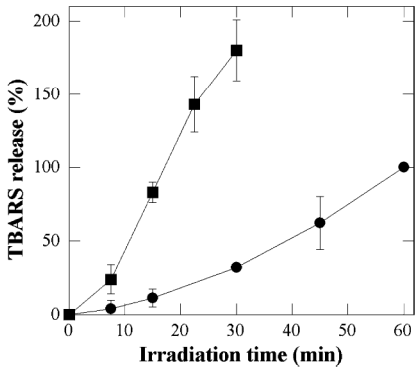

Fig. 4 P-H- and P-(Lys)$_n$-photosensitized lipid peroxidation in NCTC 2544 keratinocytes. TBARS were measured in the supernatant of cells incubated with 5 μM P-H (●) or P-(Lys)$_n$ (■) for 3 h in FCS-supplemented EMEM prior to irradiation. The percentage of TBARS released by P-(Lys)$_n$-photosensitization was expressed taking as 100% the TBARS value measured with P-H after 60 min of irradiation. Data are the mean of at least three independent experiments performed in triplicates.

Microfluorometry of P-H and P-(Lys)$_n$

One of the advantages of PDT is that the currently used and potentially usable porphyrin derivatives do not accumulate in the cell nucleus.[24] Thus in contrast to the psoralens used in the PUVA therapy of skin disorders[25] direct damage to DNA that may lead to mutations in surviving cells are less likely. However, secondary dark reactions in the cells after porphyrin photosensitization have been shown to indirectly lead to DNA alterations.[26] On the other hand it is known that because of their charge, cationic compounds accumulate in the nucleus.[27] For all the above reasons it is interesting to study the role of the conjugation on the intracellular localization of P-H and P-(Lys)$_n$ before further developing this series of molecules. The two studied porphyrins fluoresce in the red with maximum emission near 650 nm. Fluorescence microscopy can therefore be used for unraveling the sites of localization of P-H and P-(Lys)$_n$ in the NCTC 2544 keratinocytes. Fig. 5 shows the phase contrast and fluorescence images obtained for control cells (untreated cells) and cells treated overnight with P-H and P-(Lys)$_n$ in FCS-supplemented culture medium. These images obtained after an overnight incubation (18 h) were similar to those obtained after a 3 h incubation (data not shown). Fluorescence images were obtained with an excitation in the near UV range (330–380 nm) and an emission in the visible range (610–700 nm). As expected[28] the auto-fluorescence arises from the whole cytoplasm with larger intensities in the peri-nuclear area and the mitochondrial network (Fig. 5A and 5D). However, the auto-fluorescence level is low as compared to that obtained with treated cells (see quantified levels in Fig. 5 legend). Upon incubation with P-H, a diffuse fluorescence is observed in the whole cytoplasm as well as more intense localized fluorescence spots suggesting cytoplasmic and plasma membrane localization in addition to the accumulation in lysosomes or

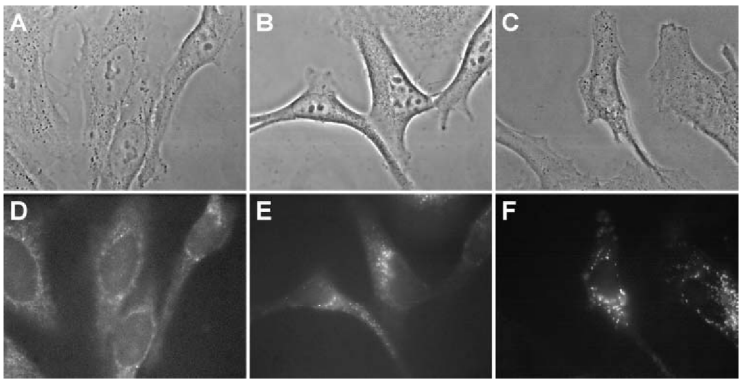

Fig. 5 Phase contrast images (A, B, C) and fluorescence micrographs (D, E, F) obtained in NCTC 2544 keratinocytes incubated for 18 h in EMEM + 10% FCS with no additives (A, D), with 5 μM P-H (B, E) or with 5 μM P-(Lys)$_n$ (C, F). Fluorescence images were obtained with an Nikon × 100 oil immersion objective. Exposure time: 2 s. Signal attenuation: 1/16. Dichroic mirror: 400 nm. Excitation: 330–380 nm. Emission: 610–700 nm. 256 Grey levels between: −30–120 (D), −140–650 (E) and −150–2500 (F).

lysosome like structures (Fig. 5B and 5E). In agreement with the uptake data, the fluorescence recorded after 1 h of incubation with P-(Lys)$_n$ is much larger than that obtained with P-H (Fig. 5C and 5F). Moreover, the P-(Lys)$_n$ fluorescence is more specifically localized in the lysosome-like structures. Lysosomal localization of P-(Lys)$_n$ was confirmed by double labeling with the lysosome specific probe, LysoTracker Green whose fluorescence emission is centered around 515 nm (see experimental section and legend of Fig. 6 for details). LysoTracker Green is a lysosomotropic weak base staining low pH (about 5–6) cell compartments. As shown in Fig. 6, the red fluorescence image (Fig. 6B) and the green fluorescence image (Fig. 6C) closely resemble. However, these two fluorescence images do not perfectly superimpose, suggesting that in addition to lysosomes, P-(Lys)$_n$ also localizes in non-lysosomal structures, most probably early endosomes or pinocytic vesicles. These early endocytotic vesicles have a pH slightly more basic than that of lysosomes and are therefore poorly or not labeled by LysoTracker Green. In relation to this observation, Hamblin *et al.* showed that the conjugation of chlorin e_6 to poly-L-lysine (positively charged at neutral pH) leads to a more substantial increase in the fluorescence of the photosensitizer.[29] It should be noted that the specific accumulation of these two porphyrins in the mitochondria of NCTC 2544 keratinocytes is unlikely in view of data obtained with the specific mitochondria probe rhodamine 123, which show a mitochondrial network extending all over the cell (data not shown, see also ref. 29). Finally, it should be noted that the low fluorescence level of P-(Lys)$_n$ and in a lesser extent of P-H in the nuclear area, strongly suggests that there is little, if any, photosensitizer in the nucleus, despite the positive charges of these molecules. However, the same re-localization as that observed during or after the incubation with other porphyrin derivatives[24] could mean that may confer a carcinogenic potential on these molecules.

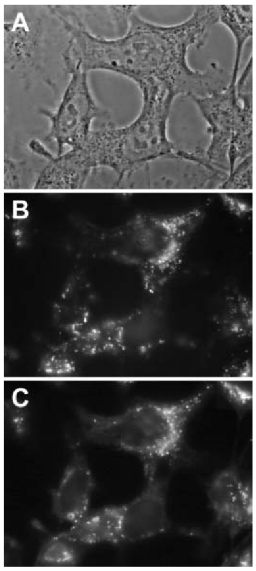

Fig. 6 Phase contrast images (A) and fluorescence micrographs (B, C) obtained with 2544 keratinocytes incubated for 17 h with 5 μM P-(Lys)$_n$ in EMEM + 10% FCS and then for 1 h with 5 μM P-(Lys)$_n$ and 125 nM LysoTracker Green in EMEM + 10% FCS. Fluorescence images were obtained with a Nikon × 100 oil immersion objective. Exposure time: 2 s. Signal attenuation: 1/16. Dichroic mirror: 400 nm. Excitation: 330–380 nm. Emission: 610–700 nm (B) and 510–565 nm (C). 256 Grey levels between: −190–2900 (B) and −130–3100 (C).

Effect of the presence of proteins in the incubation medium

The experiments described above were also performed after incubating the cells with porphyrins in serum free medium. Though incubation in FCS-supplemented medium is closer to the *in vivo* situation, this study may unravel a role of serum proteins in the uptake process. As shown in Fig. 7A, an extremely fast uptake is observed for both P-H and P-(Lys)$_n$. Whereas the kinetics of the P-H uptake is independent of the presence or absence of proteins, the P-(Lys)$_n$ uptake is faster in the absence of proteins than in their presence suggesting that the P-(Lys)$_n$ derivative interacts with serum proteins. This interaction most probably due to the polylysine chain may explain the lower plateau value observed in the presence of proteins (compare Fig. 7A to Fig. 2A). In this regard, solutions of the derivatives (1 μM) in culture medium with or without proteins (10% FCS) were submitted to gel exclusion chromatography. In contrast to P-H, retained on the top of the column either in the presence or in the absence of proteins, part of P-(Lys)$_n$ (about 30%) eluted with the proteins (data not shown). In the absence of proteins, P-(Lys)$_n$ eluted at longer times, strongly suggesting that it interacts with serum proteins. The higher rate of uptake of the strongly positively charged P-(Lys)$_n$ probably results from the negative charge of the outer cell plasma membrane.[11] As observed with the serum supplemented medium, the P-(Lys)$_n$

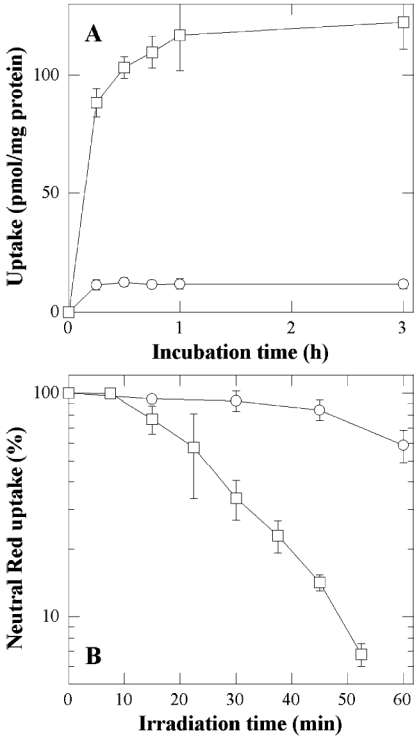

Fig. 7 Uptake of P-H (○) and P-(Lys)$_n$ (□) as a function of the incubation time (A) and cytotoxic effects photosensitized by P-H (○) and P-(Lys)$_n$ (□) as a function of the irradiation time (B). In A, cells were incubated with 1 μM of porphyrin in HBSS. In B, cells were incubated with 5 μM of porphyrin in HBSS prior to irradiation. A Neutral Red uptake of 100% corresponds to sham-irradiated untreated cells. Data are the mean of at least three independent experiments performed in triplicates.

uptake is an order of magnitude greater than that of P-H (Fig. 3A) and is practically proportional to the P-(Lys)$_4$ concentration after 1 h incubation with concentrations up to 5 μM (data not shown).

The effect of proteins on the photocytotoxicity of P-H and P-(Lys)$_4$ was assessed by incubating the cells for 1 h in HBSS with 5 μM P-H or P-(Lys)$_4$. Data reported in Fig. 3B can be compared to those obtained in the presence of FCS (see Fig. 3). First, it should be noted that P-H or P-(Lys)$_4$ are not cytotoxic in the dark. The phototoxicity data obtained with P-H or P-(Lys)$_4$ under these incubation conditions are similar to those obtained in the presence of serum proteins. A weak photocytotoxicity can only be observed with P-H at high incubation concentration (5 μM) and long irradiation time (60 min). The photocytotoxicity of P-(Lys)$_4$ is slightly higher in the absence than in the presence of proteins, consistent with a slightly greater uptake in the former case. In conclusion, as observed for the uptake, the presence of serum proteins in the incubation medium does not significantly alter the phototoxicity.

Time-microscopy was also assayed after incubation in the absence of serum proteins. Data (not shown) demonstrate the lack of influence of serum proteins. A similar conclusion can be drawn regarding the intracellular localization since similar patterns are observed by microfluorimetry after incubation in HBSS.

Concluding remarks

In view of the low photodynamic effectiveness of P-(Lys)$_4$, it may be suggested that its larger uptake and better retention than those of P-H (assessed with cells) both highly contribute to its greater photocytotoxicity. The microfluorescence study suggests that, in addition to the uptake, the intracellular localization could contribute to the marked differences in the cell photosensitizing efficiencies. Interestingly, the most effective poly-lysine-derivatives do not accumulate in the nucleus. However, it is obvious that a better understanding of the strong effect of the poly-lysine side chain on the photocytotoxic potential of the tetrapyrrolic porphyrins requires further investigations on the relationship(s) between their cell localization and the molecular mechanisms underlying their phototoxic effect.

Acknowledgements

This work was supported in part by grants from the Gulbenkian Foundation (to INSERM/GRICES exchange agreement) and by the Franco-Portuguese "Pessoa" exchange Program (07938NH) and "Fundação para a Ciência e a Tecnologia" (Área de Organic Chemistry Research Unit). The fluorescence microscopy experiments were performed with the equipment of the "Centre de Microscopie du Muséum". The authors wish to thank Dr M. Gibbs and M. Dellinger for their advice.

References

1 T. J. Dougherty, C. J. Gomer, B. W. Henderson, G. Jori, D. Kessel, M. Korbelik, J. Moan and Q. Peng, Photodynamic therapy, *J. Natl. Cancer Inst.*, 1998, **90**, 889–905.

2 R. K. Pandey and G. Zheng, Porphyrins as photosensitizers in photodynamic therapy, in *The Porphyrin Handbook*, ed. K. M. Kadish, K. M. Smith and R. Guillard, Academic Press, San Diego, 2000, vol. 6, pp. 157–230.

3 R. Bonnett, *Chemical Aspects of Photodynamic Therapy*, Gordon and Breach Science Publishers, London, 2000.

4 C. Schmidt, Interdisciplinary and International Mechanisms of action of photodynamic therapy with chlorin-type photosensitizers in the treatment of age-related macular degeneration, *Surv. Ophthalmol.*, 2000, **45**, 195–214.

5 A. M. Sieber, J. Warloe, A. Berner and K. E. Gederaas, A follow-up study of the recurrence and cosmesis in completely responding superficial and nodular basal cell carcinomas treated with methyl 5-aminolevulinate-based photodynamic therapy alone and with prior curettage, *Br. J. Dermatol.*, 2001, **145**, 469–475.

6 X. Chen, J. Hai, D. A. Drake and C. M. Drain, Efficient synthesis and photodynamic activity of porphyrin-saccharide conjugates: targeting and incapacitating cancer cells, *Bioconjug. Chem.*, 2004, **15**, 1067–1079.

7 H. Kato, K. Furukawa, M. Sato, T. Okunaka, Y. Kuroki, M. Kawahara, M. Tanaka, T. Miyazawa, T. Yana, K. Muto, T. Shirabe and H. Hamamoto, Phase II clinical study of photodynamic therapy using mono-L-aspartyl chlorin e6 and diode laser for early superficial squamous cell carcinoma of the lung, *Lung Cancer*, 2003, **42**, 103–111.

8 J. P. C. Tomé, M. G. P. M. S. Neves, A. C. Tomé, J. A. S. Cavaleiro, M. Soncin, M. Magnoni, S. Perro and G. Jori, Synthesis and antibacterial activity of new poly-S-lysine porphyrin conjugates, *J. Med. Chem.*, 2004, **47**, 6649–6652.

9 M. R. Hamblin and T. Hasan, Photodynamic therapy: a new antimicrobial approach to infectious disease?, *Photochem. Photobiol. Sci.*, 2004, **3**, 436–450.

10 D. Gad, T. Zahra, K. P. Francis, T. Hasan and M. R. Hamblin, Targeted photodynamic therapy of established soft-tissue infections in mice, *Photochem. Photobiol. Sci.*, 2004, **3**, 451–458.

11 P. Th. Korn, Cell membrane structure and synthesis, *Ann. Rev. Physiol.*, 1969, **31**, 303–336.

12 O. H. Lowry, N. J. Rosebrough, A. L. Farr and R. J. Randall, Protein measurement with the Folin phenol reagent, *J. Biol. Chem.*, 1951, **193**, 265–275.

13 P. Morlière, T. Bosca, M. A. Miranda, J. V. Castell and R. Santus, Primary photochemical processes of the psoralenic cross-linker 4′-aminomethyl-4,5′,8-trimethylpsoralen: a study by laser flash photolysis and steady state irradiation, *Photochem. Photobiol.*, 1984, **40**, 535–541.

14 P. Morliere, S. Salvador, M. Anbouiy, A. Rister and R. Santus, Sensitization of skin fibroblasts to UVA by traces of iron, *Biochim. Biophys. Acta*, 1997, **1334**, 297–300.

15 R. M. Lemmon, R. V. Use tollon, E. C. Gomez, Quantitative in vivo assessment of photosensitivity by a fibroblast-neutral red assay, *J. Invest. Dermatol.*, 1982, **78**, 277–279.

16 Commission Directive 2000/33/EC, *Official Journal of the European Communities*, 6.6.2000, pp. L136/90–L136/97.

17 P. Filipe, J. N. Silva, J. Haigle, J. P. Freitas, A. Fernandes, R. Santus and P. Morliere, Contrasting action of flavonoids on phototoxic effects induced in human skin fibroblasts by UVA alone or UVA plus cyamemazine, a phenothiazine neuroleptic, *Photochem. Photobiol. Sci.*, 2005, **4**, 420–428.

18 P. Morlière, A. Moysan, R. Santus, G. Huppe, J.-C. Mazière and L. Dubertret, UVA-induced lipid peroxidation in cultured human skin fibroblasts, *Biochim. Biophys. Acta*, 1991, **1084**, 261–268.

19 C. A. Parker, *Photoluminescence of Solutions*, Elsevier, Amsterdam, 1968, pp. 326–326.

20 M. R. Hamblin, J. L. Miller, L. Rizvi and R. Oseroff, Hydroxyaluminium chloride, a polyethylene chain and Tetrakis(4-sulfonatophenyl)porphine: cellular uptake, localization and photosensitivity towards macrophages and tumor cells, *J. Photochem. Photobiol. B: Biol.*, 1997, **38**, 145–157.

21 E. Kohen, R. Santus and J. G. Hirschberg, *Photobiology*, Academic Press, San Diego, 1995, pp. 53–85.

22 P. Morliere, A. Moysan, R. Santus, G. Huppe, J.-C. Mazière and L. Dubertret, UVA-induced lipid peroxidation in cultured human fibroblasts, *Biochim. Biophys. Acta*, 1991, **1084**, 261–268.

23 P. Morlière, J. Haigle, P. Filipe, J. Silva and R. Santus, An insight into the mechanisms of the phototoxic response induced by cyamemazine: a study with cultured fibroblasts and keratinocytes, *Photochem. Photobiol.*, 2004, **79**, 163–171.

24 K. Berg, *Mechanisms of cell damage in photodynamic therapy*, in *The fundamental bases of phototherapyed*, A. Young, H. Honigsmann and G. Jori, OEMF, Milan, 1996, pp. 181–207.

97 T. Dall'Acqua, S. Marciani, M. Marzi, D. Zamboni and G. Rodighiero, Kinetic analysis of the photoreaction (Psoralen)-between psoralen and DNA, *Photochem. Photobiol.*, 1979, **29**, 489–495.

98 G. Onédraogo and R. W. Redmond, Secondary reactive species and the diversity of photosensitized effects in cells: DNA damage promoted via initial membrane sensitization, *Photochem. Photobiol.*, 2005, **77**, 443–450.

99 R. P. Haugland, *Handbook of Fluorescent Probes and Research Chemicals*, Molecular Probes Inc., Eugene, Oregon, 2005, pp. 277–280.

100 M. Dellinger, M. Géze, R. Santus, T. Kuhen, C. Kaiser, J. G. Hirschberg and M. Morris, Imaging of cells by autofluorescence: a new tool in the probing of photopharmaceutical effects at the intracellular level, *Biotechnol. Appl. Biochem.*, 1999, **29**, 25–33.

101 M. Géze, L. M. Cavaliere, M. Bazin and R. Santus, Sub-cellular localization of second generation PDT photosensitizers studied by microspectrofluorometry, in *Analytical use of fluorescent probes in oncology*, ed. E. Kessler and I. G. Hilderbrand, Plenum Press, New York, 1996, pp. 113–131.

ARTICLE III

CHAIN-DEPENDENT PHOTOCYTOTOXICITY OF TRICATIONIC PORPHYRIN CONJUGATES AND RELATED MECHANISMS OF CELL DEATH IN PROLIFERATING HUMAN SKIN KERATINOCYTES

Biochemical Pharmacology xxx (2010) xxx–xxx

Contents lists available at ScienceDirect

Biochemical Pharmacology

journal homepage: www.elsevier.com/locate/biochempharm

Chain-dependent photocytotoxicity of tricationic porphyrin conjugates and related mechanisms of cell death in proliferating human skin keratinocytes

João Nuno Silva [a,b,c,d], Antoine Galmiche [b,c,d], João P.C. Tomé [e], Agnès Boullier [b,c,d], Maria G.P.M.S. Neves [e], Eduarda M.P. Silva [e], Jean-Claude Capiod [f], José A.S. Cavaleiro [e], René Santus [g], Jean-Claude Mazière [b,c,d], Paulo Filipe [a], Patrice Morlière [b,c,d,*]

[a] Faculdade de Medicina de Lisboa, Hospital de Santa Maria, Clinica Universitária de Dermatologia, Lisboa, Portugal
[b] INSERM, ERI12, Amiens, France
[c] Université de Picardie Jules Verne, Faculté de Médecine et de Pharmacie, EA 4292, Amiens, France
[d] CHU Amiens, Laboratoire de Biochimie, Amiens, France
[e] University of Aveiro, Department of Chemistry, Aveiro, Portugal
[f] CHU Amiens, Laboratoire d'Hématologie, Amiens, France
[g] Muséum National d'Histoire Naturelle, RDDM, Photobiologie, Paris, France

ARTICLE INFO

Article history:
Received 14 June 2010
Accepted 22 July 2010
Available online xxx

xxxxxxx
LDL
Photocytotoxicity
Keratinocytes
Autophagy
Caspases
MAPK pathways

ABSTRACT

Photodynamic therapy (PDT) is a poor treatment option for nodular basal cell carcinomas and squamous cell carcinomas. As a result, the search for new photosensitizers with better effectiveness is of current interest. The photocytotoxicity of conjugates (P-R) of a water soluble tricationic porphyrin (P-T), having similar efficiency at production of singlet oxygen, the PDT botanoxin, has been assessed in vitro. Links between uptake, intracellular localization, photooxidative stress, photocytotoxicity and ability to induce programmed cell death are established. Conjugates bearing methyl (2-Me), Di-O-isopropylidene (2-glucopyranosyl (2-OGal) or N,N'-dicyclohexylcarbodioxycarbonyl (2-DDC) chains are efficiently taken-up by proliferating NCTC 2544 keratinocytes. The relative order of photocytotoxicity is 2-OGal > 2-DDC ≈ 2-Me > 2-H. The photocytotoxic potential of 2-Me, 2-OGal and 2-DDC is due to that of endogenous protoporphyrin IX induced by δ-aminolevulinic acid or its esters. The pro-drugs currently employed for PDT of skin lesions. Microfluorimetry shows that 2-Me, 2-OGal and 2-DDC localize in cytosolic pinocytotic vesicles but not in mitochondria or nucleus. Absence of annexin V binding, caspase activation or chromatin condensation suggests that cell photosensitization by P-R does not induce apoptosis. On the other hand, P-OGal photocytotoxicity correlates with appearance of cytosolic vesicles that have hall marks of autophagy compartments, being decreased with the transient transfection by an expression vector encoding GFP-LC3. ERK1/2 and JNK phosphorylation and inhibition of ERK1/2 phosphorylation suggest close relationship between normal thymocytes and MAPK pathway involvement. Given their potentially easy formulation, water-soluble P-R are promising powerful photosensitizers for PDT of skin lesions.

1. Introduction

The treatment of malignant or benign skin diseases by photodynamic therapy (PDT) has developed rapidly [1]. Current evidence indicates that topical PDT is effective in actinic keratosis, Bowen's disease and basal cell carcinoma (BCC) but it is a relatively poor treatment option for either squamous cell carcinomas or nodular BCC. In current skin PDT, topical application of δ-aminolevulinic acid (ALA) or its methyl ester (MAL), precursors of protoporphyrin IX (PPIX), is followed by illumination of the diseased area with red light. The poor water solubility of these agents requires expensive preparation of formulations for systemic or topical administration. Hence, development of new

Abbreviations: 3-MA, 3-methyladenine; ALA, 5-aminolevulinic acid; A, annexin V-FITC; BCC, Basal cell carcinoma; CHAPS, 3-[(3-cholamidopropyl)dimethylammonio]-1-propanesulfonic acid; EMEM, minimum essential medium with Earle's salts; FCS, fetal calf serum; GFP, Green fluorescent protein; HBSS, Hanks' balanced saline solution; LC3, microtubule-associated protein light-chain 3; MAL, methyl aminolevulinate; NR, neutral red; DPBS, Dulbecco's phosphate-buffered saline; PDT, photodynamic therapy; PI, propidium iodide; PPIX, protoporphyrin IX; ROS, reactive oxygen species; SDS, sodium dodecyl sulfate; TBARS, thiobarbituric acid reactive substances; TX100, triton X100.

* Corresponding author at: INSERM ERI12, Laboratoire de Biochimie, CHU Amiens - Hôpital Nord, place Victor Pauchet, 80054 Amiens Cedex 1, France.
Tel.: +33 3 22 66 86 69; fax: +33 3 22 66 85 93.
E-mail address: morliere.patrice@chu-amiens.fr (P. Morlière).

0006-2952/$ – see front matter © 2010 Elsevier Inc. All rights reserved.
doi:10.1016/j.bcp.2010.07.033

photosensitizers with better effectiveness is of current interest. Such new photoactive substances might demonstrate better clinical and histological efficacy in treating skin lesions for which topical MAL PDT is ineffective (e.g. melanoma) or might be used as a palliative treatment for patients with plaque type cutaneous T cell lymphoma. Despite superior absorbance in the 700 nm region (molar absorptivity: ~2 × 10^5 M^{-1} cm^{-1}) phthalocyanines are not currently used in the PDT of epidermal skin lesions (normally ~1–2 mm thickness). They tend to form aggregates of reduced uptake and photosensitizing properties and the phthalocyanine ring resists to biodegradation [2]. However, their encapsulation in silica nanoparticles would appear to provide a promising approach to photosensitizer uptake and delivery as it has already been shown to improve the aqueous solubility and stability of the silicon phthalocyanine 4 [3]. For these reasons, the synthesis of water-soluble derivatives of porphyrins and chlorins has been investigated. Conjugation of amino-acids, peptides and sugars to photosensitizers favours specific targeting since such groups play key roles in the recognition and metabolism in micro-organisms and cells [4,5].

In this study, new water-soluble derivatives of 5-(4-carboxyphenyl)-10,15,20-tris(4-methylpyridinium-4-yl)porphyrin tri-iodide (P-R), whose absorbance maxima are shifted to the red by 15–20 nm as compared to PPIX, have been shown to be of potential interest in dermatological PDT since a poly-S-lysine conjugate is, *in vitro*, an effective photosensitizer towards rapidly proliferating human skin keratinocytes [6]. Furthermore, tricationic porphyrins are promising molecules since they may bind to negatively charged skin cells after disruption of the *Stratum Corneum* barrier. In this study, the photocytotoxicity effectiveness of conjugates with a methyl (P-Me), a dicyclohexylureidooxy group (P-DDC), a di-*O*-isopropylidene-α-D-galactopyranosyl group (P-OGal), a α/β-D-galactopyranosyl group (P-Gal) has been evaluated in cultured proliferating human skin keratinocytes for allowing the direct comparison of results obtained with the poly-*S*-lysine conjugate (P-(Lys)$_n$) [6]. We have also determined the molecular mechanisms involved in the photo-induced cell death, the induction of a specific death mode being susceptible to result in a therapeutic advantage.

2. Materials and methods

2.1. Chemicals, culture media and routine spectroscopic equipment

Reagents for cell culture, minimum essential medium with Earle's salts (EMEM), Hanks' balanced saline solution containing 20 mM Hepes (HBSS), Dulbecco's phosphate-buffered saline (DPBS), all without phenol red, fetal calf serum (FCS), trypsin and antibiotics were purchased from Sigma Chemical Co (St. Louis, MO, USA). Chemicals and reagents were obtained from Sigma chemical Co., Merck (Darmstadt, Germany), Fluka (Saint-Quentin Fallavier, France) and Molecular Probes (Eugene, OR, USA) [6]. Inhibitors of p38 (SB203580) and JNK (SP600125) were purchased from Calbiochem (Darmstadt, Germany). Specific antibodies against caspase-3, caspase-8, caspase-9 and p62/SQSTM1 were provided by Santa Cruz Biotechnology (Heidelberg, Germany) whereas those against total p38, phospho-p38, total JNK, phospho-JNK, total Akt, phospho-Akt, total ERK, phospho-ERK were purchased from Cell Signaling (Beverley, MA, USA). The synthesis of the porphyrin conjugates (P-R) (Fig. 1) was performed as described by Tomé et al. [5,7]. The 500 μM stock solutions were prepared in water:DMSO (1:1, v/v) and stored at 0–4 °C. A UVIKON 943 spectrophotometer from Kontron Instruments (Montigny les Bretonneux, France) was used for optical absorption spectrophotometry. Fluorescence measurements were carried out with a SLM AMINCO-BOWMAN (series 2) fluorometer (Bioritech, Chamarande, France).

2.2. Cell culture and treatment

The immortalized NCTC 2544 human skin keratinocyte cell line was purchased from ICN Flow (Fontenay sous Bois, France). Cells were propagated, grown and seeded as earlier described [6]. For

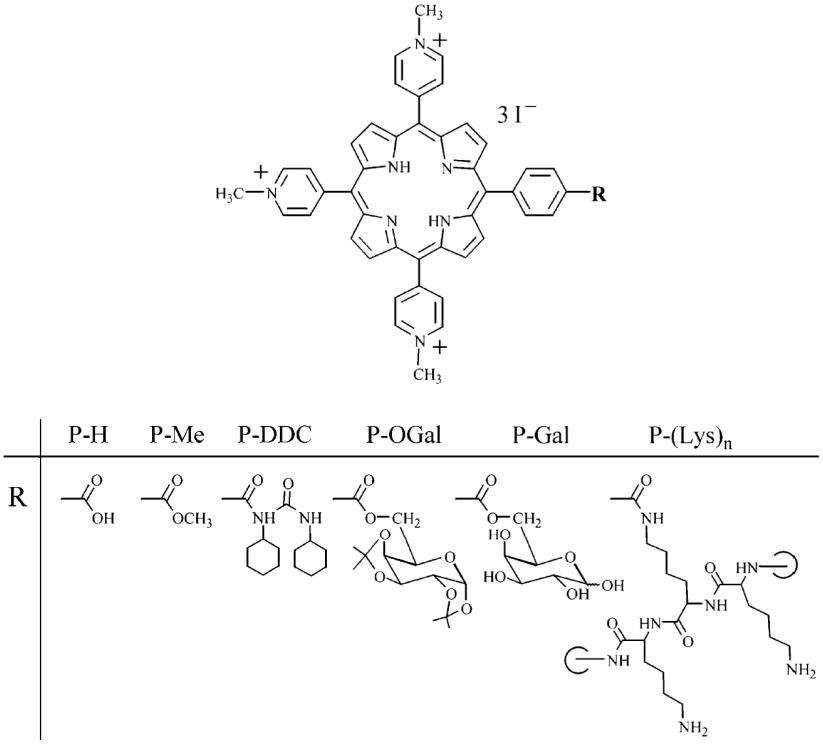

Fig. 1. Chemical structure of P-R derivatives.

fluorescence microscopy, cells were seeded on 30 mm diameter and 0.15 mm thick coverglass at a density of about 1,700 cells/cm² (2.5 mL at about 5000 cells/mL) and were grown for 4 days. The incubations were carried out with 1 mL of P-R at various concentrations and for various times in either HBSS or 10% FCS supplemented EMEM. In the case of endogenous PPIX synthesis, incubations were performed with 0.2–0.8 mM ALA in 10% FCS supplemented EMEM. After incubation, cells were washed twice with 4 mL of HBSS before measurements.

2.3. Irradiation

Washed cell monolayers, covered with 1 mL of HBSS without photosensitizer, were irradiated with broad band red light provided by a custom-built table consisting of two 300 W tungsten-halogen lamps whose light was filtered with Balzers Y54 and calflex 3000 optical filters [6,8]. Petri dishes were placed on a 30 × 25 cm thermostated (37 °C) glass table above the lamps. Under these conditions, most of the light originates from wavelengths in the range 500–750 nm as determined with a CS 1000A Minolta spectroradiometer. The lamp actinometry is described in supplementary data.

2.4. Determination of intracellular photosensitizer concentration

Immediately after P-R or ALA incubation and washings, cells were mechanically scrapped in 1 mL of water. After collection, 100 μL of an 11% SDS solution in 10 mM phosphate buffer (pH 7.0) were added to the disrupted cell suspension. Fifty μL of this solution were saved for protein determination using Lowry's method with Folin reagent. The remainder was utilized for fluorometric measurement of photosensitizer concentration, using standard P-R solutions for calibration (λ_{exc} = 427 nm and λ_{em} = 659 nm) or standard PPIX solutions (λ_{exc} = 407 nm and λ_{em} = 636 nm) [9]. Data are the mean ± SD of at least three independent experiments, each performed in triplicate.

2.5. Neutral Red uptake assay

The assessment of photocytotoxicity by the NR uptake assay has been validated by the European Union for the testing of phototoxic chemicals and for the classification and labelling of hazardous chemical (EU Commission Directive 2000/33/EC). This assay has been fully described by Filipe et al. [10].

2.6. Thiobarbituric acid reactive substances (TBARS) assay

Immediately after irradiation or sham-irradiation, 0.9 mL of supernatants was collected. After addition of 90 μL of butylated hydroxytoluene (2% w/w in ethanol) samples were kept frozen until TBARS assay. Cells were washed twice with DPBS, scrapped and collected for protein determination. TBARS were fluorometrically determined in terms of malondialdehyde equivalent as earlier described [6].

2.7. Fluorescence microscopy equipment for photosensitizer localization

An inverted fluorescence microscope (Eclipse TE 2000 DV Nikon) equipped with a CoolSNAP$_{HQ}^{TM}$ detector cooled to −30 °C (Princeton Instruments; Division of Roper Scientific, Evry, France) was used for cell microfluorometry. This system is controlled by the Metaview/Metamorph software, which is also used for image analyses. The fluorescence recording conditions (objective, camera binning and exposure time, dichroic mirrors, filters) are fully described in ref. [6]. No porphyrin fluorescence was detected with the green emission filter while negligible fluorescence of the Lyso-Tracker Green was recorded with the red emission filter. Background fluorescence obtained from cell free areas was subtracted from all the acquired images.

2.8. Flow cytometry

At various times after photosensitization, adherent cells were washed twice in ice-cold DPBS and detached with Accutase^{TM} (Sigma–Aldrich Co). Cells were transferred to 15 mL conical tubes and gently washed with serum supplemented medium by low speed centrifugation at 1500 rpm for 5 min. Cell pellets were washed once with DPBS and then re-suspended in assay buffer (0.1 M HEPES/NaOH, pH 7.4; 140 mM NaCl; 25 mM $CaCl_2$) at a concentration of 1×10^6 cells/mL. Annexin V-FITC binding was assessed using the Santa Cruz Biotechnology Apoptosis Kit (Santa Cruz Biotechnology, Heidelberg, Germany) according to the manufacturer's protocol. After 15 min of incubation in the dark with annexin V-FITC (5 μg/mL) and propidium iodide (PI) (5 μg/mL), cell fluorescence was measured in the spectral regions 505–545 nm (FL1) for annexin V-FITC (A) and 610–650 nm (FL3) for PI with a Cytomics FC 500 flow cytometer (Beckam Coulter, Villepinte, France). Data analysis was performed using Cytomics Analysis software.

2.9. DNA fragmentation assay

DNA fragmentation was assessed through determining cytoplasmic accumulation of histone-associated DNA fragments by an enzyme-linked immunosorbent assay (Roche Diagnostics, Mannheim, Germany). At different times after irradiation, the cell supernatant was removed, cells were washed twice with ice-cold DPBS and lysed with the kit buffer. Equal amounts of protein from the cytoplasmic fraction (100 μg, Bradford assay from Bio-Rad Laboratories, Marne-la-Coquette, France) were transferred into an anti-DNA precoated microtiter plate and analyzed using the ELISA procedure recommended by the manufacturer.

2.10. Caspase assays

After irradiation cells were lysed in buffer (10 mM HEPES, pH 7.4, 2 mM EDTA, 0.1% CHAPS, 5 mM dithiothreitol and 1 mM phenylmethylsulfonyl fluoride, supplemented with 10 μg/mL pepstatin, aprotinin and leupeptin), sonicated and centrifuged at 14,000 × g for 5 min at 4 °C. Supernatants were saved as representative cytosol extracts. Aminomethylcoumarin (AMC)-conjugated peptide substrates at a final concentration of 20 μM were added to 40 μg of total cytosol protein and incubated for 30 min at 37 °C. The specific substrates used were: acetyl-Asp-Glu-Val-Asp-AMC (Ac-DEVD-AMC) for caspase-3, acetyl-Ile-Glu-Thr-Asp-AMC (Ac-IETD-AMC) for caspase-8 and acetyl-Leu-Glu-His-Asp-AMC (Ac-LEHD-AMC) for caspase-9 (AnaSpec, Inc, San Jose, CA, USA). The fluorescence of coumarin dyes was measured with a 96-microwell plate reader under excitation at 360 nm and emission at 460 nm.

2.11. Immunoblot analysis

Cells were lysed in RIPA buffer supplemented with protease and phosphatase inhibitors. The protein concentration of cell extracts was determined using the Pierce BCA assay (Thermo Fisher Scientific, Cergy Pontoise, France) and equal amounts of proteins (40 μg) were separated by 12% SDS-PAGE and transferred onto nitrocellulose membranes. Membranes were immunoblotted using conventional procedures and revealed using an enhanced chemiluminescence detection kit from Amersham (Saclay, France). Western blots were scanned and quantified using the software ImageJ (National Institutes of Health).

2.12. Cell transfection with GFP-LC3

The cDNA encoding microtubule associated protein light chain 3 (LC3) protein tagged at its N-terminus with green fluorescent protein (GFP), GFP-LC3, has been used to monitor autophagy through cited fluorescence microscopy and was provided by Drs. T. Yoshimori and N. Mizushima (Department of Bioregulation and Metabolism, The Tokyo Metropolitan Institute of Medical Science, Japan) [11]. NCTC 2544 cells grown on glass coverslips were transfected with GFP-LC3 using Lipofectamine 2000 according to the supplier's protocol (Invitrogen). After transfection, cells were incubated for 3 h with 5 μM P-OGal or for 18 h with 0.8 mM ALA and irradiated for 15 min. At various times after irradiation, cells were fixed with paraformaldehyde, rinsed and mounted on glass slides using Mowiol (Calbiochem). Cells were observed under a Nikon Eclipe TE2000-U fluorescence microscope equipped with a plan APO VC 60×/1.40 objective under oil immersion. Cells with active autophagy were defined as those displaying 3 or more puncta of GFP-LC3. Results are given under each experimental condition as percentage of cells with more than 3 puncta of GFP-LC3, and are based on the counting of over 500 cells expressing GFP-LC3.

2.13. Cytochrome c immunofluorescent staining

Cells grown on glass coverslips and treated as indicated were washed with PBS, fixed with 4% paraformaldehyde, and permeabilized with 0.1% TX100. Immunolabelling was performed using a mouse antibody raised against cytochrome c (BD Bioscience, Le Pont de Claix, France) and a secondary antibody labeled with Cy3 (Jackson Immunoresearch). Nuclei were counterstained with DAPI. The stained samples were rinsed and mounted in Mowiol (Calbiochem) and the slides were examined and photographed using a Nikon Eclipse TE2000-U fluorescence microscope equipped with a plan APO VC 60×/1.40 objective under oil immersion.

2.14. Statistical analyses

Statistical analyses were performed with the Student's *t*-test. Statistical significances are provided in the figures ($^{*}p < 0.05$, $^{**}p < 0.01$).

3. Results

3.1. Uptake of P-R derivatives by cells

NCTC 2544 keratinocytes have been incubated at various durations with increasing concentrations of porphyrins in FCS-supplemented EMEM. As shown in Fig. 2A, the uptake of all derivatives is extremely fast and reaches a plateau within less than an hour. No further uptake is observed with incubation of up to 18 h. P-H and, to a lesser extent, P-Gal are poorly incorporated when compared to P-Me, P-DDC and P-OGal. After a 3 h incubation in FCS-supplemented EMEM, the uptake increases almost linearly

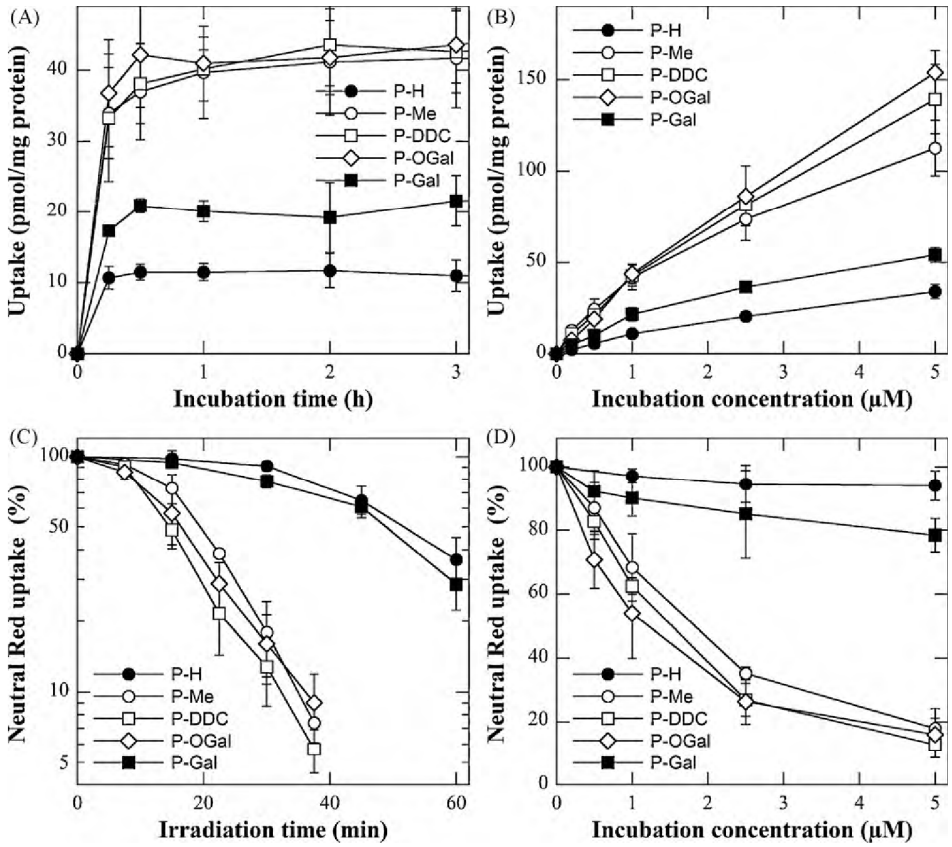

Fig. 2. (A and B) Uptake of P-H, P-Me, P-DDC, P-OGal, P-Gal (●,○,□,◇,■) by NCTC 2544 keratinocytes as a function of the time of incubation with 1 μM P-R (A) and of the P-R concentration during 3 h incubation (B) in FCS-supplemented culture medium. Data are the mean of at least three independent experiments performed in triplicates. (C and D) Cytotoxic effects photosensitized by P-H, P-Me, P-DDC, P-OGal, P-Gal (●,○,□,◇,■) as a function of the irradiation time (C) and of the incubation concentration (D) in FCS-supplemented culture medium. In C, cells were incubated for 3 h with 5 μM P-R prior to irradiation, whereas in D cells were irradiated for 30 min after incubation for 3 with the desired P-R concentration. A 100% Neutral Red (NR) uptake corresponds to sham-irradiated untreated cells. Data are the mean of at least three independent experiments performed in triplicates. Note the logarithmic *Y*-axis in C.

Table 1
Photosensitization of NCTC 2544 keratinocytes by tricationic porphyrins.

	P-H	P-Me	P-DDC	P-OGal	P-Gal	P-$(Lys)_n$ [c]
PC_{50} (μM)[a]	>>5	~1.8	~1.5	~1.2	>5	~3.1
IPC_{50} (pmol/mg protein)[b]	>>35	~55	~55	~50	>50	~260
Inhibition by N_3^- (%)[d]	100 ± 7	95 ± 11	88 ± 12	93 ± 12	100 ± 2	–

Photocytotoxic concentration (PC_{50}), intracellular phototoxic content (IPC_{50}) and inhibition of photocytotoxicity by N_3^- ions.
[a] PC_{50} is defined as the incubation concentration necessary to obtain a 50% decrease in NR uptake after a 30 min irradiation. Data were obtained from Fig. 2D.
[b] IPC_{50} is the intracellular phototoxic content corresponding to the PC_{50} obtained from Fig. 2B.
[c] Data obtained from Silva et al. [5].
[d] N_3^- ions at a non-toxic concentration of 20 mM were present during the 3 h incubation with P-R and the subsequent 30 min irradiation. Data represent survival, where 100% corresponds to survival in untreated samples.

as a function of the incubation concentration for all derivatives (Fig. 2B). The relative order of magnitude of the uptake is the same as that observed in Fig. 2A.

Though incubation in FCS-supplemented culture medium is more relevant to the *in vivo* situation, incubation in serum-free HBSS has also been performed to determine whether serum proteins play any peculiar role in the uptake process. The P-R uptake profiles as a function of incubation time or of incubation concentration are found to be similar in the presence and absence of serum (data not shown). This suggests that, in contrast to the behavior of P-$(Lys)_n$, there is no strong interaction between the other P-R shown in Fig. 1 and serum proteins [6].

3.2. Photocytotoxicity of P-R derivatives

To reach maximum uptake, cells were incubated for 3 h with porphyrins in FCS-supplemented EMEM prior to irradiation. No cytotoxicity was observed with untreated sham-irradiated cells or with untreated irradiated (up to 60 min) cells in the presence of 0.5% or less DMSO in the incubation medium (data not shown). Moreover, none of these porphyrins exhibited dark cytotoxicity at incubation concentrations up to 5 μM. Fig. 2C (irradiation with increasing light doses) demonstrates that P-Me, P-DDC and P-OGal all exhibit a much larger photocytotoxicity than P-H or P-Gal at an incubation concentration of 5 μM. Conversely, lower concentrations of P-Me, P-DDC and P-OGal are sufficient to achieve high photocytotoxicity (Fig. 2D). The incubation concentrations necessary to obtain a 50% decrease in NR uptake after a 30 min irradiation can be estimated from Fig. 2D. These values, hereafter referred to as "photocytotoxic concentrations" (PC_{50}), are reported in Table 1, which also includes earlier data obtained with the P-$(Lys)_n$ derivative. Table 1 provides another photocytotoxicity index, the "intracellular phototoxic concentration" (IPC_{50}) which represents the intracellular concentration which produces a 50% decrease in NR uptake after a 30 min irradiation. Low IPC_{50} values of ~50 pmol per mg of protein are obtained with P-Me, P-DDC or P-OGal and a relative efficiency – P-OGal > P-DDC = P-Me ≫ P-Gal > P-H – is deduced from Table 1. Experiments performed after incubation in the absence of serum proteins lead to similar data for these conjugates, further illustrating that little if any role is played by serum proteins in uptake of these porphyrins (data not shown).

3.3. Oxidative stress photo-induced by P-R derivatives

Singlet oxygen is the main cytotoxin involved in PDT with porphyrins [12]. The photophysical studies here revealed no major difference in the efficiency of P-H, P-Me, P-DDC, P-OGal and P-Gal to produce singlet oxygen in a high yield whereas P-$(Lys)_n$ was found earlier to be about 4 times less effective [6,13]. Inhibition of cell photosensitization by specific $^1O_2$ quenchers such as N_3^- ions (Table 1) demonstrates the role of singlet oxygen in photo-oxidative stress induced by the tricationic porphyrins. Lipid peroxidation has been used as an overall index of oxidative stress. It has been quantified by measuring TBARS formation in cell supernatants since previous studies demonstrate practically no intracellular TBARS formation in photosensitized cells themselves. The TBARS production is shown to increase nearly linearly with the irradiation time (Fig. 3A). The ability of P-R to trigger lipid peroxidation parallels their photocytotoxic potential, and the strongly photocytotoxic P-Me, P-DDC and P-OGal as well as P-$(Lys)_n$ (see Fig. 4 in [6]), may be seen to be the most effective TBARS producers. Again, similar data were obtained in the absence of serum proteins (data not shown).

3.4. Cytotoxicity and oxidative stress photo-induced by PPIX

To compare the effects of P-R photosensitization to those of ALA, the pro-drug used in the PDT of skin lesions, cells have been incubated with various concentrations of ALA prior to irradiation in order to induce endogenous PPIX. Subsequently, the intracellular PPIX content was determined by fluorescence measurement. The photocytotoxicity or the lipid peroxidation, or both have also been determined. Data in Fig. 3B show that the IPC_{50} is approximately 50 pmol per mg of protein. About 1.8 mol of TBARS per mol of intracellular PPIX are released after a 30 min irradiation (Fig. 3C).

3.5. Fluorescence microscopy of P-R derivatives

P-R derivatives fluoresce near 660 nm and exhibit comparable fluorescence quantum yields under similar solvent conditions [13]. Fig. 4 illustrates the phase contrast and fluorescence images obtained for control cells (sham-treated cells) and for cells treated for 3 h with P-R in FCS-supplemented culture medium. The fluorescence images have been obtained with an excitation in the near UV (330–380 nm) and an emission in the red-visible range (610–700 nm). Fig. 4G–R are matching fluorescence images of the phase contrast images (Fig. 4A–F). For ready comparison, fluorescence images are displayed on the same scale in panels G–L, while they are displayed between the minimum and maximum fluorescence levels in M–R. As expected, untreated cells exhibit a very low fluorescence arising from the cytoplasm with larger intensities in the perinuclear area and the mitochondrial network. Cells treated with P-Me, P-DDC and P-OGal fluorescence more intensely, in agreement with greater uptake. A rather diffuse fluorescence with some spots in the perinuclear area is observed from cells treated with P-H and P-Gal, suggesting a main cytoplasmic and plasma membrane localization and little accumulation at specific sites. By contrast, cells treated with P-Me, P-DDC and P-OGal exhibit stronger fluorescence, mostly localized in perinuclear spots which suggests more specific localization in lysosomes or lysosome-like structures. A double labeling of the cells (Fig. 5A–C) was performed with P-R and LysoTracker Green, a lysosome specific probe emitting a green fluorescence centered towards 510 nm. As shown for P-DDC (Fig. 5B and C) the localization patterns of the green and red fluorescences are very similar, although a total superimposition cannot be achieved. This suggests a localization in other non-lysosomal structures, most probably, endocytotic or pinocytotic vesicles

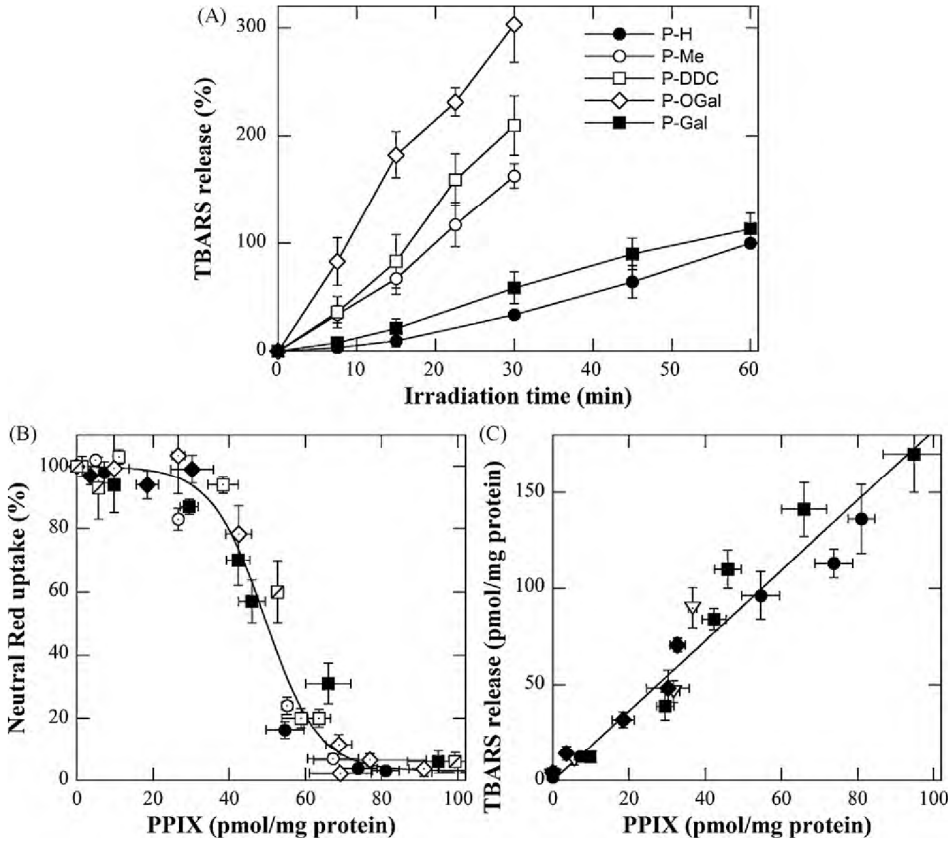

Fig. 3. (A) Lipid peroxidation photosensitized by P-H, P-Me, P-DDC, P-OGal and P-Gal (●,○,□,◇,■) after incubation for 3 h with 5 μM P-Rin FCS-supplemented culture medium prior to irradiation. TBARS released in the supernatant, normalized to the protein content, are expressed as the percentage of TBARS released after 60 min of irradiation of cells incubated with P-H (100% correspond to 37 ± 7 pmol/mg). Data are the mean of three independent experiments performed in triplicates. (B and C) Photosensitized cytotoxic effects (B) and lipid peroxidation (C) as a function of the intracellular PPIX concentration after ALA treatment. Cells were treated for 18 h without or with ALA (0.1–0.8 mM) in FCS-supplemented culture medium and irradiated for 30 min. A 100% Neutral Red uptake corresponds to sham-irradiated untreated cells. TBARS released in the supernatant were normalized to the protein content. Each symbol corresponds to an independent experiment performed in triplicates. Closed symbols in B and C correspond to data obtained from the same experiment.

beside a minor lysosomal incorporation. These vesicles have a pH higher than that of lysosomes (pH 5–6) and are therefore inefficiently labeled by LysoTracker Green®. On the other hand, lysosomal staining by the probe may be partially hidden by FRET from the probe (the donor) to P-R (the acceptor). Such behavior is observed in the case of another PDT model where tolyporphin is the photosensitizer [8]. Since P-R are positively charged, and since the inner mitochondrial membrane exhibits a negative potential, mitochondria are expected to be a preferential site for P-R localization. However, micrographs obtained with the specific mitochondrial probes, rhodamine 123 and MitoTracker® show a perinuclear network extending all over the NCTC 2544 keratinocytes (see also Gaullier et al. [14]) incompatible with the pattern of P-Me, P-DDC and P-OGal localization (Fig. 5D–F). This observation confirms previous results obtained with P-$(Lys)_n$ [6]. Although tetracationic porphyrins readily accumulate in the cell nucleus [15,16], the fluorescence depression on the nuclear area observed for all P-R strongly suggests very little, if any, localization in the nucleus of NCTC 2544 keratinocytes.

3.6. Mechanisms of the PDT-induced death in NCTC 2544 cells

Necrosis induced *in vitro* by PDT with porphyrins has long been established, and is essentially characterized by increased cell volume, organelle swelling and plasma membrane alterations [17]. Apoptosis and autophagy are induced by a variety of stress factors, notably those encountered in cancer therapies. Two reviews have been recently published on guidelines concerning the use and interpretation of assays for determining mechanisms of cell death [18,19]. It is of interest to understand the death mechanisms underlying the efficient photocytotoxicity of P-Me, P-OGal and P-DDC. As P-Me, P-OGal and P-DDC exhibit similar intracellular localization, P-OGal – the most effective photosensitizer – was chosen as representative P-R for this study.

3.7. Is apoptosis involved in P-R photocytotoxicity?

Translocation of phosphatidylserine from the inner layer to the outer layer of the plasma membrane is observed in the initial stages of apoptosis. To detect this translocation, we used annexin V, a protein that binds to cells with exposed phosphatidylserine. A simultaneous cytometric analysis of annexin V binding and propidium iodide uptake by dead cells was carried out. According to Fig. 3A, incubation with 5 μM P-OGal for 3 h, followed by a 15 min irradiation, leads to about 25% cell killing. However, no significant change in the percentage of annexin V positive cells (Fig. 6A) could be observed up to 9 h following irradiation. Similar results were observed after a 3 h incubation of cells with 1 μM P-OGal followed by 15 min of irradiation or with 5 μM P-OGal followed by 30 min of irradiation (data not shown).

Another hallmark of apoptosis is nuclear DNA breakdown into oligonucleosomal units of about 200 bp. The enzyme-linked immunosorbent assay used to quantify the cytoplasmic accumulation of histone-associated DNA fragments shows no significant increase in cytoplasmic histone-associated DNA fragments 0, 1, 3, 6, 9 12 h (Fig. 6B) or 24 h (data not shown) after PDT with 5 μM P-OGal.

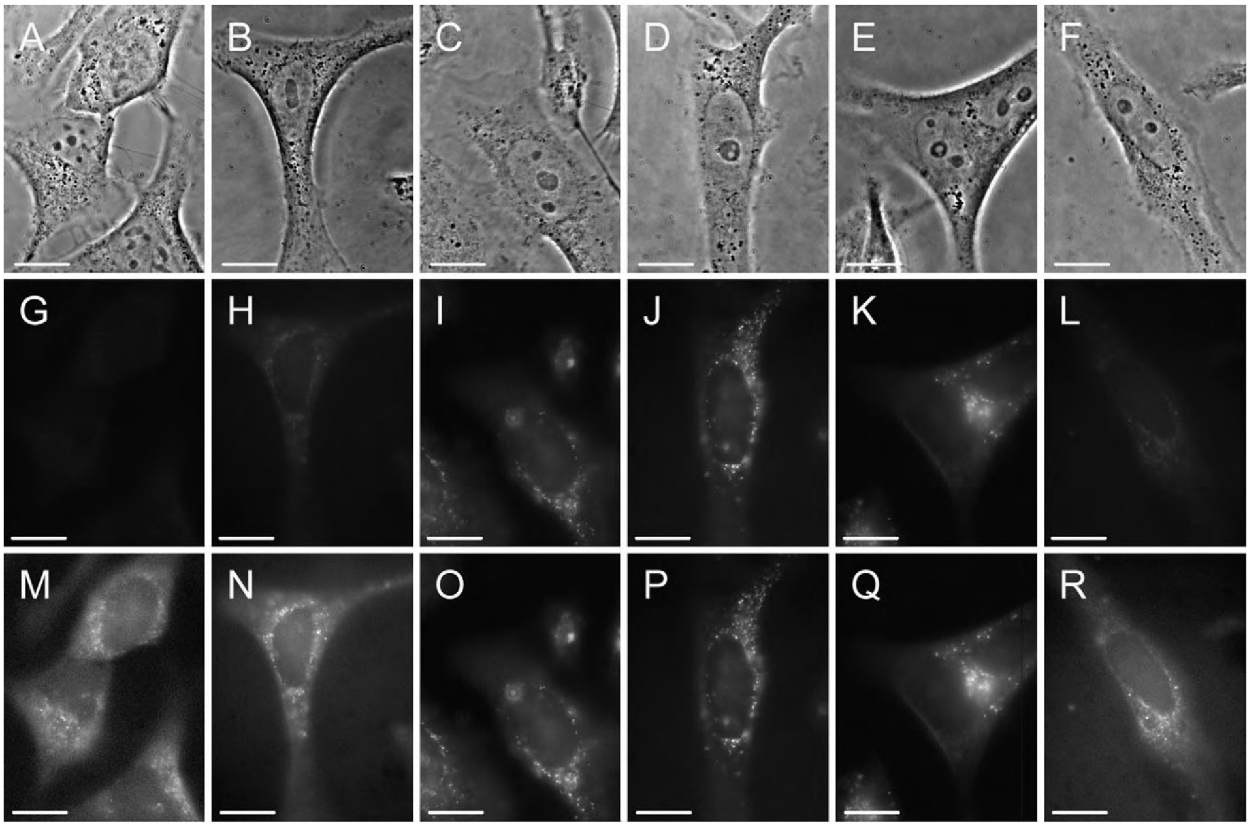

Fig. 4. (A–R) Phase contrast images (A–F) and fluorescence micrographs (G–R) obtained with NCTC 2544 keratinocytes incubated for 3 h in EMEM + 10% FCS with no additives (A, G, M), with 5 μM P-H (B, H, N), P-Me (C, I, O), P-DDC (D, J, P), P-OGal (E, K, Q) or P-Gal (F, L, R). Fluorescence images were obtained with a Nikon ×100 oil immersion objective. Exposure time: 2 s. Signal attenuation: 1/16. Dichroic mirror: 400 nm. Excitation: 330–380 nm. Emission: 610–700 nm. G–L: 256 grey levels between 0 and the maximal fluorescence recorded with P-DDC (show relative intensities). M–R: 256 grey levels between 0 and individual fluorescence (show the topography of localization). White bar = 20 μm.

Activation of intracellular proteases called caspases, is a key event during apoptosis. The caspase cascade is regulated through their partial cleavage. To further examine whether apoptosis is involved in the P-R-induced photokilling, caspase-3, caspase-8 and caspase-9 activities have been assayed. Cleavage of proteins by caspases leads to chromatin condensation and DNA degradation. Several families of PDT photosensitizers (porphyrins, chlorins, phthalocyanines.) are strong inducers of apoptosis in various cell lines [12]. Because apoptosis is a dynamic process, samples have been collected up to 24 h following PDT. No evidence for cleavage of the caspase-3, caspase-8 and caspase-9 substrates was found after P-OGal-PDT under the conditions outlined above (see Fig. S1 in supplementary data). The absence of procaspase-3, procaspase-8 and procaspase-9 cleavage in Western blots, also shown in the supplementary data, confirms the lack of caspase activities. In addition, no cytochrome *c* leakage has been observed with P-OGal photosensitized cells (Fig. 7A). To verify that under our experimental conditions, NCTC 2544 cells may readily undergo apoptosis, such cells were incubated 30 min with 10 μM 5-methoxypsoralen in DPBS and then were subjected to UVA irradiation (2.5 J/cm^2). Twenty four hours later, NCTC 2544 treatment with 5-methoxypsoralen + UVA had resulted in extensive activation of caspase-3 (6-fold increase in activity) and caspase-9 (2-fold increase in activity) in cell lysates. No change in activity was observed with caspase-8 (data not shown). These results are fully consistent with those previously presented by Viola et al. [20]. Another positive control was performed by treating cells with 5 μM campothecin. Measurement of caspase-3 activity and flow cytometry after PI and Annexin V staining readily show apoptosis induction only 9 h after treatment. These data support the conclusion that apoptosis induction after photodynamic injury induced by P-R is insignificant.

3.8. Autophagy of NCTC 2544 keratinocytes after PDT with tricationic porphyrins

Autophagy is a normal process that helps the cell get rid of damaged organelles or macromolecules. This highly regulated process is morphologically evidenced by the formation of autophagosomes and autolysosomes [18,21]. Recently, a new form of programmed cell death characterized by autophagic hallmarks has been discussed [18,19]. To determine if programmed cell death associated with PDT might exhibit such characteristics, we monitored the autophagic activity in NCTC cells exposed to P-OGal. Autophagic activity was followed using a fluorescent marker (GFP-LC3) consisting in a fusion microtubule-associated protein light-chain 3 (LC3) tagged with a green fluorescent protein (GFP). Upon autophagy induction, LC3 is proteolytically processed and recruited to autophagosomal membranes [11]. After P-OGal PDT, we have observed the subcellular redistribution of the fluorescent marker GFP-LC3 fusion protein from a uniform, cytosolic, to a punctated, vacuolar pattern [18,19] (Fig. 7A). After a 3 h incubation of cells with 5 μM P-OGal, followed by 15 min of irradiation, a time-dependent increase in the number of cells showing the characteristic vacuolar pattern of GFP-LC3 is observed (Fig. 7B). By contrast, no significant change in the accumulation of GFP-LC3 is observed (Fig. 7B) after incubation of NCTC 2544 cells with 0.8 mM ALA for 18 h followed by a 15 min irradiation, which induces similar photocytotoxic effects as those observed with P-R (see Fig. 3C).

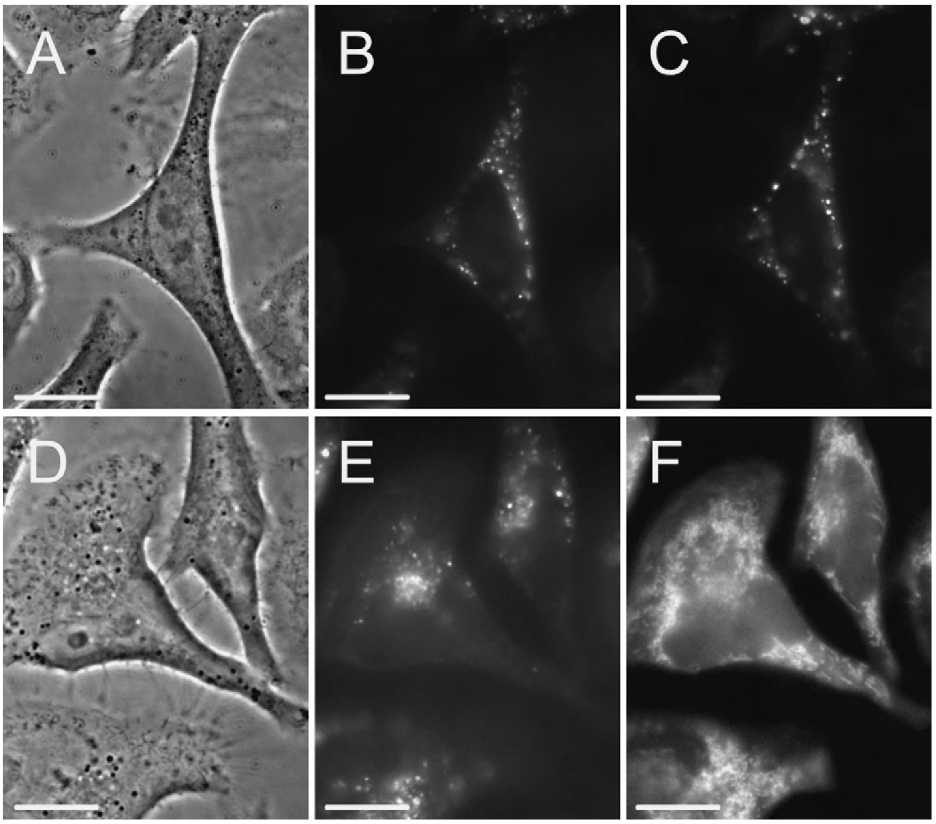

Fig. 5. Double-labeling experiments: (A–C) Phase contrast images (A) and fluorescence micrographs (B and C) obtained after incubation for 3 h with 5 μM P-DDC in EMEM + 10% FCS and then for 30 min with 5 μM P-DDC and 125 nM LysoTracker Green in EMEM + 10% FCS. (D–F) Phase contrast images (D) and fluorescence micrographs (E and F) obtained after incubation for 3 h with 5 μM P-DDC in EMEM + 10% FCS and then for 30 min with 5 μM P-DDC and 10 μM Rhodamine 123 in EMEM + 10% FCS. Objective, signal attenuation, dichroic mirror and excitation as in Fig. 4. Exposure times: 2 s with the red emission filter and then 2 s with the green emission filter. Emission: 610–700 nm (B and E) and 510–565 nm (C and F). White bar = 20 μm.

In another series of measurements, the immunoblotting analysis for the modulation of the p62 protein, also called sequestosome 1 (SQSTM1), by P-R has been performed. Since p62/SQSTM1 accumulates when autophagy is inhibited and decreases when autophagy is induced, it may be used as a marker of autophagic activity [18]. Western blotting analysis reveals that 6 h after irradiation the amount of p62/SQSTM1 is decreased by more than 60% in the P-OGal-treated cells but not in cells treated with P-OGal but not irradiated (Fig. 7D).

To further assess a possible contribution of autophagy to P-OGal-induced cell death, we have studied the effect of 3-methyladenine (3-MA), a well-characterized autophagy inhibitor [18]. After 15 min of irradiation of cells incubated for 3 h with 5 μM P-OGal and 5 mM 3-MA, the percentage of cells showing the characteristic vacuolar pattern of GFP-LC3 in the P-OGal + 3-MA-treated group is decreased to about 70% of the value obtained with the group treated with P-OGal alone (Fig. 7C). By contrast P-OGal-induced cell death is inhibited by about 40% after incubation with 5 mM 3-MA (Fig. 6C). It is well established that the inhibition of autophagy by 3-MA may potentiate apoptosis induced by a variety of chemicals [21]. Autophagy inhibition does not significantly change the percentage of annexin V positive cells measured 6 h after P-OGal-PDT (Fig. 6C). Furthermore, no leakage of mitochondrial cytochrome *c* in the cytoplasm has been observed with 3-MA-treated cells up to 6 h after irradiation (data not shown), but the p62 degradation was decreased by about 80% (Fig. 8D).

These data suggest that cells undergoing P-OGal-PDT show increased autophagy levels and that autophagy may be associated with cell death induced by P-OGal photosensitization.

3.9. MAPK participate in death of NCTC 2544 keratinocytes after PDT with tricationic porphyins

Several lines of evidence indicate that MAPK participate in closely related signaling cascades that contribute to the regulation of gene expression in response to photodynamic treatment. Activation of ERK 1/2 is generally associated with cell proliferation and survival, while p38 and JNK are linked to induction of apoptosis [12,22]. Recent reports show, however, that the role of MAPKs in cell death induced by photosensitization is largely cell type and photosensitizer-dependent [12].

The MAPK phosphorylation has been assessed in NCTC 2544 cells treated by P-OGal-PDT and lysed 0, 1, 3, 6 or 9 h after irradiation. The p38 and JNK phosphorylation was significantly increased. This increase is stronger with p38 and maximal 3 h after irradiation (Fig. 8A). After this interval, p38 and JNK phosphorylation steadily declines, becoming barely detectable 9 h after irradiation. On the other hand, no significant phosphorylation of p38 and JNK is observed before irradiation in untreated (control) cells or after sham-irradiation of P-OGal-treated cells.

Regarding Akt and ERK, the level of total Akt and ERK is unchanged whereas the p-Akt and p-ERK levels are markedly decreased after P-OGal-PDT in a time dependent manner (Fig. 8A). In contrast to results obtained with p38 and JNK, substantial amounts of phosphorylated ERK1/2 and Akt are detected prior to irradiation. Although the p-ERK and p-Akt levels remain unchanged in sham-irradiated cells and untreated controls, p-Akt decreased progressively after the photodynamic challenge while p-ERK has a significant abrupt drop at 3 h and becomes barely detectable. These results suggest that MAPKs

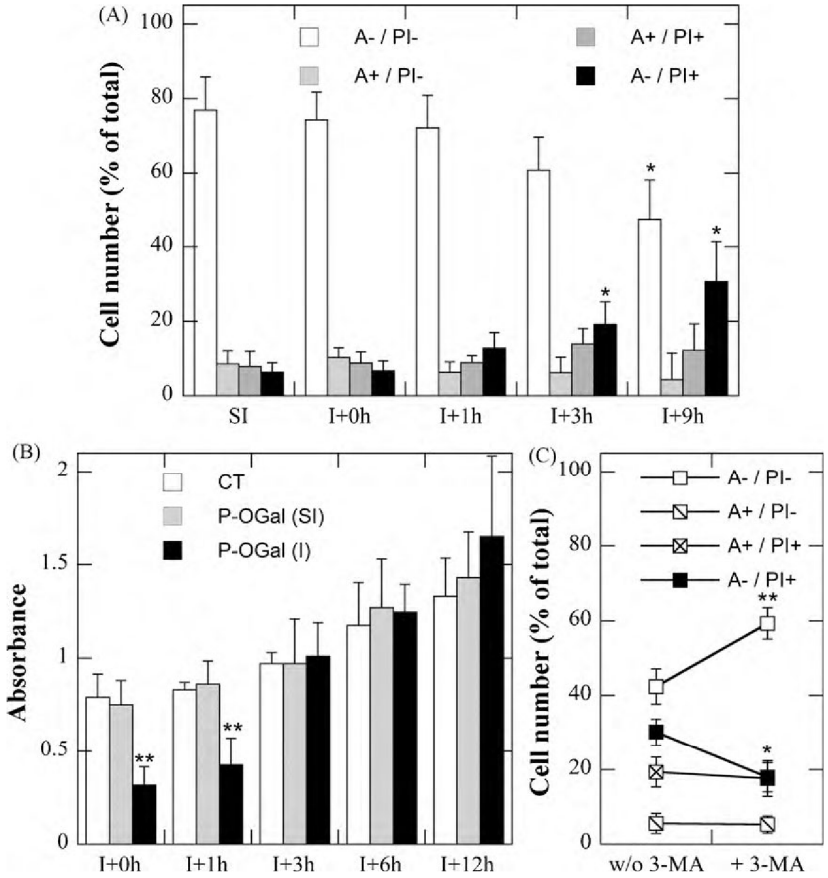

Fig. 6. (A) Flow cytometric analysis of NCTC 2544 keratinocytes after P-OGal photosensitization. Cells were incubated for 3 h with 5 μM P-OGal in FCS-supplemented culture medium, then irradiated (I) or sham-irradiated for 15 min (SI). They were stained with Annexin V-FITC and PI and analyzed by flow cytometry at the indicated times after irradiation (I+). Data are the mean of 3 independent experiments performed in triplicates. A−/PI−: viable cells; A+/PI−: still viable cells undergoing apoptosis (early apoptotic cells); A+/PI+: late apoptotic dead cells; A−/PI+: necrotic cells. $^{*}p < 0.05$ compared to matching SI. SI data were obtained immediately after sham-irradiation and were unchanged for durations up to 9 h after sham-irradiation. (B) After incubation and irradiation as in (A), cell lysates were prepared and analyzed for cytoplasmic accumulation of histone-associated DNA fragments by an enzyme-linked immunosorbent assay at the indicated times after irradiation. CT: sham-treated control cells; P-OGal (SI): treated cells but sham-irradiated for 15 min; P-OGal (I) cells treated and irradiated for 15 min. Data are the mean of 3 independent experiments performed in triplicates. $^{**}p < 0.01$ compared to matching CT. (C) Effect of 3-MA on cytotoxic effects photosensitized by P-OGal. Before irradiation, cells were treated for 3 h with 5 μM P-OGal only (w/o 3-MA) or simultaneously with 5 μM P-OGal and 5 mM 3-MA. Cells were stained with Annexin V-FITC and PI 6 h after irradiation and analyzed by flow cytometry. Data are the mean of 3 independent experiments performed in triplicates. $^{*}p < 0.05$ and $^{**}p < 0.01$ compared to 3-MA untreated cells.

activity modulation by P-OGal-PDT may be implicated in the cytotoxicity.

To examine the role of MAPKs activation in cell death, P-OGal-treated cells were pre-incubated with the p38 (SB203580) and JNK (SP600125) inhibitors. As a matter of fact, SB203580 and SP600125 inhibit p38 and JNK phosphorylation in the NCTC 2544 cells. Thus, after an osmotic stress induced by 0.4 M sorbitol for 10 min, immunoblot analysis demonstrates that 25 μM SB203580 and 25 μM SP600125 reduced p-p38 and p-JNK over 75% of the control value (data not shown). Addition of SP600125 3 h before irradiation, increases the photo-induced cell death by approximately 50%, whereas SB203580 has no significant effect (Fig. 8B). Incidentally, it must be noted that the viability of control cells treated with P-OGal and pre-incubated with SB203580 and SP600125 but left in the dark was unchanged. Fig. 8B also suggests that an insignificant effect on the percentage of annexin V positive cells is observed 6 h after P-OGal-PDT of cells pre-incubated with 25 μM of p38 and JNK inhibitors. By contrast, 6 h after irradiation, the number of cells showing the vacuolar pattern of GFP-LC3 is increased by 31% ($p < 0.001$) in cells treated with P-OGal and 25 μM SP600125 (Fig. 8C) although SP600125 has no effect on the basal level of GFP-LC3-puncta. On the contrary, no significant change has been observed in the P-OGal PDT-induced accumulation of GFP-LC3 after pre-incubation of cells with SB203580. Under the same experimental conditions, SP600125 but not SB203580 increases the p62 degradation after PDT (Fig. 8D). Taken together, these results suggest that JNK exerts a negative regulator effect on P-OGal PDT-induced autophagy and PDT-dependent programmed cell death.

4. Discussion

4.1. The nature of the conjugated chain determines the intracellular localization of tri-cationic conjugates and their cytotoxicity

The comparison of the photocytotoxic potential of P-R is straightforward since they absorb identical light under the same experimental conditions (see supplementary data). The greater photocytotoxic efficiency of P-OGal, P-DDC and P-Me compared to that of P-H and P-Gal (Fig. 2C,D) parallels the magnitude of the lipid peroxidation (Fig. 3A) suggesting that their phototoxicity and their overall ability to produce an oxidative stress correlate, irrespective of the targets in the cell lines studied.

Interestingly, P-OGal, P-DDC and P-Me favorably compare with endogenous PPIX produced by ALA treatment. Fig. 3B demonstrates that a 50% loss in Neutral Red uptake is obtained with an intracellular PPIX concentration (~50 pmol/mg of cellular protein) similar to that found for P-OGal, P-DDC and P-Me. Since light doses absorbed by equal concentrations of P-R and PPIX are essentially

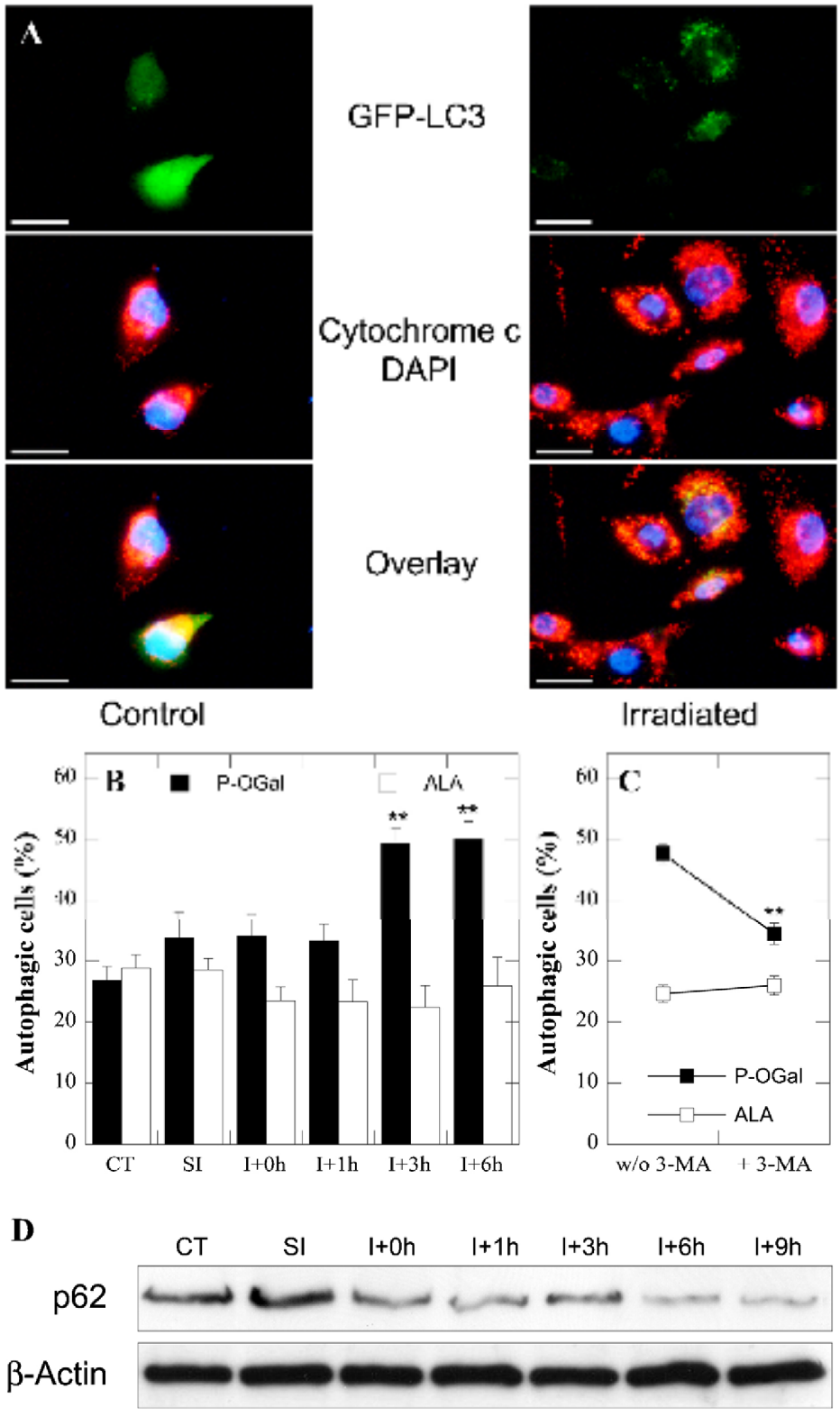
A
GFP-LC3
Cytochrome c
DAPI
Overlay
Control
Irradiated
B
P-OGal
ALA
Autophagic cells (%)
CT
SI
I+0h
I+1h
I+3h
I+6h
C
w/o 3-MA
+ 3-MA
D
CT
SI
I+0h
I+1h
I+3h
I+6h
I+9h
p62
β-Actin

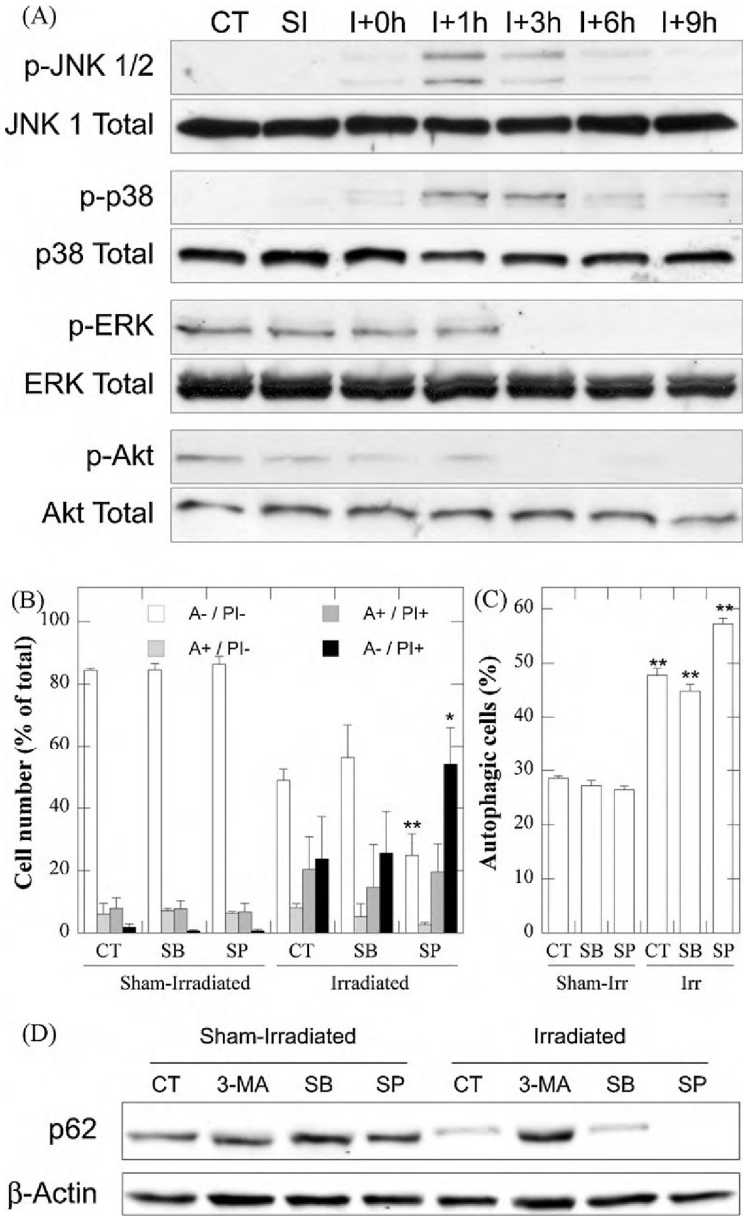

Fig. 8. MAPKs protein expressions were analyzed in lysates of NCTC 2544 cells. (A) Representative Western blots of total and phosphorylated JNK, p38, ERK and Akt either in cells untreated but left in supplemented culture medium for 3 h (control, CT) or in cells treated during 3 h with 5 μM P-OGal and then sham-irradiated (SI) or irradiated for 15 min and incubated for indicated times after irradiation (I+). Total-JNK, p38, ERK and Akt immunoblottings are used as controls for protein loading. (B) Effect of 25 μM SB203580 or 25 μM SP600125 on cytotoxic effects photosensitized by P-OGal. Before irradiation, cells were treated for 3 h with 5 μM P-OGal (CT) or with 5 μM P-OGal and 25 μM SB203580 (SB) or SP600125 (SP). Nine hours after irradiation, cells were stained with annexin V-FITC and PI and analyzed by flow cytometry. Data are the mean of 3 independent experiments performed in triplicates. $^{*}p < 0.05$ and $^{**}p < 0.01$ compared to irradiated CT. (C) Cells transfected with GFP-LC3 were treated using P-OGal without (CT) or by pre-incubation with 25 μM SB203580 (SB) or SP600125 (SP). Autophagic cells were counted and results are given as in Fig. 7B (mean ± SD of 3 independent experiments in triplicates). $^{**}p < 0.01$ compared to matching sham-irradiated cells. (D) Western blotting analysis of p62 in lysates from cells collected 9 h after P-OGal-PDT without or with pre-incubation in the presence of 5 mM 3-MA (3-MA), 25 μM SB203580 (SB) or SP600125 (SP). β-actin is shown as loading control.

identical (see supplementary data), P-OGal, P-DDC and P-Me are photosensitizers as powerful as PPIX in our cell model. Comparison of data in Figs. 2B and 3A and C demonstrates that at equivalent light doses, oxidative membrane damage is more pronounced with PPIX than with P-Me, P-DDC or P-OGal. This behavior is consistent with the higher hydrophobicity of PPIX favouring its intracellular localization in lipophilic microenvironments.

With the exception of P-$(Lys)_n$, P-R derivatives have comparable singlet oxygen formation quantum yield. Consequently, they have similar intrinsic photosensitizing potential. From Fig. 2B, it may be estimated that incubation with P-Me, P-DDC or P-OGal concentrations in the range 0.7–0.8 μM leads to the same P-R intracellular contents as incubations with 5 μM P-H or 1.4–1.6 μM P-Gal. It may be deduced from Fig. 2C and D that these differences cannot account for the observed differences in cytotoxicity.

The intracellular localization may explain different photocytotoxic responses. Microfluorometry confirms that P-H and P-Gal are taken up less by NCTC 2544 keratinocytes than is P-Me, P-DDC or

transfected with GFP-LC3 were treated with P-OGal or ALA and irradiated as described in (A), without or with simultaneous treatment with 5 mM 3-MA. Autophagic cells were counted and results are given as in B (mean ± SD of 3 independent experiments in triplicates). $^{**}p < 0.01$ compared to matching 3-MA-untreated cells. (D) Western blotting analysis of lysates from cells collected at indicated times after treatment with P-OGal and irradiation. Total cell lysates were analyzed for p62. β-actin is shown as loading control. SI data were obtained immediately after sham-irradiation and were unchanged up to 9 h after sham-irradiation. Sham-treated irradiated cells behave as CT.

P-OGal, whose fluorescence is more specifically localized in spots that may correspond to endo- or pinocytotic vesicles, but not to mitochondria and nucleus. The observations reported here demonstrate that the nature of the conjugated side chain is more critical than the electric charge of the porphyrin ring in controlling the uptake and site of localization of the P-R and, consequently, their greater photosensitizing efficiency. It may be thought that major direct damage to the mitochondria and the nucleus by $^1O_2$ produced by P-R is rather unlikely since $^1O_2$ does not diffuse a great distance from its site of production [16].

4.2. The photo-induced cell death shows hallmarks of autophagy

Beside demonstrating for the first time the chain structure dependence of the photocytotoxic potential of tri-cationic porphyrins, this study provides new information about mechanisms of cell death and MAPK-mediated stress signaling in our PDT model. It has been demonstrated that many PDT photosensitizers including those used to treat skin lesions in clinical practice, e.g. ALA and photofrin®, activate several pathways leading to apoptosis ([12] and references therein). Our results are in sharp contrast with these reports. Consistent with the absence of apoptosis, no annexin V cell staining (Fig. 6A), no oligonucleosome fragmentation (Fig. 6B) and no caspase activation (see supplementary data) are observed after P-OGal-PDT. Among other factors, these results may be related to the non-mitochondrial localization of the most photocytotoxic P-R (Fig. 4). The absence of major mitochondrial damage is also suggested by the lack of cytochrome *c* leakage (Fig. 7A). On the other hand, we show the appearance of a punctate pattern of GFP-LC3 and a decrease in the amount of p62 following PDT with P-OGal (Fig. 7A–C). Consistently, 3-methyladenine, a well-known inhibitor of autophagy, inhibits the photocytotoxicity, lowers the percentage of cells showing punctate GFP-LC3 and decreases p62 degradation (Figs. 6C, 7C and 8D). The incorporation of P-R in lysosomes or pre-lysosomes in the vicinity of the ER and the Golgi apparatus might be responsible for this conjunction of pro-autophagic and anti-apoptotic events.

There are relatively few recent reports on the induction of autophagy by photodynamic therapy and most deal with apoptosis-deficient cells or cells whose caspase activity has been inhibited [12,23]. We used apoptosis-competent cells in which porphyrin conjugates induced autophagic cell death in the absence of apoptosis inhibitor. Treatment with the autophagy inhibitor 3-MA is not associated with a significant change in the percentage of annexin V positive cells and thus with apoptosis activation (Fig. 6C). Possibly, autophagy may constitute an attempt by cells to remove photo-oxidized organelles or large cross-linked aggregates formed after photodynamic damage to protein complexes.

4.3. Consequences of P-OGal-PDT on MAPKs in NCTC 2544 cells

Several studies performed with different cell lines and photosensitizers have shown that MAPKs participate in the oxidative signaling events induced by PDT [12]. Previous research presented conflicting data concerning the roles of p38 and JNK in cell viability after PDT. Results suggest that the degree of p38 and JNK phosphorylation as well as their effect on cell death regulation after PDT may depend on cell type, photosensitizer and light dose [22,24]. In contrast to apoptosis, relatively little is known about PDT-induced autophagy signaling in terms of MAPK activation and possible cross-talk among different pathways.

The role of JNK in cell death has long been controversial as it exhibits a pro-survival function or it promotes lethality depending on the physiological or pathological condition studied [25]. The paradoxical nature of this effect could be partially due to different modes of JNK activation [26], different kinetics [27] or might depend on the nature of the chemical inducers used including reactive oxygen species [26,28]. An early transient JNK activation determines cell survival whereas sustained JNK activation can induce cell death signals [27]. Consistent with these data, we observed a rapid and transient JNK activation after P-OGal-PDT associated with a negative regulatory effect on cell mortality and autophagy (Fig. 8A). We may speculate that this effect might be partially explained by JNK1 mediated Bcl-2 phosphorylation known to inhibit the binding of Bcl-2 to Beclin 1 which activates autophagy [29]. Of note, it has recently been reported that JNK activation, induced by 2-methoxyestradiol in Ewing sarcoma cells, modulates autophagy either through Bcl2 phosphorylation or up regulation of the damaged regulated autophagy modulator [30,31].

While several reports support the role of p38 as inhibitor of autophagy [32], others imply the opposite [33]. Although we observed a p38 activation after P-OGal PDT, our data suggest that p38 is not directly implicated in induction of cell death. A downstream event in the mitogenic pathway is ERK activation through binding of ligands to extracellular growth factor receptors involved in regulation of growth and cell cycle progression. The Ras/Raf/ERK activation pathway can promote opposite pro-survival or anti-proliferative cellular responses, such as apoptosis and autophagy. This wide variety of processes triggered by the activation of a single pathway depends on the timing, duration and strength of activation, on subcellular localization and on the presence of reactive oxygen species (ROS) [34]. Available evidence suggests that the photooxidative stress induced by PDT may modulate ERK activity as does other ROS such as H_2O_2, which is produced in a variety of tumor cell lines by 1,3-dibutyl-2-thiooxo-imidazolidine-4,5-dione [35]. Depending on the photosensitizer and cell culture, ERK phosphorylation variably responds to the PDT-induced oxidative stress by irreversible inhibition [24], moderate attenuation [36], insignificant modulation [22] or transient activation [37]. It is noteworthy that ALA-PDT has no effect on ERK expression in HaCat cells [38]. We found a decrease in the p-ERK content to almost undetectable levels 3 h after P-OGal-PDT despite high pre-existing expression (Fig. 8A).

Activation of PI3-K/Akt is another important signaling pathway. The Akt acts on a variety of ways including mTOR activation, Bad phosphorylation, IκB kinase phosphorylation and caspase-9 inhibition, thereby preventing cell death [21]. The PDT effect on Akt regulation varies from de-phosphorylation and subsequent activation of caspase-assisted death [39] to phosphorylation stimulation [40]. Our results show a time-dependent decrease in the content of p-Akt after PDT treatment (Fig. 8A), consistent with increased photo-induced autophagic death.

5. Conclusions

Beside necrosis, autophagy may contribute to the death of NCTC 2544 keratinocytes by P-OGal-PDT with no evidence for significant apoptosis. JNK activation exerts a negative regulatory effect on photocytotoxicity and autophagy while p38 activation is not involved in cell death. Several studies show that ERK and PI3-K/Akt pathways are aberrant in human cancers [41] suggesting them as targets for the development of novel cancer treatments [42]. The inhibition of ERK1/2 and Akt activities suggests that water-soluble tri-cationic porphyrins may thus play a beneficial role in cancer treatment by PDT given their potentially easy formulation. However, the role of MAPKs modulation on photocytotoxicity and autophagic cell death induced by P-OGal-PDT still needs clarification. In this regard, the use of the siRNA technology would of definite interest to understand the role played by the JUNK pathway in the photo-induced death mechanism. Finally, the present study has allowed the characterization of P-OGal as the

most potent photoactive conjugate in the NCI-2244 cell model. In view of its potential interest as a PDT photosensitizer in dermatology, it would be also valuable to assess its photobiological activity towards SCC or BCC cell lines.

Acknowledgements

This work was supported by an ICCTI/CRUP/GRICES exchange agreement, a Franco-Portuguese "PESSOA" exchange program (07010XF), a co-tutelage "PAULIF" Franco-Portuguese program (J.N.S., P.F., J.C.M., R.S., P.M.) and grants from the Gulbenkian Foundation (J.N.S., P.F.) and the "Fundação para a Ciência e a Tecnologia" (J.P.C.F., M.G.P.M.S.N., E.M.P.S., J.A.S.C.). A portion of the epifluorescence microscopy experiments was performed with the equipment of the "Centre de Microscopie du Muséum". The authors wish to thank Drs. M. Géze and M. Deltinger for their advices. The authors wish to thank Pr. I.K. Patterson (Radiation Laboratory, University of Notre Dame, Notre Dame, Indiana) for his careful reading of the manuscript and improvement of the English language. We thank Drs. Yoshimori and Mizushima (Tokyo Metropolitan Institute of Medical Science, Japan) for the kind gift of the GFP-LC3 construct.

Appendix A. Supplementary data

Supplementary data associated with this article can be found, in the online version, at doi:10.1016/j.bcp.2010.07.033.

References

[1] Soler AM, Warloe T, Berner A, Giercksky KE. A follow-up study of recurrence and cosmesis in completely responding superficial and nodular basal cell carcinomas treated with methyl 5-aminolaevulinate-based photodynamic therapy alone and with prior curettage. Br J Dermatol 2001;145:467–71.

[2] Conneely A, Smyth WF, McMullan G. Study of the white-rot fungal degradation of selected phthalocyanine dyes by capillary electrophoresis and liquid chromatography. Anal Chim Acta 2002;2002:259–70.

[3] Zhao B, Yin JJ, Bilski PJ, Chignell CF, Roberts JE, He YY. Enhanced photodynamic efficacy towards melanoma cells by encapsulation of Pc4 in silica nanoparticles. Toxicol Appl Pharmacol 2009;241:62–72.

[4] Chen X, Hu H, Fang DA, Dou QM, Ellick T. Synthesis and photodynamic activity of porphyrin-sugar conjugates against drug-resistant cancer cells. Biochemistry 2004;43:10278–86.

[5] Tome JPC, Neves MGPMS, Tome AC, Cavaleiro JAS, Soncin M, Mac-Robert AJ, et al. Synthesis of glycoconjugated tetrakis(porphyrin-5-yl)-1,4-dihydrazinophthalazines and their photodynamic activity towards cancer cells. J Med Chem 2006;49:6609–15.

[6] Silva N, Hergle J, Tomé P, Neves MG, Tomé AC, Madeira J, et al. Enhancement of the photodynamic activity of meso-tetrakis(pentafluorophenyl)porphyrin in keratinocytes by conjugation to polylysine. Photochem Photobiol Sci 2008;3:1128–33.

[7] Tomé JPC, Silva EMP, Rocha AMVM, Alonso CMA, Faustino MAF, Neves MGPMS, et al. Synthesis of neutral and cationic glycoporphyrins as galactose receptor mediated photosensitizers for cancer therapy. Bioorg Med Chem 2007;15:4705–13.

[8] Mulinacci N, Madeira PJA, Santos R, Smith ED, Pinelli P, Romani A, et al. Tellyoside, a new natural glycoside from Teucrium scorodonia L. (garlic germander) showing activity against tumor cells in vitro and in vivo. Cancer Res 1998;58:3571–8.

[9] Reyftmann J-P, Morlière P, Salmon S, Santus R, Dubertret L, Lagrange D. Interaction of human serum low density lipoproteins with porphyrins: a spectroscopic and photochemical study. Photochem Photobiol 1984;40:721–9.

[10] Filipe P, Silva JN, Haigle J, Freitas JP, Fernandes A, Gomes A, et al. Green coffee antioxidants and photoprotection—both synthetic and natural hydroxycinnamates protect skin from ultraviolet-induced chronic damage. Exp Dermatol 2008;17:1046–53.

[11] Kato Y, Mitsui Y, Itoh T, Yamaguchi A, Kawakami T, Nishi T, et al. UVA-induced translocation of a gene, Apg16p, is mediated by the autophagosome in mammalian cells. Antioxid Redox Signal 2004;6:1–6.

[12] Tyrrell RM, Pidoux M. Correlations between the induction of stress proteins and the development of thermotolerance in UV-irradiated human cells. Int J Radiat Biol Relat Stud Phys Chem Med 1985;47:69–78.

[13] Kessel D, Luo Y, Deng Y, Chang CK. The role of subcellular localization in initiation of apoptosis by photodynamic therapy. Photochem Photobiol 1997;65:422–6.

[14] Gomi K, Iwai K, Ikeda MA, Takahashi A, Okamoto K, Takahashi K, et al. High-fluence photoactivation and photobleaching kinetics of benzoporphyrin derivative monoacid ring A in human bladder carcinoma cells and its correlation with cytotoxicity. Photochem Photobiol 1995;62:96–102.

[15] Kessel D, Woodburn K, Saunders R, Thomas JP. Structure–activity relationships for cationic porphyrins in photosensitization. Photochem Photobiol 1991;53:381–5.

[16] Kessel D, Thompson P, Saatio K, Nantwi KD. Tumor localization and photosensitization by sulfonated derivatives of tetraphenylporphine. Photochem Photobiol 1987;45:787–90.

[17] Kessel D, Luo Y, Mathieu P, Reiners JJ. Determinants of the apoptotic response to lysosomal photodamage. Photochem Photobiol 2000;71:196–200.

[18] Kessel D, Thompson P, Saatio K, Nantwi KD. Tumor localization and photosensitization by sulfonated derivatives of tetraphenylporphine. Photochem Photobiol 1987;45:787–90.

[19] Kessel D, Luo Y, Deng Y, Chang CK. The role of subcellular localization in initiation of apoptosis by photodynamic therapy. Photochem Photobiol 1997;65:422–6.

[20] Kessel D, Woodburn K, Saunders R, Thomas JP. Structure–activity relationships for cationic porphyrins in photosensitization. Photochem Photobiol 1991;53:381–5.

[21] Kessel D, Thompson P, Saatio K, Nantwi KD. Tumor localization and photosensitization by sulfonated derivatives of tetraphenylporphine. Photochem Photobiol 1987;45:787–90.

[22] Kessel D, Luo Y, Mathieu P, Reiners JJ. Determinants of the apoptotic response to lysosomal photodamage. Photochem Photobiol 2000;71:196–200.

[23] Kessel D, Thompson P, Saatio K, Nantwi KD. Tumor localization and photosensitization by sulfonated derivatives of tetraphenylporphine. Photochem Photobiol 1987;45:787–90.

[24] Kessel D, Luo Y, Deng Y, Chang CK. The role of subcellular localization in initiation of apoptosis by photodynamic therapy. Photochem Photobiol 1997;65:422–6.

[25] Kessel D, Woodburn K, Saunders R, Thomas JP. Structure–activity relationships for cationic porphyrins in photosensitization. Photochem Photobiol 1991;53:381–5.

[26] Ventura JJ, Hubner A, Zhang C, Flavell RA, Shokat KM, Davis RJ. Chemical genetic analysis of the time course of signal transduction by JNK. Mol Cell 2006;21:701–10.

[27] Nakano H, Nakajima A, Sakon-Komazawa S, Piao JH, Xue X, Okumura K. Reactive oxygen species mediate crosstalk between NF-kappaB and JNK. Cell Death Diff 2006;13:730–7.

[28] Shimizu S, Konishi A, Nishida Y, Mizuta T, Nishina H, Yamamoto A, et al. Involvement of JNK in the regulation of autophagic cell death. Oncogene 2010;29:2070–82.

[29] Wei Y, Pattingre S, Sinha S, Bassik M, Levine B. JNK1-mediated phosphorylation of Bcl-2 regulates starvation-induced autophagy. Mol Cell 2008;30:678–88.

[30] Lorin S, Borges A, Ribeiro Dos Santos L, Souquere S, Pierron G, Ryan KM, et al. c-Jun N-terminal kinase activation is essential for DRAM-dependent induction of autophagy and apoptosis in p53-null fibrosarcoma cells. Cancer Res 2009;69:6021–1.

[31] Lorin S, Pierron G, Ryan KM, Cocogne P, Djavaheri-Mergny M. Evidence for the interplay between JNK and p53-DRAM signalling pathways in the regulation of autophagy. Autophagy 2010;6:153–4.

[32] Weber JL, Jones SA. New insights into the function of Atg5. IUBMB Life 2010;62:1–19–25.

[33] Zhang Y, Wang P, Tashiro S, Onodera S, Ikejima T. Involvement of p90 ribosomal S6 kinase-1 pathways in oridonin-induced autophagy in HeLa cells: a protective mechanism against apoptosis. Biochem Biophys Res Commun 2008;377:1278–83.

[34] Cagnol S, Chambard JC. ERK and cell death: mechanisms of ERK-induced cell death—apoptosis, autophagy and senescence. FEBS J 2010;277:2–21.

[35] Wong CH, Iskandar KA, Yadav SK, Hotchandani N, Lim T, Parwaz A, Simultaneous induction of non-canonical autophagy and apoptosis in cancer cells by ROS-dependent ERK and JNK activation. PLoS One 2010;5:e9996.

[36] Schiene SM, van Montfort C, Dudeczek DP, Zimmer A, Fuellen Beck S, Kaufmann J, et al. Sindbis virus induces apoptosis through activation of both initiator and effector caspases. Virus Res 2004;99:731–37.

[37] Gupta S, Singh A. Sustained activation of the extracellular signal regulated kinase pathway protects cells from photodynamic therapy mediated by sodium n-aspartyl chlorin e6. Cancer Res 2007;67:6227–35.

[38] Kiefer JD, Hudson S, Brooks A, Jayaraman A, Bottaro J, Sen JJ. Activation of JNK and p38 but not eIK3/MAP kinases in human skin cells by 3-amino enolinate-phenylpyrazine. Life Sci 1998;62:4377–380.

[39] Mata-Cantero A, Kabasakal T, Nadi B, Gleich H, Connally T, Young TA, et al. Photodynamic therapy induces caspase-dependent apoptosis in rat UVB model. Invest Ophthalmol Vis Sci 2007;48:4741–7.

[40] Buytaert E, Wang A, Dewaele M, Breckpot K, Bockaert K, Galsky M, et al. Multiple components of photodynamic therapy can phosphorylate Akt. Photochem Photobiol 2007;83:1020–22.

[41] Schaub-Schaub F, Herbst R, Tarasiuk O. Nitrogen-activated protein kinase cascade in breast cancer. Adv Exp Cancer 2010;14:937–14.

[42] Cheng JQ, Lindsley CW, Cheng GZ, Yang H, Nicosia SV. The Akt/PKB pathway: molecular target for cancer drug discovery. Oncogene 2005;24:7482–92.

Chain-dependent photocytotoxicity of tricationic porphyrin conjugates and related mechanisms of cell death in proliferating human skin keratinocytes

João Nuno Silva, Antoine Galmiche, João P.C. Tomé, Agnès Boullier, Maria G.P.M.S. Neves, Eduarda M.P. Silva, Jean-Claude Capiod, José A.S. Cavaleiro, René Santus, Jean-Claude Mazière, Paulo Filipe and Patrice Morlière

Actinometry of the custom-built table used for irradiation of cell monolayers

The effectiveness of a photodynamic photosensitizer is mostly related to 4 parameters : 1/ the intracellular concentration, 2/ the ability to absorb light which is directly related to molar extinction coefficients, 3/ the intrinsic ability to produce singlet oxygen and 4/ the intracellular targets which are closely related to the intracellular localization. The two first parameters govern the amount of absorbed light. As a result of the polychromatic light provided by the lamp, it is necessary to carry out a careful actinometry of the custom-built irradiation table. The spectral output has been provided by a CS 1000A Minolta spectroradiometer (Bremen, Germany). The absolute calibration has been performed by chemical actinometry using the photodynamic degradation of 50 µM His by 20 µM hematoporphyrin in air saturated 50 mM pH 7.3 phosphate buffer. The quantum yield of His degradation was first measured under irradiation with 365 nm monochromatic light delivered by a filtered high-pressure mercury lamp described in Morliere et al. (1). Then, the **His** degradation was performed with red light.

The relative absorbed light is equal to $S \times \int (I_\lambda \times (1-10^{-A_\lambda})) \times d\lambda) \times dt$, where **S** is the surface of the Petri dish, A_λ the optical density at the wavelength λ and I_λ the relative light intensity at the wavelength λ, obtained with the radiometer. Thus, the absolute spectral distribution can be calculated assuming that the His degradation quantum yield is the same under irradiation with red and 365 nm lights. The integration over the wavelength range yields a light fluence rate of 5.0×10^{-7} photons s^{-1} cm^{-2} corresponding to 15.2 mW cm^{-2}.

For the sake of comparison with other reports of the literature, an equivalent intensity (I_{eq}) of monochromatic light can be estimated with the relationship: $\int I_\lambda \times \varepsilon_\lambda \times d\lambda = I_{eq} \times \varepsilon_\lambda$ where I_λ is the incident light fluence rate and ε_λ the molar extinction coefficient in PBS at wavelength λ. As the visible absorption spectra in a given solvent are very similar for P-H, P-Me, P-DDe, P-Gal et P-OGal, there is practically no difference in the integrated fluence rates ($\int I_\lambda \times \varepsilon_\lambda \times d\lambda$: 19.0 ± 0.6 $\times 10^{-2}$ photons s^{-1} cm^{-1} in PBS, 9.9 ± 0.7 $\times 10^{-2}$ photons s^{-1} cm^{-2} in SDS and 9.7 ± 0.5 $\times 10^{-2}$ photons s^{-1} cm^{-2} in TX100). Assuming an extinction coefficient of 2000 mol^{-1} l cm^{-1}, this calculation yields an equivalent light fluence rate of ~4.5 × 10^{15} photons s^{-1} cm^{-2} in PBS, ~4.95 × 10^{15} photons s^{-1} cm^{-2} in SDS and ~4.85 × 10^{15} photons s^{-1} cm^{-2} in TX100. This calculation is valid for weakly absorbing solutions, which is met with cell monolayers. It also shows that the light doses absorbed by **P-R** are very close to each other under identical concentration and solvent conditions. Moreover, it suggests that these absorbed light doses do not strongly depend on the environment. In the case of PPIX induced by incubation of NCTC cells with ALA, it can be estimated that the integrated light fluence rates for PPIX are equal to 10.2 ± 10^{15} photons s^{-1} cm^{-2} and 9.4 ± 10^{15} photons s^{-1} cm^{-2} in SDS and TX100, respectively. Therefore, the light doses absorbed by P-R and PPIX at equal concentration are rather identical.

Reference

Morlière, P., Bosca, F., Miranda, M.A., Castell, J.V., and Santus, R. (2004) *Photochem. Photobiol.* 80, 535-541.

Lack of caspase activation after PDT of NCTC 2544 keratinocytes with P-OGal

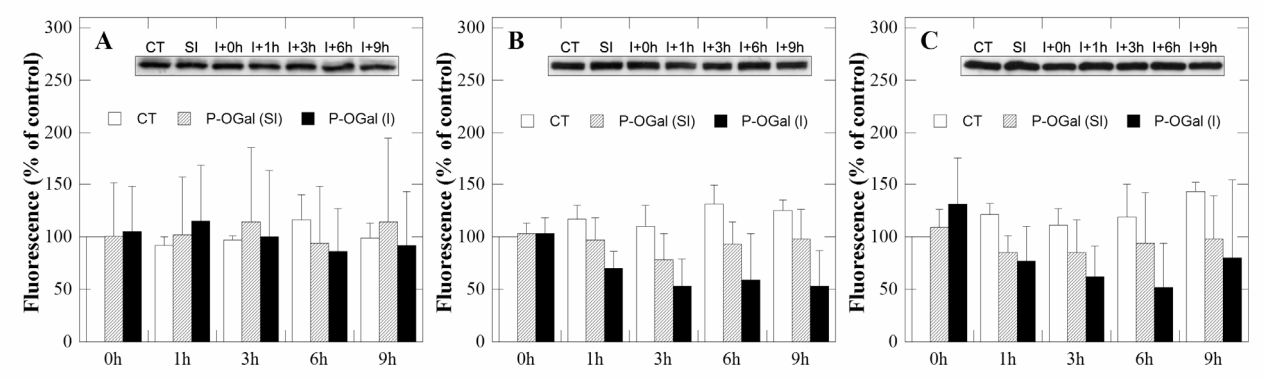

Fig. S1: Effect of P-OGal photodynamic therapy on caspase-3 (A), caspase-8 (B) and caspase-9 (C) activation. Cells were incubated for 3 h with 5 µM P-OGal in FCS-supplemented culture medium, then irradiated (I) or sham-irradiated (SI) for 15 min. Controls (CT) are sham-incubated cells that have been sham-irradiated. At the indicated times after irradiation, cells were harvested and the lysates were assayed for protease activity with the following substrates: Ac-DEVD-AMC (caspase 3), Ac-IETD-AMC (caspase-8) and Ac-LEHD-AMC (caspase 9). Data are expressed as percentage of the enzyme activity measured in controls immediately after the irradiation and are represented as mean − SDM of three independent experiments. Inserts: Western blots confirm no change in caspase expressions up to 9h after PDT. At the indicated times after irradiation, cells were harvested and the lysates were subjected to immunoblot analysis as described in the experimental procedures.

5.3 MAIN RESULTS AND DISCUSSION

5.3.1 CELLULAR UPTAKE OF P-R DERIVATIVES

The P-R uptake as a function of incubation time is presented in Fig. 2A (Article II) for P-$(Lys)_n$ and in Fig. 2A (Article III) for P-H, P-Me, P-DDC, P-Gal and P-OGal. The uptake of P-H, P-Me, P-DDC, P-Gal and P-OGal is extremely rapid and reaches a plateau within less than a hour after the beginning of the incubation. In the case of P-$(Lys)_n$ it takes longer (3 hours) to reach this plateau. The five conjugates are more efficiently taken up by cells than P-H. The uptake of all derivatives increases almost linearly as a function of the incubation concentration. The P-R incubation has also been performed in serum-free HBSS to determine whether serum proteins play any peculiar role in the uptake process. Only P-$(Lys)_n$ slightly interacts with serum proteins (see Fig. 7 (Article II)).

5.3.2 PHOTOCYTOTOXICITY OF P-R DERIVATIVES

The photocytotoxicity efficiency of the P-R derivatives has been estimated by the Neutral Red assay. The following relative order of PDT efficiency -- P-OGal > P-DDC = P-Me > P-$(Lys)_n$ >> P-Gal > P-H -- has been established (Fig. 2C and 2D and Table 1 in Article III)). A clear relationship between photocytotoxicity effectiveness and structure is evidenced as P-H, P-Me, P-DDC, P-Gal and P-OGal have a similar intrinsic $^1O_2$ production capacity and absorb similar light doses. On the other hand, P-$(Lys)_n$ has a lower intrinsic $^1O_2$ production capacity than P-H and P-Gal but it is a stronger photocytotoxic agent (see Fig. 3 in Article II and Table 1 in Article III). Therefore, other factors than the intrinsic $^1O_2$ production capacity must be invoked to explain this superior photosensitizing effect on cells. These are the modulation of the cellular uptake and the intracellular localization/partition within cytosolic sites and cell membranes. It is important to note that P-OGal, P-DDC and P-Me favorably compare with endogenous PPIX induced by treating cells with ALA (see Fig. 3B in Article III). Since the amounts of light absorbed by intracellular P-R and PPIX are rather identical, P-OGal, P-DDC and P-Me are as powerful photosensitizers as PPIX in our cellular model.

5.3.3 PHOTO-OXIDATIVE STRESS INDUCED BY P-R DERIVATES

Singlet oxygen is the main cytotoxin involved in PDT [25]. The photophysical studies presented in Chapter 4 revealed no major difference in the singlet oxygen quantum yields of

P-H, P-Me, P-DDC, P-OGal and P-Gal whereas P-Lys was found to be about 4 times less effective. As presented in Table 1 (Article III) cell photosensitization is inhibited by N_3^- ions, which are specific $^1O_2$ quenchers, further demonstrating the role of singlet oxygen in the photo-oxidative stress induced by these tricationic porphyrins.

Lipid peroxidation was chosen as an overall index of the "intensity" of the photo-oxidative stress. Lipid peroxidation was assayed by measuring TBARS formation [497]. Measurements of TBARS formation induced by P-R are reported in Fig. 4 (Article II) and in Fig. 3A (Article III). The TBARS production is shown to increase nearly linearly with the irradiation time. The most effective TBARS producers are P-OGal, P-DDC, P-Me. As a matter of fact, the greater photocytotoxic efficiency of P-OGal, P-DDC, P-Me and P-$(Lys)_n$ compared to that of P-H and P-Gal also applies to the lipid peroxidation initiation. It thus suggests a correlation between photocytotoxicity of the studied derivatives and their overall ability to produce an oxidative stress.

It is also demonstrated that oxidative membrane damages are more pronounced with PPIX than with P-Me, P-DDC and P-OGal (see Fig. 3C (Article III)). This is in agreement with the highest hydrophobicity of PPIX, which favours its intracellular localization in lipophilic environments.

5.3.4 FLUORESCENCE MICROSCOPY OF P-R DERIVATIVES TREATED CELLS

Phase contrast and fluorescence images obtained with cells exposed to P-R exposed are illustrated in Fig 5 (Article II) and Fig 4 (Article III). A sensitive fluorescence microscopy system has been used to avoid the interference of photobleaching, photodamage and dye relocalization during image acquisition. Intracellular fluorescence experiments have confirmed that P-H and P-Gal are less taken up by NCTC 2544 keratinocytes than P-Me, P-DDC and P-OGal. Moreover, the fluorescence of P-Me, P-DDC, P-OGal and P-$(Lys)_n$ is more specifically localized in spots that may correspond to endo- or pinocytotic vesicles. The rather diffuse fluorescence observed in cells treated with P-H and P-Gal suggests a main cytoplasmic and plasma membrane localization. It should be noted that the mitochondria and the nucleus are not primary sites of P-R localization. These observations demonstrate that the methyl (P-Me), the Di-O-isopropylidene-α-D-galactopyranosyl (P-OGal) and the *N,N´*-dicyclohexylureidooxycarbonyl (P-DDC) groups on the conjugated side chain are more critical than the electric charge of the porphyrin ring in controlling their uptake and localization site and, as a consequence, their greater photosensitizing efficiency.

5.3.5 MECHANISMS OF THE PDT-INDUCED DEATH IN NCTC 2544 CELLS

After describing the chain structure dependence of the photocytotoxic potential by tri-cationic porphyrin conjugates, we have established the nature of the programmed cell death mechanisms induced by P-R and their relative importance. As P-Me, P-OGal and P-DDC exhibit similar intracellular localization, P-OGal -- the most effective photosensitizer -- was chosen as representative P-R for this study.

a) *Role of apoptosis*

It has been established by Oleinick's group that PDT was a strong inducer of apoptosis [498], as previously discussed in Section 2.2. The translocation of phosphatidylserine from the inner layer to the outer layer of the plasma membrane is an early marker of apoptosis. Apoptosis was thus assayed by simultaneous cytometric analysis of annexin V binding and propidium iodide uptake. As presented in Fig 5A (Article III) no significant change in the percentage of annexin V positive cells is observed up to 9 h after irradiation. Similar results were obtained with different P-OGal concentrations, P-OGal incubation durations and light doses. Another well established marker of apoptosis is the nuclear DNA breakdown into oligonucleosomal units. As shown in Fig. 5B (Article III), no significant increase in cytoplasmic histone-associated DNA fragments is found up to 24 h after P-OGal PDT as assayed by an enzyme-linked immunosorbent assay. Furthermore, no caspase-3, caspase-8 and caspase-9 activities and no procaspase-3, procaspase-8 and procaspase-9 cleavage have been observed up to 12 h after P-OGal-PDT. These results and those showing the absence of cytochrome *c* leakage in photosensitized cells are presented in Fig. S1 (Article III). All these data support the lack of apoptosis induction by P-OGal PDT in NCTC 2544 cells.

These results raise the following question: *Are NCTC 2544 cells capable of entering apoptosis or are they apoptosis deficient cells?* To answer these questions, we have used two positive controls (5-methoxypsoralen+UVA and campothecin). Apoptosis induction has been observed as soon as 9 h after campothecin treatment whereas extensive activation of caspase-3 (6-fold increase in activity) has been measured 24h after 5-methoxypsoralen+UVA.

Therefore, our observations are in sharp contrast with most of the published reports that attribute cell death after photodynamic therapy to apoptosis [384]. The absence of internally triggered apoptosis is consistent with the non-mitochondrial localization of the photocytotoxic P-R.

b) *Role of autophagy*

As apoptosis plays no significant role in the photocytotoxicity induced by P-R, we look for an alternative cell death pathway, namely autophagy. Although autophagy was originally described as a cell survival response, it has also been implicated as a death pathway in numerous studies [353, 499-500].

As for apoptosis, we have used multiple criteria to score the development of autophagy after P-OGal-PDT. First, autophagic activity has been studied using a fluorescent marker (GFP-LC3) consisting in a fusion microtubule-associated protein light-chain 3 (LC3) tagged with a green fluorescent protein (GFP). The proteolysis process and recruitment to autophagosomal membranes of LC3, a marker of autophagy, has been followed by fluorescence microscopy and is presented in Fig. 6A (Article III). After P-OGal-PDT, the development of multiple cytosolic vacuoles labeled with a punctated pattern of GFP-LC3 is observed associated to a time-dependent increase in the number of cells showing the characteristic vacuolar pattern of GFP-LC3 (Fig. 6B in Article III). Another accepted marker of autophagy is the p62/SQSTM1 degradation. The western blotting analysis presented in Fig. 6D (Article III) reveals that after irradiation the amount of p62/SQSTM1 decreases (~60%) in the P-OGal-treated cells. To confirm these data, ALA-induced phototoxicity was used as a negative control. By contrast, none of the above autophagy markers is modified in the photocytotoxicity induced by equitoxic ALA in NCTC 2544 cells.

Autophagy induction in P-OGal-induced cell death is further confirmed in our work by treatment of cells with 3-methyladenine (3-MA), a well-characterized autophagy inhibitor. Cell pre-incubation with 3-MA suppresses, as expected, the GFP-LC3 puntacted pattern (Fig. 6C (Article III)) and the p62 degradation (Fig. 7D (Article III)).

To assess the contribution of autophagy in cell death induced by P-R, cytometric analysis of annexin V binding and propidium iodide uptake by dead cells was undertaken. As presented in Fig. 5C (Article III), P-OGal-induced cell death is inhibited by about 40% after incubation with 3-MA. Furthermore, no evidence of apoptosis induction is observed after autophagy inhibition by 3-MA. These experiments suggest that: 1) autophagy plays a pro-death role in our system; 2) autophagy occurs independently of apoptosis but in association with necrosis.

There are a few recent reports on the induction of autophagic cell death by photodynamic therapy and most were performed with apoptosis deficient cells. Moreover, in several studies, autophagy was only observed after inhibition of caspase activity [364, 501-502]. It is of utmost importance to note that we used an apoptosis competent cell model in which the

tri-cationic porphyrin conjugates induced predominantly autophagic cell death in the absence of any apoptosis inhibitor. The incorporation of P-R in lysosomes or pre-lysosomes in the vicinity of the Endoplasmic Reticulum and the Golgi apparatus and non-mitochondrial localization might be responsible for this conjunction of non-apoptotic events although its relationship with autophagy has to be elucidated. We may attribute the autophagy induced by P-OGal photodynamic therapy to an attempt to remove photo-oxidized organelles or to degrade large cross-linked protein aggregates which cannot be removed by the ubiquitin-proteasome system. Depending on the degree of cellular damage, persistence of autophagy may conduct cells to a metabolic collapse and, ultimately, to autophagic cell death. In addition, autophagy may be initiated by several signaling molecules whose expression is modulated during photodynamic therapy in response to oxidative stress. This modulation may switch this process from a survival to a lethal pathway.

5.3.6 MAPK PARTICIPATION IN DEATH OF NCTC 2544 CELLS AFTER PDT WITH P-R DERIVATIVES

The above presented results strongly suggest that autophagy is implicated is cell death induced by P-R. As a consequence, one may raise the following question: *Do photosensitizers activate/inactivate any specific molecular pathway that modulates the autophagic process?* We thus probed oxidative signaling events associated with the photodynamic induced cell killing, particularly those mediated by the MAPKs JNK and p38 (typically associated with apoptosis/autophagy) and ERK1/2 and AKT (typically associated with cell survival and proliferation).

Immunoblot assays performed to assess JNK, p38, ERK1/2 and AKT phosphorylation are presented in Fig 7A (Article III). A rapid, albeit transient, appearance of activated p38 and JNK is observed in photodynamically stressed NCTC cells. By contrast, a striking decrease in the content of p-ERK and p-AKT is observed, the former showing a large decrease to almost undetectable levels despite its high pre-existing level. The role of MAPKs is further evidenced by adding JNK (SP600125) and p38 (SB203580) inhibitors. After confirming the inhibitor specificity by submitting the NCTC 2544 to an osmotic stress, cytometric analysis of their effect on the annexin V binding and propidium iodide uptake has been performed. SP600125, but not SB203580, increases the photo-induced cell death as reported in Fig 7B (Article III). This cytotoxic effect is not due to the direct toxic effect of SP600125 as the viability of control cells treated with P-OGal and pre-incubated with SB203580 and SP600125 but left in the dark is unchanged. Furthermore, no significant effect on the

percentage of annexin V positive cells is observed after P-OGal -PDT of cells pre-incubated with p38 and JNK inhibitors

To better understand how SP600125 increases the photo-induced cell death, the fluorescence detection of GFP-LC3-puncta and the p62 immunoblot assays have been performed. As presented in Fig.7C (Article III), GFP-LC3 is increased in cells treated with P-OGal and SP600125 while SP600125 has no effect on the basal level of GFP-LC3-puncta. As expected, SP600125 but not SB203580 increases the p62 degradation after PDT. Altogether these results confirm that JNK exerts a negative regulator effect on P-OGal PDT-induced autophagy and PDT-dependent programmed cell death.

These results corroborate several studies performed with different cell lines and photosensitizers, that demonstrate the MAPKs participation in the oxidative signalling events induced by PDT [442]. However, the precise role of p38 and JNK MAPK in cell viability after PDT is still unclear, as previously discussed in Section 2.2.3. Taken together the results suggest that the degree of p38 and JNK phosphorylation as well as their effect on the cell death regulation after PDT may depend on the cell type, the photosensitizer used and the light dose administered [396, 406]. In contrast to the PDT-induced apoptosis, relatively little is known about the PDT-induced autophagy signalling in terms of MAPK activation and possible cross-talk among different pathways.

The role of JNK in cell death has long been controversial as it exhibits a pro-survival effect or triggers cell killing depending on the physiological or pathological condition studied [503]. This paradoxical effect is partially due to different modes of JNK activation [504]. Apparently, an early transient phase of JNK activation determines cell survival, whereas sustained JNK activation can induce cell death signals. As an example, sustained activation of JNK has been implicated in reactive oxygen species-induced necrosis [505] and etoposide- and staurosporine-induced autophagy in Bax/Bak DKO cells [506]. Our results are in accordance with the previous data as we observed a rapid and transient activation of JNK after P-OGal PDT associated with a negative regulatory effect on cell mortality and autophagy. We may speculate that this effect might be partially explained by the JNK1 mediated Bcl-2 phosphorylation. Bcl-2 phosphorylation was shown to inhibit the binding of Bcl-2 to Beclin 1 leading to autophagy activation [507].

Conflicting data also exist regarding the role of p38 in apoptosis and autophagy. Several reports support the role of p38 as inhibitor of autophagy [508-509] while others suggest that it is an inducer of autophagy [510]. Although we observed an activation of p38 after P-OGal PDT, our data suggest that p38 is not directly implicated in cell death induction in our system.

A downstream event in the mitogenic pathway is the activation of ERK. The activation of the Ras/Raf-1/ERK1/2 pathway is able to promote opposite pro-survival or antiproliferative cellular responses, such as apoptosis and autophagy. This wide variety of processes triggered by the activation of a single pathway has been shown to depend on the timing, duration and strength of this activation, as well as on specific subcellular localization and on the presence of reactive oxygen species [511]. As presented in Section 2.2.3, available evidence suggests that PDT may modulate ERK activity. Depending on the photosensitizer and cellular lines, ERK has been found to variably respond to the PDT-induced oxidative stress by irreversible inhibition [403], moderate attenuation [512], no significant modulation [406] or even a transient activation of ERK1/2 [407]. We found a decrease in the content of p-ERK after P-R conjugates PDT to almost undetectable levels 3 h after PDT despite high pre-existing expression (Fig. 7A). The role of the indicated trend of ERK1/2 in cell death mechanisms observed in our PDT model is to be clarified in further studies.

Activation of the PI3-K/AKT is another important signaling pathway known to inhibit apoptosis and promote cell survival. AKT acts on a variety of ways including activation of mTOR, phosphorylation of Bad, phosphorylation of IκB kinase and inhibition of caspase-9 [513]. Data about the PDT effect on AKT phosphorylation are somewhat conflicting varying from dephosphorylation and subsequent activation of caspase-assisted death [514] to stimulation of AKT phosphorylation [411]. Our results show a time dependent decrease in the content of p-AKT after PDT treatment with P-R conjugates. A recent study showed that transcription factor FoXO3 functions downstream of AKT/PKB and increases the expression of many autophagy related genes. The transcription factor FoXO3 is inhibited by AKT in a TOR independent pathway [515]. We may thus speculate that AKT inhibition by P-OGal PDT would ultimately augment $FoXO_3$ activity and would contribute to autophagy induction.

Noteworthy, several studies have shown that ERK and PI3-K/AKT signaling pathways may be aberrant in various human cancers [516-517]. As tricationic porphyrin conjugates inhibit ERK1/2 and PI3-K/AKT signaling pathways, we might suggest their potential beneficial role in cancer treatment.

5.4 CONCLUSIONS

This work was undertaken to study the photocytotoxicity effectiveness of tricationic porphyrin conjugates and the related mechanisms of cell death. Considering the results described above we can conclude that:

1- All compounds are potentially interesting considering their photocytotoxic efficacy in cultured proliferating human skin keratinocytes. In particular, P-OGal, P-DDC, P-Me favorably compared with endogenous PPIX produced by ALA treatment. The following relative PDT efficiency has been estimated: P-OGal > P-DDC = P-Me > P-$(Lys)_n$ >> P-Gal > P-H.

2- The cell uptake and intracellular localization contribute to the different photocytotoxic responses. It is suggested that the nature of the conjugated side chain is more critical than the electric charge of the porphyrin ring in controlling the uptake and site of localization of P-R, and consequently the photocytotoxic efficacy.

3- In our apoptosis-competent cell system, autophagy plays a major role in the cell death photo-induced by tricationic porphyrin conjugates. Apoptosis is not activated probably because of the non-mitochondrial localization of P-R.

4- MAPK JNK exerts a negative regulator effect on P-OGal PDT-induced autophagy. A close relationship between tricationic porphyrin conjugates PDT and MAPK pathway impairment is also suggested through activation of p38 and inhibition of the AKT and EGFR-ERK signaling pathways.

CHAPTER 6

CONCLUSIONS AND PERSPECTIVES

CONCLUSIONS AND PERSPECTIVES

The objective of this work was to unravel the photobiological/biochemical characteristics of five tri-cationic porphyrin conjugates - new photoactive substances which may be suitable for therapeutic applications in dermatology.

In the first part of our work, we have conducted a rather thorough study of their photophysical and photochemical properties with emphasis on the influence of the structure of the conjugated chain on their excited singlet and triplet state properties.

Regarding the first excited singlet state, absorbance spectra, extinction coefficients, fluorescence spectra and fluorescence quantum yields of the tri-cationic porphyrin conjugates have been determined in solvents of different polarity mimicking the numerous microenvironmental conditions that prevail in living cells. Using ultrafast spectroscopy, we demonstrated that the presence of galactosyl moieties or of a polylysine chain linked to the porphyrin macrocycle allows molecular interactions between the conjugated chain and the aromatic ring within a few tenths of picoseconds. It may therefore be anticipated that, once incorporated into cells, such flexibility may favor the interaction of the conjugate with appropriate complex biological assemblies. Furthermore, we found that their fluorescence quantum yield and lifetime of all compounds is compatible with their further use for fluorescence studies in cultured cells and, possibly, for the detection of tumor tissues in clinical practice.

The rather long lifetime (up to ~60 µs) and the high quantum yield of formation (~0.5) of their first excited triplet state lead to effective production of singlet oxygen, the cytotoxin involved in PDT. From the analysis of these results it is suggested that all compounds are potentially interesting although the poly-*S*-lysine conjugate which produces less singlet oxygen seems *a priori* less relevant.
At this stage of the work, it was clear that with the exception of the polylysine conjugate, the possible difference in the photocytotoxic activity of the conjugates could not be explained by a higher intrinsic photodynamic efficiency. Other factors could be implicated such as a difference in their cellular uptake and/or in their intracellular localization/partition within cytosolic sites and cell membranes.

As a consequence, the second part of our work was dedicated to the study of the photocytotoxic effectiveness of the tri-cationic porphyrin derivatives towards cultured proliferating human skin keratinocytes. Their photosensitizing capacity was examined as a function of their physicochemical characteristics, cellular uptake and intracellular localization.

We found that all the studied compounds were photocytotoxic towards cultured proliferating human skin keratinocytes. However, the following relative order of PDT efficiency could be established: P-OGal > P-DDC = P-Me > P-$(Lys)_n$ >> P-Gal > P-H. In particular, P-OGal, P-DDC, P-Me favorably compared with endogenous PPIX produced by ALA treatment, the "*gold standard*" of topical PDT in Dermatology. As previously hypothesized, the cell uptake and intracellular localization contributed to the different photocytotoxic responses. It was observed that the nature of the conjugated side chain is more critical than the electric charge of the porphyrin ring in controlling the uptake and site of localization of P-R and, consequently, the photocytotoxic efficacy.

A particular attention was paid to the assessment of cell death pathways and molecular mechanisms involved in the photocytotoxicity induced by tri-cationic porphyrin derivatives. We found that autophagy along with necrosis play a major role in the cell death photo-induced by tricationic porphyrin conjugates. This observation disagrees with the majority of the published reports that attribute the PDT-induced cell death to apoptosis. In fact, apoptosis was not observed - even after autophagy inhibition - probably because of the non-mitochondrial localization of P-R.

To shed light on the molecular mechanisms involved, we studied the role of MAPK in the photocytotoxicity induced by P-OGal, the most effective tri-cationic porphyrin derivative. We showed that JNK exerts a negative regulatory effect on P-OGal PDT-induced autophagy. We found a close relationship between PDT with tricationic porphyrin conjugates and MAPK pathway impairment through activation of p38 and inhibition of the AKT and EGFR-ERK signaling pathways. The induction of a specific death mode and the inhibition of the AKT and EGFR-ERK signaling pathways may be susceptible to result in a therapeutic advantage.

The conclusion that can be drawn after completion of this work is that the potential interest of P-OGal as a PDT photosensitizer in dermatology warrants further *in vitro* and *in vivo* studies. Here are some interesting issues.

1- It will be interesting to study the role of autophagy in PDT-induced cell death by the

most effective tri-cationic porphyrin conjugates. The clarification of the role of MAPK's modulation in photocytotoxicity and associated autophagy is of major interest. In this regard, the use of the siRNA technology would be of definite interest to understand the role played by the JUNK pathway in the photo-induced death mechanism.

2- It will also be valuable to assess tri-cationic porphyrin conjugates photobiological activity towards squamous cell and basal cell carcinoma cell lines. As topical PDT is indicated for these diseases, these studies may raise up a definitive therapeutic interest.

3- This work shows that P-OGal, P-DDC, P-Me and P-$(Lys)_n$ are potentially interesting considering their photocytotoxic efficacy in proliferating human skin keratinocytes in culture. These tri-cationic porphyrin conjugates should thus be assayed in *in vivo* murine models of skin tumors allowing assessment of their acute toxicity, pharmacokinetics, selectivity and efficacy. These will be followed by the study of the relationship between cellular uptake, intracellular/intratumoral localization, photocytotoxicity, cell death mechanisms and signaling pathways induced by PDT *in vivo*.

4- Finally, should these further studies on animal tumor models be successful then photopatch tests on human volunteers could be performed as a prerequisite for - and in the hope of future clinical use.

Reference

1. ACKROYD R., KELTY C., BROWN N.*, et al.* The history of photodetection and photodynamic therapy. *Photochem Photobiol*, 2001, 74, p. 656-669.
2. BOUGHTON H.C., ed. The Valley Echo; 1923/4.
3. FINSEN N. Phototherapy. *London: Arnold*, 1901, p.
4. FITZPATRICK T.B., PATHAK M.A. Historical aspects of methoxsalen and other furocoumarins. *J Invest Dermatol*, 1959, 32, p. 229-231.
5. RAAB O. Uber die Wirkung fluoreszierender Stoffe auf Influsorien. *Z Biol*, 1900, 39, p. 524-546.
6. VON TRAPPEINER H J.A. Therapeutische Versuche mit fluoreszierenden stoffen. *Med Worchenschr*, 1903, 47, p. 2042-2044.
7. VON TRAPPEINER H J.A. Uber Wirkung der photodynamischen (fluorieszierenden) Stoffe auf Protozan und Enzyme. *Dtsche Arch Klin Med*, 1904, 80, p. 427-487.
8. VON TRAPPEINER H J.A. Die Sensibilisierende Wirkung fluorieszierender Substanzer. Gesammte Untersuchungen über die photodynamische Erscheinung. *FCW Vogel, Leipzig*, 1907, p.
9. PRIME O. *Les accidentes toxiques par l'eosinate de sodium*, 1900.
10. HAUSMANN W. Die sensibilisierende Wirkung des Hämatoporphyrins. *Biochem Z*, 1911, 30, p. 276-316.
11. MEYER-BETZ F. Untersuchungen über die biologische (photodynamische) Wirkung des Hämatoporphyrins und anderer Derivate des Blut- und Gallenfarbstoffs. *Dtsche Arch Klin Med*, 1913, 112, p. 476-503.
12. POLICARD A. Etude sur les aspects offerts par des tumeurs expérimentales examinées à la lumière de Wood. *C R Soc Biol*, 1924, 91, p. 1423-1424.
13. BLUM H.F. *Photodynamic Action and Diseuses Caused by Light*. New York: Rhinehold, 1941.
14. RONCHESE F. The fluorescence of cancer under the Wood light. *Oral Surg Oral Med Oral Pathol*, 1954, 7, p. 967-971.
15. FIGGE F.H., WEILAND G.S., MANGANIELLO L.O. Cancer detection and therapy; affinity of neoplastic, embryonic, and traumatized tissues for porphyrins and metalloporphyrins. *Proc Soc Exp Biol Med*, 1948, 68, p. 640.
16. RASMUSSEN-TAXDAL D.S., WARD G.E., FIGGE F.H. Fluorescence of human lymphatic and cancer tissues following high doses of intravenous hematoporphyrin. *Surg Forum*, 1955, 5, p. 619-624.
17. WINKELMAN J. Intracellular localization of "hematoporphyrin" in a transplanted tumor. *J Natl Cancer Inst*, 1961, 27, p. 1369-1377.
18. WINKELMAN J. The distribution of tetraphenylporphinesulfonate in the tumor-bearing rat. *Cancer Res*, 1962, 22, p. 589-596.
19. WINKELMAN J. Metabolic studies on the accumulation of tetraphenylporphinesulfonate in tumours. *Experientia*, 1967, 23, p. 949-950.
20. LIPSON R.L., BALDES E.J., OLSEN A.M. The use of a derivative of hematoporhyrin in tumor detection. *J Natl Cancer Inst*, 1961, 26, p. 1-11.
21. DOUGHERTY T.J. A brief history of clinical photodynamic therapy development at Roswell Park Cancer Institute. *J Clin Laser Med Surg*, 1996, 14, p. 219-221.
22. DOUGHERTY T.J. Activated dyes as antitumor agents. *J Natl Cancer Inst*, 1974, 52, p. 1333-1336.
23. WEISHAUPT K.R., GOMER C.J., DOUGHERTY T.J. Identification of singlet oxygen as the cytotoxic agent in photoinactivation of a murine tumor. *Cancer Res*, 1976, 36, p. 2326-2329.
24. SCHUITMAKER J.J., BAAS P., VAN LEENGOED H.L.*, et al.* Photodynamic therapy: a promising new modality for the treatment of cancer. *J Photochem Photobiol B*, 1996, 34, p. 3-12.

25. DOUGHERTY T.J., GOMER C.J., HENDERSON B.W.*, et al.* Photodynamic therapy. *J Natl Cancer Inst*, 1998, 90, p. 889-905.
26. VAN LIER J. *Photosensitization: reaction pathways*: New York: Plenum press, 1990.
27. PRASAD P. *Introduction to biophotonics*. Hoboken: Wiley, 2003.
28. VALEUR B. *Molecular fluorescence: principles and applications*. Weinheim: Wiley, 2001.
29. KOHEN E., SANTUS R., HIRSCHBERG J.G. *Fluorescence pros in oncology*. London: Imperial College Press, 2002.
30. OCHSNER M. Photophysical and photobiological processes in the photodynamic therapy of tumours. *J Photochem Photobiol B*, 1997, 39, p. 1-18.
31. HATZ S., LAMBERT J.D., OGILBY P.R. Measuring the lifetime of singlet oxygen in a single cell: addressing the issue of cell viability. *Photochem Photobiol Sci*, 2007, 6, p. 1106-1116.
32. NIEDRE M., PATTERSON M.S., WILSON B.C. Direct near-infrared luminescence detection of singlet oxygen generated by photodynamic therapy in cells in vitro and tissues in vivo. *Photochem Photobiol*, 2002, 75, p. 382-391.
33. HATZ S., POULSEN L., OGILBY P.R. Time-resolved singlet oxygen phosphorescence measurements from photosensitized experiments in single cells: effects of oxygen diffusion and oxygen concentration. *Photochem Photobiol*, 2008, 84, p. 1284-1290.
34. FOOT C.S. *Mechanisms of photo-oxygenation*. New York: Alan R Liss, 1984, p. 3-18.
35. REDMOND R.W., GAMLIN J.N. A compilation of singlet oxygen yields from biologically relevant molecules. *Photochem Photobiol*, 1999, 70, p. 391-475.
36. JUZENIENE A., NIELSEN K.P., MOAN J. Biophysical aspects of photodynamic therapy. *J Environ Pathol Toxicol Oncol*, 2006, 25, p. 7-28.
37. MACDONALD I.J., MORGAN J., BELLNIER D.A.*, et al.* Subcellular localization patterns and their relationship to photodynamic activity of pyropheophorbide-a derivatives. *Photochem Photobiol*, 1999, 70, p. 789-797.
38. BOYLE R.W., DOLPHIN D. Structure and biodistribution relationships of photodynamic sensitizers. *Photochem Photobiol*, 1996, 64, p. 469-485.
39. NENCKI M., SIEBER N. *Arch Explt Path Pharmakol*, 1884, 18, p. 401.
40. KUSTER W.Z. *Z Physiol Chem*, 1912, 82, p. 463.
41. KISCHER H., KLARER J., JUSTUS L. *Ann Chem*, 1926, 450, p. 181.
42. NYMAN E.S., HYNNINEN P.H. Research advances in the use of tetrapyrrolic photosensitizers for photodynamic therapy. *J Photochem Photobiol B*, 2004, 73, p. 1-28.
43. SCHWARTZ S. K. A.K., VERMUND H. Some relationships of porphyrins, X-rays and tumours. *Univ Minn Med Bull*, 1955, 27, p. 7–8.
44. KESSEL D., BYRNE C.J., WARD A.D. Photophysical and photobiological properties of diporphyrin ethers. *Photochem Photobiol*, 1991, 53, p. 469-474.
45. KESSEL D., BYRNE C.J., WARD A.D. Configuration of triporphyrin ethers probed by fluorescence measurements. *J Photochem Photobiol B*, 1992, 13, p. 153-160.
46. BONNETT R., BERENBAUM M.C. HPD - a study of its components and their properties. *Adv Exp Med Biol*, 1983, 160, p. 241-250.
47. MOAN J., SANDBERG S., CHRISTENSEN T.*, et al.* Hematoporphyrin derivative: chemical composition, photochemical and photosensitizing properties. *Adv Exp Med Biol*, 1983, 160, p. 165-179.
48. DOUGHERTY T.J., POTTER W.R., WEISHAUPT K.R. The structure of the active component of hematoporphyrin derivative. *Prog Clin Biol Res*, 1984, 170, p. 301-314.
49. KESSEL D., CHANG C.K., MUSSELMAN B. Chemical, biologic and biophysical studies on 'hematoporphyrin derivative'. *Adv Exp Med Biol*, 1985, 193, p. 213-227.
50. *Photodynamic, tumour therapy: 2nd and 3rd generation photosensitizers*. New Delhi: Harwood Academic Publishers, 1998.
51. BONNETT R. Photosensitizers of the porphyrin and phthalocyanine series for photodynamic therapy. *Chem Soc Rev*, 1995, 24, p. 19–33.

52. PUSHPAN S.K., VENKATRAMAN S., ANAND V.G.*, et al.* Porphyrins in photodynamic therapy - a search for ideal photosensitizers. *Curr Med Chem Anticancer Agents*, 2002, 2, p. 187-207.
53. ALLISON R.R., DOWNIE G.H., CUENCA R.*, et al.* Photosensitizers in clinical PDT. *Photodiagn Photodyn Ther*, 2004, 1, p. 27–42.
54. CASTANO A.P., DEMIDOVA T.N., HAMBLIN M.R. Mechanisms in photodynamic therapy: part one - photosensitizers, photochemistry and cellular localization. *Photodiagn Photodyn Ther*, 2004, 1, p. 279–293.
55. DETTY M.R., GIBSON S.L., WAGNER S.J. Current clinical and preclinical photosensitizers for use in photodynamic therapy. *J Med Chem Soc Rev*, 2004, 47, p. 3897–3915.
56. WILSON B.C., JEEVES W.P., LOWE D.M.*, et al. Light propagation in animal tissues in the wavelength range 375–825 nanometers*. New York: Liss Inc, 1984, p. 115–132.
57. JORI G. Far-red-absorbing photosensitizers: their use in the photodynamic therapy of tumours. *J Photochem Photobiol A*, 1992, 62, p. 371-378.
58. COPPER M.P., TAN I.B., OPPELAAR H.*, et al.* Meta-tetra(hydroxyphenyl)chlorin photodynamic therapy in early-stage squamous cell carcinoma of the head and neck. *Arch Otolaryngol Head Neck Surg*, 2003, 129, p. 709-711.
59. CAMPBELL S.M., GOULD D.J., SALTER L.*, et al.* Photodynamic therapy using meta-tetrahydroxyphenylchlorin (Foscan) for the treatment of vulval intraepithelial neoplasia. *Br J Dermatol*, 2004, 151, p. 1076-1080.
60. SESSLER J.L., DOW W.C., O'CONNOR D. Biomedical applications of lanthanide(III) texaphyrins as potential PDT sensitizers. *J Alloys Compd*, 1997, 249, p. 146-152.
61. HENDERSON B.W., DOUGHERTY T.J. How does photodynamic therapy work? *Photochem Photobiol*, 1992, 55, p. 145-157.
62. KUBLER A.C., HAASE T., STAFF C.*, et al.* Photodynamic therapy of primary nonmelanomatous skin tumours of the head and neck. *Lasers Surg Med*, 1999, 25, p. 60-68.
63. BERENBAUM M.C., AKANDE S.L., BONNETT R.*, et al.* meso-Tetra(hydroxyphenyl)porphyrins, a new class of potent tumour photosensitisers with favourable selectivity. *Br J Cancer*, 1986, 54, p. 717-725.
64. VAN GEEL I.P., OPPELAAR H., OUSSOREN Y.G.*, et al.* Photosensitizing efficacy of MTHPC-PDT compared to photofrin-PDT in the RIF1 mouse tumour and normal skin. *Int J Cancer*, 1995, 60, p. 388-394.
65. FRIEDBERG J.S., MICK R., STEVENSON J.*, et al.* A phase I study of Foscan-mediated photodynamic therapy and surgery in patients with mesothelioma. *Ann Thorac Surg*, 2003, 75, p. 952-959.
66. RAUSCHNING W., TAN I.B., DOLIVET G. Photodynamic therapy PDT with mTHPC in the palliation of advanced head and neck cancer in patients who have failed prior therapies and are unsuitable for radiatiotherapy, surgery or systemic chemotherapy. *J Clin Oncol*, 2004, 22, p. 5596.
67. BIEL M. Advances in photodynamic therapy for the treatment of head and neck cancers. *Lasers Surg Med*, 2006, 38, p. 349-355.
68. LOVAT L.B., JAMIESON N.F., NOVELLI M.R.*, et al.* Photodynamic therapy with m-tetrahydroxyphenyl chlorin for high-grade dysplasia and early cancer in Barrett's columnar lined esophagus. *Gastrointest Endosc*, 2005, 62, p. 617-623.
69. ETIENNE J., DORME N., BOURG-HECKLY G.*, et al.* Photodynamic therapy with green light and m-tetrahydroxyphenyl chlorin for intramucosal adenocarcinoma and high-grade dysplasia in Barrett's esophagus. *Gastrointest Endosc*, 2004, 59, p. 880-889.
70. MOORE C.M., NATHAN T.R., LEES W.R.*, et al.* Photodynamic therapy using meso tetra hydroxy phenyl chlorin (mTHPC) in early prostate cancer. *Lasers Surg Med*, 2006, 38, p. 356-363.
71. NATHAN T.R., WHITELAW D.E., CHANG S.C.*, et al.* Photodynamic therapy for prostate cancer recurrence after radiotherapy: a phase I study. *J Urol*, 2002, 168, p. 1427-1432.

72. PEREIRA S.P., AYARU L., ROGOWSKA A.*, et al.* Photodynamic therapy of malignant biliary strictures using meso-tetrahydroxyphenylchlorin. *Eur J Gastroenterol Hepatol*, 2007, 19, p. 479-485.
73. HANSCH A., FREY O., GAJDA M.*, et al.* Photodynamic treatment as a novel approach in the therapy of arthritic joints. *Lasers Surg Med*, 2008, 40, p. 265-272.
74. TRIESSCHEIJN M., RUEVEKAMP M., ANTONINI N.*, et al.* Optimizing meso-tetra-hydroxyphenyl-chlorin-mediated photodynamic therapy for basal cell carcinoma. *Photochem Photobiol*, 2006, 82, p. 1686-1690.
75. CALZAVARA-PINTON P.G., SZEIMIES R.M., ORTEL B.*, et al.* Photodynamic therapy with systemic administration of photosensitizers in dermatology. *J Photochem Photobiol B*, 1996, 36, p. 225-231.
76. SHELEG S.V., ZHAVRID E.A., KHODINA T.V.*, et al.* Photodynamic therapy with chlorin e(6) for skin metastases of melanoma. *Photodermatol Photoimmunol Photomed*, 2004, 20, p. 21-26.
77. HRUZA L., LUI H., HRUZA G. Response of psoriasis to photodynamic therapy using benzoporphyrin derivative monoacid ring A. *Lasers Surg Med*, 1995, 4, p. 43.
78. MOAN J., PENG Q. An outline of the hundred-year history of PDT. *Anticancer Res*, 2003, 23, p. 3591-3600.
79. HUANG Z. A review of progress in clinical photodynamic therapy. *Technol Cancer Res Treat*, 2005, 4, p. 283-293.
80. CALZAVARA-PINTON P.G., VENTURINI M., SALA R. Photodynamic therapy: update 2006. Part 1: Photochemistry and photobiology. *J Eur Acad Dermatol Venereol*, 2007, 21, p. 293-302.
81. WOHRLE D., HIRTH A., BOGDAHN-RAI T.*, et al.* Photodynamic therapy of cancer: second and third generations of photosensitizers. *Russ Chem Bull*, 1998, 47, p. 807–816.
82. DERYCKE A.S., DE WITTE P.A. Transferrin-mediated targeting of hypericin embedded in sterically stabilized PEG-liposomes. *Int J Oncol*, 2002, 20, p. 181-187.
83. SOLBAN N., RIZVI I., HASAN T. Targeted photodynamic therapy. *Lasers Surg Med*, 2006, 38, p. 522-531.
84. KONAN Y.N., GURNY R., ALLEMANN E. State of the art in the delivery of photosensitizers for photodynamic therapy. *J Photochem Photobiol B*, 2002, 66, p. 89-106.
85. MOORE M.R., MCCOLL K.E., GOLDBERG A. The porphyrias. *Diabete Metab*, 1979, 5, p. 323-336.
86. BATLLE A.M. Porphyrins, porphyrias, cancer and photodynamic therapy--a model for carcinogenesis. *J Photochem Photobiol B*, 1993, 20, p. 5-22.
87. SASSA S. Hematologic aspects of the porphyrias. *Int J Hematol*, 2000, 71, p. 1-17.
88. KAUPPINEN R. Porphyrias. *Lancet*, 2005, 365, p. 241-252.
89. NORMAN R.A. Past and future: porphyria and porphyrins. *Skinmed*, 2005, 4, p. 287-292.
90. XU W., KOZAK C.A., DESNICK R.J. Uroporphyrinogen-III synthase: molecular cloning, nucleotide sequence, expression of a mouse full-length cDNA, and its localization on mouse chromosome 7. *Genomics*, 1995, 26, p. 556-562.
91. FERREIRA G.C., ANDREW T.L., KARR S.W.*, et al.* Organization of the terminal two enzymes of the heme biosynthetic pathway. Orientation of protoporphyrinogen oxidase and evidence for a membrane complex. *J Biol Chem*, 1988, 263, p. 3835-3839.
92. BERLIN N.I., NEUBERGER A., SCOTT J.J. The metabolism of delta -aminolaevulic acid. 2. Normal pathways, studied with the aid of 14C. *Biochem J*, 1956, 64, p. 90-100.
93. BERLIN N.I., NEUBERGER A., SCOTT J.J. The metabolism of delta -aminolaevulic acid. 1. Normal pathways, studied with the aid of 15N. *Biochem J*, 1956, 64, p. 80-90.
94. BATLLE A.M.D.C., LLAMBIAS E.B.C., WIDER E.*, et al.* Porphyrin biosynthesis in the soybean callus tissue system-XV. The, effect of growth conditions. *Int J Biochem*, 1975, 6, p. 591–606.
95. MALIK Z., LUGACI H. Destruction of erythroleukaemic cells by photoactivation of endogenous porphyrins. *Br J Cancer*, 1987, 56, p. 589-595.

96. MOAN J., PENG Q., EVENSEN J.F.*, et al.* Photosensitizing efficiencies, tumor- and cellular uptake of different photosensitizing drugs relevant for photodynamic therapy of cancer. *Photochem Photobiol*, 1987, 46, p. 713-721.
97. KENNEDY J.C., POTTIER R.H., PROSS D.C. Photodynamic therapy with endogenous protoporphyrin IX: basic principles and present clinical experience. *J Photochem Photobiol B*, 1990, 6, p. 143-148.
98. PIACQUADIO D.J., CHEN D.M., FARBER H.F.*, et al.* Photodynamic therapy with aminolevulinic acid topical solution and visible blue light in the treatment of multiple actinic keratoses of the face and scalp: investigator-blinded, phase 3, multicenter trials. *Arch Dermatol*, 2004, 140, p. 41-46.
99. FRITSCH C., STEGE H., SAALMANN G.*, et al.* Green light is effective and less painful than red light in photodynamic therapy of facial solar keratoses. *Photodermatol Photoimmunol Photomed*, 1997, 13, p. 181-185.
100. BRAATHEN L.R., SZEIMIES R.M., BASSET-SEGUIN N.*, et al.* Guidelines on the use of photodynamic therapy for nonmelanoma skin cancer: an international consensus. International Society for Photodynamic Therapy in Dermatology, 2005. *J Am Acad Dermatol*, 2007, 56, p. 125-143.
101. PENG Q., WARLOE T., BERG K.*, et al.* 5-Aminolevulinic acid-based photodynamic therapy. Clinical research and future challenges. *Cancer*, 1997, 79, p. 2282-2308.
102. TAYLOR E.L., BROWN S.B. The advantages of aminolevulinic acid photodynamic therapy in dermatology. *J Dermatolog Treat*, 2002, 13 Suppl 1, p. S3-11.
103. RUD E., GEDERAAS O., HOGSET A.*, et al.* 5-aminolevulinic acid, but not 5-aminolevulinic acid esters, is transported into adenocarcinoma cells by system BETA transporters. *Photochem Photobiol*, 2000, 71, p. 640-647.
104. GAULLIER J.M., BERG K., PENG Q.*, et al.* Use of 5-aminolevulinic acid esters to improve photodynamic therapy on cells in culture. *Cancer Res*, 1997, 57, p. 1481-1486.
105. UEHLINGER P., ZELLWEGER M., WAGNIERES G.*, et al.* 5-Aminolevulinic acid and its derivatives: physical chemical properties and protoporphyrin IX formation in cultured cells. *J Photochem Photobiol B*, 2000, 54, p. 72-80.
106. GEDERAAS O.A., HOLROYD A., BROWN S.B.*, et al.* 5-Aminolaevulinic acid methyl ester transport on amino acid carriers in a human colon adenocarcinoma cell line. *Photochem Photobiol*, 2001, 73, p. 164-169.
107. PENG Q., SOLER A.M., WARLOE T.*, et al.* Selective distribution of porphyrins in skin thick basal cell carcinoma after topical application of methyl 5-aminolevulinate. *J Photochem Photobiol B*, 2001, 62, p. 140-145.
108. PENG Q., WARLOE T., MOAN J.*, et al.* Distribution of 5-aminolevulinic acid-induced porphyrins in noduloulcerative basal cell carcinoma. *Photochem Photobiol*, 1995, 62, p. 906-913.
109. MARTIN A., TOPE W.D., GREVELINK J.M.*, et al.* Lack of selectivity of protoporphyrin IX fluorescence for basal cell carcinoma after topical application of 5-aminolevulinic acid: implications for photodynamic treatment. *Arch Dermatol Res*, 1995, 287, p. 665-674.
110. AHMADI S., MCCARRON P.A., DONNELLY R.F.*, et al.* Evaluation of the penetration of 5-aminolevulinic acid through basal cell carcinoma: a pilot study. *Exp Dermatol*, 2004, 13, p. 445-451.
111. FRITSCH C., HOMEY B., STAHL W.*, et al.* Preferential relative porphyrin enrichment in solar keratoses upon topical application of delta-aminolevulinic acid methylester. *Photochem Photobiol*, 1998, 68, p. 218-221.
112. KUIJPERS D.I., THISSEN M.R., THISSEN C.A.*, et al.* Similar effectiveness of methyl aminolevulinate and 5-aminolevulinate in topical photodynamic therapy for nodular basal cell carcinoma. *J Drugs Dermatol*, 2006, 5, p. 642-645.
113. BARR H., KENDALL C., REYES-GODDARD J.*, et al.* Clinical aspects of photodynamic therapy. *Sci Prog*, 2002, 85, p. 131-150.

114. MOLONEY F.J., COLLINS P. Randomized, double-blind, prospective study to compare topical 5-aminolaevulinic acid methylester with topical 5-aminolaevulinic acid photodynamic therapy for extensive scalp actinic keratosis. *Br J Dermatol*, 2007, 157, p. 87-91.
115. MALIK E., BERG C., MEYHOFER-MALIK A*., et al.* Fluorescence diagnosis of endometriosis using 5-aminolevulinic acid. *Surg Endosc*, 2000, 14, p. 452-455.
116. KELTY C.J., BROWN N.J., REED M.W*., et al.* The use of 5-aminolaevulinic acid as a photosensitiser in photodynamic therapy and photodiagnosis. *Photochem Photobiol Sci*, 2002, 1, p. 158-168.
117. SZEIMIES R.M., LANDTHALER M. Photodynamic therapy and fluorescence diagnosis of skin cancers. *Recent Results Cancer Res*, 2002, 160, p. 240-245.
118. STULBERG D.L., CRANDELL B., FAWCETT R.S. Diagnosis and treatment of basal cell and squamous cell carcinomas. *Am Fam Physician*, 2004, 70, p. 1481-1488.
119. STUMMER W., PICHLMEIER U., MEINEL T*., et al.* Fluorescence-guided surgery with 5-aminolevulinic acid for resection of malignant glioma: a randomised controlled multicentre phase III trial. *Lancet Oncol*, 2006, 7, p. 392-401.
120. CASAS A., BATLLE A. Aminolevulinic acid derivatives and liposome delivery as strategies for improving 5-aminolevulinic acid-mediated photodynamic therapy. *Curr Med Chem*, 2006, 13, p. 1157-1168.
121. FOTINOS N., CAMPO M.A., POPOWYCZ F*., et al.* 5-Aminolevulinic acid derivatives in photomedicine: Characteristics, application and perspectives. *Photochem Photobiol*, 2006, 82, p. 994-1015.
122. TAUB A.F. Photodynamic therapy in dermatology: history and horizons. *J Drugs Dermatol*, 2004, 3, p. S8-25.
123. BABILAS P., LANDTHALER M., SZEIMIES R.M. Photodynamic therapy in dermatology. *Eur J Dermatol*, 2006, 16, p. 340-348.
124. NESTOR M.S., GOLD M.H., KAUVAR A.N*., et al.* The use of photodynamic therapy in dermatology: results of a consensus conference. *J Drugs Dermatol*, 2006, 5, p. 140-154.
125. HILLEMANNS P., UNTCH M., PROVE F*., et al.* Photodynamic therapy of vulvar lichen sclerosus with 5-aminolevulinic acid. *Obstet Gynecol*, 1999, 93, p. 71-74.
126. FEHR M.K., HORNUNG R., SCHWARZ V.A*., et al.* Photodynamic therapy of vulvar intraepithelial neoplasia III using topically applied 5-aminolevulinic acid. *Gynecol Oncol*, 2001, 80, p. 62-66.
127. RASPAGLIESI F., FONTANELLI R., ROSSI G*., et al.* Photodynamic therapy using a methyl ester of 5-aminolevulinic acid in recurrent Paget's disease of the vulva: a pilot study. *Gynecol Oncol*, 2006, 103, p. 581-586.
128. LONING M., DIDDENS H., FRIEDRICH M*., et al.* [Fluorescence diagnosis and photodynamic therapy with 5-aminolevulinic acid induced protoporphyrin IX in gynecology: an overview]. *Zentralbl Gynakol*, 2006, 128, p. 311-317.
129. SABBAN F., COLLINET P., COSSON M*., et al.* [Fluorescence imaging technique: diagnostic and therapeutic interest in gynecology]. *J Gynecol Obstet Biol Reprod (Paris)*, 2004, 33, p. 734-738.
130. LONING M., DIDDENS H., KUPKER W*., et al.* Laparoscopic fluorescence detection of ovarian carcinoma metastases using 5-aminolevulinic acid-induced protoporphyrin IX. *Cancer*, 2004, 100, p. 1650-1656.
131. KRIEGMAIR M., ZAAK D., KNUECHEL R*., et al.* 5-Aminolevulinic acid-induced fluorescence endoscopy for the detection of lower urinary tract tumors. *Urol Int*, 1999, 63, p. 27-31.
132. KRIEGMAIR M., ZAAK D., KNUECHEL R*., et al.* Photodynamic cystoscopy for detection of bladder tumors. *Semin Laparosc Surg*, 1999, 6, p. 100-103.
133. CHATTERTON K., RAY E., O'BRIEN T.S. Fluorescence diagnosis of bladder cancer. *Br J Nurs*, 2006, 15, p. 595-597.

134. HUNGERHUBER E., STEPP H., KRIEGMAIR M.*, et al.* Seven years' experience with 5-aminolevulinic acid in detection of transitional cell carcinoma of the bladder. *Urology*, 2007, 69, p. 260-264.
135. ACKROYD R., BROWN N.J., DAVIS M.F.*, et al.* Photodynamic therapy for dysplastic Barrett's oesophagus: a prospective, double blind, randomised, placebo controlled trial. *Gut*, 2000, 47, p. 612-617.
136. HAGE M., SIERSEMA P.D., VAN DEKKEN H.*, et al.* 5-aminolevulinic acid photodynamic therapy versus argon plasma coagulation for ablation of Barrett's oesophagus: a randomised trial. *Gut*, 2004, 53, p. 785-790.
137. KELTY C.J., ACKROYD R., BROWN N.J.*, et al.* Endoscopic ablation of Barrett's oesophagus: a randomized-controlled trial of photodynamic therapy vs. argon plasma coagulation. *Aliment Pharmacol Ther*, 2004, 20, p. 1289-1296.
138. SMOLKA J., MATEASIK A., CUNDERLIKOVA B.*, et al.* In vivo fluorescence diagnostics and photodynamic therapy of gastrointestinal superficial polyps with aminolevulinic acid. A clinical and spectroscopic study. *Neoplasma*, 2006, 53, p. 418-423.
139. DOVER J.S., BHATIA A.C., STEWART B.*, et al.* Topical 5-aminolevulinic acid combined with intense pulsed light in the treatment of photoaging. *Arch Dermatol*, 2005, 141, p. 1247-1252.
140. ZAKHARY K., ELLIS D.A. Applications of aminolevulinic Acid-based photodynamic therapy in cosmetic facial plastic practices. *Facial Plast Surg*, 2005, 21, p. 110-116.
141. NOOTHETI P.K., GOLDMAN M.P. Aminolevulinic acid-photodynamic therapy for photorejuvenation. *Dermatol Clin*, 2007, 25, p. 35-45.
142. STENDER I.M., BECH-THOMSEN N., POULSEN T.*, et al.* Photodynamic therapy with topical delta-aminolevulinic acid delays UV photocarcinogenesis in hairless mice. *Photochem Photobiol*, 1997, 66, p. 493-496.
143. SHARFAEI S., VIAU G., LUI H.*, et al.* Systemic photodynamic therapy with aminolaevulinic acid delays the appearance of ultraviolet-induced skin tumours in mice. *Br J Dermatol*, 2001, 144, p. 1207-1214.
144. SHARFAEI S., JUZENAS P., MOAN J.*, et al.* Weekly topical application of methyl aminolevulinate followed by light exposure delays the appearance of UV-induced skin tumours in mice. *Arch Dermatol Res*, 2002, 294, p. 237-242.
145. LIU Y., VIAU G., BISSONNETTE R. Multiple large-surface photodynamic therapy sessions with topical or systemic aminolevulinic acid and blue light in UV-exposed hairless mice. *J Cutan Med Surg*, 2004, 8, p. 131-139.
146. SZEIMIES R.M., RADNY P., SEBASTIAN M.*, et al.* Photodynamic therapy with BF-200 ALA for the treatment of actinic keratosis: results of a prospective, randomized, double-blind, placebo-controlled phase III study. *Br J Dermatol*, 2010, p.
147. BERG K., ANHOLT H., BECH O.*, et al.* The influence of iron chelators on the accumulation of protoporphyrin IX in 5-aminolaevulinic acid-treated cells. *Br J Cancer*, 1996, 74, p. 688-697.
148. MACROBERT A.J., BOWN, S.G., PHILLIPS, D. . What are the ideal photoproperties for a sensitizer? *Photosensitizing Compounds: Their Chemistry, Biology and Clinical Use* / ed. by BOCK G., HARNETT, S. . Chichester: Wiley, 1989, p. 4–16.
149. BONNETT R., MARTINEZ G. Photobleaching of sensitisers used in photodynamic therapy. *Tetrahedron*, 2001, 57, p. 9513–9547.
150. JORI G. Photosensitized processes in vivo: proposed phototherapeutic applications. *Photochem Photobiol*, 1990, 52, p. 439-443.
151. STERNBERG E.D., DOLPHIN, D., BRUCKNER, C. . Porphyrin-based photosensitizers for use in photodynamic therapy. *Tetrahedron*, 1998, 54, p. 4151-4202.
152. KOCHEVAR I.E. Singlet oxygen signaling: from intimate to global. *Sci STKE*, 2004, 2004, p. pe7.
153. MOAN J., BERG K. The photodegradation of porphyrins in cells can be used to estimate the lifetime of singlet oxygen. *Photochem Photobiol*, 1991, 53, p. 549-553.

154. BONNETT R., MARTINEZ G. Photobleaching of compounds of the 5,10,15,20-Tetrakis(m-hydroxyphenyl)porphyrin Series (m-THPP, m-THPC, and m-THPBC). *Org Lett*, 2002, 4, p. 2013-2016.
155. MOAN J., STRECKYTE G., BAGDONAS S.*, et al.* Photobleaching of protoporphyrin IX in cells incubated with 5-aminolevulinic acid. *Int J Cancer*, 1997, 70, p. 90-97.
156. MANG T.S., DOUGHERTY T.J., POTTER W.R.*, et al.* Photobleaching of porphyrins used in photodynamic therapy and implications for therapy. *Photochem Photobiol*, 1987, 45, p. 501-506.
157. MOAN J. Effect of bleaching of porphyrin sensitizers during photodynamic therapy. *Cancer Lett*, 1986, 33, p. 45-53.
158. ROTOMSKIENE J., KAPOCIUTE R., ROTOMSKIS R.*, et al.* Light-induced transformations of hematoporphyrin diacetate and hematoporphyrin. *J Photochem Photobiol B*, 1988, 2, p. 373-379.
159. STRECKYTE G., ROTOMSKIS R. Phototransformations of porphyrins in aqueous and micellar media. *J Photochem Photobiol B*, 1993, 18, p. 259-263.
160. ROTOMSKIS R., BAGDONAS S., STRECKYTE G. Spectroscopic studies of photobleaching and photoproduct formation of porphyrins used in tumour therapy. *J Photochem Photobiol B*, 1996, 33, p. 61-67.
161. BAGDONAS S., MA L.W., IANI V.*, et al.* Phototransformations of 5-aminolevulinic acid-induced protoporphyrin IX in vitro: a spectroscopic study. *Photochem Photobiol*, 2000, 72, p. 186-192.
162. KRIEG M., WHITTEN D.G. Self-sensitized photo-oxidation of protoporphyrin IX and related porphyrins in erythrocyte ghosts and microemulsions: A novel photo-oxidation pathway involving singlet oxygen. *J Photochem*, 1984, 25, p. 235–252.
163. ERICSON M.B., GRAPENGIESSER S., GUDMUNDSON F.*, et al.* A spectroscopic study of the photobleaching of protoporphyrin IX in solution. *Lasers Med Sci*, 2003, 18, p. 56-62.
164. MOAN J., JUZENAS P., BAGDONAS S. *Degradation and transformation of photosensitisers during light exposure*. Trivandrum: Transworld Research Network, 2000, p. 121–132.
165. ROTOMSKIS R., BAGDONAS S., STRECKYTE G.*, et al.* Phototransformation of Sensitisers: 3. Implications for Clinical Dosimetry. *Lasers Med Sci*, 1998, 13, p. 271–278.
166. GEORGAKOUDI I., NICHOLS M.G., FOSTER T.H. The mechanism of Photofrin photobleaching and its consequences for photodynamic dosimetry. *Photochem Photobiol*, 1997, 65, p. 135-144.
167. GEORGAKOUDI I., FOSTER T.H. Singlet oxygen- versus nonsinglet oxygen-mediated mechanisms of sensitizer photobleaching and their effects on photodynamic dosimetry. *Photochem Photobiol*, 1998, 67, p. 612-625.
168. MOAN J. The photochemical yield of singlet oxygen from porphyrins in different states of aggregation. *Photochem Photobiol*, 1984, 39, p. 445–449.
169. BELITCHENKO I., MELNIKOVA V., BEZDETNAYA L.*, et al.* Characterization of photodegradation of meta-tetra(hydroxyphenyl)chlorin (mTHPC) in solution: biological consequences in human tumor cells. *Photochem Photobiol*, 1998, 67, p. 584-590.
170. GROSSWEINER L.I. Optical dosimetry in photodynamic therapy. *Lasers Surg Med*, 1986, 6, p. 462-466.
171. JONGEN A.J., STERENBORG H.J. Mathematical description of photobleaching in vivo describing the influence of tissue optics on measured fluorescence signals. *Phys Med Biol*, 1997, 42, p. 1701-1716.
172. OSTERLOH J., VICENTE M.G. Mechanisms of porphyrinoid localization in tumors. *Journal of Porphyrins and Phthalocyanines*, 2002, 6, p. 305-324.
173. GOMER C.J., LUNA M., FERRARIO A.*, et al.* Cellular targets and molecular responses associated with photodynamic therapy. *J Clin Laser Med Surg*, 1996, 14, p. 315-321.
174. MOOR A.C. Signaling pathways in cell death and survival after photodynamic therapy. *J Photochem Photobiol B*, 2000, 57, p. 1-13.

175. KESSEL D. Correlation between subcellular localization and photodynamic efficacy. *Journal of Porphyrins and Phthalocyanines*, 2004, 8, p. 1009-1014.
176. PAZOS M.C., NADER H.B. Effect of photodynamic therapy on the extracellular matrix and associated components. *Braz J Med Biol Res*, 2007, 40, p. 1025-1035.
177. ATLANTE A., MORENO G., PASSARELLA S*., et al.* Hematoporphyrin derivative (Photofrin II) photosensitization of isolated mitochondria: impairment of anion translocation. *Biochem Biophys Res Commun*, 1986, 141, p. 584-590.
178. HILF R., WARNE N.W., SMAIL D.B*., et al.* Photodynamic inactivation of selected intracellular enzymes by hematoporphyrin derivative and their relationship to tumor cell viability in vitro. *Cancer Lett*, 1984, 24, p. 165-172.
179. GIBSON S.L., HILF R. Photosensitization of mitochondrial cytochrome c oxidase by hematoporphyrin derivative and related porphyrins in vitro and in vivo. *Cancer Res*, 1983, 43, p. 4191-4197.
180. KROEMER G., ZAMZAMI N., SUSIN S.A. Mitochondrial control of apoptosis. *Immunol Today*, 1997, 18, p. 44-51.
181. HIRSCH T., DECAUDIN D., SUSIN S.A*., et al.* PK11195, a ligand of the mitochondrial benzodiazepine receptor, facilitates the induction of apoptosis and reverses Bcl-2-mediated cytoprotection. *Exp Cell Res*, 1998, 241, p. 426-434.
182. VERMA A., FACCHINA S.L., HIRSCH D.J*., et al.* Photodynamic tumor therapy: mitochondrial benzodiazepine receptors as a therapeutic target. *Mol Med*, 1998, 4, p. 40-45.
183. PERLIN D.S., MURANT R.S., GIBSON S.L*., et al.* Effects of photosensitization by hematoporphyrin derivative on mitochondrial adenosine triphosphatase-mediated proton transport and membrane integrity of R3230AC mammary adenocarcinoma. *Cancer Res*, 1985, 45, p. 653-658.
184. KESSEL D., LUO Y. Photodynamic therapy: a mitochondrial inducer of apoptosis. *Cell Death Differ*, 1999, 6, p. 28-35.
185. BERG K., MOAN J. Lysosomes as photochemical targets. *Int J Cancer*, 1994, 59, p. 814-822.
186. OKADA C.Y., RECHSTEINER M. Introduction of macromolecules into cultured mammalian cells by osmotic lysis of pinocytic vesicles. *Cell*, 1982, 29, p. 33-41.
187. MOAN J., BERG K., ANHOLT H*., et al.* Sulfonated aluminium phthalocyanines as sensitizers for photochemotherapy. Effects of small light doses on localization, dye fluorescence and photosensitivity in V79 cells. *Int J Cancer*, 1994, 58, p. 865-870.
188. BERG K., SELBO P.K., PRASMICKAITE L*., et al.* Photochemical internalization: a novel technology for delivery of macromolecules into cytosol. *Cancer Res*, 1999, 59, p. 1180-1183.
189. DIETZE A., SELBO P.K., PRASMICKAITE L*., et al.* Photochemical internalization (PCI): a new modality for light activation of endocytosed therapeuticals. *J Environ Pathol Toxicol Oncol*, 2006, 25, p. 521-536.
190. PENG Q., FARRANTS G.W., MADSLIEN K*., et al.* Subcellular localization, redistribution and photobleaching of sulfonated aluminum phthalocyanines in a human melanoma cell line. *Int J Cancer*, 1991, 49, p. 290-295.
191. KESSEL D. Chemical and biochemical determinants of porphyrin localization. *Porphyrin Localization and Treatment Tumors* / ed. by DOIRON D.R., GOMER, C.J. New York: Alan R. Liss, 1984 p. 405–418.
192. JUZENIENE A., PENG Q., MOAN J. Milestones in the development of photodynamic therapy and fluorescence diagnosis. *Photochem Photobiol Sci*, 2007, 6, p. 1234-1245.
193. DUBBELMAN T.M., PRINSZE, C., PENNING, L.C., VAN STEVENINCK, J. New York: Marcel Decker, 1992, p. 37-46.
194. UZDENSKY A., KOLPAKOVA E., JUZENIENE A*., et al.* The effect of sub-lethal ALA-PDT on the cytoskeleton and adhesion of cultured human cancer cells. *Biochim Biophys Acta*, 2005, 1722, p. 43-50.

195. UZDENSKY A.B., JUZENIENE A., KOLPAKOVA E.*, et al.* Photosensitization with protoporphyrin IX inhibits attachment of cancer cells to a substratum. *Biochem Biophys Res Commun*, 2004, 322, p. 452-457.
196. WOODS J.A., TRAYNOR N.J., BRANCALEON L.*, et al.* The effect of photofrin on DNA strand breaks and base oxidation in HaCaT keratinocytes: a comet assay study. *Photochem Photobiol*, 2004, 79, p. 105-113.
197. HAYLETT A.K., WARD T.H., MOORE J.V. DNA damage and repair in Gorlin syndrome and normal fibroblasts after aminolevulinic acid photodynamic therapy: a comet assay study. *Photochem Photobiol*, 2003, 78, p. 337-341.
198. EVENSEN J.F., MOAN J. Photodynamic action and chromosomal damage: a comparison of haematoporphyrin derivative (HpD) and light with X-irradiation. *Br J Cancer*, 1982, 45, p. 456-465.
199. KVAM E., STOKKE T. Sites of photodynamically induced DNA repair in human cells. *Photochem Photobiol*, 1994, 59, p. 437-440.
200. GUTTER B., SPECK W.T., ROSENKRANZ H.S. The photodynamic modification of DNA by hematoporphyrin. *Biochim Biophys Acta*, 1977, 475, p. 307-314.
201. GOMER C.J., RUCKER N., FERRARIO A.*, et al.* Expression of potentially lethal damage in Chinese hamster cells exposed to hematoporphyrin derivative photodynamic therapy. *Cancer Res*, 1986, 46, p. 3348-3352.
202. MOAN J., WAKSVIK H., CHRISTENSEN T. DNA single-strand breaks and sister chromatid exchanges induced by treatment with hematoporphyrin and light or by x-rays in human NHIK 3025 cells. *Cancer Res*, 1980, 40, p. 2915-2918.
203. EVANS H.H., HORNG M.F., RICANATI M.*, et al.* Mutagenicity of photodynamic therapy as compared to UVC and ionizing radiation in human and murine lymphoblast cell lines. *Photochem Photobiol*, 1997, 66, p. 690-696.
204. MCNAIR F.I., MARPLES B., WEST C.M.*, et al.* A comet assay of DNA damage and repair in K562 cells after photodynamic therapy using haematoporphyrin derivative, methylene blue and meso-tetrahydroxyphenylchlorin. *Br J Cancer*, 1997, 75, p. 1721-1729.
205. BALL D.J., MAYHEW S., WOOD S.R.*, et al.* A comparative study of the cellular uptake and photodynamic efficacy of three novel zinc phthalocyanines of differing charge. *Photochem Photobiol*, 1999, 69, p. 390-396.
206. BERG K., MADSLIEN K., BOMMER J.C.*, et al.* Light induced relocalization of sulfonated meso-tetraphenylporphines in NHIK 3025 cells and effects of dose fractionation. *Photochem Photobiol*, 1991, 53, p. 203-210.
207. KESSEL D. Relocalization of cationic porphyrins during photodynamic therapy. *Photochem Photobiol Sci*, 2002, 1, p. 837-840.
208. RUCK A., BECK G., BACHOR R.*, et al.* Dynamic fluorescence changes during photodynamic therapy in vivo and in vitro of hydrophilic A1(III) phthalocyanine tetrasulphonate and lipophilic Zn(II) phthalocyanine administered in liposomes. *J Photochem Photobiol B*, 1996, 36, p. 127-133.
209. COLLAUD S., JUZENIENE A., MOAN J.*, et al.* On the selectivity of 5-aminolevulinic acid-induced protoporphyrin IX formation. *Curr Med Chem Anticancer Agents*, 2004, 4, p. 301-316.
210. HAMBLIN M.R., NEWMAN E.L. On the mechanism of the tumour-localising effect in photodynamic therapy. *J Photochem Photobiol B*, 1994, 23, p. 3-8.
211. JORI G. Tumour photosensitizers: approaches to enhance the selectivity and efficiency of photodynamic therapy. *J Photochem Photobiol B*, 1996, 36, p. 87-93.
212. MOAN J., VAN DEN AKKER J.T., JUZENAS P.*, et al.* On the basis for tumor selectivity in the 5-aminolevulinic acid-induced synthesis of protoporphyrin IX. *J Porphyrins Phthalocyanines*, 2001, 5, p. 170–176.
213. MOAN J., CUNDERLIKOVA B., JUZENIENE A.*, et al. Tumour selectivity of Photodynamic Therapy*. Ravnetrykk, Tromsø: Ø. S. Bruland and T. Flægstad, 2003, p. 208–211.

214. POTTIER R., KENNEDY J.C. The possible role of ionic species in selective biodistribution of photochemotherapeutic agents toward neoplastic tissue. *J Photochem Photobiol B*, 1990, 8, p. 1-16.
215. GERWECK L.E., SEETHARAMAN K. Cellular pH gradient in tumor versus normal tissue: potential exploitation for the treatment of cancer. *Cancer Res*, 1996, 56, p. 1194-1198.
216. KORBELIK M., KROSL G., OLIVE P.L.*, et al.* Distribution of Photofrin between tumour cells and tumour associated macrophages. *Br J Cancer*, 1991, 64, p. 508-512.
217. MAZIERE J.C., MORLIERE P., SANTUS R. The role of the low density lipoprotein receptor pathway in the delivery of lipophilic photosensitizers in the photodynamic therapy of tumours. *J Photochem Photobiol B*, 1991, 8, p. 351-360.
218. VAUPEL P., KALLINOWSKI F., OKUNIEFF P. Blood flow, oxygen and nutrient supply, and metabolic microenvironment of human tumors: a review. *Cancer Res*, 1989, 49, p. 6449-6465.
219. JAIN R.K. Transport of molecules in the tumor interstitium: a review. *Cancer Res*, 1987, 47, p. 3039-3051.
220. SUBARSKY P., HILL R.P. The hypoxic tumour microenvironment and metastatic progression. *Clin Exp Metastasis*, 2003, 20, p. 237-250.
221. REED M.W., MULLINS A.P., ANDERSON G.L.*, et al.* The effect of photodynamic therapy on tumor oxygenation. *Surgery*, 1989, 106, p. 94-99.
222. TROMBERG B.J., ORENSTEIN A., KIMEL S.*, et al.* In vivo tumor oxygen tension measurements for the evaluation of the efficiency of photodynamic therapy. *Photochem Photobiol*, 1990, 52, p. 375-385.
223. FINGAR V.H. Vascular effects of photodynamic therapy. *J Clin Laser Med Surg*, 1996, 14, p. 323-328.
224. SITNIK T.M., HAMPTON J.A., HENDERSON B.W. Reduction of tumour oxygenation during and after photodynamic therapy in vivo: effects of fluence rate. *Br J Cancer*, 1998, 77, p. 1386-1394.
225. BUSCH T.M. Local physiological changes during photodynamic therapy. *Lasers Surg Med*, 2006, 38, p. 494-499.
226. FUKUDA H., CASAS A., BATLLE A. Use of ALA and ALA derivatives for optimizing ALA-based photodynamic therapy: a review of our experience. *J Environ Pathol Toxicol Oncol*, 2006, 25, p. 127-143.
227. LAHAV M., EPSTEIN O., SCHOENFELD N.*, et al.* Increased porphobilinogen deaminase activity in patients with malignant lymphoproliferative diseases. A helpful diagnostic test. *JAMA*, 1987, 257, p. 39-42.
228. KONDO M., HIROTA N., TAKAOKA T.*, et al.* Heme-biosynthetic enzyme activities and porphyrin accumulation in normal liver and hepatoma cell lines of rat. *Cell Biol Toxicol*, 1993, 9, p. 95-105.
229. GIBSON S.L., CUPRIKS D.J., HAVENS J.J.*, et al.* A regulatory role for porphobilinogen deaminase (PBGD) in delta-aminolaevulinic acid (delta-ALA)-induced photosensitization? *Br J Cancer*, 1998, 77, p. 235-242.
230. VAN HILLEGERSBERG R., VAN DEN BERG J.W., KORT W.J.*, et al.* Selective accumulation of endogenously produced porphyrins in a liver metastasis model in rats. *Gastroenterology*, 1992, 103, p. 647-651.
231. POURZAND C., REELFS O., KVAM E.*, et al.* The iron regulatory protein can determine the effectiveness of 5-aminolevulinic acid in inducing protoporphyrin IX in human primary skin fibroblasts. *J Invest Dermatol*, 1999, 112, p. 419-425.
232. BECH O., PHILLIPS D., MOAN J.*, et al.* A hydroxypyridinone (CP94) enhances protoporphyrin IX formation in 5-aminolaevulinic acid treated cells. *J Photochem Photobiol B*, 1997, 41, p. 136-144.

233. CHANG S.C., MACROBERT A.J., PORTER J.B*., et al.* The efficacy of an iron chelator (CP94) in increasing cellular protoporphyrin IX following intravesical 5-aminolaevulinic acid administration: an in vivo study. *J Photochem Photobiol B*, 1997, 38, p. 114-122.
234. CURNOW A., MCILROY B.W., POSTLE-HACON M.J*., et al.* Enhancement of 5-aminolaevulinic acid-induced photodynamic therapy in normal rat colon using hydroxypyridinone iron-chelating agents. *Br J Cancer*, 1998, 78, p. 1278-1282.
235. XIE W., MCCAHON P., JAKOBSEN K*., et al.* Evaluation of the ability of digital infrared imaging to detect vascular changes in experimental animal tumours. *Int J Cancer*, 2004, 108, p. 790-794.
236. SONG C., APPLEYARD V., MURRAY K*., et al.* Thermographic assessment of tumor growth in mouse xenografts. *Int J Cancer*, 2007, 121, p. 1055-1058.
237. DIETEL W., BOLSEN K., DICKSON E*., et al.* Formation of water-soluble porphyrins and protoporphyrin IX in 5-aminolevulinic-acid-incubated carcinoma cells. *J Photochem Photobiol B*, 1996, 33, p. 225-231.
238. JUZENAS P., SORENSEN R., IANI V*., et al.* Uptake of topically applied 5-aminolevulinic acid and production of protoporphyrin IX in normal mouse skin: dependence on skin temperature. *Photochem Photobiol*, 1999, 69, p. 478-481.
239. MOAN J., BERG K., GADMAR O.B*., et al.* The temperature dependence of protoporphyrin IX production in cells and tissues. *Photochem Photobiol*, 1999, 70, p. 669-673.
240. BOUWSTRA J.A., HONEYWELL-NGUYEN P.L. Skin structure and mode of action of vesicles. *Adv Drug Deliv Rev*, 2002, 54 Suppl 1, p. S41-55.
241. FUCHS C., RIESENBERG R., SIEGERT J*., et al.* H-dependent formation of 5-aminolaevulinic acid-induced protoporphyrin IX in fibrosarcoma cells. *J Photochem Photobiol B*, 1997, 40, p. 49-54.
242. WYLD L., REED M.W., BROWN N.J. The influence of hypoxia and pH on aminolaevulinic acid-induced photodynamic therapy in bladder cancer cells in vitro. *Br J Cancer*, 1998, 77, p. 1621-1627.
243. WYSS-DESSERICH M.T., SUN C.H., WYSS P*., et al.* Accumulation of 5-aminolevulinic acid-induced protoporphyrin IX in normal and neoplastic human endometrial epithelial cells. *Biochem Biophys Res Commun*, 1996, 224, p. 819-824.
244. ORTEL B., CHEN N., BRISSETTE J*., et al.* Differentiation-specific increase in ALA-induced protoporphyrin IX accumulation in primary mouse keratinocytes. *Br J Cancer*, 1998, 77, p. 1744-1751.
245. ORTEL B., SHARLIN D., O'DONNELL D*., et al.* Differentiation enhances aminolevulinic acid-dependent photodynamic treatment of LNCaP prostate cancer cells. *Br J Cancer*, 2002, 87, p. 1321-1327.
246. ICKOWICZ SCHWARTZ D., GOZLAN Y., GREENBAUM L*., et al.* Differentiation-dependent photodynamic therapy regulated by porphobilinogen deaminase in B16 melanoma. *Br J Cancer*, 2004, 90, p. 1833-1841.
247. GIBSON S.L., NGUYEN M.L., HAVENS J.J*., et al.* Relationship of delta-aminolevulinic acid-induced protoporphyrin IX levels to mitochondrial content in neoplastic cells in vitro. *Biochem Biophys Res Commun*, 1999, 265, p. 315-321.
248. PLAETZER K., KRAMMER B., BERLANDA J*., et al.* Photophysics and photochemistry of photodynamic therapy: fundamental aspects. *Lasers Med Sci*, 2009, 24, p. 259-268.
249. PRASAD P.N. *Introduction to biophotonics*. Hoboken: Wiley, 2003.
250. NIEMZ M.H. *Laser-tissue interactions. Fundamentals and applications.* . Berlin Heidelberg New York: Springer, 2004.
251. NIEMZ M.H. *Laser-tissue interactions*. Berlin: Springer, 1996.
252. DOLMANS D.E., FUKUMURA D., JAIN R.K. Photodynamic therapy for cancer. *Nat Rev Cancer*, 2003, 3, p. 380-387.
253. SVAASAND L.O. Optical dosimetry for direct and interstitial photoradiation therapy of malignant tumors. *Prog Clin Biol Res*, 1984, 170, p. 91-114.

254. POTTER W.R., MANG, T.S. Photofrin II levels by in vivo fluorescence photometry. *Porphyrin Localization and Treatment of Tumors* / ed. by DOIRON D.R., GOMER, C.J. New York: Alan R. Liss, 1984, p. 177–186.
255. DOUGHERTY T.J. Photochemistry in the treatment of cancer. *Adv Photochem*, 1992, 17, p. 275-311.
256. ANDERSON R.R., PARRISH J.A. The optics of human skin. *J Invest Dermatol*, 1981, 77, p. 13-19.
257. NIELSEN K.P., JUZENIENE A., JUZENAS P.*, et al.* Choice of optimal wavelength for PDT: the significance of oxygen depletion. *Photochem Photobiol*, 2005, 81, p. 1190-1194.
258. WANG H.W., ZHU T.C., PUTT M.E.*, et al.* Broadband reflectance measurements of light penetration, blood oxygenation, hemoglobin concentration, and drug concentration in human intraperitoneal tissues before and after photodynamic therapy. *J Biomed Opt*, 2005, 10, p. 14004.
259. WILSON B.C., JEEVES W.P., LOWE D.M. In vivo and post mortem measurements of the attenuation spectra of light in mammalian tissues. *Photochem Photobiol*, 1985, 42, p. 153-162.
260. SVAASAND L.O. Photodynamic and photohyperthermic response of malignant tumors. *Med Phys*, 1985, 12, p. 455-461.
261. MICHAILOV N., PEEVA M., ANGELOV I.*, et al.* Fluence rate effects on photodynamic therapy of B16 pigmented melanoma. *J Photochem Photobiol B*, 1997, 37, p. 154-157.
262. BUSCH T.M., WILEYTO E.P., EMANUELE M.J.*, et al.* Photodynamic therapy creates fluence rate-dependent gradients in the intratumoral spatial distribution of oxygen. *Cancer Res*, 2002, 62, p. 7273-7279.
263. BABILAS P., SCHACHT V., LIEBSCH G.*, et al.* Effects of light fractionation and different fluence rates on photodynamic therapy with 5-aminolaevulinic acid in vivo. *Br J Cancer*, 2003, 88, p. 1462-1469.
264. HENDERSON B.W., BUSCH T.M., VAUGHAN L.A.*, et al.* Photofrin photodynamic therapy can significantly deplete or preserve oxygenation in human basal cell carcinomas during treatment, depending on fluence rate. *Cancer Res*, 2000, 60, p. 525-529.
265. HENDERSON B.W., BUSCH T.M., SNYDER J.W. Fluence rate as a modulator of PDT mechanisms. *Lasers Surg Med*, 2006, 38, p. 489-493.
266. BRANCALEON L., MOSELEY H. Laser and non-laser light sources for photodynamic therapy. *Lasers Med Sci*, 2002, 17, p. 173-186.
267. MANG T.S. Lasers and light sources for PDT: past, present and future. *Photodiagn Photodyn Ther*, 2004, 1, p. 43-48.
268. MCCAUGHAN L. Lasers in photodynamic therapy. *Nurs Clin North Am*, 1990, 25, p. 725-738.
269. STERENBORG H.J., VAN GEMERT M.J. Photodynamic therapy with pulsed light sources: a theoretical analysis. *Phys Med Biol*, 1996, 41, p. 835-849.
270. FERRARIO A., RUCKER N., RYTER S.W.*, et al.* Direct comparison of in-vitro and in-vivo Photofrin-II mediated photosensitization using a pulsed KTP pumped dye laser and a continuous wave argon ion pumped dye laser. *Lasers Surg Med*, 1991, 11, p. 404-410.
271. AL-WATBAN F.A., ZHANG X.Y. The comparison of effects between pulsed and CW lasers on wound healing. *J Clin Laser Med Surg*, 2004, 22, p. 15-18.
272. KAWAUCHI S., MORIMOTO Y., SATO S.*, et al.* Differences between cytotoxicity in photodynamic therapy using a pulsed laser and a continuous wave laser: study of oxygen consumption and photobleaching. *Lasers Med Sci*, 2004, 18, p. 179-183.
273. STRASSWIMMER J., GRANDE D.J. Do pulsed lasers produce an effective photodynamic therapy response? *Lasers Surg Med*, 2006, 38, p. 22-25.
274. CLARK C., BRYDEN A., DAWE R.*, et al.* Topical 5-aminolaevulinic acid photodynamic therapy for cutaneous lesions: outcome and comparison of light sources. *Photodermatol Photoimmunol Photomed*, 2003, 19, p. 134-141.

275. PANJEHPOUR M., OVERHOLT B.F., HAYDEK J.M. Light sources and delivery devices for photodynamic therapy in the gastrointestinal tract. *Gastrointest Endosc Clin N Am*, 2000, 10, p. 513-532.
276. BROWN S.B. The role of light in the treatment of non-melanoma skin cancer using methyl aminolevulinate. *J Dermatolog Treat*, 2003, 14 Suppl 3, p. 11-14.
277. HAMZAVI I., LUI H. Using light in dermatology: an update on lasers, ultraviolet phototherapy, and photodynamic therapy. *Dermatol Clin*, 2005, 23, p. 199-207.
278. MORTON C.A., BROWN S.B., COLLINS S*., et al.* Guidelines for topical photodynamic therapy: report of a workshop of the British Photodermatology Group. *Br J Dermatol*, 2002, 146, p. 552-567.
279. JUZENIENE A., JUZENAS P., MA L.W*., et al.* Effectiveness of different light sources for 5-aminolevulinic acid photodynamic therapy. *Lasers Med Sci*, 2004, 19, p. 139-149.
280. CLARK C., DAWE R.S., MOSELEY H*., et al.* The characteristics of erythema induced by topical 5-aminolaevulinic acid photodynamic therapy. *Photodermatol Photoimmunol Photomed*, 2004, 20, p. 105-107.
281. SOLER A.M., ANGELL-PETERSEN E., WARLOE T*., et al.* Photodynamic therapy of superficial basal cell carcinoma with 5-aminolevulinic acid with dimethylsulfoxide and ethylendiaminetetraacetic acid: a comparison of two light sources. *Photochem Photobiol*, 2000, 71, p. 724-729.
282. GRUNER S., VOLK H.D., NOACK F*., et al.* Inhibition of HLA-DR antigen expression and of the allogeneic mixed leukocyte reaction by photochemical treatment. *Tissue Antigens*, 1986, 27, p. 147-154.
283. MOSELEY H., ALLEN J.W., IBBOTSON S*., et al.* Ambulatory photodynamic therapy: a new concept in delivering photodynamic therapy. *Br J Dermatol*, 2006, 154, p. 747-750.
284. KESSEL D., LUGUYA R., VICENTE M.G. Localization and photodynamic efficacy of two cationic porphyrins varying in charge distributions. *Photochem Photobiol*, 2003, 78, p. 431-435.
285. FEOFANOV A., SHARONOV G., GRICHINE A*., et al.* Comparative study of photodynamic properties of 13,15-N-cycloimide derivatives of chlorin p6. *Photochem Photobiol*, 2004, 79, p. 172-188.
286. TIJERINA M., KOPECKOVA P., KOPECEK J. Mechanisms of cytotoxicity in human ovarian carcinoma cells exposed to free Mce6 or HPMA copolymer-Mce6 conjugates. *Photochem Photobiol*, 2003, 77, p. 645-652.
287. NOODT B.B., BERG K., STOKKE T*., et al.* Different apoptotic pathways are induced from various intracellular sites by tetraphenylporphyrins and light. *Br J Cancer*, 1999, 79, p. 72-81.
288. PENG Q., MOAN J., NESLAND J.M. Correlation of subcellular and intratumoral photosensitizer localization with ultrastructural features after photodynamic therapy. *Ultrastruct Pathol*, 1996, 20, p. 109-129.
289. KESSEL D., CONLEY M., VICENTE M.G*., et al.* Studies on the subcellular localization of the porphycene CPO. *Photochem Photobiol*, 2005, 81, p. 569-572.
290. MARCHAL S., FRANCOIS A., DUMAS D*., et al.* Relationship between subcellular localisation of Foscan and caspase activation in photosensitised MCF-7 cells. *Br J Cancer*, 2007, 96, p. 944-951.
291. OLEINICK N.L., MORRIS R.L., BELICHENKO I. The role of apoptosis in response to photodynamic therapy: what, where, why, and how. *Photochem Photobiol Sci*, 2002, 1, p. 1-21.
292. GRANVILLE D.J., CARTHY C.M., HUNT D.W*., et al.* Apoptosis: molecular aspects of cell death and disease. *Lab Invest*, 1998, 78, p. 893-913.
293. LUO Y., KESSEL D. Initiation of apoptosis versus necrosis by photodynamic therapy with chloroaluminum phthalocyanine. *Photochem Photobiol*, 1997, 66, p. 479-483.
294. TSAI T., HONG R.L., TSAI J.C*., et al.* Effect of 5-aminolevulinic acid-mediated photodynamic therapy on MCF-7 and MCF-7/ADR cells. *Lasers Surg Med*, 2004, 34, p. 62-72.

295. PLAETZER K., KIESSLICH T., KRAMMER B.*, et al.* Characterization of the cell death modes and the associated changes in cellular energy supply in response to AlPcS4-PDT. *Photochem Photobiol Sci*, 2002, 1, p. 172-177.
296. JIANG H., GRANVILLE D.J., NORTH J.R.*, et al.* Selective action of the photosensitizer QLT0074 on activated human T lymphocytes. *Photochem Photobiol*, 2002, 76, p. 224-231.
297. ALI S.M., OLIVO M. Bio-distribution and subcellular localization of Hypericin and its role in PDT induced apoptosis in cancer cells. *Int J Oncol*, 2002, 21, p. 531-540.
298. WYLD L., REED M.W., BROWN N.J. Differential cell death response to photodynamic therapy is dependent on dose and cell type. *Br J Cancer*, 2001, 84, p. 1384-1386.
299. KAMUHABWA A.R., AGOSTINIS P.M., D'HALLEWIN M.A.*, et al.* Cellular photodestruction induced by hypericin in AY-27 rat bladder carcinoma cells. *Photochem Photobiol*, 2001, 74, p. 126-132.
300. LEIST M., NICOTERA P. The shape of cell death. *Biochem Biophys Res Commun*, 1997, 236, p. 1-9.
301. CINCOTTA L., FOLEY J.W., MACEACHERN T.*, et al.* Novel photodynamic effects of a benzophenothiazine on two different murine sarcomas. *Cancer Res*, 1994, 54, p. 1249-1258.
302. CHAN W.S., BRASSEUR N., LA MADELEINE C.*, et al.* Evidence for different mechanisms of EMT-6 tumor necrosis by photodynamic therapy with disulfonated aluminum phthalocyanine or photofrin: tumor cell survival and blood flow. *Anticancer Res*, 1996, 16, p. 1887-1892.
303. KORBELIK M., KROSL G. Cellular levels of photosensitisers in tumours: the role of proximity to the blood supply. *Br J Cancer*, 1994, 70, p. 604-610.
304. ZILBERSTEIN J., BROMBERG A., FRANTZ A.*, et al.* Light-dependent oxygen consumption in bacteriochlorophyll-serine-treated melanoma tumors: on-line determination using a tissue-inserted oxygen microsensor. *Photochem Photobiol*, 1997, 65, p. 1012-1019.
305. FOSTER T.H., MURANT R.S., BRYANT R.G.*, et al.* Oxygen consumption and diffusion effects in photodynamic therapy. *Radiat Res*, 1991, 126, p. 296-303.
306. VAN GEEL I.P., OPPELAAR H., MARIJNISSEN J.P.*, et al.* Influence of fractionation and fluence rate in photodynamic therapy with Photofrin or mTHPC. *Radiat Res*, 1996, 145, p. 602-609.
307. CHIN W., LAU W., LAY S.L.*, et al.* Photodynamic-induced vascular damage of the chick chorioallantoic membrane model using perylenequinones. *Int J Oncol*, 2004, 25, p. 887-891.
308. KRAMMER B. Vascular effects of photodynamic therapy. *Anticancer Res*, 2001, 21, p. 4271-4277.
309. CHEN Q., CHEN H., HETZEL F.W. Tumor oxygenation changes post-photodynamic therapy. *Photochem Photobiol*, 1996, 63, p. 128-131.
310. FINGAR V.H., WIEMAN T.J., HAYDON P.S. The effects of thrombocytopenia on vessel stasis and macromolecular leakage after photodynamic therapy using photofrin. *Photochem Photobiol*, 1997, 66, p. 513-517.
311. FINGAR V.H., WIEMAN T.J., KARAVOLOS P.S.*, et al.* The effects of photodynamic therapy using differently substituted zinc phthalocyanines on vessel constriction, vessel leakage and tumor response. *Photochem Photobiol*, 1993, 58, p. 251-258.
312. MCMAHON K.S., WIEMAN T.J., MOORE P.H.*, et al.* Effects of photodynamic therapy using mono-L-aspartyl chlorin e6 on vessel constriction, vessel leakage, and tumor response. *Cancer Res*, 1994, 54, p. 5374-5379.
313. GILISSEN M.J., VAN DE MERBEL-DE WIT L.E., STAR W.M.*, et al.* Effect of photodynamic therapy on the endothelium-dependent relaxation of isolated rat aortas. *Cancer Res*, 1993, 53, p. 2548-2552.
314. REEVES K.J., REED M.W., BROWN N.J. Is nitric oxide important in photodynamic therapy? *J Photochem Photobiol B*, 2009, 95, p. 141-147.
315. TABER S.W., WIEMAN T.J., FINGAR V.H. The effects of aspirin on microvasculature after photodynamic therapy. *Photochem Photobiol*, 1993, 57, p. 856-861.

316. FINGAR V.H., TABER S.W., HAYDON P.S*., et al.* Vascular damage after photodynamic therapy of solid tumors: a view and comparison of effect in pre-clinical and clinical models at the University of Louisville. *In Vivo*, 2000, 14, p. 93-100.
317. BUSCH T.M., XING X., YU G*., et al.* Fluence rate-dependent intratumor heterogeneity in physiologic and cytotoxic responses to Photofrin photodynamic therapy. *Photochem Photobiol Sci*, 2009, 8, p. 1683-1693.
318. WANG H.W., PUTT M.E., EMANUELE M.J*., et al.* Treatment-induced changes in tumor oxygenation predict photodynamic therapy outcome. *Cancer Res*, 2004, 64, p. 7553-7561.
319. DAVIDS L.M., KLEEMANN B., KACEROVSKA D*., et al.* Hypericin phototoxicity induces different modes of cell death in melanoma and human skin cells. *J Photochem Photobiol B*, 2008, 91, p. 67-76.
320. CASTANO A.P., DEMIDOVA T.N., HAMBLIN M.R. Mechanisms in photodynamic therapy: part two – cellular signalling, cell metabolism and modes of cell death. *Photodiag Photodyn Ther*, 2005, p. 1–23.
321. MILLER J.D., BARON E.D., SCULL H*., et al.* Photodynamic therapy with the phthalocyanine photosensitizer Pc 4: the case experience with preclinical mechanistic and early clinical-translational studies. *Toxicol Appl Pharmacol*, 2007, 224, p. 290-299.
322. LOCKSHIN R.A., ZAKERI Z. Programmed cell death and apoptosis: origins of the theory. *Nat Rev Mol Cell Biol*, 2001, 2, p. 545-550.
323. LOCKSHIN R.A., ZAKERI Z. Apoptosis, autophagy, and more. *Int J Biochem Cell Biol*, 2004, 36, p. 2405-2419.
324. SUN Y., PENG Z.-L. Programmed cell death and cancer. *Postgrad Med J*, 2009, 85, p. 134-140.
325. KERR J.F., WYLLIE A.H., CURRIE A.R. Apoptosis: a basic biological phenomenon with wide-ranging implications in tissue kinetics. *Br J Cancer*, 1972, 26, p. 239-257.
326. HENGARTNER M.O. The biochemistry of apoptosis. *Nature*, 2000, 407, p. 770-776.
327. GREEN D.R., EVAN G.I. A matter of life and death. *Cancer Cell*, 2002, 1, p. 19-30.
328. KRIESER R.J., WHITE K. Engulfment mechanism of apoptotic cells. *Curr Opin Cell Biol*, 2002, 14, p. 734-738.
329. FADOK V.A., BRATTON D.L., ROSE D.M*., et al.* A receptor for phosphatidylserine-specific clearance of apoptotic cells. *Nature*, 2000, 405, p. 85-90.
330. LIU X., KIM C.N., YANG J*., et al.* Induction of apoptotic program in cell-free extracts: requirement for dATP and cytochrome c. *Cell*, 1996, 86, p. 147-157.
331. LAUBER K., APPEL H.A., SCHLOSSER S.F*., et al.* The adapter protein apoptotic protease-activating factor-1 (Apaf-1) is proteolytically processed during apoptosis. *J Biol Chem*, 2001, 276, p. 29772-29781.
332. ADAMS J.M., CORY S. Apoptosomes: engines for caspase activation. *Curr Opin Cell Biol*, 2002, 14, p. 715-720.
333. IGNEY F.H., KRAMMER P.H. Death and anti-death: tumour resistance to apoptosis. *Nat Rev Cancer*, 2002, 2, p. 277-288.
334. JIN Z., EL-DEIRY W.S. Overview of cell death signaling pathways. *Cancer Biol Ther*, 2005, 4, p. 139-163.
335. AHMAD N., GUPTA S., FEYES D.K*., et al.* Involvement of Fas (APO-1/CD-95) during photodynamic-therapy-mediated apoptosis in human epidermoid carcinoma A431 cells. *J Invest Dermatol*, 2000, 115, p. 1041-1046.
336. ALI S.M., CHEE S.K., YUEN G.Y*., et al.* Photodynamic therapy induced Fas-mediated apoptosis in human carcinoma cells. *Int J Mol Med*, 2002, 9, p. 257-270.
337. YOKOTA T., IKEDA H., INOKUCHI T*., et al.* Enhanced cell death in NR-S1 tumor by photodynamic therapy: possible involvement of Fas and Fas ligand system. *Lasers Surg Med*, 2000, 26, p. 449-460.
338. ZHUANG S., DEMIRS J.T., KOCHEVAR I.E. p38 mitogen-activated protein kinase mediates bid cleavage, mitochondrial dysfunction, and caspase-3 activation during apoptosis induced by singlet oxygen but not by hydrogen peroxide. *J Biol Chem*, 2000, 275, p. 25939-25948.

339. LI H., ZHU H., XU C.J*., et al.* Cleavage of BID by caspase 8 mediates the mitochondrial damage in the Fas pathway of apoptosis. *Cell*, 1998, 94, p. 491-501.
340. DESAGHER S., OSEN-SAND A., NICHOLS A*., et al.* Bid-induced conformational change of Bax is responsible for mitochondrial cytochrome c release during apoptosis. *J Cell Biol*, 1999, 144, p. 891-901.
341. CORY S., ADAMS J.M. The Bcl2 family: regulators of the cellular life-or-death switch. *Nat Rev Cancer*, 2002, 2, p. 647-656.
342. ZHUANG S., LYNCH M.C., KOCHEVAR I.E. Caspase-8 mediates caspase-3 activation and cytochrome c release during singlet oxygen-induced apoptosis of HL-60 cells. *Exp Cell Res*, 1999, 250, p. 203-212.
343. ZHUANG S., KOCHEVAR I.E. Ultraviolet A radiation induces rapid apoptosis of human leukemia cells by Fas ligand-independent activation of the Fas death pathways. *Photochem Photobiol*, 2003, 78, p. 61-67.
344. NAGY B., YEH W.C., MAK T.W*., et al.* FADD null mouse embryonic fibroblasts undergo apoptosis after photosensitization with the silicon phthalocyanine Pc 4. *Arch Biochem Biophys*, 2001, 385, p. 194-202.
345. KESSEL D., LUO Y., DENG Y*., et al.* The role of subcellular localization in initiation of apoptosis by photodynamic therapy. *Photochem Photobiol*, 1997, 65, p. 422-426.
346. REINERS J.J., JR., CARUSO J.A., MATHIEU P*., et al.* Release of cytochrome c and activation of pro-caspase-9 following lysosomal photodamage involves Bid cleavage. *Cell Death Differ*, 2002, 9, p. 934-944.
347. TEITEN M.H., MARCHAL S., D'HALLEWIN M.A*., et al.* Primary photodamage sites and mitochondrial events after Foscan photosensitization of MCF-7 human breast cancer cells. *Photochem Photobiol*, 2003, 78, p. 9-14.
348. INANAMI O., YOSHITO A., TAKAHASHI K*., et al.* Effects of BAPTA-AM and forskolin on apoptosis and cytochrome c release in photosensitized Chinese hamster V79 cells. *Photochem Photobiol*, 1999, 70, p. 650-655.
349. CARRE V., JAYAT C., GRANET R*., et al.* Chronology of the apoptotic events induced in the K562 cell line by photodynamic treatment with hematoporphyrin and monoglucosylporphyrin. *Photochem Photobiol*, 1999, 69, p. 55-60.
350. LUTHI A.U., MARTIN S.J. The CASBAH: a searchable database of caspase substrates. *Cell Death Differ*, 2007, 14, p. 641-650.
351. TSUJIMOTO Y., SHIMIZU S. Another way to die: autophagic programmed cell death. *Cell Death Differ*, 2005, 12 Suppl 2, p. 1528-1534.
352. SHIMIZU S., KANASEKI T., MIZUSHIMA N*., et al.* Role of Bcl-2 family proteins in a non-apoptotic programmed cell death dependent on autophagy genes. *Nat Cell Biol*, 2004, 6, p. 1221-1228.
353. YU L., ALVA A., SU H*., et al.* Regulation of an ATG7-beclin 1 program of autophagic cell death by caspase-8. *Science*, 2004, 304, p. 1500-1502.
354. CUERVO A.M. Autophagy: in sickness and in health. *Trends Cell Biol*, 2004, 14, p. 70-77.
355. CODOGNO P., MEIJER A.J. Autophagy and signaling: their role in cell survival and cell death. *Cell Death Differ*, 2005, 12 Suppl 2, p. 1509-1518.
356. REGGIORI F., KLIONSKY D.J. Autophagosomes: biogenesis from scratch? *Curr Opin Cell Biol*, 2005, 17, p. 415-422.
357. LEVINE B., YUAN J. Autophagy in cell death: an innocent convict? *J Clin Invest*, 2005, 115, p. 2679-2688.
358. KLIONSKY D.J. Autophagy: from phenomenology to molecular understanding in less than a decade. *Nat Rev Mol Cell Biol*, 2007, 8, p. 931-937.
359. MIZUSHIMA N., KLIONSKY D.J. Protein turnover via autophagy: implications for metabolism. *Annu Rev Nutr*, 2007, 27, p. 19-40.
360. MAIURI M.C., ZALCKVAR E., KIMCHI A*., et al.* Self-eating and self-killing: crosstalk between autophagy and apoptosis. *Nat Rev Mol Cell Biol*, 2007, 8, p. 741-752.

361. WEI M.C., ZONG W.X., CHENG E.H.*, et al.* Proapoptotic BAX and BAK: a requisite gateway to mitochondrial dysfunction and death. *Science*, 2001, 292, p. 727-730.
362. DEGENHARDT K., MATHEW R., BEAUDOIN B.*, et al.* Autophagy promotes tumor cell survival and restricts necrosis, inflammation, and tumorigenesis. *Cancer Cell*, 2006, 10, p. 51-64.
363. LEVINE B., KROEMER G. Autophagy in the Pathogenesis of Disease. *Cell*, 2008, 11, p. 27-42.
364. BUYTAERT E., CALLEWAERT G., HENDRICKX N.*, et al.* Role of endoplasmic reticulum depletion and multidomain proapoptotic BAX and BAK proteins in shaping cell death after hypericin-mediated photodynamic therapy. *FASEB J*, 2006, 20, p. 756-758.
365. KESSEL D., VICENTE M.G., REINERS JR. J.J. Initiation of apoptosis and autophagy by photodynamic therapy. *Autophagy*, 2006, 2, p. 289-290.
366. KESSEL D., CASTELLI M., REINERS JR. J.J. Apoptotic response to photodynamic therapy versus the Bcl-2 antagonist HA14-1. *Photochem Photobiol*, 2002, 76, p. 314-319.
367. XUE L.Y., CHIU S.M., OLEINICK N.L. Photochemical destruction of the Bcl-2 oncoprotein during photodynamic therapy with the phthalocyanine photosensitizer Pc 4. *Oncogene*, 2001, 20, p. 3420-3427.
368. PATTINGRE S., TASSA A., QU X.*, et al.* Bcl-2 antiapoptotic proteins inhibit Beclin 1-dependent autophagy. *Cell*, 2005, 122, p. 927-939.
369. OBERSTEIN A., JEFFREY P.D., SHI Y. Crystal structure of the Bcl-XL-Beclin 1 peptide complex: Beclin 1 is a novel BH3-only protein. *J Biol Chem*, 2007, 282, p. 13123-13132.
370. VANTIEGHEM A., XU Y., ASSEFA Z.*, et al.* Phosphorylation of Bcl-2 in G2/M phase-arrested cells following photodynamic therapy with hypericin involves a CDK1-mediated signal and delays the onset of apoptosis. *J Biol Chem*, 2002, 277, p. 37718-37731.
371. CHIU S.M., XUE L.Y., USUDA J.*, et al.* Bax is essential for mitochondrion-mediated apoptosis but not for cell death caused by photodynamic therapy. *Br J Cancer*, 2003, 89, p. 1590-1597.
372. VERCAMMEN D., BEYAERT R., DENECKER G.*, et al.* Inhibition of caspases increases the sensitivity of L929 cells to necrosis mediated by tumor necrosis factor. *J Exp Med*, 1998, 187, p. 1477-1485.
373. GOLSTEIN P., KROEMER G. Cell death by necrosis: towards a molecular definition. *Trends Biochem Sci*, 2007, 32, p. 37-43.
374. LOTZE M.T., TRACEY K.J. High-mobility group box 1 protein (HMGB1): nuclear weapon in the immune arsenal. *Nat Rev Immunol*, 2005, 5, p. 331-342.
375. MOUBARAK R.S., YUSTE V.J., ARTUS C.*, et al.* Sequential activation of poly(ADP-ribose) polymerase 1, calpains, and Bax is essential in apoptosis-inducing factor-mediated programmed necrosis. *Mol Cell Biol*, 2007, 27, p. 4844-4862.
376. HOLLER N., ZARU R., MICHEAU O.*, et al.* Fas triggers an alternative, caspase-8-independent cell death pathway using the kinase RIP as effector molecule. *Nat Immunol*, 2000, 1, p. 489-495.
377. FESTJENS N., VANDEN BERGHE T., CORNELIS S.*, et al.* RIP1, a kinase on the crossroads of a cell's decision to live or die. *Cell Death Differ*, 2007, 14, p. 400-410.
378. LOPEZ-SANCHEZ N., RODRIGUEZ J.R., FRADE J.M. Mitochondrial c-Jun NH2-terminal kinase prevents the accumulation of reactive oxygen species and reduces necrotic damage in neural tumor cells that lack trophic support. *Mol Cancer Res*, 2007, 5, p. 47-60.
379. KIM C.H., HAN S.I., LEE S.Y.*, et al.* Protein kinase C-ERK1/2 signal pathway switches glucose depletion-induced necrosis to apoptosis by regulating superoxide dismutases and suppressing reactive oxygen species production in A549 lung cancer cells. *J Cell Physiol*, 2007, 211, p. 371-385.
380. CIPRIANI G., RAPIZZI E., VANNACCI A.*, et al.* Nuclear poly(ADP-ribose) polymerase-1 rapidly triggers mitochondrial dysfunction. *J Biol Chem*, 2005, 280, p. 17227-17234.
381. YU S.W., WANG H., POITRAS M.F.*, et al.* Mediation of poly(ADP-ribose) polymerase-1-dependent cell death by apoptosis-inducing factor. *Science*, 2002, 297, p. 259-263.

382. ZHANG S., LIN Y., KIM Y.S*., et al.* c-Jun N-terminal kinase mediates hydrogen peroxide-induced cell death via sustained poly(ADP-ribose) polymerase-1 activation. *Cell Death Differ*, 2007, 14, p. 1001-1010.
383. LEIST M., JAATTELA M. Four deaths and a funeral: from caspases to alternative mechanisms. *Nat Rev Mol Cell Biol*, 2001, 2, p. 589-598.
384. ALMEIDA R.D., MANADAS B.J., CARVALHO A.P*., et al.* Intracellular signaling mechanisms in photodynamic therapy. *Biochim Biophys Acta*, 2004, 1704, p. 59-86.
385. CHANG L., KARIN M. Mammalian MAP kinase signalling cascades. *Nature*, 2001, 410, p. 37-40.
386. GRAVES L.M., GUY H.I., KOZLOWSKI P*., et al.* Regulation of carbamoyl phosphate synthetase by MAP kinase. *Nature*, 2000, 403, p. 328-332.
387. WADA T., PENNINGER J.M. Mitogen-activated protein kinases in apoptosis regulation. *Oncogene*, 2004, 23, p. 2838-2849.
388. KRISHNA M., NARANG H. The complexity of mitogen-activated protein kinases (MAPKs) made simple. *Cell Mol Life Sci*, 2008, 65, p. 3525-3544.
389. MATSUZAWA A., ICHIJO H. Redox control of cell fate by MAP kinase: physiological roles of ASK1-MAP kinase pathway in stress signaling. *Biochim Biophys Acta*, 2008, 1780, p. 1325-1336.
390. SONG J.J., RHEE J.G., SUNTHARALINGAM M*., et al.* Role of glutaredoxin in metabolic oxidative stress. Glutaredoxin as a sensor of oxidative stress mediated by H2O2. *J Biol Chem*, 2002, 277, p. 46566-46575.
391. TOURNIER C., HESS P., YANG D.D*., et al.* Requirement of JNK for stress-induced activation of the cytochrome c-mediated death pathway. *Science*, 2000, 288, p. 870-874.
392. KYRIAKIS J.M., BANERJEE P., NIKOLAKAKI E*., et al.* The stress-activated protein kinase subfamily of c-Jun kinases. *Nature*, 1994, 369, p. 156-160.
393. HUANGFU W.C., OMORI E., AKIRA S*., et al.* Osmotic stress activates the TAK1-JNK pathway while blocking TAK1-mediated NF-kappaB activation: TAO2 regulates TAK1 pathways. *J Biol Chem*, 2006, 281, p. 28802-28810.
394. HADDAD J.J. Discordant tissue-specific expression of SAPK/MAPK(JNK)-related cofactors in hypoxia and hypoxia/reoxygenation in a model of anoxia-tolerance. *Protein Pept Lett*, 2007, 14, p. 373-380.
395. JOHNSON G.L., LAPADAT R. Mitogen-activated protein kinase pathways mediated by ERK, JNK, and p38 protein kinases. *Science*, 2002, 298, p. 1911-1912.
396. ASSEFA Z., VANTIEGHEM A., DECLERCQ W*., et al.* The activation of the c-Jun N-terminal kinase and p38 mitogen-activated protein kinase signaling pathways protects HeLa cells from apoptosis following photodynamic therapy with hypericin. *J Biol Chem*, 1999, 274, p. 8788-8796.
397. THRANE E.V., SCHWARZE P.E., THORESEN G.H*., et al.* Persistent versus transient map kinase (ERK) activation in the proliferation of lung epithelial type 2 cells. *Exp Lung Res*, 2001, 27, p. 387-400.
398. CUI W., YAZLOVITSKAYA E.M., MAYO M.S*., et al.* Cisplatin-induced response of c-jun N-terminal kinase 1 and extracellular signal--regulated protein kinases 1 and 2 in a series of cisplatin-resistant ovarian carcinoma cell lines. *Mol Carcinog*, 2000, 29, p. 219-228.
399. ANDERSON C.N., TOLKOVSKY A.M. A role for MAPK/ERK in sympathetic neuron survival: protection against a p53-dependent, JNK-independent induction of apoptosis by cytosine arabinoside. *J Neurosci*, 1999, 19, p. 664-673.
400. AGOSTINIS P., VANDENBOGAERDE A., DONELLA-DEANA A*., et al.* Photosensitized inhibition of growth factor-regulated protein kinases by hypericin. *Biochem Pharmacol*, 1995, 49, p. 1615-1622.
401. HUANG Y.H., LEE T.H., CHAN K.J*., et al.* Anemonin is a natural bioactive compound that can regulate tyrosinase-related proteins and mRNA in human melanocytes. *J Dermatol Sci*, 2008, 49, p. 115-123.

402. SANTONOCITO C., CONCOLINO P., LAVIERI M.M*., et al.* Comparison between three molecular methods for detection of blood melanoma tyrosinase mRNA. Correlation with melanoma stages and S100B, LDH, NSE biochemical markers. *Clin Chim Acta*, 2005, 362, p. 85-93.
403. ASSEFA Z., GARMYN M., BOUILLON R*., et al.* Differential stimulation of ERK and JNK activities by ultraviolet B irradiation and epidermal growth factor in human keratinocytes. *J Invest Dermatol*, 1997, 108, p. 886-891.
404. TAO J., SANGHERA J.S., PELECH S.L*., et al.* Stimulation of stress-activated protein kinase and p38 HOG1 kinase in murine keratinocytes following photodynamic therapy with benzoporphyrin derivative. *J Biol Chem*, 1996, 271, p. 27107-27115.
405. KLOTZ L.O., FRITSCH C., BRIVIBA K*., et al.* Activation of JNK and p38 but not ERK MAP kinases in human skin cells by 5-aminolevulinate-photodynamic therapy. *Cancer Res*, 1998, 58, p. 4297-4300.
406. XUE L., HE J., OLEINICK N.L. Promotion of photodynamic therapy-induced apoptosis by stress kinases. *Cell Death Differ*, 1999, 6, p. 855-864.
407. TONG Z., SINGH G., RAINBOW A.J. Sustained activation of the extracellular signal-regulated kinase pathway protects cells from photofrin-mediated photodynamic therapy. *Cancer Res*, 2002, 62, p. 5528-5535.
408. VAUZOUR D., VAFEIADOU K., RICE-EVANS C*., et al.* Activation of pro-survival Akt and ERK1/2 signalling pathways underlie the anti-apoptotic effects of flavanones in cortical neurons. *J Neurochem*, 2007, 103, p. 1355-1367.
409. ZHUANG S., KOCHEVAR I.E. Singlet oxygen-induced activation of Akt/protein kinase B is independent of growth factor receptors. *Photochem Photobiol*, 2003, 78, p. 361-371.
410. YANG P., PEAIRS J.J., TANO R*., et al.* Oxidant-mediated Akt activation in human RPE cells. *Invest Ophthalmol Vis Sci*, 2006, 47, p. 4598-4606.
411. BOZKULAK O., WONG S., LUNA M*., et al.* Multiple components of photodynamic therapy can phosphorylate Akt. *Photochem Photobiol*, 2007, 83, p. 1029-1033.
412. WONG T.W., TRACY E., OSEROFF A.R*., et al.* Photodynamic therapy mediates immediate loss of cellular responsiveness to cytokines and growth factors. *Cancer Res*, 2003, 63, p. 3812-3818.
413. VERHEIJ M., RUITER G.A., ZERP S.F*., et al.* The role of the stress-activated protein kinase (SAPK/JNK) signaling pathway in radiation-induced apoptosis. *Radiother Oncol*, 1998, 47, p. 225-232.
414. TANG P.M., ZHANG D.M., XUAN N.H*., et al.* Photodynamic therapy inhibits P-glycoprotein mediated multidrug resistance via JNK activation in human hepatocellular carcinoma using the photosensitizer pheophorbide a. *Mol Cancer*, 2009, 8, p. 56.
415. TONG J., ELOWE S., NASH P*., et al.* Manipulation of EphB2 regulatory motifs and SH2 binding sites switches MAPK signaling and biological activity. *J Biol Chem*, 2003, 278, p. 6111-6119.
416. FORREST V.J., KANG Y.H., MCCLAIN D.E*., et al.* Oxidative stress-induced apoptosis prevented by Trolox. *Free Radic Biol Med*, 1994, 16, p. 675-684.
417. HOPCIA K.L., MCCAREY Y.L., SYLVESTER F.C*., et al.* Radiation-induced apoptosis in HL60 cells: oxygen effect, relationship between apoptosis and loss of clonogenicity, and dependence of time to apoptosis on radiation dose. *Radiat Res*, 1996, 145, p. 315-323.
418. GODAR D.E., LUCAS A.D. Spectral dependence of UV-induced immediate and delayed apoptosis: the role of membrane and DNA damage. *Photochem Photobiol*, 1995, 62, p. 108-113.
419. DELLINGER M. Apoptosis or necrosis following Photofrin photosensitization: influence of the incubation protocol. *Photochem Photobiol*, 1996, 64, p. 182-187.
420. GIROTTI A.W. Lipid hydroperoxide generation, turnover, and effector action in biological systems. *J Lipid Res*, 1998, 39, p. 1529-1542.
421. LEMAITRE D., VERICEL E., POLETTE A*., et al.* Effects of fatty acids on human platelet glutathione peroxidase: possible role of oxidative stress. *Biochem Pharmacol*, 1997, 53, p. 479-486.

422. BASU-MODAK S., LUSCHER P., TYRRELL R.M. Lipid metabolite involvement in the activation of the human heme oxygenase-1 gene. *Free Radic Biol Med*, 1996, 20, p. 887-897.
423. VILE G.F., BASU-MODAK S., WALTNER C.*, et al.* Heme oxygenase 1 mediates an adaptive response to oxidative stress in human skin fibroblasts. *Proc Natl Acad Sci U S A*, 1994, 91, p. 2607-2610.
424. NOWIS D., MAKOWSKI M., STOKLOSA T.*, et al.* Direct tumor damage mechanisms of photodynamic therapy. *Acta Biochim Pol*, 2005, 52, p. 339-352.
425. HAQQ C., NOSRATI M., SUDILOVSKY D.*, et al.* The gene expression signatures of melanoma progression. *Proc Natl Acad Sci U S A*, 2005, 102, p. 6092-6097.
426. SPECHT K.G., RODGERS M.A. Depolarization of mouse myeloma cell membranes during photodynamic action. *Photochem Photobiol*, 1990, 51, p. 319-324.
427. OGATA M., INANAMI O., NAKAJIMA M.*, et al.* Ca(2+)-dependent and caspase-3-independent apoptosis caused by damage in Golgi apparatus due to 2,4,5,7-tetrabromorhodamine 123 bromide-induced photodynamic effects. *Photochem Photobiol*, 2003, 78, p. 241-247.
428. HUBMER A., HERMANN A., UBERRIEGLER K.*, et al.* Role of calcium in photodynamically induced cell damage of human fibroblasts. *Photochem Photobiol*, 1996, 64, p. 211-215.
429. PENNING L.C., RASCH M.H., BEN-HUR E.*, et al.* A role for the transient increase of cytoplasmic free calcium in cell rescue after photodynamic treatment. *Biochim Biophys Acta*, 1992, 1107, p. 255-260.
430. AGARWAL M.L., LARKIN H.E., ZAIDI S.I.*, et al.* Phospholipase activation triggers apoptosis in photosensitized mouse lymphoma cells. *Cancer Res*, 1993, 53, p. 5897-5902.
431. BERRIDGE M.J., IRVINE R.F. Inositol phosphates and cell signalling. *Nature*, 1989, 341, p. 197-205.
432. SCHWAB B.L., GUERINI D., DIDSZUN C.*, et al.* Cleavage of plasma membrane calcium pumps by caspases: a link between apoptosis and necrosis. *Cell Death Differ*, 2002, 9, p. 818-831.
433. FOSTER T.H., PRIMAVERA M.C., MARDER V.J.*, et al.* Photosensitized release of von Willebrand factor from cultured human endothelial cells. *Cancer Res*, 1991, 51, p. 3261-3266.
434. FREAS W., HART J.L., GOLIGHTLY D.*, et al.* Vascular interactions of calcium and reactive oxygen intermediates produced following photoradiation. *J Cardiovasc Pharmacol*, 1991, 17, p. 27-35.
435. LUNA M.C., WONG S., GOMER C.J. Photodynamic therapy mediated induction of early response genes. *Cancer Res*, 1994, 54, p. 1374-1380.
436. KICK G., MESSER G., PLEWIG G.*, et al.* Strong and prolonged induction of c-jun and c-fos proto-oncogenes by photodynamic therapy. *Br J Cancer*, 1996, 74, p. 30-36.
437. VOLANTI C., MATROULE J.Y., PIETTE J. Involvement of oxidative stress in NF-kappaB activation in endothelial cells treated by photodynamic therapy. *Photochem Photobiol*, 2002, 75, p. 36-45.
438. MATROULE J.Y., HELLIN A.C., MORLIERE P.*, et al.* Role of nuclear factor-kappa B in colon cancer cell apoptosis mediated by aminopyropheophorbide photosensitization. *Photochem Photobiol*, 1999, 70, p. 540-548.
439. JADESKI L.C., HUM K.O., CHAKRABORTY C.*, et al.* Nitric oxide promotes murine mammary tumour growth and metastasis by stimulating tumour cell migration, invasiveness and angiogenesis. *Int J Cancer*, 2000, 86, p. 30-39.
440. GOMES E.R., ALMEIDA R.D., CARVALHO A.P.*, et al.* Nitric oxide modulates tumor cell death induced by photodynamic therapy through a cGMP-dependent mechanism. *Photochem Photobiol*, 2002, 76, p. 423-430.
441. YAMAMOTO F., OHGARI Y., YAMAKI N.*, et al.* The role of nitric oxide in delta-aminolevulinic acid (ALA)-induced photosensitivity of cancerous cells. *Biochem Biophys Res Commun*, 2007, 353, p. 541-546.
442. BUYTAERT E., DEWAELE M., AGOSTINIS P. Molecular effectors of multiple cell death pathways initiated by photodynamic therapy. *Biochim Biophys Acta*, 2007, 1776, p. 86-107.

443. HONG X., JIANG F., KALKANIS S.N.*, et al.* Intracellular free calcium mediates glioma cell detachment and cytotoxicity after photodynamic therapy. *Lasers Med Sci*, 2009, 24, p. 777-786.
444. ROLAND C.L., HARKEN A.H., SARR M.G.*, et al.* ICAM-1 expression determines malignant potential of cancer. *Surgery*, 2007, 141, p. 705-707.
445. CHRISTENSEN T., MOAN, T. Photodynamic Effect of Hematoporphyrin (HP) On Cells Cultivated in Vitro. *Lasers in Photomedicine and Photobiology* / ed. by SACCHI R.P.A.C.A. Berlin, Heidelberg, New York: Springer-Verlag, 1980, p. 87-91.
446. DAHLE J., ANGELL-PETERSEN, E., STEEN, H. B., MOAN, J. Bystander effects in cell death induced by photodynamic treatment UVA radiation and inhibitors of ATP synthesis. *Photochem Photobiol*, 2001, 73, p. 378-387.
447. KORBELIK M., DOUGHERTY G.J. Photodynamic therapy-mediated immune response against subcutaneous mouse tumors. *Cancer Res*, 1999, 59, p. 1941-1946.
448. HENDRZAK-HENION J.A., KNISELY T.L., CINCOTTA L.*, et al.* Role of the immune system in mediating the antitumor effect of benzophenothiazine photodynamic therapy. *Photochem Photobiol*, 1999, 69, p. 575-581.
449. HUNT D.W., LEVY J.G. Immunomodulatory aspects of photodynamic therapy. *Expert Opin Investig Drugs*, 1998, 7, p. 57-64.
450. HUNT D.W., CHAN A.H. Influence of photodynamic therapy on immunological aspects of disease - an update. *Expert Opin Investig Drugs*, 2000, 9, p. 807-817.
451. HRYHORENKO E.A., OSEROFF A.R., MORGAN J.*, et al.* Antigen specific and nonspecific modulation of the immune response by aminolevulinic acid based photodynamic therapy. *Immunopharmacology*, 1998, 40, p. 231-240.
452. NORTH J., NEYNDORFF H., LEVY J.G. Photosensitizers as virucidal agents. *J Photochem Photobiol B*, 1993, 17, p. 99-108.
453. PRIGNANO F., LOTTI T., SPALLANZANI A.*, et al.* Sequential effects of photodynamic treatment of basal cell carcinoma. *J Cutan Pathol*, 2009, 36, p. 409-416.
454. KOON H.K., LO K.W., LEUNG K.N.*, et al.* Photodynamic therapy-mediated modulation of inflammatory cytokine production by Epstein-Barr virus-infected nasopharyngeal carcinoma cells. *Cell Mol Immunol*, 2010, p.
455. KRUTMANN J., ATHAR M., MENDEL D.B.*, et al.* Inhibition of the high affinity Fc receptor (Fc gamma RI) on human monocytes by porphyrin photosensitization is highly specific and mediated by the generation of superoxide radicals. *J Biol Chem*, 1989, 264, p. 11407-11413.
456. OBOCHI M.O., RATKAY L.G., LEVY J.G. Prolonged skin allograft survival after photodynamic therapy associated with modification of donor skin antigenicity. *Transplantation*, 1997, 63, p. 810-817.
457. REDDAN J.C., ANDERSON C.Y., XU H.*, et al.* Immunosuppressive effects of silicon phthalocyanine photodynamic therapy. *Photochem Photobiol*, 1999, 70, p. 72-77.
458. EVANS S., MATTHEWS W., PERRY R.*, et al.* Effect of photodynamic therapy on tumor necrosis factor production by murine macrophages. *J Natl Cancer Inst*, 1990, 82, p. 34-39.
459. MORTON C.A., MCKENNA K.E., RHODES L.E. Guidelines for topical photodynamic therapy: update. *Br J Dermatol*, 2008, 159, p. 1245-1266.
460. ALEXIADES-ARMENAKAS M.R., GERONEMUS R.G. Laser-mediated photodynamic therapy of actinic keratoses. *Arch Dermatol*, 2003, 139, p. 1313-1320.
461. TARSTEDT M., ROSDAHL I., BERNE B.*, et al.* A randomized multicenter study to compare two treatment regimens of topical methyl aminolevulinate (Metvix)-PDT in actinic keratosis of the face and scalp. *Acta Derm Venereol*, 2005, 85, p. 424-428.
462. DRAGIEVA G., PRINZ B.M., HAFNER J.*, et al.* A randomized controlled clinical trial of topical photodynamic therapy with methyl aminolaevulinate in the treatment of actinic keratoses in transplant recipients. *Br J Dermatol*, 2004, 151, p. 196-200.

463. FREEMAN M., VINCIULLO C., FRANCIS D*., et al.* A comparison of photodynamic therapy using topical methyl aminolevulinate (Metvix) with single cycle cryotherapy in patients with actinic keratosis: a prospective, randomized study. *J Dermatolog Treat*, 2003, 14, p. 99-106.
464. MORTON C., HORN M., LEMAN J*., et al.* Comparison of topical methyl aminolevulinate photodynamic therapy with cryotherapy or Fluorouracil for treatment of squamous cell carcinoma in situ: Results of a multicenter randomized trial. *Arch Dermatol*, 2006, 142, p. 729-735.
465. BROOKES P.T., JHAWAR S., HINTON C.P*., et al.* Bowen's disease of the nipple-a new method of treatment. *Breast*, 2005, 14, p. 65-67.
466. USMANI N., STABLES G.I., TELFER N.R*., et al.* Subungual Bowen's disease treated by topical aminolevulinic acid-photodynamic therapy. *J Am Acad Dermatol*, 2005, 53, p. S273-276.
467. BALL S.B., DAWBER R.P. Treatment of cutaneous Bowen's disease with particular emphasis on the problem of lower leg lesions. *Australas J Dermatol*, 1998, 39, p. 63-68.
468. SOUZA C.S., FELICIO L.B., BENTLEY M.V*., et al.* Topical photodynamic therapy for Bowen's disease of the digit in epidermolysis bullosa. *Br J Dermatol*, 2005, 153, p. 672-674.
469. GUILLEN C., SANMARTIN O., ESCUDERO A*., et al.* Photodynamic therapy for in situ squamous cell carcinoma on chronic radiation dermatitis after photosensitization with 5-aminolaevulinic acid. *J Eur Acad Dermatol Venereol*, 2000, 14, p. 298-300.
470. VARMA S., HOLT P.J., ANSTEY A.V. Erythroplasia of queyrat treated by topical aminolaevulinic acid photodynamic therapy: a cautionary tale. *Br J Dermatol*, 2000, 142, p. 825-826.
471. THISSEN M.R., SCHROETER C.A., NEUMANN H.A. Photodynamic therapy with delta-aminolaevulinic acid for nodular basal cell carcinomas using a prior debulking technique. *Br J Dermatol*, 2000, 142, p. 338-339.
472. ANGELL-PETERSEN E., SORENSEN R., WARLOE T*., et al.* Porphyrin formation in actinic keratosis and basal cell carcinoma after topical application of methyl 5-aminolevulinate. *J Invest Dermatol*, 2006, 126, p. 265-271.
473. RHODES L.E., DE RIE M., ENSTROM Y*., et al.* Photodynamic therapy using topical methyl aminolevulinate vs surgery for nodular basal cell carcinoma: results of a multicenter randomized prospective trial. *Arch Dermatol*, 2004, 140, p. 17-23.
474. HORN M., WOLF P., WULF H.C*., et al.* Topical methyl aminolaevulinate photodynamic therapy in patients with basal cell carcinoma prone to complications and poor cosmetic outcome with conventional treatment. *Br J Dermatol*, 2003, 149, p. 1242-1249.
475. FOLEY P. Clinical efficacy of methyl aminolevulinate (Metvix) photodynamic therapy. *J Dermatolog Treat*, 2003, 14 Suppl 3, p. 15-22.
476. ZANE C., VENTURINI M., SALA R*., et al.* Photodynamic therapy with methylaminolevulinate as a valuable treatment option for unilesional cutaneous T-cell lymphoma. *Photodermatol Photoimmunol Photomed*, 2006, 22, p. 254-258.
477. HILLEMANNS P., WANG X., STAEHLE S*., et al.* Evaluation of different treatment modalities for vulvar intraepithelial neoplasia (VIN): CO(2) laser vaporization, photodynamic therapy, excision and vulvectomy. *Gynecol Oncol*, 2006, 100, p. 271-275.
478. HAMDAN K.A., TAIT I.S., NADEAU V*., et al.* Treatment of grade III anal intraepithelial neoplasia with photodynamic therapy: report of a case. *Dis Colon Rectum*, 2003, 46, p. 1555-1559.
479. HONGCHARU W., TAYLOR C.R., CHANG Y*., et al.* Topical ALA-photodynamic therapy for the treatment of acne vulgaris. *J Invest Dermatol*, 2000, 115, p. 183-192.
480. ITOH Y., NINOMIYA Y., TAJIMA S*., et al.* Photodynamic therapy of acne vulgaris with topical delta-aminolaevulinic acid and incoherent light in Japanese patients. *Br J Dermatol*, 2001, 144, p. 575-579.
481. POLLOCK B., TURNER D., STRINGER M.R*., et al.* Topical aminolaevulinic acid-photodynamic therapy for the treatment of acne vulgaris: a study of clinical efficacy and mechanism of action. *Br J Dermatol*, 2004, 151, p. 616-622.

482. TOME J.P., NEVES M.G., TOME A.C*., et al.* Synthesis and antibacterial activity of new poly-S-lysine-porphyrin conjugates. *J Med Chem*, 2004, 47, p. 6649-6652.
483. TOME J.P., SILVA E.M., PEREIRA A.M*., et al.* Synthesis of neutral and cationic tripyridylporphyrin-D-galactose conjugates and the photoinactivation of HSV-1. *Bioorg Med Chem*, 2007, 15, p. 4705-4713.
484. ROBEL I., SUBRAMANIAN V., KUNO M*., et al.* Quantum dot solar cells. harvesting light energy with CdSe nanocrystals molecularly linked to mesoscopic TiO2 films. *J Am Chem Soc*, 2006, 128, p. 2385-2393.
485. MORLIERE P., BOSCA F., MIRANDA M.A*., et al.* Primary photochemical processes of the phototoxic neuroleptic cyamemazine: a study by laser flash photolysis and steady-state irradiation. *Photochem Photobiol*, 2004, 80, p. 535-541.
486. PARKER C.A. Photoluminescence of Solutions. / ed. Amsterdam: Elsevier, 1968, p. 208-216.
487. MORLIERE P., MAZIERE J.C., SANTUS R*., et al.* Tolyporphin: a natural product from cyanobacteria with potent photosensitizing activity against tumor cells in vitro and in vivo. *Cancer Res*, 1998, 58, p. 3571-3578.
488. LOWRY O.H., ROSEBROUGH N.J., FARR A.L*., et al.* Protein measurement with the Folin phenol reagent. *J Biol Chem*, 1951, 193, p. 265-275.
489. BORENFREUND E., BORRERO O. In vitro cytotoxicity assays. Potential alternatives to the Draize ocular allergy test. *Cell Biol Toxicol*, 1984, 1, p. 55-65.
490. LASAROW R.M., ISSEROFF R.R., GOMEZ E.C. Quantitative in vitro assessment of phototoxicity by a fibroblast-neutral red assay. *J Invest Dermatol*, 1992, 98, p. 725-729.
491. GUTTERIDGE J.M., HALLIWELL B. Iron toxicity and oxygen radicals. *Baillieres Clin Haematol*, 1989, 2, p. 195-256.
492. WAGNIERES G.A., STAR W.M., WILSON B.C. In vivo fluorescence spectroscopy and imaging for oncological applications. *Photochem Photobiol*, 1998, 68, p. 603-632.
493. BRAICHOTTE D.R., SAVARY J.F., MONNIER P*., et al.* Optimizing light dosimetry in photodynamic therapy of early stage carcinomas of the esophagus using fluorescence spectroscopy. *Lasers Surg Med*, 1996, 19, p. 340-346.
494. BENSASSON R.V., LAND E.J., TRUSCOTT T.G. *Flash Photolysis and Pulse Radiolysis. Contributions to the Chemistry of Biology and Medicine*. New York: Pergamon Press, 1983, p. 11-14, 67-72.
495. KIMEL S., TROMBERG B.J., ROBERTS W.G*., et al.* Singlet oxygen generation of porphyrins, chlorins, and phthalocyanines. *Photochem Photobiol*, 1989, 50, p. 175-183.
496. WOODBURN K.W., VARDAXIS N.J., HILL J.S*., et al.* Evaluation of porphyrin characteristics required for photodynamic therapy. *Photochem Photobiol*, 1992, 55, p. 697-704.
497. MORLIERE P., MOYSAN A., SANTUS R*., et al.* UVA-induced lipid peroxidation in cultured human fibroblasts. *Biochim Biophys Acta*, 1991, 1084, p. 261-268.
498. AGARWAL M.L., CLAY M.E., HARVEY E.J*., et al.* Photodynamic therapy induces rapid cell death by apoptosis in L5178Y mouse lymphoma cells. *Cancer Res*, 1991, 51, p. 5993-5996.
499. GOZUACIK D., KIMCHI A. Autophagy as a cell death and tumor suppressor mechanism. *Oncogene*, 2004, 23, p. 2891-2906.
500. EDINGER A.L., THOMPSON C.B. Death by design: apoptosis, necrosis and autophagy. *Curr Opin Cell Biol*, 2004, 16, p. 663-669.
501. XUE L.Y., CHIU S.M., AZIZUDDIN K*., et al.* Protection by Bcl-2 against apoptotic but not autophagic cell death after photodynamic therapy. *Autophagy*, 2008, 4, p. 125-127.
502. GUILLON-MUNOS A., VAN BEMMELEN M.X., CLARKE P.G. Autophagy can be a killer even in apoptosis-competent cells. *Autophagy*, 2006, 2, p. 140-142.
503. DAVIS R.J. Signal transduction by the JNK group of MAP kinases. *Cell*, 2000, 103, p. 239-252.
504. VENTURA J.J., HUBNER A., ZHANG C*., et al.* Chemical genetic analy-sis of the time course of signal transduction by JNK. *Mol Cell*, 2006, 21, p. 701-710.
505. NAKANO H., NAKAJIMA A., SAKON-KOMAZAWA S*., et al.* Reactive oxygen species mediate crosstalk between NF-kappaB and JNK. *Cell Death Differ*, 2006, 13, p. 730-737.

506. SHIMIZU S., ARAKAWA S., NISHIDA Y. Autophagy takes an alternative pathway. *Autophagy*, 2010, 6, p. 290-291.
507. WEI Y., SINHA S., LEVINE B. Dual role of JNK1-mediated phosphorylation of Bcl-2 in autophagy and apoptosis regulation. *Autophagy*, 2008, 4, p. 949-951.
508. WEBBER J.L. Regulation of autophagy by p38alpha MAPK. *Autophagy*, 2010, 6, p. 292-293.
509. WEBBER J.L., TOOZE S.A. Coordinated regulation of autophagy by p38alpha MAPK through mAtg9 and p38IP. *EMBO J*, 2010, 29, p. 27-40.
510. ZHANG Y., WU Y., TASHIRO S.*, et al.* Involvement of PKC signal pathways in oridonin-induced autophagy in HeLa cells: a protective mechanism against apoptosis. *Biochem Biophys Res Commun*, 2009, 378, p. 273-278.
511. CAGNOL S., CHAMBARD J.C. ERK and cell death: mechanisms of ERK-induced cell death--apoptosis, autophagy and senescence. *FEBS J*, 2010, 277, p. 2-21.
512. SCHIEKE S.M., VON MONTFORT C., BUCHCZYK D.P.*, et al.* Singlet oxygen-induced attenuation of growth factor signaling: possible role of ceramides. *Free Radic Res*, 2004, 38, p. 729-737.
513. KONDO Y., KANZAWA T., SAWAYA R.*, et al.* The role of autophagy in cancer development and response to therapy. *Nat Rev Cancer*, 2005, 5, p. 726-734.
514. MATSUBARA A., NAKAZAWA T., NODA K.*, et al.* Photodynamic therapy induces caspase-dependent apoptosis in rat CNV model. *Invest Ophthalmol Vis Sci*, 2007, 48, p. 4741-4747.
515. MAMMUCARI C., MILAN G., ROMANELLO V.*, et al.* FoxO3 controls autophagy in skeletal muscle in vivo. *Cell Metab*, 2007, 6, p. 458-471.
516. SEBOLT-LEOPOLD J.S., HERRERA R. Targeting the mitogen-activated protein kinase cascade to treat cancer. *Nat Rev Cancer*, 2004, 4, p. 937-947.
517. CHENG J.Q., LINDSLEY C.W., CHENG G.Z.*, et al.* The Akt/PKB pathway: molecular target for cancer drug discovery. *Oncogene*, 2005, 24, p. 7482-7492.

ANNEXES

Annex I - Photophysical properties of a photocytotoxic fluorinated chlorine conjugated to four β-cyclodextrins

JN Silva, A Silva, J Tomé, A Ribeiro, M Domingues, J Cavaleiro, A Silva, M Neves, A Tomé, O Serra, F Bosca, P Filipe, R Santus, P Morlière, Photochem. Photobiol. Sci., 2008, 7, 834–843

Annex II - Photodynamic therapies: Principles and present medical applications

JN Silva, P Filipe, P Morlière, J-C Mazière, JP Freitas, J Cirne de Castro, R Santus, Bio-Medical Materials and Engineering 16 (2006) 147–154

Annex III - Photodynamic therapy: Dermatology and ophthalmology as main fields of current applications in clinic

JN Silva, P Filipe, P Morlière, J-C Mazière, JP Freitas, M Marques Gomes, R Santus, Bio-Medical Materials and Engineering 18 (2008) 319–327

PAPER www.rsc.org/pps | Photochemical & Photobiological Sciences

Photophysical properties of a photocytotoxic fluorinated chlorin conjugated to four β-cyclodextrins†

João Nuno Silva,[a] Ana M. G. Silva,‡[b] João P. Tomé,[b] Anderson O. Ribeiro,[c] M. Rosário M. Domingues,[b] José A. S. Cavaleiro,[b] Artur M. S. Silva,[b] M. Graça P. M. S. Neves,[b] Augusto C. Tomé,[b] Osvaldo A. Serra,[c] Francisco Bosca,[d] Paulo Filipe,[e] René Santus[e] and Patrice Morlière*[f,g]

Received 8th January 2008, Accepted 9th April 2008
First published as an Advance Article on the web 7th May 2008
DOI: 10.1039/b800348c

A *meso*-tetrakis(pentafluorophenyl)-chlorin with the reduced pyrrole ring linked to an isoxazolidine ring (FC) has been conjugated to four β-cyclodextrins (CDFC). The CDFC exhibits excellent water solubility and is a potent photosensitizer towards proliferating NCTC 2544 human keratinocytes. The study by conventional steady state absorption and fluorescence spectroscopies and by time-resolved femto- and nanosecond laser flash spectroscopies suggests that in ethanol and pH 7 buffer the β-cyclodextrins ensure the hydrophobic tetrakis(pentafluorophenyl)-chlorin macrocycle and strongly interact with the chlorin rings in the singlet and triplet manifolds. In these solvents, femtosecond spectroscopy suggests the FC conjugate undergoes intramolecular relaxation to the upper excited singlet states induced by photochemical and/or conformational changes at a rate of about 5 ps^{-1} to fluorescent states whose lifetimes (~8 ns). This interaction is destroyed upon addition of Triton X-100 to buffer. Both FC and CDFC strongly fluoresce (Φ_F ~ 0.5) in micelles. Similar behavior is observed in the triplet level. In ethanol and buffer, the initial formation of triplet states absorbing at 460 nm within 1–5 μs yielding a longer-lived triplet with spectral properties indistinguishable from that of original differences in absorbance spectra. The determination of the molar absorbance in the 440–460 nm region (ε ~ 35 000 M^{-1} cm^{-1}) leads to an estimate of ~0.2 for the triplet formation quantum yield of FC in ethanol and of FC and CDFC in Triton X-100 micelles. Quenching of the CDFC triplets by dissolved oxygen in buffer paralleled $^1O_2$ in a good yield consistent with the effective photocytotoxicity of the chlorin–cyclodextrin conjugate towards cultured NCTC 2544 human keratinocytes. By contrast, FC which aggregates in buffer produces little if any $^1O_2$.

Introduction

Photodynamic therapy (PDT) is an alternative treatment to pre-existing therapies in several clinical situations in oncology and ophthalmology. Presently authorized photoactive substances are tetrapyrrolic derivatives producing singlet oxygen as the major cytotoxin upon illumination of the tumor site with visible light after systemic administration of a photosensitizer.[1,2] In dermatology, the treatment of basal and squamous cell carcinoma and of the pre-cancerous lesions of solar keratoses by PDT involves topical application of the esters of 5-aminolevulinic acid, the precursor of protoporphyrin IX.[3] Most effective tetrapyrroles are lipophilic and are carried by blood lipoproteins which deliver them not only to the tumor but also to every organ.[4] The poor water solubility of tetrapyrroles is another limiting factor implying the preparation of special formulations for their systemic or topical administration. Several strategies are currently used to overcome these difficulties. The synthesis of porphyrins and chlorins bearing water soluble groups conferring tumor selectivity, such as tumor-specific antibodies or peptides and sugars has been carried out.[5,6] Accordingly the synthesis of β-cyclodextrin conjugates of porphyrins for dermatological applications is of interest since cyclodextrins have been used to improve hair and systemic dermal drug delivery by enhancing drug release and/or permeation and the reduction of drug degradation in topical preparations. In addition, cyclodextrins reduce drug-induced local irritation.[9–13]

It has been previously shown that a bis-β-cyclodextrin derivative of *meso*-tetrakis(pentafluorophenyl)-porphyrin which specifically binds to serum albumin was the most effective PDT

[a]Universidade de Lisboa, Faculdade de Medicina, Clínica Universitária de Dermatologia, 1699 Lisboa, Portugal
[b]University of Aveiro, Department of Chemistry, Campus Universitário de Santiago, 3810-193 Aveiro, Portugal
[c]University of São Paulo, Department of Chemistry, FFCLRP, Ribeirão Preto, Brazil
[d]Universidad Politécnica de Valencia, Instituto de Tecnología Química, 46022 Valencia, Spain
[e]UMR8640, CNRS – Laboratoire de Photophysique et Photochimie Moléculaire, Département de Chimie, Ecole Normale Supérieure, 24 rue Lhomond, 75231, Paris, France
[f]INSERM ERI12, 80054 Amiens, France. Groupe Universitaire de Picardie, Jules Verne, Faculté de Médecine et de Pharmacie, 80036 Amiens CHU Amiens, Laboratoire de Biochimie, 80054 Amiens, France
[g]Medical assoc. at CHU Amiens, Nord, Laboratoire de Biochimie, INSERM ERI12, place Victor Pauchet, 80054 Amiens Cedex 1, France. E-mail: morliere.patrice@chu-amiens.fr; Fax: +33 3 22 66 89 17; Tel: +33 3 22 66 86 69

† Electronic supplementary information (ESI) available: Characterization of the chlorins by mass spectrometry and details of the methods used to determine triplet molar extinction coefficients. See DOI: 10.1039/b800348c

‡ University of Porto, Faculty of Science, REQUIMTE, Department of Chemistry, 4169-007 Porto, Portugal.

agent when administered to mice bearing aggressive subcutaneous tumors induced by implanted mammary carcinoma cells.[14] While the conjugation with cyclodextrin provides fair water solubility, fluorination of porphyrinoid photosensitizers enhances their photodynamic activity.[15] It is therefore interesting to study the contribution of cyclodextrin conjugation and of fluorination on the physico-chemical basis of this increased photosensitizing potency. Along these lines, we have synthesized a *meso*-tetrakis(pentafluorophenyl)-chlorin bearing a *N*-benzylisoazolidine ring (FC) conjugated to four β-cyclodextrins (CDFC) to further assess the potential interest of this new class of chlorins as PDT photosensitizers. In the light of the effective photocytotoxic effectiveness of CDFC towards cultured human keratinocytes and to help understanding the photobiological properties of CDFC we have also undertaken a study of the photophysics of these fluorinated tetrapyrrole derivatives. We have determined their excited singlet and triplet state properties by means of time-resolved femto and nanosecond spectroscopies. A micro-environmental-dependent interaction of the cyclodextrin moieties with the fluorinated chlorin ring in the singlet and triplet excited states is observed in buffer and ethanol but it is abolished upon incorporation of CDFC into neutral Triton X100 micelles. In buffered aqueous solutions, the presence of four β-cyclodextrin macrocycles prevents CDFC from stacking interactions between hydrophobic chlorin macrocycles leading to a long-lived triplet state which forms $^1O_2$ in a good yield upon quenching by oxygen.

Materials and methods

Chemicals

Reagents for cell culture, minimum essential medium with Earle's salts (EMEM), Hanks' buffered saline solution containing 20 mM Hepes (HBSS), Dulbecco's phosphate-buffered saline (PBS), all without phenol red, fetal calf serum (FCS), trypsin and antibiotics were purchased from Gibco (Cergy-Pontoise, France). 1-Hexadecanol (Hex) and the Folin reagent were supplied by Sigma Chemical Co. (St Louis, MO, USA). Neutral Red (NR) was a Fluka (Saint-Quentin La Verier, France) product whereas Triton X100 (TX100), sodium dodecyl sulfate (SDS), absolute ethanol and DMSO (spectroscopic grade solvents) were supplied by Merck (Darmstadt, Germany). All other chemicals and solvents used in this work were of the purest available grade and were used without further purification. Phosphate buffer (10 mM, pH 7) was prepared in pure water obtained with a reverse osmosis system from Seral Pure Ces. The water exhibits a resistivity of 18 MΩ cm^{-1} and a total organic content of < 10 ppm.

Synthesis of the chlorins FC and CDFC

Synthesis of chlorin FC. The 1,3-dipolar cycloaddition reaction of *meso*-tetrakis(pentafluorophenyl)-porphyrin (prepared by a published procedure)[16] with *N*-benzylnitrone, generated *in situ* from paraformaldehyde and *N*-benzylhydroxylamine hydrochloride, in the presence of K_2CO_3, led to chlorin FC (Fig. 1). Briefly, a toluene solution (2 mL) of *meso*-tetrakis(pentafluorophenyl)-porphyrin (28.2 mg, 0.03 mmol), *N*-benzylhydroxylamine hydrochloride (18.4 mg, 0.11 mmol), paraformaldehyde (8.7 mg, 0.29 mmol) and K_2CO_3 (32.0 mg, 0.23 mmol) was heated at 60 °C, under a nitrogen atmosphere for 6 d. After further addition of *N*-benzylhydroxylamine hydrochloride (18.4 mg), paraformaldehyde (8.7 mg) and K_2CO_3 (32.0 mg), the resulting mixture was heated for two more days. The reaction mixture was cooled, filtered and washed with CH_2Cl_2. The solvents were evaporated to dryness and the residue was purified by flash chromatography using hexane–CH_2Cl_2 (2 : 3) as the eluent. The unchanged starting porphyrin (4.3 mg, 15%) was the first fraction to be collected followed by the chlorin FC (7.5 mg, 52% yield).

^{1}H NMR ($CDCl_3$, 300 MHz) δ: −2.08 (s, 2H, NH), 3.39–3.88 (m, 10H), 5.40–5.50 (m, 1H), 6.80–7.19 (m, 6H), 8.45–8.55 (m, 4H), 8.72 (broad s, 2H). LSI-MS *m/z*: 1110 (M + H) (see electronic supplementary information, ESI‡).

Synthesis of chlorin CDFC. A solution of chlorin FC (16.5 mg, 0.02 mmol) and β-cyclodextrin (200 mg, 0.17 mmol) in dry DMF (5 mL) was stirred at room temperature under a nitrogen atmosphere in the presence of K_2CO_3 (2.8 mg, 0.17 mmol), for 5 d. After that time, the reaction mixture was washed with an aqueous solution of citric acid and then neutralised with $NaHCO_3$. The resulting mixture was purified by a reverse-phase chromatography using CH_3CN–H_2O (1 : 4) to elute the chlorin CDFC. The chlorin CDFC was crystallised from acetone to give 20.0 mg (24% of yield) of a dark green powder. MALDI-MS *m/z*: 5571 $[M + 2H]^+$ (see ESI‡).

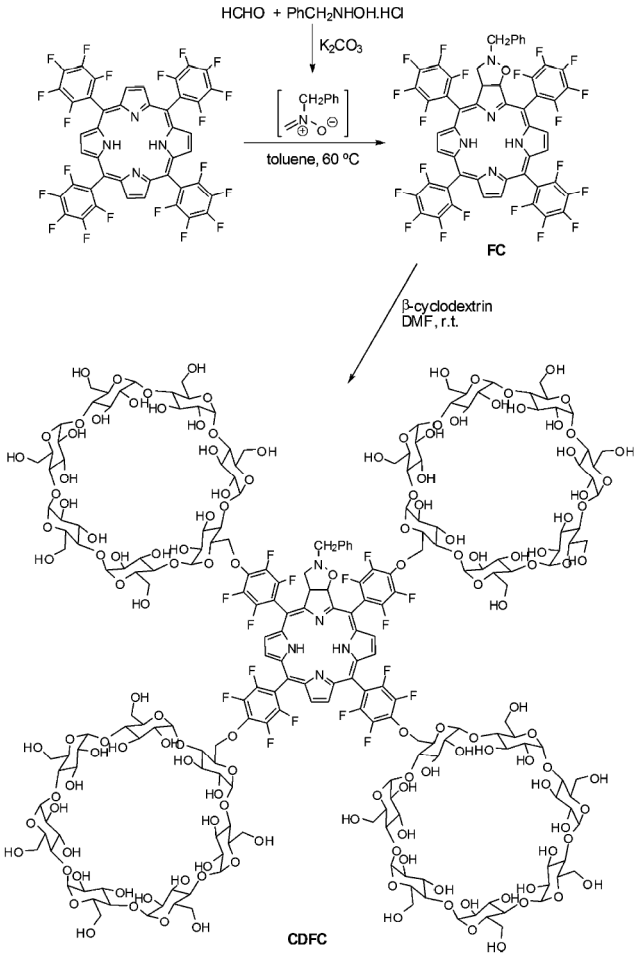

Fig. 1 Reaction scheme and structure of FC and CDFC.

Laser flash spectroscopy

Femtosecond transient absorption measurements were conducted at the Radiation Laboratory of the University of Notre Dame (Indiana, USA) using a Clark-MXR 2010 laser system (transient and an optical detection system provided by Ultrafast Systems (Helios). The source for the pump and probe pulses is the fundamental of the Clark laser system (775 nm, 1 mJ pulse^{-1}, 1 kHz repetition rate). A second harmonic generator is introduced into the path of the laser beam to provide 387 nm (3.20 eV, 130 fs) laser pulses for the pump. 5% of the fundamental is used to create a white light continuum. Before creating the white light probe the fundamental is fed through a delay providing the experimental time window of 1.5 ns with a maximum step resolution of 7 fs. The energy of the pump beam (2 mm diameter) is 5 μJ pulse^{-1} on the sample cell (2 mm light path) where it merged with the analyzing white light with an angle < 10°. After passing through the cell the white light is focused onto a 300 μm core fiber connected to a CCD spectrograph enabling time-resolved spectra recording (425–850 nm). Usually 5000 excitation pulses are averaged to obtain the transient spectrum at a set delay time. Kinetics at appropriate wavelengths are extracted from the time-resolved spectra. The 3D data are analyzed with the surface Xplorer Iite software.[17]

Nanosecond laser flash experiments were carried out using the 7th harmonic (λ_{exc} = 355 nm) of a Quantel pulsed Nd:YAG spectrum laser system (Brilliant instrument). The single pulses were ca. 10 ns (fwhm), and the energy was ca. 15 mJ pulse^{-1} at the laser output. A Xenon lamp was employed as detecting light source. The laser flash photolysis apparatus consisted of the pulsed laser, the Xe lamp, a monochromator, and a photomultiplier (PMT) system made up of a PMT, UPMT housing, and a PMT power supply. The output signal from the Tektronix oscilloscope was transferred to a personal computer for study. Samples were contained in 10 × 10 mm cells made of Suprasil quartz and were deaerated for at least 20 min with dry nitrogen or when desired, saturated with oxygen prior to the experiments. Decays were generally recorded after automatically averaging 6 to 8 traces whereas for transient spectrum acquisition absorbances (generally 5 nm intervals) resulted from averaging 3–4 data at each wavelength.

All laser spectroscopic measurements were conducted at room temperature with solutions of the photosensitizers whose absorbance was ca. 0.3 (387 nm) and 0.4 (355 nm).

Routine equipment

Flash chromatography was carried out using silica gel Merck (230–400 mesh), and the preparative thin layer chromatography was carried out with 20 × 20 cm glass plates coated with silica gel 60 (1 mm thick). Analytical TLC was carried out with pre-coated sheets with silica gel (0.2 mm thick, Merck). Waters Sep-Pak$^{®}$ Vac 35 cc (10 g) cartridges were used for solid phase extraction.

UV/Vis absorption measurements were performed with either a UVIKON 943 or a Shimadzu UV-2101PC spectrometer. A SLM AMINCO-BOWMAN (series 2) (Bioritech, Chamarande, France) fluorometer equipped with excitation and emission correction spectra was used for fluorescence measurements. Fluorescence spectra and quantum yields were obtained with solutions whose absorbance at the excitation wavelength (usually 407 nm) was ≈0.1. *meso*-Tetraphenylporphyrin was used as a reference for which Φ_F = 0.13 in toluene.[8] *meso*-Tetraphenylporphyrin is particularly suitable as a reference quantum counter for TC and CDTC since its absorbance and fluorescence spectra are close to those of the chlorins.

Fluorescence lifetimes were measured from optical cells with a light path of 5 mm containing solutions of photosensitizers whose absorbances were ≈ 0.3 using the Horiba-Jobin Yvon Nanoled single photon counting system with excitation at 373 nm with 700 ps laser pulses. The emission wavelength was set at 656 nm. Fluorescence decay measurements were further analyzed using the DAS6 software library.

Photosensitized histidine degradation

Air-saturated 10 mM phosphate buffer solutions (pH 7) containing 200 μM L-His and 5 μM TC or CDTC or meso-tetrasulfonatophenyl porphyrin ($TPPS_4$) were irradiated with increasing light doses at 365 nm. His loss was monitored by HPLC using a Whatman Partisil 10/25 SCX cation exchange column and 15 mM $NH_4H_2PO_4$ whose pH was adjusted to 2.3 by addition of phosphoric acid as mobile phase, as earlier described.[19] Irradiations, in a 1 × 1 cm cuvette (2.5 mL), were performed with an OSRAM HBO 200 W high pressure mercury lamp whose 365 nm Hg emission line was isolated as detailed before.[4] Chemical actinometry based on the photoreduction of ferrioxalate by the UV radiation was carried out according to Parker.[20]

Cell culture and treatment

The NCTC 2544 immortalized human keratinocyte cell line was purchased from ICN (Low Germany sous Bois, France). Cultures were grown in DMEM supplemented with 10% FCS, 100 U mL^{-1} penicillin and 100 μg mL^{-1} streptomycin without other additives (weekly passages 1:10 splitting ratio). Cells were trypsinized and their monolayers were seeded at about 75000 cells per 35 mm diameter plastic Petri dish containing 2.5 mL of DMEM supplemented with FCS. They were grown for 4 d at 80–90% confluence. Cells were incubated for various times with 1 mL of irradiation (1% FCS supplemental DMEM) containing the desired concentration of CDTC. After incubation, cells were thoroughly washed twice with 2 mL of HBSS before further irradiation (photosensitizer uptake photogenotoxicity). Irradiations were carried out with 1 mL of HBSS, devoid of photosensitizer, covering the cell monolayers. Sham-irradiated cells, used as controls, consisted in cells kept in the dark for the same duration and under the same environmental conditions as the irradiated cells.

Cellular uptake of CDTC

Immediately after washing, cells were mechanically scraped in 1 mL of water. After collection, 100 μL of an 11% SDS solution in 10 mM, pH 7.0 phosphate buffer were added to the cell suspension. Fifty μL of this solution were saved for protein determination using the method of Lowry with the Folin reagent.[21] The rest was used for fluorometric measurement of the photosensitizer concentration, using photosensitizer solutions of known concentrations for calibration with excitation and emission wavelengths respectively set at 409 and 649 nm. The photosensitizer concentration was

normalized to the protein content and the data are the mean ± standard deviation (SD) of at least three independent experiments, each performed in triplicates.

Irradiation

Irradiation of cell monolayers with broad band red light was carried out with a custom-built table consisting of two 300 W tungsten-halogen lamps whose light was filtered with Balzers Y54 and calflex 3000 optical filters. The lamps were placed below the 30 × 25 cm table thermostated at 37 °C. Under these conditions, most of the light arises from wavelengths in the range 500–750 nm as determined with a CS 1000A Minolta spectroradiometer. The methodology used for absolute calibration of the light fluence rate (15.2 mW cm^{-2}) has been previously published in detail.[22]

Neutral Red uptake assay

As detailed earlier, the photocytotoxic effect was determined by the NR uptake assay.[22] Challenged cells were washed and further incubated at 37 °C for 3 h with the supplemented culture medium before loading with NR. This 3 h lag was chosen to allow the initial damage to propagate but was short enough to avoid important proliferation of undamaged cells (population doubling time is about 1 day) which may alter data. The NR uptake is a widely used assay for evaluating the photocytotoxicity of exogenous drugs or hazardous compounds. It has been validated by the European Union for testing phototoxic chemicals and for the classification and labelling of hazardous chemical (EU Commission Directive 2000/33/EC).[22,23] Data are presented as the percentage of NR uptake with respect to a control consisting of sham-irradiated untreated cells. The data are the mean ± SD of at least three independent experiments, each performed in triplicates.

Results and discussion

Uptake and photocytotoxicity of the cyclodextrin conjugate

For easy and direct comparison, the photocytotoxic potential of CDFC was assessed using the same experimental procedure as that described in our previous work using tri-cationic porphyrins as photosensitizers.[22] As a consequence, prior to irradiation, the CDFC uptake was measured after incubating the NCTC 2544 keratinocytes for 3 h with increasing concentrations of the photosensitizer in FCS supplemented EMEM. Under these conditions, the CDFC uptake is practically proportional to the incubation concentration and the intracellular concentration is quite similar to that measured with the tri-cationic 5-(4-carboxyphenyl)-10,15,20-tris(1-methylpyridinium)-porphyrin poly-S-lysine conjugate (P-(Lys)$_{1.1}$) (Fig. 2A).

The CDFC photocytotoxicity estimated by the NR uptake assay was also compared to that of P-(Lys)$_{1.1}$. After incubation with 1 to 5 μM CDFC or 5 μM P-(Lys)$_{1.1}$ in FCS-supplemented EMEM NCTC 2544 keratinocytes were irradiated with increasing light doses (Fig. 2B). Control experiments were performed with cells incubated with CDFC but sham-irradiated (up to 60 min). No alteration of the NR uptake was observed with these controls as compared to native cells. Moreover, CDFC exhibits no cytotoxic effect in the dark for incubation concentrations up to 5 μM (data not shown). It turns out that CDFC is as effective a photosensitizer as our reference P-(Lys)$_{1.1}$. Thus 0% survival was observed with both CDFC and P-(Lys)$_{1.1}$ after incubation with 5 μM of the photosensitizers and irradiation for 30 min.

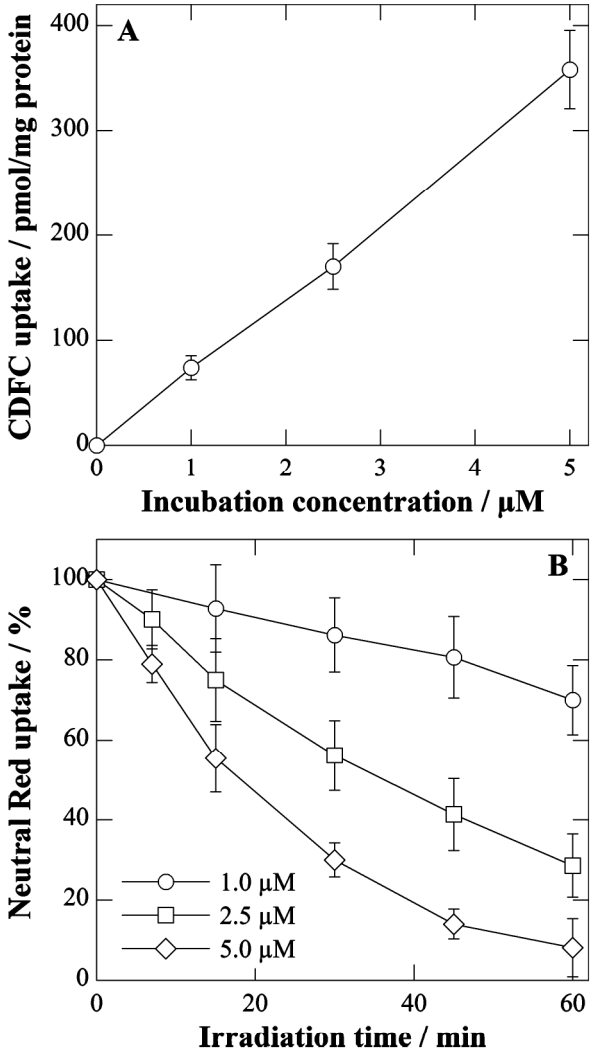

Fig. 2 (A) Uptake of CDFC as a function of the incubation concentration. Cells were incubated for 3 h with the desired chlorin concentration in FCS-supplemented EMEM. Data are the mean of at least three independent experiments performed in triplicates. (B) Cytotoxic effects photosensitized by CDFC as a function of the irradiation time and of the incubation concentration. Prior to irradiation, cells were incubated for 3 h with CDFC in FCS-supplemented EMEM and then irradiated for 30 min. A Neutral Red uptake of 100% corresponds to sham-irradiated untreated cells. Data are the mean of at least three independent experiments performed in triplicates.

In view of this excellent in vitro photocytotoxic activity, the photophysical properties of the cyclodextrin conjugate and the effect of the conjugation on the excited state properties of the chlorin ring were studied.

First singlet excited state properties of FC and CDFC

Steady state results. The absorbance spectra of CDFC in ethanol, buffer or in TX100 micelles show the characteristic features of the chlorins with the strong Soret band with maximum absorbance at ~400 nm and the four Q bands with the more

pronounced (ε ≈ 20000 M⁻¹ cm⁻¹ at ≈ 650 nm) (Table 1). The substitution of a fluorine atom at the *para* position on the four phenyl rings of FC by a β-cyclodextrin has only small effects on the position of the wavelengths of maximum absorbance of CDFC in all the solvents but the molar absorbance is notably decreased in pH 7 buffer as compared to ethanol (Fig. 3A). However, a higher molar absorbance is restored by addition of TX100. The fluorescence spectrum and the fluorescence quantum yield ($\Phi_F \approx 0.75$) of the CDFC derivative are practically unchanged in going from ethanol to buffer solutions containing Triton X100. On the other hand, addition of TX100 leads to $\Phi_F = 0.9$ for CDFC in water in comparison to that of FC in ethanol and TX100. Whereas interaction of TX100 in the micromolar range with the cavity of β-cyclodextrin cannot be excluded for CDFC, in the case of FC the pronounced polyoxyethylene glycol groups favor hydrophobic ring-ring interaction with the chlorin ring and solubilization of FC in the micellar environment.[3] Due to its limited solubility in buffer (≈ 1 μM), FC tends to readily aggregate leading to broadening of all absorption bands with strong decrease in absorbance and to a red shift and a strong quenching of the fluorescence. On the other hand, FC, in contrast to CDFC, is readily soluble in a non-polar solvent such as toluene where it strongly fluoresces ($\Phi_F = 0.61$, Table 1).

The CDFC fluorescence decay by two parallel monomolecular processes in ethanol may be explained by the presence of two structurally different molecular arrangements. It may be supposed that in such structures, the chlorin FC macrocycle is "encaged" in three-dimensional networks created by the four β-cyclodextrin rings around the chlorin with its bulky benzyl-benzimidazolidine ring. In buffer only the long-lived component is observed suggesting that, in this more polar solvent, a single positioning of the four β-cyclodextrin moieties around the chlorin FC macrocycle is imposed by the interaction of the strongly polar water molecules with the hydrophobic chlorin ring. Distinct properties of singlet excited CDFC suggesting specific arrangement of the β-cyclodextrins in ethanol and water are supported by femtosecond spectroscopy.

Ultrafast spectroscopy results. Time resolved ultrafast (picosecond) absorption spectroscopy from the lowest excited singlet state (S_1) of FC and CDFC is of practical interest since it may unravel specific interaction of the β-cyclodextrins moieties with the chlorin ring in the S_1 state. Being given that the fluorescence lifetimes of FC and CDFC are of the order of several nanoseconds, there exists a spectroscopic window extending from light absorption to several hundred picoseconds in which a quasi stable S_1 state is reached allowing study by appropriate technology of transient absorption from the S_1 state to upper excited singlet states (S_n) of the molecules. Thus, in principle the study of excited singlet states by ultra-fast spectroscopy is comparable to that of the well-known absorption spectroscopy of the triplet states.

Fig. 1A shows the transient absorbance changes observed with CDFC in buffer and ethanol at short and "long" time after excitation with 0.15 ps, 387 nm laser light pulses. The strong negative absorbance change in the 650–680 nm region is mainly due to the fluorescence of CDFC (see Fig. 3B) with some contribution of the bleaching of the S_0 CDFC absorbance. In this regard, the ≈ 50% drop recorded within 1.5 ns in buffer (Fig. 4A) and in ethanol (which are not shown) cannot be explained on

Table 1 Absorbance and fluorescence characteristics of tetrakis(4-carboxyphenyl)-chlorin (FC) and meso-(tetra-β-cyclodextrin-tetrakis-fluorophenyl)-chlorin (CDFC) in various solvents[a]

CDFC						FC				
	Absorbance		Fluorescence			Absorbance		Fluorescence		
Solvent	λ_{max}/nm	ε/M⁻¹ cm⁻¹	λ_{max}/nm	Φ_F	τ_F/ns	λ_{max}/nm	ε/M⁻¹ cm⁻¹	λ_{max}/nm	Φ_F	τ_F/ns
Ethanol	407	135 000	646	0.70	1.36 (20.3%) 7.46 (79.7%)	403	85 000	654	0.61	7.0
	502	13 300				501	17 000			
	528	5 200				526	≈ 1 000			
	588	4 000				594	≈ 700			
	645	24 000				646	42 500			
pH 7 buffer[b]	404	99 500	648	≈ 0.2	0.37	401	55 000[d]	661	0.0013[d]	
	503	9 000				502	2 600[d]			
	529	3 600				531				
	588	3 000				594				
	614	22 800								
Triton X100[c]	402	122 000	648	0.90	6.30	403	179 000	656	0.55	
	502	11 000				503	19 600			
	528	4 200				530	4 400			
	592	3 900				595	5 000			
	615	23 000				650	45 100			
Toluene						407	162 500	653	0.61	
						504	17 300			
						532	12 600			
						597	12 100			
						650	43 200			

[a] λ_{max}: wavelengths of maxima of absorbance and fluorescence; ε: molar absorbance; Φ_F: fluorescence quantum yield; τ_F: fluorescence lifetime. [b] 10 mM phosphate buffer. [c] 0.3% Triton X100 in pH 7, 10 mM phosphate buffer. [d] Unstable solution due to poor solubility.

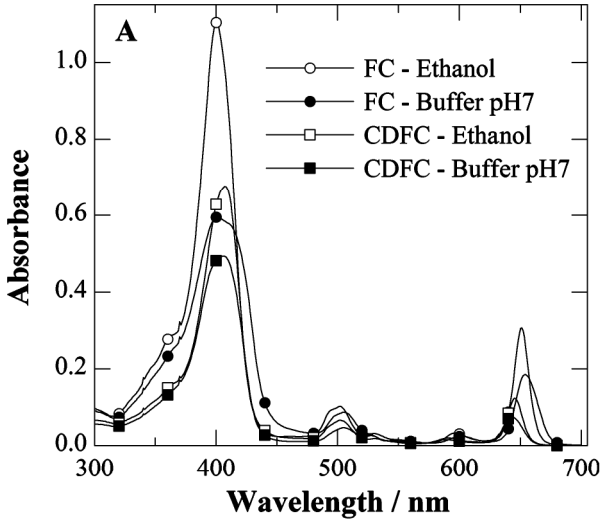

Fig. 3 (A) Absorbance spectra of FC (●)(○) and CDFC (□)(■) in pH 7, 10 mM buffer (●)(■) and in ethanol (○)(□). (B) Fluorescence spectra of FC and CDFC in pH 7, 10 mM phosphate buffer and in ethanol. Symbols are the same as in (A). The excitation wavelength was 400 and 407 nm for FC and CDFC, respectively. The absorbance of the solutions (light path: 1 cm) was ≤0.05 in all the cases. The sensitivity of the detection was increased 100-fold for FC in buffer. The temperature was 23 °C.

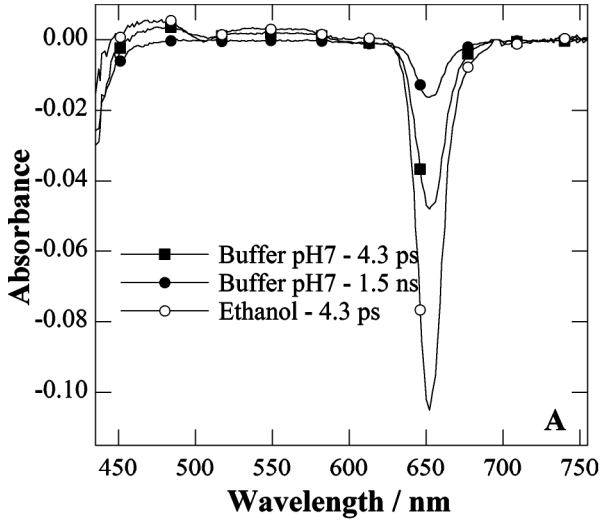

Fig. 4 (A) Transient difference absorbance spectra obtained 4.3 ps (■)(○) and 1510 ps (●) with femtosecond 387 nm laser flash photolysis of CDFC in air-saturated pH 7, 10 mM phosphate buffer (■)(●) and ethanol (○). (B) Decays of the transient absorbance at 475 nm after femtosecond 387 nm laser flash photolysis of CDFC in pH 7, air-saturated 10 mM phosphate buffer (■), ethanol (□) or TX100 (⊠) shown in Fig. 2B and of FC in ethanol (○).

the basis of the fluorescence lifetimes reported in Table 1. Positive absorbance changes are observed in the visible wavelength range and the time dependence at 475 nm is presented in Fig. 4B. With the CDFC derivative, the S_1S_n absorption is considerably reduced (about 2/3) via a monomolecular process (rate constant ~5 ps^{-1}) which parallels the fluorescence drop of Fig. 4A, an almost constant fluorescence being observed at times greater than 30 ps (data not shown). On the other hand, a comparable decay is not observed with FC (Fig. 4B). This observation is consistent with an interaction of the β-cyclodextrins with the chlorin ring perturbing the CDFC S_1 state and leading to the Φ_F drop observed in ethanol and buffer with CDFC (Table 1). Thus the radiative energy loss may possibly be due to increased non-radiative internal conversion and/or to reaction of the S_1 state with proximal OH groups of the four β-cyclodextrins and/or solvent molecules encaged in the CD cavities whose local concentration is by force quite high.

In this regard, slight modification of the CDFC ground state absorbance spectrum is observed after laser flash experiments. Interestingly, when CDFC is incorporated into TX100 micelles, the fluorescence lifetime (Table 1) remains close to those measured in buffer or ethanol and a much smaller S_1S_n absorption (Fig. 4B) and a much higher Φ_F (Table 1) are observed. These results suggest an important conformational reorganization induced by the TX100 micelles whose relatively small molecular size, *e.g.* ~0.5 nm, increases strongly intramolecular constraints including the reorganization of the cyclodextrin "cage" and the interaction with the chlorin ring.[25]

Triplet state properties of FC and CDFC

Porphyrins and chlorins are archetypes of the so-called photodynamic agents. They are recognized as type II photodynamic agents through activation of dioxygen molecules by energy transfer

from their lowest excited triplet state ($^3T_1$) to oxygen triplet ground state to form singlet oxygen ($^1O_2$). Type I electron transfer reactions although much less favoured, are also possible because tetrapyrroles are electron donors to strong electrophiles such as nitroaromatic rules.[4] As a result, it is essential to characterise the triplet state properties of a potential PDT photosensitizer such as CDFC. Transient absorbance spectrum, quantum yield of $^3T_1$ formation and rate constant of interaction of $^3T_1$ with oxygen are the most relevant parameters which may help to understand its interesting photophysical activity. Fluorescence lifetimes of the order of 10 ns (Table 1) suggest that the triplet states of FC and CDFC are populated with a rate constant of $>10^8$ s^{-1} consistent with a $S_1(\pi,\pi^*) \rightarrow {}^3T_1(\pi,\pi^*)$ process.

Triplet state transient spectra. Fig. 5A shows the transient difference absorbance spectra of CDFC measured at various times after 355 nm nanosecond laser flash spectroscopy of CDFC in de-

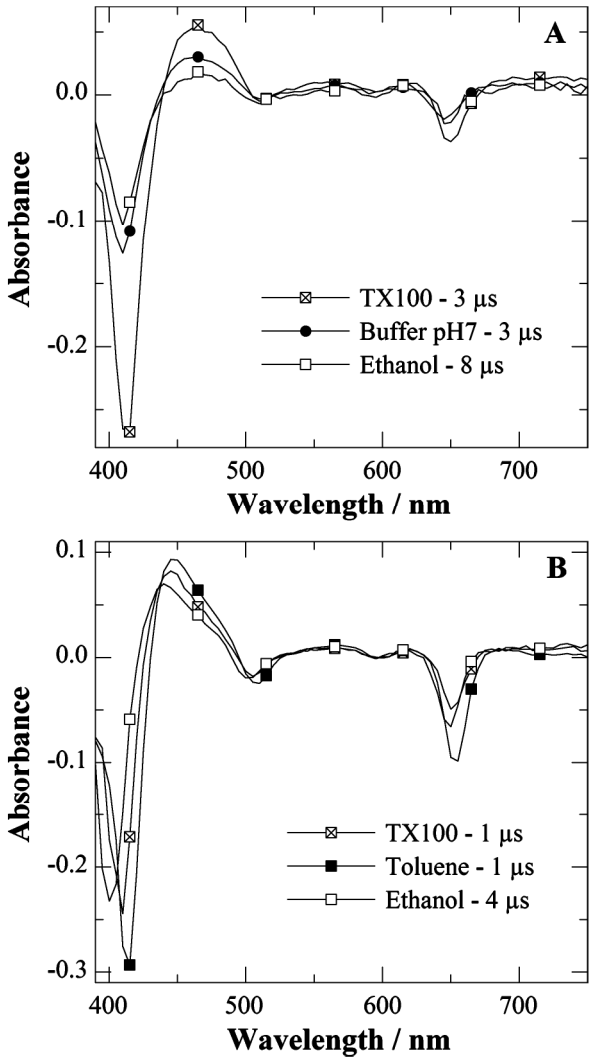

Fig. 5 (A) Transient difference absorbance spectra obtained 3 µs (●)(☒) and 8 µs (□) after 355 nm laser flash photolysis of 16 µM CDFC in pH 7, 10 mM phosphate buffer (●), TX100 (☒) and ethanol (□). All the solutions were saturated with N_2. (B) Transient difference absorbance spectra obtained 1 µs (☒)(■) and 4 µs (□) after 355 nm laser flash photolysis of 12 µM FC in toluene (■), TX100 (☒) and ethanol (□). All the solutions were saturated with N_2.

aerated buffer, ethanol and TX100. It can be seen that the spectral shapes are practically independent of solvents and time delays after the laser pulse. All the transient species show a strong broad absorbance with maximum around 460 nm and minor maxima at about 560, 670 and 720 nm corresponding to transitions between $^3T_1$ to higher triplet levels. $^3T_1$ as generally observed with this class of molecules.[22,23] The negative absorbance observed in the absorbance region of the Soret and main Q bands result from the depopulation of ground state molecules by the exciting laser flash to produce $^3T_1$ molecules.

The decay of these transient triplet absorptions strongly depends on solvents. While the CDFC triplet slowly decays in the aerated TX100 micellar solution by a simple first order process with a lifetime of 2.5 µs (Table 2), more complex kinetics are observed in ethanol and water (Fig. 6). In these two last solvents, a fast initial decay yields a longer lived species whose spectral characteristics (Fig. 5A) are apparently the same as those of the short-lived components. The first order decay of these long-lived transients apparently leads to partial recovery of the ground state absorbance of Soret and first Q bands (Fig. 6) supporting the contention that these species have structural chemical features similar to the ground state CDFC. A major difference between the longer lived species of CDFC in ethanol and in the buffered solution is that in the aqueous medium the longer lived species lifetime is 427 µs while it is only 1.2 µs in ethanol in which only partial recovery of the CDFC ground state absorbance is observed after the triplet molecules have decayed. However femto- and nano-second laser spectroscopy data do not make it possible to conclude whether in ethanol the photochemistry involves upper singlet states or the triplet state of CDFC.

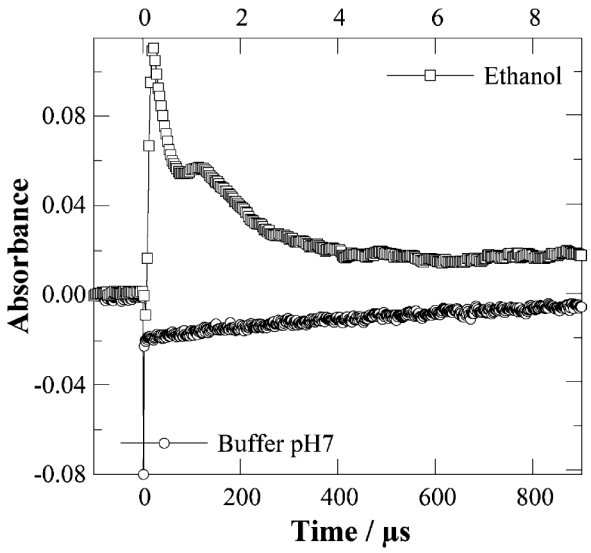

Fig. 6 Decay of the transient absorbance at 460 nm in N_2-saturated solutions after nanosecond 355 nm laser flash photolysis of 16 µM CDFC in ethanol (□) and recovery of absorbance at 650 nm in pH 7, 10 mM phosphate buffer (○).

The contribution of the four β-cyclodextrins to the triplet state properties of CDFC is evidenced by the study of FC whose difference absorbance spectra after laser flash excitation under various solvent conditions are presented in Fig. 5B. While the bandwidth of the difference absorbance band of FC in the

Table 2 Triplet-state parameters of meso-tetrakis(pentafluorophenyl)-chlorin (FC) and meso-tetrakis-3-cyclodextrin-(tetrafluorophenyl)-chlorin (CDFC) in various solvents at 25 °C

FC					CDFC			
Solvent	λ_{max}/nm[a]	ε/M^{-1} cm^{-1}	τ_T/μs	$\Delta(\varepsilon_T)^{\lambda}$ × 10^{-3}/M^{-1} cm^{-1}	λ_{max}/nm	ε/M^{-1} cm^{-1}	τ_T/μs	$\Delta(\varepsilon_T)^{\lambda}$ × 10^{-3}/M^{-1} cm^{-1}
Ethanol	450	50000	140 ± 1	1.5 ± 0.1	460	20000[b]	0.25 ± 0.01[b] 1.18 ± 0.04[b]	2.2 ± 0.3[b]
pH 7 buffer					452	33000[c]	2.7 ± 0.6[c] 2.7 ± 0.4[c]	1.8 ± 0.2[c]
Triton X100	455	53000	217 ± 2	2.8 ± 0.2[d]	455	32000	213 ± 1	0.61 ± 0.05[d]
Toluene	445	~42000 32000	240 ± 2					

[a] λ_{max}: wavelength of maximum absorbance of difference transient absorption spectrum or molar absorbance of triplet–triplet. This maximum estimated by method B unless otherwise stated. [b] τ_T: triplet lifetime in de-aerated solution. $\Delta(\varepsilon_T)^{\lambda}$: molar extinction coefficient at λ_{max} corrected for triplet quenching by oxygen. [c] 20 mM phosphate buffer and 0.15 M NaCl. [d] 0.3% Triton X100 in pH 7, 10 mM phosphate buffer and 0.15 M NaCl. [e] Two species (see text). τ_T and $\Delta(\varepsilon_T)^{\lambda}$ hold for the longer lived species. [f] Assuming Φ_T solvent-independent to be same as in buffer (1.0 with error of 0.2). [g] Method A.

440–500 nm region with a maximum at about 450 nm, is somewhat narrower than that of CDFC, the wavelengths of the secondary maxima in the visible region are rather similar for the two derivatives. In contrast to CDFC, the FC transient absorptions decay by simple first order processes characterized by rather long lifetimes in all the solvents (Table 2).

The triplet nature of all these species is supported by their quenching by oxygen in O_2- and air-saturated solutions which follows pseudo-first order kinetics. However, the similar reaction rate constant $k_q(O_2)$ obtained with the CDFC derivative in TX100 micelles suggests that the bulky cyclodextrin assembly in the chlorin-ring vicinity intervenes in the quenching process (Table 2).

Determination of triplet molar extinction coefficients. Triplet identification was further ascertained using the $^3T_1$ state of FC of a 17 μM FC solution in toluene as an energy donor to 3-carotene (3-car). Upon pulse-laser excitation, the $^3T_1$ state energy is transferred to 3-car. Direct population of the 3-carotene triplet (^{3}3-car) is negligible since the intersystem crossing yield is exceedingly small.[29] However the β-car $^3T_1$ state can be populated by energy transfer from molecules with $^3T_1$ states of higher energy. By this means, using the so-called comparative method, a molar extinction coefficient of ^{3}β-car has been determined to be ε = 100000 M^{-1} cm^{-1} at 520 nm. This wavelength has two advantages since it is close to the absorbance maximum of ^{3}β-car in toluene, and the β-car ground state molar absorbance at 520 nm is only 1900 M^{-1} cm^{-1}.[30,31] Assuming a transfer efficiency of unity from the long-lived FC triplet state to the β-car triplet, the concentration of molecules in the first excited FC triplet state can be obtained from which molar extinction coefficients are measured (method A). By this method, the molar extinction coefficient of triplet FC at 450 nm, the wavelength of maximum absorbance, can be estimated to be ε = 53000 M^{-1} cm^{-1} (see ESI†).

Another method (method B) allowing an estimate of the ε ($^3T_1$) triplet FC is based on the determination of the ratio (a) of the FC molecules in the $^3T_1$ state [^{3}FC] to the total ground state [FC_0] concentration. At any time (t) after the laser pulse and at any wavelength (λ), the transient difference absorbance $\Delta Abs(t)$ must be for simple first order processes: $\Delta Abs(t) = Abs(^3FC)(t) - a \times Abs(FC_0)$.[27,32] With this method, ε of ^{3}FC at 450 nm is found to be 42000 M^{-1} cm^{-1}, in fair agreement with the value estimated by the energy transfer method (see ESI†). Thus, an average value of 50000 M^{-1} cm^{-1} would be realistic being given the uncertainty inherent to such determinations. Molar extinction coefficients estimated using method B are given for both FC and CDFC in all the studied solvents. Overall, it can be seen that these values are smaller for CDFC. However, they are consistent with molar extinction coefficients previously reported for meso-tetrakis-(hydroxyphenyl)-chlorin (Foscan®) and glucosyl-conjugated derivatives synthesized in cyclodextrins.[27]

Triplet quantum yield of FC and CDFC. Knowing the molar absorbance of the FC $^3T_1$ state, it is possible to estimate the ^3T-formation quantum yield (Φ_T) by the comparative method.[33] The meso-tetraphenylporphyrin (TPP) was used as an actinometer since its Φ_T is 0.8 in toluene and $\Delta\varepsilon = \varepsilon(^3T) - \varepsilon(S_0) = 35000$ M^{-1} cm^{-1} at 450 nm.[34] To this end a solution of TPP with an absorbance corresponding to that of 13 μM FC at 355 nm was prepared in toluene to ensure equal population of singlet states of FC and TPP under excitation with the same laser energy.[3] Conveniently, ground state depletion effects are negligible (see ESI†). The Φ_T of FC can be easily calculated to 0.7 based on the maximum difference transient absorbance of TPP and FC triplet and the $\Delta\varepsilon$ value of FC (35000 M^{-1} cm^{-1}) at 450 nm.[34] Fig. 5B suggests that the Φ_T value of 0.7 is probably valid for the other media in view of the spectral similarities of FC triplet in the studied solvents. As for CDFC, its insolubility in toluene and the complex triplet behavior in ethanol preclude any direct Φ_T determination. However, using the FC triplet as an actinometer for the CDFC triplet in TX100 (Fig. 5A), it can be suggested that the Φ_T of CDFC in this solvent is about the same as that of FC taking into account the lower molar extinction coefficient of triplet CDFC in TX100 (see Table 2). It can be seen that in all the cases $\Phi_T - \Phi_\Delta$ is ≤ 0.1, suggesting the intervention of internal conversion processes in the deactivation of the excited molecules in support to ultra-fast spectroscopic data.

Quantum yield of $^1O_2$ formation in buffered aqueous solution

The formation of a long-lived CDFC triplet state (Fig. 6), quenched by dioxygen at diffusion controlled rate (Table 2) in

buffered aqueous solutions suggests the production of O_2. The $^1O_2$ generation was detected using Ellman's reagent as O_2 probe since its photosensitized oxidation occurs *via* a type II photodynamic mechanism in buffered aqueous solutions[19,20]. The quantity of O_2 produced was assessed using comparative methodology with meso-tetra(4-sulfonatophenyl)porphyrin (TPPS$_4$) as a reference water-soluble photosensitizer for which the quantum efficiency of $^1O_2$ generation in cell culture has been reported to be 0.6[21]. The 655 nm light dose-dependences of the consumption of Ellman's reagent at low light doses follows first order kinetics, as seen in the presence of DPBF in solutions containing TPPS$_4$ or CDFC or FC as photosensitizers. The first order reaction rate constants normalized to the fraction of absorbed light ($1 - 10^{-A_{655}}$, A_{655} being the absorbance of the solutions at 655 nm) are proportional to the quantum efficiency of $^1O_2$ generation. Assuming $\Phi(^1O_2) = 0.6$ for TPPS$_4$, it turns out that $\Phi(^1O_2) = 0.4$ and < 0.05 for CDFC and FC, respectively. Thus, although the Φ_Δ of CDFC could not be readily determined in buffer and being given the uncertainties inherent to the comparative methods used for Φ_Δ (see above) and $\Phi(^1O_2)$ determination, it may be proposed that the quenching of the CDFC triplets by dioxygen generates $^1O_2$ with high efficiency. On the other hand, the negligible O_2 generation by FC is readily understandable since in buffer, FC rapidly aggregates and precipitates (see section on FC singlet excited state properties).

Conclusions

The goals of this work was to synthesize an effective water-soluble chlorin photosensitizer for which or other members of the same family as vectorization for multimodal photochemotherapy applications is granted. It appears that up to four β-cyclodextrins can be conjugated to a bulky meso-ethynylalkoxyphenyl chlorin with the reduced pyrrole ring linked to a monosaccharide may provide a water-soluble photosensitizer active towards cultured proliferating human keratinocytes. The cell-penetrating property of the photosensitizer is an enticing lead for potential PDT. Cyclodextrins are used as topical drug carriers both by keeping hydrophobic drug molecules in solution and delivering them to the skin, where they can interact with lipophilic cell components of the skin after disturbance of the barrier function[5,6]. Moreover, for topical PDT, skin lesions are usually submitted to prior curettage which decreases the stratum corneum barrier properties thereby possibly enhancing skin penetration of the conjugates.

This work demonstrates that the first excited triplet state of such derivatives can be highly populated in a variety of microenvironments thereby generating O_2, a major cytotoxin. Accordingly, an obvious and immediate development of this work, owing to the fairly good fluorescence of the functionalized chlorin ring, will be the study of the time-dependent intracellular localization of the conjugate in cultured living cells by micro(spectro)fluorometric techniques. The full or partial removal of β-cyclodextrins through slow hydrolysis of the ether bonds by O-alkyl cleavage enzymes may be an effective way of modulating the intracellular localization/partition of the chlorin core within hydrophilic cytosolic sites and cell membranes, thus developing an effective photo-oxidative stress at multiple sites. Such a study is a prerequisite for a further extension of this work to skin tumor bearing animals.

Acknowledgements

JNS, PF and RS are grateful to Professor P. Kaiser (Radiation Laboratory, University of Notre Dame) for having given us the possibility to use the femtosecond laser flash spectroscopic set-up and to Dr I. Rebel and Dr P. Sudeep of his laboratory for their advice regarding experimental details. We also thank Dr C. Veyret-Bizet at the Museum d'Histoire Naturelle for help in some routine spectroscopic measurements. PF and JNS thank the Portuguese Society of Dermatology for several travel grants to USA and France during the course of this study. The Aveiro and Ribeirão Preto groups thank the CAPES/GRICES program for funding.

References

1 T. J. Dougherty, C. J. Gomer, B. W. Henderson, G. Jori, D. Kessel, M. Korbelik, J. Moan and Q. Peng, Photodynamic therapy, *J. Natl. Cancer Inst.*, 1998, **90**, 889–905.
2 R. K. Pandey and T. Zheng, Porphyrins as photosensitizers in photodynamic therapy, in *The Porphyrin Handbook*, ed. K. M. Kadish, K. M. Smith and R. Guilard, Academic Press, San Diego, 2000, pp. 157–230.
3 C. Schmidt-Erfurth and T. Hasan, Mechanisms of action of photodynamic therapy with verteporfin for the treatment of age-related macular degeneration, *Surv. Ophthalmol.*, 2000, **45**, 195–214.
4 A. M. Soler, L. Warloe, A. Berner and K. L. Gederaas, A follow-up study of recurrence and systemic immunosuppressive response in basal and nodular basal cell carcinomas treated with topical 5-aminolevulinic acid-based photodynamic therapy: one and two year follow-up, *Br. J. Dermatol.*, 2001, **145**, 467–471.
5 J.-P. Rochaix, P. Moulinoux, S. Golstein, R. Santus, L. Dubertret and D. Lagrange, Interaction of human serum low density lipoproteins with porphyrins: a spectroscopic and photochemical study, *Photochem. Photobiol.*, 1986, **43**, 721–729.
6 G. Jori, M. Beltramini, T. Reddi, D. Salvatori, A. Pagnan, L. Zinovi, L. Fanin and T. Tarrow, Evidence for a major role of plasma lipoproteins as tumour-porphyrin carriers in vivo, *Cancer Lett.*, 1984, **24**, 291–297.
7 K. Chen, L. Hui, H. A. Tose and C. M. Hain, Efficient synthesis and photodynamic activity of porphyrin-cyclodextrin conjugates targeting and photokilling cancer cells, *Bioconjug. Chem.*, 2004, **15**, 1019–1029.
8 H. Kato, K. Furukawa, M. Sato, T. Okimaka, Y. Kuroki, M. Kawahara, M. Tokuoka, T. Miyazawa, T. Yano, K. Mukai, T. Shinashi and T. Horiuchi, Phase II clinical study of photodynamic therapy using mono-L-aspartyl chlorin e6 and diode laser for early stage superficial squamous cell carcinoma of the lung, *Lung Cancer*, 2003, **42**, 103–111.
9 S. L. Chang and A. K. Banga, Transdermal iontophoretic delivery of hydrocortisone from cyclodextrin solutions, *J. Pharm. Pharmacol.*, 1988, **50**, 533–610.
10 R. T. Lopez, T. H. O'Dell, M. V. Bentley and T. Mora, Influence of cyclodextrin complexation on the in vitro permeation and skin metabolism of dexamethasone, *Int. J. Pharm.*, 2000, **200**, 177–187.
11 H. Marsada and H. Arima, Dynamic aspects in microdermal and dermal delivery, *Adv. Drug Deliv. Rev.*, 1999, **36**, 81–99.
12 K. Uekama, T. Hirayama and T. Irie, Cyclodextrin drug carrier systems, *Chem. Rev.*, 1998, **98**, 2045–2076.
13 M. Tanaka, Y. Iwata, Y. Kawada, K. Tomizuka, H. Matsuda, H. Arima and S. Tsuchiya, Effect of 2-hydroxypropyl-beta-cyclodextrin on percutaneous absorption of methyl nicotinate, *J. Pharm. Pharmacol.*, 1995, **47**, 597–599.
14 I. Rubinov, A. Synytsya, P. Petrusova, M. Kuc, M. Dvorak and V. Kral, Novel porphyrin conjugates with a potent photodynamic antitumor effect: differential efficacy of mono- and bis-beta-cyclodextrin derivatives *in vitro* and *in vivo*, *Photochem. Photobiol.*, 2006, **82**, 432–438.
15 G. Li, A. Graham, W. Potter, Z. D. Grossman, A. Oseroff, T. J. Dougherty and R. K. Pandey, A simple and efficient approach for the synthesis of fluorinated and nonfluorinated octaethylporphyrin-based benzochlorins with variable lipophilicity, their *in vivo* tumor uptake, and the preliminary *in vitro* photosensitizing efficacy, *J. Org. Chem.*, 2001, **66**, 1316–1325.

16 M. G. A. R. Gonsalves, J. M. T. B. Vieira and M. M. Pereira, Some recent aspects related to the synthesis of meso-substituted porphyrins, *J. Heterocycl. Chem.*, 1991, **28**, 635–640.
17 I. Robel, V. Subramanian, M. Kuno and P. V. Kamat, Quantum dot solar cells. Harvesting light energy with CdSe nanocrystals molecularly linked to mesoscopic TiO_2 films, *J. Am. Chem. Soc.*, 2006, **128**, 2385–2393.
18 T. T. Figueiredo, R. A. W. Johnstone, A. M. P. Santos-Naylor, D. Bicknell and P. Douglas, Determination of fluorescence yields, triplet lifetimes and singlet oxygen yields of some insoluble porphyrins and metalloporphyrins in aqueous solvents and in aqueous media, *Photochem. Photobiol.*, 1990, **52**, 159–164.
19 P. Mathieu, T. Bonet, M. A. Miranda, J. V. Castell and R. Sastre, Primary photochemical processes of the photoreactive xenobiotic oxolinic acid: a study by laser flash photolysis and steady-state irradiation, *Photochem. Photobiol.*, 2004, **80**, 535–541.
20 C. A. Parker, *Photoluminescence of Solutions*, Elsevier Publishing Co., Amsterdam, 1968, pp. 262–276.
21 H. Levy, N. J. Rosenblatt, A. E. Lurie and R. J. Bendel, Precise measurement of the Folin phenol reagent, *J. Biol. Chem.*, 1951, **193**, 265–275.
22 J. S. Silva, J. Basílio, J. P. Pinto, M. G. Neves, A. C. Tomé, J.-C. Mazière, C. Moreno, R. Santus, J. A. Cavaleiro, P. Filipe and P. Morlière, Photosensitization of the photodynamic activity of a cationic porphyrin towards proliferating keratinocytes by encapsulation in poly-L-lysine, *Photochem. Photobiol. Sci.*, 2006, **5**, 179–183.
23 Commission Directive 2000/39/EC, *Official Journal of the European Communities*, 8.6.2000 L 139/190–L 139/197.
24 X. Wang, J. Wang, Y. Wang, Z. Z. Chen and R. Tang, Study on the multi-spectral mechanism of cisplatin-calf thymus DNA interaction in the presence of 6-mercaptonicotinic acid-modified gold nanoparticles, *J. Photochem. Photobiol. A*, 2006, **183**, 194–201.
25 H. H. Patterle, Shape and size of the nonelectrolyte molecule Lithium Xylonate in aqueous solution, *J. Phys. Chem.*, 1958, **84**, 2569–2577.
26 P. Kohen, R. Sharma and I. G. Hirschberg, *Photobiology*, Academic Press, San Diego, 1995, pp. 23–35.
27 A. Barrisa-Sánchez, A. Kasselouri, M. C. Desrochers, J. Bois, P. Maillard, H. M. da Silveira, A. C. Tedesco, P. Prognon and J. Delaite, Photo-Lysed liposomes of chlorin e6 and de-Uleine and perdeuterio and their associations with cyclodextrins, *J. Photochem. Photobiol. B*, 2005, **81**, 154–162.
28 A. Harriman, Luminescence of porphyrins and metalloporphyrins. Part 4.—Heavy-atom effects, *J. Chem. Soc. Faraday Trans. 2*, 1976, **77**, 1281–1291.
29 R. T. Dullinger, W. H. Woodruff and M. A. J. Rodgers, The lifetime of excited singlet state of β-carotene: consequences in photosynthetic harvesting, *Photochem. Photobiol.*, 1981, **33**, 273–277.
30 B. R. Nielsen, K. Jorgensen and F. H. Skibsted, Triplet–triplet extinction coefficients, rate constants of triplet decay and rate constants of oxygen quenching of triplet state carotenoids generated by the LED photosensitizer β-apo-8′-carotenal at 298 K, *J. Photochem. Photobiol. A: Chem.*, 2001, **142**, 127–133.
31 R. V. Benavides, D. J. Land and T. G. Truscott, *Flash photolysis and pulse radiolysis: Contributions to the chemistry of biology and medicine*, Pergamon Press, New York, 1983, pp. 11–16.
32 Y. H. Meyer and P. Plaza, Ultrafast excited singlet state absorption and fluorescence of carotenes in solution, *J. Photochem. Photobiol. A: Chem.*, 1995, **2000**, 331–349.
33 S. Baier, D. J. Land, W. G. Rowan and M. W. Bates, Singlet oxygen generation of porphyrins, chlorins and phthalocyanines, *Photochem. Photobiol.*, 1996, **58**, 322–328.
34 V. J. Stella, V. M. Rao, E. A. Zannou and V. V. Zia, Mechanisms of drug release from cyclodextrin complexes, *Adv. Drug Deliv. Rev.*, 1999, **36**, 3–16.
35 P. Loftsson and M. Masson, Cyclodextrins in topical drug formulations: theory and practice, *Int. J. Pharm.*, 2001, **225**, 15–30.

Bio-Medical Materials and Engineering 16 (2006) S.47–S15
IOS Press

Photodynamic therapies: Principles and present medical applications

João N. Silva[a], Paulo Filipe[a], Patrice Morlière[b], Jean Claude Mazière[b], João P. Freitas[a], José L. Cirne de Castro[c] and René Santus[b,*]

[a] *Clínica Universitária de Dermatologia, Hospital de Santa Maria, Lisbon, Portugal*
[b] *INSERM ERI 12, Laboratoire de Biochimie, CHU Amiens, Amiens, France*
[c] *INSERM U 697, Institut de Recherche sur la Peau, Hôpital Saint Louis et Muséum National d'Histoire Naturelle, Paris, France*

Abstract. Photodynamic therapy (PDT) by porphyrins and related tetrapyrrolic derivatives is an emerging new treatment modality of tumors of lung, esophagus and skin and of age related macular degeneration. Phase II clinical trials in other pathologies such as re-stenoses after angioplasty are also underway. Under systemic conditions, the prospect of porphyrin photosensitizers by serum low density lipoproteins and their specific delivery to tumor cells and vasculature is a determinant of treatment effectiveness. However, this effectiveness can be improved by increasing the selectivity of the photosensitizer uptake by tumors and by using photosensitizers absorbing light in the 650–800 nm range where tissues have the highest transmittance. Another treatment showing great promise is the PDT of skin cancers after topical application of the protoporphyrin IX precursor delta aminolevulinic acid (or its ester forms). In all the cases, the photosensitizers should be rapidly cleared to avoid a long lasting skin photosensitivity.

1. Introduction

Phototherapies solely involve the irradiation of human body with light. On the other hand, photochemotherapies combine the action of a photoactive drug (or photosensitizer) with irradiation with near UV or visible light. The treatment of neonatal jaundice by blue/green light or of psoriasis by UVB light are examples of phototherapies. Nowadays, two types of photochemotherapies are encountered in the hospital practice. First, in the seventies, PUVA therapy based on the combination of psoralens with illumination of diseases areas with the UVA radiation was developed. Psoriasis, a benign skin proliferative disease well responds to PUVA therapy [1]. In the nineties, photodynamic therapy (PDT) emerged as a new treatment modality of tumors and other proliferative diseases or pre-cancerous status [2]. A mixture of porphyrins called Photofrin® was first authorized in 1994 for the treatment of lung and esophagus cancers. In addition to hollow organs, the main body sites presently concerned with PDT are skin and eyes; e.g. organs that are easily accessible to irradiation by conventional (skin and eyes) or fiber optics (hollow organs). The main difference between PUVA therapy and PDT is that in contrast to the former, the latter requires well-oxygenated tissues since its effectiveness results from oxygen activation after absorption of light by the photosensitizer [2]. PDT has two major advantages. First, it can be carried

*Corresponding author: René Santus, INSERM U697, Institut de Recherche sur la Peau, Pavillon Bazin, Hôpital Claude Vellefaux, 75475 Paris cedex 10, France. Tel.: +33 (0) 1 40 37 93 26; E-mail: santus@rmnhn.fr.

out with patients for whom previous therapies have failed without introducing unacceptable additional systemic toxicity. Second, it can be repeated several times.

2. Basic photophysics of PDT

This concept is based on photodynamic reactions. These are oxygen-dependent photosensitized reactions in which a substrate (S) (here, a biomolecule) is destroyed only in the presence of a chromophore molecule called a photosensitizer (P) that absorbs light. At low P concentration, according to the Beer–Lambert law the amount of light absorbed is proportional to the incident light dose and to the absorbance of the photosensitizer. Light absorption promotes P from the singlet ground state to the first singlet excited state whose deactivation occurs in the nanosecond time scale either by emitting a fluorescence or by converting P into a long-lived (several microseconds to milliseconds) excited state called a triplet state. There are two types of photodynamic reactions. The so-called "type 1 photodynamic reactions" involve the formation of radical species. The photosensitizer (P) in its triplet state is semi-reduced (formation of $P^{\bullet-}$) by reacting with S which is semi oxidized (formation of $S^{\bullet+}$). Then, molecular oxygen reacts with $S^{\bullet+}$ and $P^{\bullet-}$ to yield the oxidized S and the $O_2^{\bullet-}$ radical-anion, respectively. Alternatively, in a "type 2 photodynamic reaction", the photosensitizer in its triplet state returns to the ground state by transferring its excess electronic energy to molecular oxygen thereby producing singlet oxygen ($^1O_2$), a major cytotoxin. Amino acids such as Trp, His, Cys, Met, purines (essentially guanine), vitamins E and C and polyunsaturated fatty acids are examples of biologically relevant photodynamic substrates. Well-known photosensitizers include several families of aromatic and heterocyclic compounds such as pyrenes, xanthenes, phenothiazines, porphyrins and chlorins [3]. The PDT photosensitizers are generally tetrapyrrole derivatives, e.g. porphyrins and chlorins which mainly induce type 2 photodynamic reactions with singlet oxygen production.

3. Critical parameters of PDT effectiveness

These are tissue light penetration and specificity of photosensitizer delivery.

3.1. Light penetration

From above considerations on photodynamic reactions, it is clear that the PDT effectiveness depends on the light absorbed by the photosensitizer. Tissues transmit light only if it is not totally absorbed by endogenous chromophores. Unfortunately, all tissues contain oxyhemoglobin whose maximum absorbance in the visible is at 571 nm. Oxyhemoglobin still notably absorbs at 630 nm, a wavelength corresponding to the maximum of the lowest energy absorption band of Photofrin® and of protoporphyrin IX (PP), another important PDT photosensitizer that will be considered below. Moreover, these two photosensitizers are characterized by rather low molar absorbances at this wavelength. Depending on tissue vascularisation light penetration defined as the tissue depth at which the light dose is reduced to 1/3 of its initial value roughly varies from 1 to 6 mm at 630 nm. In fact the best "therapeutic window" is located between 660 and 800 nm [4]. As a result, new photosensitizers which have been authorized for today medical practice still appreciably absorb above 630 nm.

3.2. Specificity of photosensitizer delivery to diseased tissues

The simultaneous discovery in 1981 by our group [5] and G. Jori's group [6] that hydrophobic porphyrins were preferentially transported by serum lipoproteins and especially LDL played a significant role in the understanding of the mechanisms underlying the accumulation of porphyrins in tumors and other proliferating tissues. It could be anticipated at that time that porphyrin uptake by cells was governed by LDL endocytosis via the ApoB/E receptor. As a consequence, we demonstrated that increasing the number of LDL receptors by cultivating human fibroblasts in a lipid deprived medium strongly enhanced the porphyrin uptake [7] (Fig. 1). Since a marked increase in the number of LDL receptors is well established for a number of malignant cells, it provides a reasonable explanation for the relatively selective uptake of PDT photosensitizers in tumors areas as compared to normal tissues despite the fact that all cells express LDL receptors. Another important factor of porphyrin accumulation in diseased areas is the presence of an important vasculature with numerous endothelial cells expressing LDL receptors. The involvement of the LDL endocytotic pathway in the Photofrin® uptake by tumor tissues was confirmed by Kessel [8] with mouse tumor models. He showed that in addition to the tumor, the other sites of Photofrin accumulation were the liver, kidneys, lungs and skin; these organs being known as expressing a large number of apoB/E receptors. The selectivity ratio "tumor/normal tissue" is only 2–3 for Photofrin®. This modest specificity is also partly due to the structural complexity of Photofrin® which contains several components which can also bind to serum albumin and HDL. Most recent systemic PDT photosensitizers are well defined chemicals or isomers that can be chosen according to their transport and delivery process. Strongly hydrophobic PDT photosensitizers are difficult to handle. They

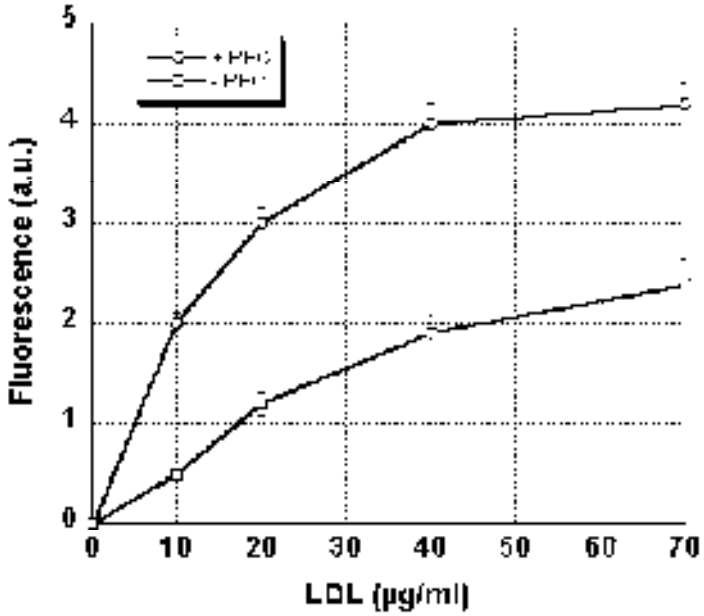

Fig. 1. Influence of the degree of expression of the ApoB/E receptor on the uptake of Photofrin®. Human fibroblasts were pre-incubated during 24 h in Dulbecco's modified minimum essential culture medium supplemented with 2% delipidized serum (+REC: maximal expression of receptors) or with 10% native serum (−REC: repression of receptors). Then cells were incubated during 1 h at 37°C with increasing concentration of LDL loaded with Photofrin® and the intracellular Photofrin® fluorescence expressed in arbitrary units per mg of proteins was measured at 625 nm upon excitation in the Soret band.

can be solubilized in adequate formulations such as liposomes of dipalmitoylphosphatidylcholine which specifically interact with LDL.

4. Mechanisms of tissue destruction by PDT photosensitizers: An outline

At the cell level, a general rule can be drawn from microfluorometric studies on single living cells or by biochemical methods. The presently used porphyrin and chlorin derivatives are localized in the cytoplasmic compartment. With Photofrin®, all organelles (mitochondria, lysosomes, endoplasmic reticulum) are targets of photodynamic reactions [9]. Furthermore, because of their amphiphilic character, tetrapyrroles tend to accumulate in membranes. As a result of their photodynamic action, a strong lipid peroxidation occurs with formation of eicosanoides and prostaglandine-like by-products which trigger the inflammatory response. From a structural point of view, blebs are readily observed at the cell surface [11] suggesting that necrosis is *a major primary death mechanism*. An important consequence of the chain reactions of lipid peroxidation is the propagation of the initial damage to other cell sites including the nucleus, thus causing non-repairable lethal DNA damage after the end of the irradiation [12].

At the tissue or organ level, in addition to the direct cell photokilling which may not be the most effective mode of action of PDT, the macroscopic response of PDT is a thrombotic necrosis due to the destruction of the neovascularisation as a result of the uptake of porphyrins by endothelial cells (see above). Another important consequence of PDT is the strong increase in the number of PMN neutrophils which doubles during the first 10 minutes after the irradiation [13].

5. Present medical applications of PDT

To date, two main fields of application are officially recognized by Health Authorities in developed countries. These are ophthalmology and oncology. It may also be noted that PDT is undergoing phase II/III clinical trials for the treatment of re-stenosis after angioplasty.

5.1. Ophthalmology

A single indication deals with the treatment of "wet" choroidal neovascularization or age-related macular degeneration (AMD) by verteporfin (Visudyne®), a 1 : 1 mixture of two regio isomers of benzoporphyrin monoacid (verteporfin). The specific delivery of the photosensitizer (6 mg/m^2 of body area) after i.v. infusion is due to the uptake by the endothelial cells of the photosensitizer via the LDL pathway [14]. The laser irradiation is carried out 15 min later using 50 J/cm^2 of 689 nm light. Inherent to all PDT treatment [2], the only secondary effect is a remanent skin and eyes phototoxicity during 2 days after verteporfin administration, a considerably shorter time than that observed with Photofrin® in other applications where skin photosensitivity can last for several weeks.

5.2. Oncology

Present study sites that are eligible for PDT with Photofrin® are the hollow organs and skin although excellent response of head and neck cancers to PDT with Foscan® (meta-tetrahydroxyphenyl)chlorin) [15] have led to recent official approval of this photosensitizer in Switzerland.

5.2.1. Lung

The main indications of Photofrin® are small tracheal and bronchial tumors for which excellent survival over several years is observed. Relapses at sites after the surgical removal of tumor may also be treated by PDT. Small cell carcinomas do not respond well to PDT [7]. The PDT of lung cancers has been more intensively developed in Japan where the official approval of new photosensitizers of the chlorin family such as N aspartyl chlorin e6 [16] is under way.

5.2.2. Esophagus

Plane or infiltrating tumors of the upper esophagus constitute the best indications for Photofrin® PDT in the GI tract. Furthermore, PDT seems to be an excellent treatment of the pre-cancerous Barrett esophagus [17].

For systemic PDT, a general treatment scheme can be summarized as follows.

i.v. injection (day 0) → transport of photosensitizer to tissues (0 to 3 h) → clearance of photosensitizer (72 to 72 h) → illumination of tumor sites by laser light → fiber optics → biological alterations of tumor components and onset of tumor necrosis → removal of debris by fibroscopy (24 h after irradiation).

If necessary, PDT can generally be repeated after healing.

5.2.3. Skin diseases

The treatment of malignant or benign diseases of the skin by PDT is rapidly developing in many countries because of an original approach based on the combination of three factors [18]: (i) topical application (2 to 4 h) of (ii) δ aminolevulinic acid (ALA) a natural precursor of protoporphyrin IX used as a prodrug, followed by (iii) irradiation with red light of the disease area with a conventional light source. Protoporphyrin IX being a quite powerful photosensitizer [19], only those cells having accumulated ALA are very effectively killed.

The use of ALA as a prodrug allows to by-pass the first step of the PP biosynthesis governed by ALA synthase, a mitochondrial enzyme finely down-regulated by heme after incorporation of iron in PP by ferrochelatase. As a result of ALA accumulation in proliferative cells in topically treated diseased area, PP synthesis is de regulated and large excess of PP is produced by cells. However, the hydrophilic nature of ALA may be a limitation in cutaneous lesion treatment, as it results in poor penetration into the skin. Recently, the methyl ester of ALA (methyl-5-aminolevulinate HCl, MAL) was successfully used which is more lipophilic than its acid. This characteristic provides a better distribution across the cellular membranes [20]. In addition, MAL and ALA are transported into cancer cells via different mechanisms, which may result in differences in their cellular uptake [21]. Furthermore, MAL seems to be more selective than ALA in actinic keratosis (AK) [22] and basal cell carcinoma (BCC) lesions [23].

Current evidence indicates that topical PDT is effective in AK, superficial BCC (Fig. 2) and Bowen's disease (Fig. 3). PDT may be of particular interest when site, size or number of lesions limits the efficacy and/or acceptability of conventional therapies. Concerning efficacy, MAL-PDT was at least as effective as cryotherapy in the treatment of AK and BCC lesions [24] and produced complete BCC lesions response rates similar to those seen with excision surgery [25]. A high degree of excellent cosmetic outcome of MAL PDT compared with other therapies (e.g. surgery, cryotherapy, fluorouracil) was observed. Topical ALA-PDT alone is a relatively poor option for both nodular BCCs and squamous cell carcinomas.

In addition to these approved indications, PDT has been applied to almost every type of cutaneous cancer and numerous benign skin disorders. Nevertheless, experience in other skin diseases remains limited or disappointing [26]. An area where there might exist a potential benefit is mycosis fungoides.

Fig. 2. A male patient with BCC at the right zygomatic region. The tumoral lesion is shown (A), while in (B) complete clinical with minimal scarring is seen 12 months after 3 treatments of MAL-PDT.

Fig. 3. A male patient with Bowen's disease at the scalar region. A erythematous, hyperkeratotic plaque (A) before treatment is shown (A), while in (B) a scar is seen at the lesion site, while the control area remains intact, at week 6 after 3 treatments of MAL-PDT.

a cutaneous T-cell lymphoma characterized by T-cell clonality with epidermotropism. We treated with MAL-PDT over 10 CTCL patients ranging from stage IA to stage IIB (Fig. 4). MAL-PDT has shown good clinical and histological efficacy in treating plaque type CTCL lesions. PDT may, therefore, be an useful additional treatment for patients with CTCL but is not suitable as monotherapy in tumor CTCL lesions [77].

In topical PDT, a general treatment scheme can be summarized as follows. After preparing the lesion by removing crusts and scales with the aid of a gentle abrasion or a non bleeding curettage, a 1 mm thick layer of the MAL cream is applied and the lesion covered by an occlusive dressing. The dressing is

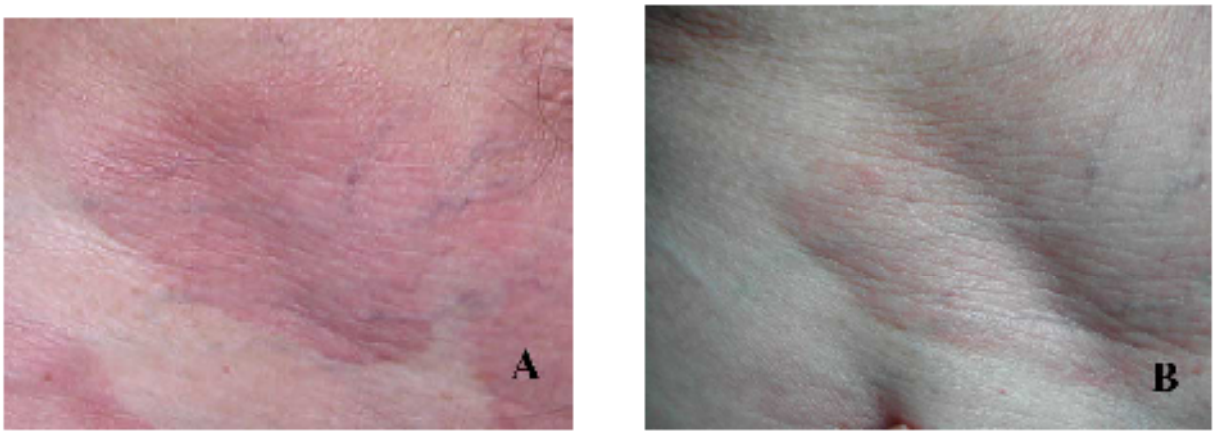

Fig. 1. Clinical response of MF lesion treated with MAL-PDT (3 treatments). The abdominal plaque showing baseline lesion (A) and treatment after 12 weeks (B).

removed after 3 hours based on the optimal time for porphyrin formation [28]. The area is cleaned using normal saline and immediately exposed to red light (570–670 nm) with a total light dose of 75 J/cm^2 and light intensity not exceeding 200 mW/cm^2 according to the observation of the complete photobleaching in BCC with this dose [23]. For the ALA ointment, a longer incubation time of 4–8 hours is needed due to slower uptake and lower selectivity.

Topical MAL-PDT is generally well tolerated in dermatology practice. Adverse events have usually mild to moderate intensity, being localized and transient. Nevertheless, they may limit patients' compliance. The most frequent adverse events result from local phototoxicity reactions, such as, burning sensation, erythema, crusting and pain. A decrease in the incidence of local adverse events is usually observed after the second cycle of PDT.

Acknowledgements

This work was made possible through grants of the "Fundação Gulbenkian" (54944, MM/n° 010000), the INSERM/GRICES exchange program and the France/Portugal bilateral "Pessoa Scientific Cooperation program".

References

[1] A. Tarstedt, A. Grigoriev, T. Hongslo, J.M. Gajer and P. Wennerholm, Photochemotherapy for severe psoriasis without oral concomitant with methoxsalen: a randomized, double-blind comparison study, *J. Am. Acad. Dermatol.* **25** (1991), 852–858.

[2] T.J. Dougherty, C.J. Gomer, B.W. Henderson, G. Jori, D. Kessel, M. Korbelik, J. Moan and Q. Peng, Photodynamic therapy, *J. Natl. Cancer Inst.* **90** (1998), 889–905.

[3] T. Kohen, R. Santus and J.G. Lindenberg, *Photobiology*, Academic Press, San Diego, 1995, pp. 23–95.

[4] B.C. Wilson, W.P. Jeeves and D.M. Lowe, Post mortem measurements of the emission spectra of light in mammalian tissues, *Photochem. Photobiol.* **42** (1985), 153–162.

[5] J.P. Reyftmann, P. Morliere, S. Goldstein, R. Santus, L. Dubertret and D. Lagrange, Interaction of human low density lipoproteins with porphyrins: a spectroscopic study, *Photochem. Photobiol.* **40** (1984), 721–729.

[6] G. Jori, M. Di Venosa, D. Reddi, D. Salvati, A. Pagnan, A. Zanon, A. Corio and L. Tiozzo, Evidence for the major role of plasma lipoproteins as tumor porphyrin carriers, *Cancer Lett.* **24** (1984), 201–207.

[7] C. Candide, P. MacLoc, J.-C. Maziere, S. Goldstein, R. Santus, L. Dubertret, J.P. Reyftmann and J. Polonowski, In vitro interaction of the photoreactive antibacterial porphyrin derivative Photofrin II with low density lipoprotein and its delivery to cultured human fibroblasts, *FEBS Lett.* 207 (1986), 131–138.
[8] D. Kessel, Porphyrin-lipoprotein association as a factor in porphyrin localization, *Cancer Lett.* 33 (1986), 183–188.
[9] K. Berg, Mechanisms of cell damage in photodynamic therapy, in: *The Fundamental Bases of Phototherapy*, A. Young, T. Dubertret and C. Lois, eds, OEMF, Milan, 1996, pp. 18–26.
[10] M. Cave, J.M. Gualtier, M. Razin and R. Santus, Sub-cellular localization of second generation PDT photosensitizers studied by microspectrofluorometry, in: *Analytical Uses of Fluorescent Probes in Oncology*, E. Kohen and J.G. Hirschberg, eds, Plenum Press, New York, 1996, pp. 13–21.
[11] J.J. Reyftmann, L. Kieran, P. Morliere, R. Santus, C. Kerian, W.L. Mangel, J.C. Dubertret and J.G. Hirschberg, A microspectrofluorometric study of porphyrin-photosensitized lysis living cells. I. Membrane alterations, *Photochem. Photobiol.* 44 (1986), 49–57.
[12] G. Oleinick and R.W. Redmond, Secondary reactive species and the range of photosensitized lethal effects on cell DNA damage mediated via initial membrane sensitization, *Photochem. Photobiol.* 57 (1993), 199–203.
[13] M. Korbelik and G. Krosl, Enhanced cytotoxic properties of cancer cells treated with photofrin in photodynamic therapy, *Photochem. Photobiol.* 60 (1994), 247–252.
[14] C. Schmidt-Erfurth and T. Hasan, Mechanisms of action of photodynamic therapy with verteporfin for the treatment of age-related macular degeneration, *Surv. Ophthalmol.* 45 (2000), 195–214.
[15] J.C. Savary, P.H. Meunier, C. Verollet, J. Mirveral, G. Wagnieres, D. Braichotte and H. Van den Bergh, Photodynamic therapy for early squamous cell carcinomas of the esophagus, pouch and mouth with m-tetrahydroxyphenylchlorin, *Arch. Otolaryngol. Head Neck Surg.* 123 (1997), 162–168.
[16] T. Kato, K. Terrahara, M. Sato, T. Okimoto, Y. Kusunoki, M. Kawahara, M. Okuroka, T. Miyazawa, T. Yana, K. Matsui, T. Shimada and T. Horiuchi, Phase II clinical study of photodynamic therapy using mono-L-aspartyl chlorin e6 and diode laser for early superficial squamous cell carcinoma of the lung, *Lung Cancer* 42 (2003), 103–111.
[17] B.F. Overholt, M. Panjehpour and J.M. Haydek, Photodynamic therapy for Barrett's esophagus: follow-up in 100 patients, *Gastrointest. Endosc.* 49 (1999), 1–7.
[18] J.C. Kennedy and R.H. Pottier, Endogenous protoporphyrin IX, a clinically useful photosensitizer for photodynamic therapy, *J. Photochem. Photobiol. B. Biol.* 14 (1992), 275–292.
[19] P. Morliere, L. Kieran, J.P. Reyftmann, R. Santus, C. Kerian, J. C. Maziere, S. Goldstein, W. L. Mangel and J. Dubertret, Photosensitization by porphyrins delivered to L cells fibroblasts by human serum low density lipoproteins. A microspectrofluorometric study, *Photochem. Photobiol.* 46 (1987), 189–191.
[20] J.M. Gaullier, K. Berg, Q. Peng, H. Anholt, P.K. Selbo, L.W. Ma and J. Moan, Use of 5-aminolevulinic acid esters to improve photodynamic therapy on cells in culture, *Cancer Res.* 57 (1997), 1481–1486.
[21] O.A. Cetemans, A. Holroyd, S.B. Brown et al., 5-Aminolevulinic acid methyl ester is not a substrate for the human colon adenocarcinoma cell line, *Photochem. Photobiol.* 73 (2001), 164–169.
[22] C. Fritsch, S. Homey, W. Stahl, D. Vetron, J. Moan and K. Berg, Preferential oxative porphyrin enrichment in solar keratoses upon topical application of delta aminolevulinic acid methylester, *Photochem. Photobiol.* 68 (1998), 218–221.
[23] E. Angell-Petersen, K.E. Gierkesky and J. Moan, Protoporphyrin IX accumulation in basal cell carcinoma and normal skin after topical application of methyl aminolevulinate (M-ALA) [poster presentation], in: *29th Annual Meeting of the American Society for Photobiology*, 2002 July 3–7, Quebec City.
[24] D.M. Pariser, N.J. Lowe, D.M. Stewart, M.T. Jarratt, A.W. Lucky, R.J. Pariser and P.S. Yamauchi, Photodynamic therapy with topical methyl aminolevulinate for actinic keratosis: results of a prospective randomized multicenter trial, *J. Am. Acad. Dermatol.* 48(Suppl. 2) (2003), 227–232.
[25] A.C. Rhodes, M. de Rie, Y. Enstrom, R. Groves, L. Morken, V. Gerritsen, G.A. Wong, J.J. Grob, S. Yazdi and J. Wolf, Photodynamic therapy using topical methyl aminolevulinate vs surgery for nodular basal cell carcinoma: results of a multicenter randomized prospective trial, *Arch. Dermatol.* 140 (2004), 17–23.
[26] C.A. Morton, S.B. Brown, S. Collins, S. Ibbotson, H. Jamieson, H. Kurwa, A. Langmack, K. McKenna, H. Moseley, A.O. Pearse, M. Sheridan, D.K. Taylor, G. Wong and L.E. Rhodes, Guidelines for topical photodynamic therapy: report of workshop of the British Photodermatology Group, *British J. Dermatol.* 146 (2002), 552–567.
[27] J. Silva, S. Filipe and J.L. Correia de Cavalho, Topical photodynamic therapy with methyl aminolevulinate in the treatment of cutaneous T cell lymphoma: case communication], in: *Second Congress of the Portuguese Society for Photodynamic Therapy*, 2002 March 2, Sintra, Italy.
[28] Q. Peng, A.M. Soler, T. Warloe, J.M. Nesland and K.E. Gierkesky, Selective distribution of porphyrins in skin with basal cell carcinoma after topical application of methyl 5-aminolevulinate, *J. Photochem. Photobiol. B. Biol.* 62 (2001), 140–145.

Bio-Medical Materials and Engineering 18 (2008) 219–227
DOI 10.3233/BME-2008-0516
IOS Press

Photodynamic therapy: Dermatology and ophthalmology as main fields of current applications in clinic

João N. Silva[a,*], Paulo Filipe[a], Patrice Morlière[b], Jean-Claude Mazière[b], João P. Freitas[c], Manuel Marques Gomes[a] and René Santus[b]

[a] *Clínica Universitária de Dermatologia, Hospital de Santa Maria, Lisbon, Portugal*
[b] *INSERM ERI 12, Laboratoire de Biochimie, CHU Amiens, Amiens, France*
[c] *INSERM U 697, Institut de Recherche sur la Peau, Hôpital Saint Louis et Muséum National d'Histoire Naturelle, Paris, France*

Abstract. Photodynamic therapy (PDT) of skin tumors or pre-cancerous lesions and of age related macular degeneration combines the administration of porphyrins or porphyrin precursors and illumination with red light at the diseased sites. Photosensitizers absorbing light beyond 630 nm where tissues have the highest transmittance produce singlet oxygen, a highly reactive activated oxygen species and a major cytotoxin. The PDT of age related macular degeneration is performed with red laser light after i.v. injection of verteporfin (Visudyne®), a lipophobic porphyrin, carried by serum lipoproteins whose endocytosis leads to accumulation of the porphyrin in endothelial cells of choroidal neovessels. In the PDT of skin cancers, local synthesis of the photosensitizer occurs after topical application of the natural pro-drug porphyrin IX precursor 5-aminolevulinic acid or its ester forms on the lesions. In all the cases, the photosensitizers should be rapidly excreted to avoid a long lasting skin photosensitivity.

Keywords: Photodynamic therapy, verteporfin, aminolevulinic acid, age related macular degeneration, actinic keratoses, basal cell carcinoma, squamous cell carcinoma, cutaneous T cell lymphoma

1. Introduction

Photodynamic therapy (PDT) was proposed twenty years ago as a local treatment of light-accessible tumors and other proliferative diseases after delivery of photoactive substances (photosensitizers) to diseased tissues. When first authorized in 1994 as a palliative treatment of lung and esophagus cancers, this therapy was based on the systemic administration of a mixture of porphyrins called Photofrin® followed by illumination with visible or red light after photosensitizer accumulation at the tumor site [6]. It becomes rapidly evident that skin and eyes that are readily accessible to irradiation by conventional or laser light were – in addition to hollow organs – first line candidates for applications of this new treatment modality.

*Address for correspondence: João N. Silva, Clínica Universitária de Dermatologia, Hospital de Santa Maria, 1600 Lisbon, Portugal. E-mail: mcjsilva@fmed.pt.

2. The molecular basis of PDT

These therapies rest upon photodynamic reactions. In such reactions requiring molecular oxygen, a biological substrate (S) is destroyed only in the presence of a photosensitizer (P) that absorbs light. Light absorption promotes P from its singlet ground state to the first singlet excited state whose deactivation occurs in the nanosecond time scale either by emitting a fluorescence – which can be used as a diagnosis tool – or by converting P into a long-lived excited state called a triplet state having a lifetime ranging from several microseconds to milliseconds. There are two types of photodynamic reactions. The so called "type 1 photodynamic reactions" involve the formation of radical species. The photosensitizer (P) in its triplet state is semi-reduced (formation of $P^{\cdot-}$) by reacting with S which is semi-oxidized (formation of $S^{\cdot+}$). Then, molecular oxygen reacts with $S^{\cdot+}$ and $P^{\cdot-}$ to produce the oxidized S and the $O_2^{\cdot-}$ radical-anion, respectively. Alternatively, in a "type 2 photodynamic reaction", the photosensitizer in its triplet state returns to the ground state by transferring excess electronic energy to molecular oxygen thereby producing singlet oxygen ($^1O_2$), a major cytotoxin. The main photodynamic substrates of biological interest are amino acids such as Trp, His, Cys, Met in the free form or incorporated into peptides and proteins, purine bases (essentially guanine), vitamins E and C and polyunsaturated fatty acid. Photosensitizers used for PDT are generally tetrapyrrole derivatives, e.g. porphyrins and chlorins which mainly induce type 2 photodynamic reactions with singlet oxygen production [16].

3. Photobiological aspects of porphyrin photosensitization

In cells, porphyrin and chlorin derivatives are localized in the cytoplasmic compartment. Therefore, all organelles (mitochondria, lysosomes, endoplasmic reticulum) are possible targets of photodynamic reactions [2]. Furthermore, because of their amphiphilic character, tetrapyrroles tend to accumulate in membranes. Upon illumination, blebs are readily observed at the cell surface suggesting that necrosis is a major primary death mechanism [10]. A strong lipid peroxidation occurs with formation of eicosanoides and prostaglandin like by products which trigger an inflammatory response. At the tissue or organ level, in addition to the direct cell photokilling, the macroscopic response of PDT may also be a thrombotic necrosis due to the destruction of the neo-vascularization as a result of the uptake of porphyrins by endothelial cells. In this regard, we demonstrated twenty years ago that hydrophobic porphyrins were readily incorporated into serum lipoproteins and especially into LDL [22]. Accordingly, Jori et al. reported the presence of hematoporphyrin in serum lipoproteins of patients after i.v. injection of hematoporphyrin [14]. These findings provided a clue for increased delivery of hydrophobic photosensitizers to tumor cells because cancerous cells generally have an increased number of LDL receptors. However, the presence of LDL receptors on all normal cells limits the selectivity of the photosensitizer accumulation at the tumor site by porphyrin loaded LDL endocytosis. The specificity of photosensitizer delivery to diseased tissues therefore plays a key role in PDT. Ocular PDT and the PDT of skin diseases illustrate two different mechanisms of photosensitizer delivery at the treatment site. In the case of ocular PDT, verteporfin – benzoporphyrin monoacid (Visudyne®) – in liposomal formulation is rapidly transferred to plasma low density lipoproteins after intravenous injection. Target cells with a high expression of low density lipoprotein receptors such as neovascular endothelial cells accumulate the photosensitizer, sparing normal vessels because of them intact blood retina barrier [24]. A totally different mechanism is operative in the PDT of skin diseases. After gentle abrasion or non-bleeding curettage of the lesion, topical application of cream containing δ-aminolevulinic acid (ALA) or its methyl ester (MAL), the natural

precursor of protoporphyrin IX (PP) leads to the biosynthesis of PP by proliferative cells or parasites in the treated area [15].

The PDT effectiveness depends on the light absorbable by the photosensitizer at the treatment site. Tissues transmit light only if it is not totally absorbed by endogeneous chromophores. Vascularized tissues contain oxyhemoglobin with maximum absorbance in the visible at 574 nm and still notable absorbance at 630 nm, a wavelength corresponding to the maximum of the lowest energy absorption band of Photofrin® and protoporphyrin IX (PP), the latter being the main PDT photosensitizer in dermatology. The best "therapeutic window" is located between 660 and 800 nm. New photosensitizers which have been authorized for today medical practice still appreciably absorb above 650 nm.

4. Treatment of ophthalmic diseases by PDT

Besides early official approval for palliative PDT with Photofrin® of cancers or pre cancerous lesions (Barrett's esophagus) of hollow organs, excellent response of head and neck cancers to PDT with Foscan® (meta-tetrahydroxyphenylchlorin) has more recently led to approval of this photosensitizer in Switzerland. However, mainstream clinical practice of PDT is limited to ophthalmology and skin diseases. The standard application of ocular PDT is the treatment of several subtypes of neo-vascular age-related macular degeneration (AMD) and choroidal neovascularization (CNV) secondary to pathologic myopia. Irradiation with 50 J/cm^2 of 689 nm light provided by a diode laser (irradiance = 600 mW/cm^2) five minutes after a 10-min infusion of the photosensitizer (6 mg/m^2 body surface area) results in visual stabilization and improvement of visual acuity after 5 treatments performed over 2 years. The only secondary effect is a transient skin and eyes photosensitivity during 2 days after verteporfin administration. The main advantage of PDT over conventional laser treatment is the selective thrombosis of new vessels while preserving adjacent neuroretinal structures. PDT has been performed with some remarkable results in several other ocular pathologies involving CNV (retinal angiomatosis proliferans, chorioditis and idiopathic CNV) and diseases without CNV such as choroidal hemangioma [17].

5. Skin disease and PDT

Very simple modalities explain the rapid development of the treatment of malignant or benign diseases of the skin by PDT [27]. The topical application of ALA is followed by illumination of the disease area with red light. As a result of ALA accumulation in proliferative cells, PP synthesis is de-regulated and large excess of PP is produced by abnormal cells. Only those cells having accumulated ALA are very effectively killed. However, the hydrophilic nature of ALA may be a limitation as it poorly penetrates into the skin. The methyl ester of ALA (MAL) which is more lipophilic and has a better distribution across the cellular membranes than its acid has been successfully used. The treatment can be summarized as follows. After preparing the lesion by removing crusts and scales, a 1 mm thick layer of the MAL cream is applied and the lesion covered by an occlusive dressing. The dressing is removed after 3 hours based on the optimal time for porphyrin formation. The area is cleaned using normal saline and immediately exposed to red light (570–670 nm) from a conventional light source with a total light dose of 75 J/cm^2 and irradiance not exceeding 200 mW/cm^2 [27]. For ALA, a longer incubation time of 4–8 hours is needed due to slower uptake and lower selectivity. Topical MAL-PDT is generally well tolerated in dermatology practice. Adverse events have usually mild to moderate intensity, being localized, transient and easily managed. The most frequent adverse events result from local phototoxicity reactions, such

as, burning sensation, erythema, crusting and pain. A decrease in the incidence of local adverse events is usually observed after the second cycle of PDT.

In general, surgical excision is the most effective treatment of epithelial skin tumours. However, alternative modalities are necessary for extensive or multiple disseminated lesions to improve functional and cosmetic results. Current evidence indicates that topical PDT is effective in actinic keratosis (AK), Bowen's disease (BD) and superficial basal cell carcinoma (sBCC). ALA-PDT and MAL-PDT are now approved for the treatment of these skin lesions in USA and Europe/Australia, respectively. PDT is of particular interest when site, size or number of lesions limits the efficacy and/or acceptability of conventional therapies.

Actinic keratosis is one of the best studied indications for PDT in Dermatology. In most clinical studies, a complete response (CR) rate of 69–93% was achieved at 3 months with the use of two MAL-PDT treatments 7 days apart [18,20,29]. Tarstedt et al. found that a single treatment with MAL-PDT, repeated after 3 months only in case lesions remained, was as effective as routinely using two treatments 7 days apart [30]. MAL-PDT efficacy has been compared with other treatment modalities for AK. A comparative study of MAL and cryotherapy was conducted by Morton et al. [18]. They performed a multicentre controlled comparison of 119 patients randomized for intraindividual right–left treatment with either MAL-PDT or cryotherapy. Overall response rates were similar between the groups at week 24 (89.1% cleared for MAL-PDT and 86.1% for cryotherapy; $p = 0.20$), but the cosmetic outcome was superior for the PDT group. Another recent randomized intrapatient comparative trial evaluated MAL-PDT and topical 5 fluorouracil (5-FU) cream in the treatment of post transplant epidermal dysplasia [21]. Treatment with two cycles of topical MAL-PDT, 1 week apart, was randomly assigned to one area of epidermal dysplasia, and 5-FU cream was applied twice daily for 3 weeks to a clinically and histologically comparable area. At 6 months, lesion CR rates were 89% with MAL-PDT and 11% with 5-FU. MAL-PDT demonstrated a superior cosmetic result and was preferred by patients. PDT can also be an effective noninvasive method to treat actinic cheilitis of the lower lip with a CR rate of 47% and partial cure rate of 46% at month 3 [5].

Bowen's disease is a form of *in situ* squamous cell carcinoma (SCC) with a significant potential to lateral spread. Lesions vary in size from a few millimeters to several centimeters in diameter. The head and neck are most commonly affected, followed by the limbs. These anatomic localisms may raise difficulties if surgery is to be considered. Prognosis of Bowen disease is favourable, with less than 5% of cases advancing to invasive SCC. There is now much support for the use of topical PDT as a tissue-sparing, non-invasive, high efficacy and good tolerability treatment for BD. The strongest evidence comes from a comparative trial involving 195 patients comparing MAL-PDT, placebo-PDT, cryotherapy and 5-FU for the treatment of BD. Results indicated that lesion CR rates at 3 months were 93% with MAL-PDT, 21% with placebo PDT, 86% with cryotherapy and 83% with 5-FU. At 24 months following final treatment lesion CR rate was 68% for MAL-PDT [19]. Topical MAL-PDT alone is a relatively poor option for SCC due to the relatively high recurrences rates and metastatic potential of this tumor.

Basal cell carcinoma (BCC) is one of the most common cancers. Surgical excision and Mohs micrographic surgery remain the mainstay of therapy of low-risk and high-risk BCC, respectively. Both methods produce high cure rates, but they may not be appropriate treatments for elderly patients who are either not surgical candidates or refuse to undergo surgery and whenever cosmetic outcome is important. There have been several trials on the use of topical MAL-PDT in superficial and nodular BCC. Results from histologically controlled studies showed 3 month clearance rates with MAL-PDT ranging from 80% (mid-facial, recurrent or large lesions) to 97% in primary superficial BCC (sBCC) [13,32]. MAL-PDT was shown to be equivalent to cryotherapy in the treatment of sBCC with comparable CR

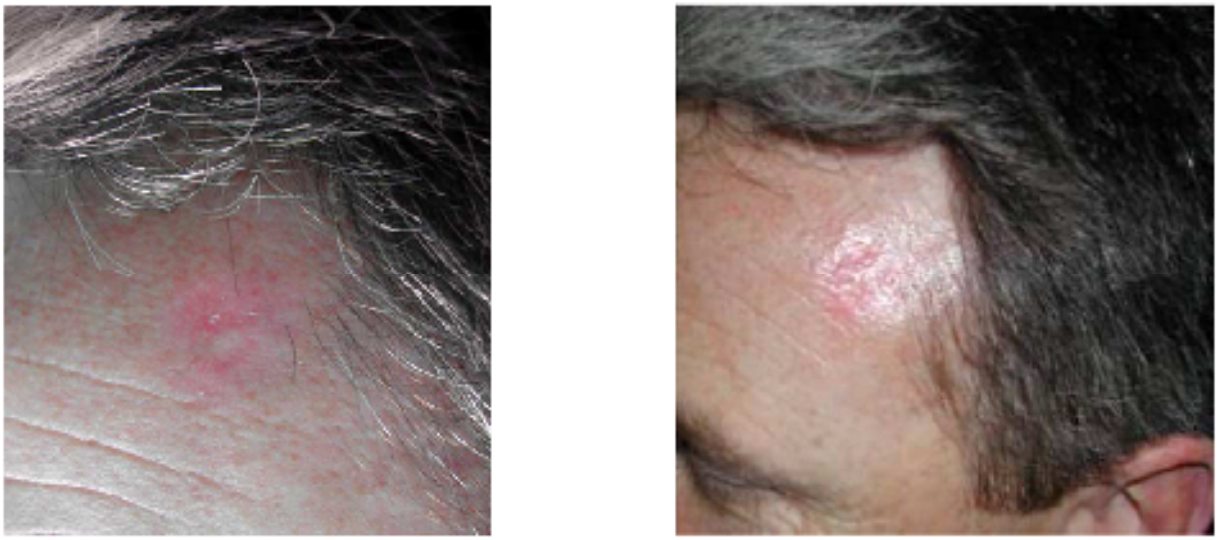

(a) (b)

Fig. 1. (a) 48-year-old man with superficial BCC on the left forehead, prior to MAL-PDT. (b) 6 months after 3 sessions of MAL-PDT: histologically confirmed complete clearance – only presence of slight erythema.

rates up to 60 months (75% vs 74%, respectively) [1]. A high degree of excellent cosmetic outcome of MAL-PDT compared with other therapies (e.g. surgery, cryotherapy, 5-fluorouracil) was also observed. We have treated over 50 sBCC with MAL-PDT. Most of the patients had a solitary lesion located on the face, dorsum or limbs. A single cycle of MAL-PDT involving two treatments was applied 1-week apart (Fig. 1). In nodular BCC (nBCC), the thickness of the skin lesion reduces PDT efficacy and surgical excision continues to be the conventional treatment. MAL-PDT CRs range from 75–91% at 3 months to 77% at 60 months [13,31]. Rhodes et al. performed a prospective, randomized, multicenter study of topical MAL-PDT and simple excision surgery in the treatment of primary nodular BCC [23]. At 3 months after the last treatment, CR rates were 91% with MAL-PDT and 98% in the surgery group. The cumulative 5-year lesion recurrence rate with MAL-PDT was 14% compared with 4% for excision surgery and the sustained lesion complete response rate at 5 years was statistically superior with excision surgery compared with MAL-PDT (96% vs 77%; p < 0.01). The cosmetic outcome at 60 months for patients in CR was rated as good or excellent in 87% for MAL-PDT vs 53% in the surgery group. The authors concluded that although surgery showed superior long-term efficacy in nBCC, the moderately low 5-year lesion recurrence rate with MAL-PDT together with the favourable long-term cosmetic outcome supports a clinical role for this modality in the treatment of nBCC.

In addition to these approved indications, PDT has been applied to almost every type of cutaneous cancer and numerous benign skin disorders. Acne and human papilloma virus warts have been the focus of several studies, while a few case reports have evaluated the utility of PDT for cutaneous T-cell lymphoma, vascular tumors, psoriasis, lichen sclerosus, lichen planus and scleroderma. An area where there might exist a potential benefit is Mycosis fungoides, a cutaneous T cell lymphoma characterized by T-cell clonality with epidermotropism. We have treated with MAL-PDT over 15 CTCL patients ranging from stage IA to stage IIB (Fig. 2). MAL-PDT has shown good clinical and histological efficacy in treating patch and plaque type CTCL lesions. PDT may, therefore, be an useful additional palliative treatment for patients with CTLC [27,53].

(a) (b)

Fig. 2. (a) 63 year old man with cutaneous T-cell lymphoma plaque on the abdomen prior to MAL-PDT. (b) 12 months after 3 courses of MAL-PDT: complete clearance – residual hyperpigmentation.

Recently, ALA-PDT has been used in the treatment of cutaneous leishmaniasis, an important health problem caused by the flagellated protozoa, *L. major* and *L. tropica*. It is endemic in 88 countries with a yearly incidence of 1.5 million cases. As there is no vaccine, drugs must be used with increasing development of resistance and strong side effects such as kidney damage by amphotericin B, a second line treatment after antimony derivatives. Encouraging results with respect to Leishmania eradication and low scar formation has been reported with PDT [9]. As with other diseases of the skin, healing and cosmetic outcome with ALA-PDT repeated once a week for a month was excellent and no clinical sign of recurrence has been noted [11]. It should be noted that *leishmania* parasites are deficient in the enzymes required for heme biosynthesis [5] and then rely on external PP biosynthesis from the diseased cells after ALA topical application.

Another developing field of interest is the potential use of PDT for nonmelanoma skin cancer (NMSC) prevention. The incidence of NMSC has been increasing by 2–3% per year in the USA. Skin cancer prevention mostly rely on sun avoidance and sun protection with sunscreens and clothing. Frequent medical visits for high-risk patients (e.g. fair-skinned individuals, patients with previous history of BCC or SCC and those who are immunosuppressed) are also performed to detect and treat early lesions. Transplant patients demand particular attention as they have a 10-fold increased risk of BCC and a 150-fold increased risk of developing SCC which appear to be more aggressive in these patients in comparison with immunocompetent individuals. Additional preventive measures, such as topical PDT, are needed in view of the limited number of options currently available. In skin cancer prevention experiments using hairless mice, Stender et al. and Shurfaci et al. showed that weekly topical ALA PDT can delay the appearance of AK and SCC induced by chronic UV radiation exposure [26,28]. A similar preventive effect was shown using topical MAL PDT [25]. The recent availability of a transgenic mouse heterozygous for the PTCH gene provided for the first time an animal model to study prevention strategies for BCC. Caty et al. recently showed that weekly suberythematous topical MAL-PDT sessions were able to delay the development of microscopic BCCs in PTCH mice chronically exposed to UV radiation [1]. Prospective clinical studies designed to evaluate skin cancer prevention have been difficult to perform mainly because of ethical issues and the long delay between the carcinogenic stimulus and the appear-

ance of skin lesions. There are few studies concerning the efficacy of PDT as a preventive treatment in immunosuppressed patients. Two prospective randomized trials have shown MAL-PDT to be effective for preventing AK in organ-transplant recipients [7,8]. On the other hand, a randomized-controlled trial with paired observations involving 40 organ-transplant recipients showed that topical ALA-PDT using violet light (400–450 nm) did not significantly prevent the development of new SCC within a 2-year follow up period [12].

6. Conclusions

Photodynamic therapy has proved to be an effective mainstream treatment of certain ocular and skin diseases. In ophthalmology, it may be anticipated that PDT may be useful in the treatment of other diseases involving choroidal neo-vascularization (CNV) such as idiopathic CNV. Also, potential synergistic action may be expected using PDT in combination with anti VEGF agents now available on the market.

Numerous clinical trials have demonstrated that topical PDT is an effective and safe treatment of various malignant and non malignant skin diseases. However the present applications of PDT in dermatology are limited to tumors or lesions with small thickness. As a result, an important refinement of PDT would be the development of new topical photosensitizers with better penetration than ALA and notably absorbing light at longer wavelengths than PP. Once again, the possibility of combining these photosensitizers with chemotherapeutic agents should also be investigated.

Acknowledgements

We gratefully acknowledge grants from "La Ligue contre le Cancer, Comité de la Somme". J.N. Silva and P. Filipe thank the "Sociedade Portuguesa de Dermatologia e Venereologia" for travel grants.

References

[1] N. Basset-Seguin, S. Ibbotson and ... Emtestam, MAL-PDT versus cryotherapy for treatment of primary superficial basal cell carcinoma: results of a five year prospective randomized trial, *J. Invest. Dermatol.* **126** (2006), 539.

[2] K. Berg, Mechanisms of cell damage in photodynamic therapy, in: *The Biochemical Bases of Photomedicine*, A. Young, T. Honjyamura and G. Jori, eds, OEMC Milan, 1998, pp. 18–26.

[3] C. Berking, T. Herzinger, M.J. Hagg, M. Brenner, C. Borelli and K. Degitz, The efficacy of photodynamic therapy in actinic cheilitis of the lower lip: a prospective study of 15 patients, *Dermatol. Surg.* **33** (2007), 825–830.

[4] V. Clay, S. Lee, C. Watt and R. Bissonnette, Multiple large surface photodynamic therapy sessions with topical methyl aminolevulinate in PDT-naïve heterozygous mice, *Int. J. Dermatol.* **154** (2006), 740–742.

[5] C.S. Chang and K.P. Chang, Heme requirement and acquisition by extracellular and intracellular stages of Leishmania mexicana amastigotes, *Mol. Biochem. Parasitol.* **16** (1985), 267–276.

[6] T.J. Dougherty, C.J. Gomer, B.W. Henderson, G. Jori, D. Kessel, M. Korbelik, J. Moan and Q. Peng, Photodynamic therapy, *J. Natl. Cancer Inst.* **90** (1998), 889–905.

[7] G. Dragieva, J. Hafner, R. Dummer, P. Schmid-Grendelmeier, M. Roos, B.M. Prinz, G. Burg, U. Braunwalder and W. Kempf, Topical photodynamic therapy in the treatment of actinic keratoses and Bowen's disease in transplant recipients, *Transplantation* **77** (2004), 1545–1547.

[8] G. Dragieva, B.M. Prinz, J. Hafner, R. Dummer, G. Burg, U. Braunwalder and W. Kempf, A randomized controlled clinical trial of topical photodynamic therapy with methyl aminolevulinate in the treatment of actinic keratoses in transplant recipients, *Br. J. Dermatol.* **151** (2004), 196–200.

[9] K. Gardeła, Z. ... ska, O.D. ... ek, I. Rauch, M. Megahed, E. Ruzicka and G. Hrisch, Treatment of cutaneous leishmaniasis by photodynamic therapy, *J. Am. Acad. Dermatol.* **48** (2003), 893–896.

[10] M. Göze, J.M. Gaullier, M. Bazin and S. Sauma, Sub-cellular localization of second generation PDT photosensitizers studied by microspectrofluorometry, in: *Analysis at Use of Photosensitizers in Oncology*, J. Kahlert and J.C. Stockert, eds, Plenum Press, New York, 1996, pp. 13–21.

[11] Y. Ün Yanlar, O. Serper, M. Mirchamsy, M.H. Mirmohseni and Z.K. Hassani, Photodynamic therapy as a new treatment of cutaneous leishmaniasis, *Lasers. Medi. Health J.* **12** (2006), 932–938.

[12] M.G. de Graaff, C. Kennedy, R. Wolterbeek, A.J.C. Gallen, R. Wennekes, N. Bavinck, Photodynamic therapy does not prevent cutaneous squamous-cell carcinoma in organ-transplant recipients: results of a randomized-controlled trial, *J. Invest. Dermatol.* 126 (2006), 569–574.

[13] M. Lassus, P. Wolf, H.C. Wulf, E. Warloe, C. Hirsch and L.L. Rhodes, Topical 5-ethyl aminolevulinate photodynamic therapy in patients with basal cell carcinoma prone to complications and poor cosmetic outcome with conventional therapy, *Br. J. Dermatol.* **149** (2003), 1242–1249.

[14] G. Jori, M. Beltramin, L. Soncin, R. Salvato, A. Pagnan, L. Zinon, L. Tomio and L. Ferro, Evidence for the exploitation of tumour lipoproteins as tumour-photodynamic carriers, *Cancer Lett.* **24** (1984), 297–303.

[15] C.J. Kelty, N.J. Brown, M.W.R. Reed and R. Ackroyd, The use of 5-aminolevulinic acid as a tumour marker in photodynamic therapy and photodiagnosis, *Photochem. Photobiol. Sci.* 1 (2002), 158–168.

[16] A. Kohen, R. Sandlas and J.C. Stockert, *Photobiology*, Academic Press, San Diego, CA, 1995, pp. 23–95.

[17] S. Mensel, I. Barbazetto, C.H. Meyer, S. Peter and M. Stur, Ocular photodynamic therapy – standard applications and new indications (Part I), *Ophthalmologica* 221 (2007), 2–6–228.

[18] C. Morton, S. Campbell, G. Gupta, S. Kerdraon, J. Lear, I. Zeki, S. Walton, N. Ravenscroft, G. Thomas and P. Soyer, Intraindividual, right–left comparison of topical methyl aminolaevulinate photodynamic therapy and cryotherapy in subjects with actinic keratoses: a multicentre, randomized controlled study, *Br. J. Dermatol.* 155 (2006), 1020–1026.

[19] C.A. Morton, M. Hout, S.C. Lesher, A randomised placebo-controlled, European study comparing MAL-PDT with cryotherapy and 5-fluorouracil in subjects with Bowen's disease: results from a 21 months follow up, Poster presented at the 16th World Congress on Cancer of the Skin, Vienna, 2005.

[20] D.M. Pariser, N.J. Lowe, D.M. Stewart, M.T. Jorizzo, A.W. Dudley, R.J. Pariser and P.S. Yamauchi, Photodynamic therapy with topical methyl aminolevulinate for actinic keratoses: results of a prospective randomized multicenter trial, *J. Am. Acad. Dermatol.* 48 (2003), 227–232.

[21] C.M. Panich, J.M. McFadyen, J. Warwick, P. Kernan, I.M. Leigh, C.M. Proby and C.A. Harrison, Short course of post-transplant, post-malignant skin diseases: a randomized intraindividual comparative study of 5-fluorouracil cream and topical photodynamic therapy, *Br. J. Dermatol.* 156 (2007), 320–328.

[22] J.P. Reyftmann, P. Morliere, S. Goldstein, R. Santus, T. Dubertret and D. Lagrange, Interaction of human low density lipoproteins with porphyrins: a spectroscopic study, *Photochem. Photobiol.* **40** (1984), 721–727.

[23] L.L. Rhodes, M.A. de Rie, R. Leenhouts, R.C. Yu, I. Beckham, V. Goulden, C.A. Wong, M.A. Rholand, A. Ansley and P. Wolf, Nine year follow-up of a randomized, prospective trial of topical methyl aminolevulinate photodynamic therapy vs surgery for nodular basal cell carcinoma, *Arch. Dermatol.* 143 (2007), 1343–1350.

[24] L. Schmidt, A. Faludi, I. Lazar, L. Dragomán, L.D. Kozma and R. Biczók, Vascular targeting in photodynamic occlusion of subretinal vessels, *Ophthalmologe* **101** (1964), 1953–1961.

[25] S. Sternfeld, P. Invernizzi, F. Muzi and R. Bissonnette, Weekly topical application of methyl aminolevulinate followed by light exposure delays the appearance of UV-induced skin tumors in mice, *Arch. Dermatol. Res.* 294 (2002), 237–242.

[26] S. Szeimies, G. Viola, H. Luis, J. Boehncke and R. Bissonnette, Systemic photodynamic therapy with aminolaevulinic acid delays the appearance of ultraviolet-induced skin tumours in mice, *Br. J. Dermatol.* **144** (2001), 1207–1214.

[27] J.N. Silva, P. Filipe, P. Morliere, J.C. Mazière, J.P. Santus, F.L. Pina da Cunha and R. Santus, Photodynamic therapies: principles and present medical applications, *Biomed. Mater. Eng.* 16 (2006), S147–S151.

[28] I.M. Stender, N. Reed, T. Thomsen, L. Pedersen and J.C. Wulf, Photodynamic therapy with topical 5-aminolevulinic acid delays UV photocarcinogenesis in hairless mice, *Photochem. Photobiol.* 66 (1997), 493–496.

[29] R.M. Szeimies, S. Karrer, S. Radakovic-Fijan, A. Tanew, P.F. Calzavara-Pinton, C. Zane, A. Sidoroff, M. Hempel, J. Ulrich, E. Avedaño, H. Meleti, M. Mulder, J. Sattmann, H.C. Dijkman, J.W. Baron, K. Korn and A.L. Bezdahn, Photodynamic therapy using topical methyl 5-aminolevulinate compared with cryotherapy for actinic keratosis: a prospective, randomized study, *J. Am. Acad. Dermatol.* 47 (2002), 258–262.

[30] M. Tarstedt, I. Rosdahl, S. Berne, K. Svanberg and A.M. Wennberg, A randomized multicenter study to evaluate two treatment regimens of topical methyl aminolevulinate (Metvix) PDT in actinic keratosis of the face and scalp, *Acta Derm. Venereol.* 85 (2005), 124–128.

[31] W.D. Togo, A. Morton, R.A. El-Azhary, N.J. Lowe, M. Innaft and D.M. Pariser, Comparison of topical methyl aminolevulinate photodynamic therapy versus placebo photodynamic therapy in nodular BCC, *J. Am. Acad. Dermatol. Venereol.* **18** (2004), 433–441.

[32] C. Vanicullo, T. Elliott, K. Gebauer, L. Spelman and R. Ngyen, MAL-PDT in patients with basal cell carcinoma: results of an Australian multicentre study, Poster presented to the International Skin Cancer Conference 2001, Vienna, 2001.
[33] C. Zane, M. Venturini, R. Sala, P. Calzavara-Pinton, Photodynamic therapy with methylaminolevulinate as a valuable treatment option for mucosotropic cutaneous T-cell lymphoma, *Photodermatol. Photoimmunol. Photomed.* **22** (2006), 254–258.

PUBLICATIONS

PUBLICATIONS

Chain-dependent photocytotoxicity of tricationic porphyrin conjugates and related mechanisms of cell death in proliferating human skin keratinocytes.
Silva JN, Galmiche A, Tomé JP, Boullier A, Neves MG, Silva EM, Capiod JC, Cavaleiro JA, Santus R, Mazière JC, Filipe P, Morlière P. Biochem Pharmacol. 2010 Aug 4.

Tricationic porphyrin conjugates: evidence for chain-structure-dependent relaxation of excited singlet and triplet States.
Silva JN, Bosca F, Tomé JP, Silva EM, Neves MG, Cavaleiro JA, Patterson LK, Filipe P, Mazière JC, Santus R, Morlière P. J Phys Chem B. 2009 Dec 31;113(52):16695-704.

Stratum corneum is an effective barrier to TiO2 and ZnO nanoparticle percutaneous absorption.
Filipe P, **Silva JN**, Silva R, Cirne de Castro JL, Marques Gomes M, Alves LC, Santus R, Pinheiro T. Skin Pharmacol Physiol. 2009;22(5):266-75.

The alkyl chain length of 3-alkyl-3',4',5,7-tetrahydroxyflavones modulates effective inhibition of oxidative damage in biological systems: illustration with LDL, red blood cells and human skin keratinocytes.
Filipe P, Silva AM, Seixas RS, Pinto DC, Santos A, Patterson LK, **Silva JN**, Cavaleiro JA, Freitas JP, Mazière JC, Santus R, Morlière P. Biochem Pharmacol. 2009 Mar 15;77(6):957-64.

Changes of iron concentrations in skin and plasma of patients with hemochromatosis along therapy
Pinheiro T, Barreiros A, Alves L, Neres M, Fleming R, **Silva JN**, Filipe P, Silva R. J Radioanal Nucl Chem (2009) 281:161–164

Imaging iron in skin and liver: Non-invasive tools for hemochromatosis therapy.
Pinheiro T, Fleming R, Gonçalves A, Neres M, Alves L, **Silva JN**, Filipe P, Silva R. Nuclear Instruments and Methods in Physics Research B 267 (2009) 2140–2143

Photodynamic therapy: Dermatology and ophthalmology as main fields of current applications in clinic.
Silva JN, Filipe P, Morlière P, Mazière JC, Freitas JP, Gomes MM, Santus R. Biomed Mater Eng. 2008;18(4-5):319-27.

Solar urticaria treated successfully with intravenous high-dose immunoglobulin: a case report.
Correia I, **Silva JN**, Filipe P, Gomes M. Photodermatol Photoimmunol Photomed. 2008 Dec;24(6):330-1.

Photophysical properties of a photocytotoxic fluorinated chlorin conjugated to four beta-cyclodextrins.
Silva JN, Silva AM, Tomé JP, Ribeiro AO, Domingues MR, Cavaleiro JA, Silva AM, Neves MG, Tomé AC, Serra OA, Bosca F, Filipe P, Santus R, Morlière P. Photochem Photobiol Sci. 2008 Jul;7(7):834-43.

Skin cancers and precancerous lesions in Parkinson's disease patients.
Ferreira J, **Silva JM**, Freire R, Pignatelli J, Guedes LC, Feijó A, Rosa MM, Coelho M, Costa J, Noronha A, Hewett R, Gomes AM, de Castro JL, Rascol O, Sampaio C. Mov Disord. 2007 Jul 30;22(10):1471-5.

Nuclear microscopy: a tool for imaging elemental distribution and percutaneous absorption in vivo.
Veríssimo A, Alves LC, Filipe P, **Silva JN**, Silva R, Ynsa MD, Gontier E, Moretto P, Pallon J, Pinheiro T. Microsc Res Tech. 2007 Apr;70(4):302-9.

Enhancement of the photodynamic activity of tri cationic porphyrins towards proliferating keratinocytes by conjugation to poly-S-lysine.
Silva JN, Haigle J, Tomé J, Neves M, Tomé A, Mazière J-C, Mazière C, Santus R, Cavaleiro J, Filipe P, Morlière P. Photochem. Photobiol*. Sci.*, 2006, *5*, 126–133.

Photodynamic therapies: principles and present medical applications.
Silva JN, Filipe P, Morlière P, Mazière JC, Freitas JP, Cirne de Castro JL, Santus R. Biomed Mater Eng. 2006;16(4 Suppl):S147-54.

Using skin to assess iron accumulation in human metabolic disorders
Guinote I, Fleming R, Silva R, Filipe P, **Silva JN**, Veríssimo A, Napoleão P, Alves L, Pinheiro T. Nuclear Instruments and Methods in Physics Research B 249 (2006) 697–701

Contrasting action of flavonoids on phototoxic effects induced in human skin fibroblasts by UVA alone or UVA plus cyamemazine, a phototoxic neuroleptic.
Filipe P, **Silva JN**, Haigle J, Freitas JP, Fernandes A, Santus R, Morlière P. Photochem Photobiol Sci. 2005 May;4(5):420-8.

Polyhydroxylated 2-styrylchromones as potent antioxidants.
Filipe P, Silva AM, Morlière P, Brito CM, Patterson LK, Hug GL, **Silva JN**, Cavaleiro JA, Mazière JC, Freitas JP, Santus R. Biochem Pharmacol. 2004 Jun 15;67(12):2207-18.

Anti- and pro-oxidant effects of quercetin in copper-induced low density lipoprotein oxidation. Quercetin as an effective antioxidant against pro-oxidant effects of urate.
Filipe P, Haigle J, **Silva JN**, Freitas J, Fernandes A, Mazière JC, Mazière C, Santus R, Morlière P. Eur J Biochem. 2004 May;271(10):1991-9.

An insight into the mechanisms of the phototoxic response induced by cyamemazine in cultured fibroblasts and keratinocytes.
Morlière P, Haigle J, Aissani K, Filipe P, **Silva JN**, Santus R. Photochem Photobiol. 2004 Feb;79(2):163-71.

Flavonoids and urate antioxidant interplay in plasma oxidative stress.
Filipe P, Lança V, **Silva JN**, Morlière P, Santus R, Fernandes A. Mol Cell Biochem. 2001 May;221(1-2):79-87.

Antioxidant effect of drugs used in cardiovascular therapy.
Silva JM, Filipe PM, Fernandes AC, Manso CF. Rev Port Cardiol. 1998 Jun;17(6):495-503.

Effect of silibinin on oxidative damage of blood constituents.
Filipe PM, Fernandes AC, **Silva JN**, Freitas JP, Manso CF. C R Seances Soc Biol Fil. 1997;191(5-6):821-35